Refining the climate, glacier, and volcanic history of Iceland during the Holocene

David John Harning

Faculty of Earth Sciences
University of Iceland
2019

Refining the climate, glacier, and volcanic history of Iceland during the Holocene

David John Harning

Dissertation submitted in partial fulfillment of a
Philosophiae Doctor degree in Geological Sciences

PhD Committee

Dr. Áslaug Geirsdóttir [1]
Dr. Gifford H. Miller [2]
Dr. Julio Sepúlveda [2]
Dr. Thomas M. Marchitto [2]
Dr. Robert S. Anderson [2]
Dr. Alexandra Jahn [3]

[1] Faculty of Earth Sciences, University of Iceland
[2] INSTAAR and Department of Geological Sciences, University of Colorado Boulder
[3] INSTAAR and Department of Atmospheric and Oceanic Sciences, University of Colorado Boulder

Faculty of Earth Sciences
School of Engineering and Natural Sciences
University of Iceland
Reykjavik, April 2019

Refining the climate, glacier, and volcanic history of Iceland during the Holocene
Holocene climate, glacier, and volcanic history of Iceland
Dissertation submitted in partial fulfillment of a *Philosophiae Doctor* degree in Geological Sciences

Faculty of Earth Sciences
School of Engineering and Natural Sciences
University of Iceland
Askja, Sturlugata 7
101 Reykjavík
Iceland

Telephone: 525 4000

Bibliographic information:
Harning, D.J., 2019, *Refining the climate, glacier, and volcanic history of Iceland during the Holocene*, PhD dissertation, Faculty of Earth Sciences, University of Iceland, 238 pp.

Author ORCID: https://orcid.org/0000-0002-2648-1346

Printing: Háskolaprent
Reykjavík, Iceland, April 2019

Abstract

Iceland's position at the confluence of major oceanic and atmospheric fronts results in a highly sensitive climate evident in both instrumental and paleo records. However, open questions still remain regarding the pre-instrumental evolution of climate, glacier, and volcanic activity at this hemispherically relevant location. This dissertation capitalizes on and merges a range of analytical techniques in an effort to refine our understanding of Icelandic climate variability, glacier extent, and tephrochronology during the Holocene epoch, with a focus on Northwest Iceland. In order to provide robust age control in our records, this research required the development of a tephrochronological framework for West Iceland, a region that lacks the otherwise widely-dispersed rhyolitic marker tephras. Glacier proxies (threshold lake sediment records and emerging dead vegetation from receding ice margins) provide firm constraints on the Holocene activity of Drangajökull, an ice cap in northwest Iceland, and high-resolution lake sediment proxy records (TOC, $\delta^{13}C$, C/N and biogenic silica) collected adjacent to the glacier elucidate the concomitant climate. Furthermore, we explore two lipid biomarker paleothermometers (alkenones and branched glycerol dialkyl glycerol tetraether, GDGTs) in one of these lakes and its catchment soils for the first time in Iceland to quantify the evolution of Holocene summer temperature.

Similar to other Icelandic ice cap histories, our records collectively illustrate that a warm early Holocene (2 to 5 ^{o}C above modern) likely resulted in the complete demise of Drangajökull shortly after 9 ka. Subsequent to peak early Holocene summer warmth, lake sediment climate proxies indicate punctuated declines in algal productivity and increases in soil erosion alongside steadily decreasing northern hemisphere (NH) summer insolation. As summers continued to cool, Drangajökull re-nucleated by ~2.3 ka and episodically expanded to its maximum dimension during the Little Ice Age (0.7-0.1 ka), when summer temperatures are estimated to be ~1 ^{o}C below modern. Triggers for cold anomalies are linked to variable combinations of freshwater pulses from waning Pleistocene ice sheets, low total solar irradiance, explosive and effusive volcanism, and internal modes of climate variability, with cooling likely sustained by ocean/sea-ice feedbacks.

In addition to the lake record, GDGTs were also applied in two other settings: a Holocene soil archive in central Iceland and in the marine realm along the North Iceland Shelf. For the latter, we also developed an Icelandic GDGT-temperature calibration based on marine surface sediment that highlights the reduced uncertainty (± 0.4 ^{o}C) achievable for local rather than global calibrations (e.g., ± 4.0 ^{o}C). Local calibrations are particularly important for areas where the temperature relationship of GDGTs deviates from the overall linear correlation observed in global calibrations (i.e., cold and warm regions), such as Iceland. Although clearly reflected in the maximum dimensions of Drangajökull, the Little Ice Age cooling is obscured in all lake, soil and marine organic geochemical records investigated in this dissertation. For the former two, the erosion of older soils, nutrients and relic GDGTs likely compromise the records and imply warmth. On the other hand, the development of thick sea ice inferred from highly branched isoprenoid biomarkers on the North Iceland Shelf insulated the subsurface waters during the peak Little Ice Age, likely preventing the ventilation of heat from below the surface layer to the atmosphere. This dissertation provides critical and nuanced observations necessary for evaluating modeling simulations aiming to forecast the poorly constrained climate of the coming century.

Útdráttur

Næmni Íslands fyrir veðurfarsbreytingum kemur fram í samfelldum veðurathugunum og veðurvísum og skýrist að einhverju leyti af stöðu landsins á skilum kaldra og tempraðra sjávar- og loftmassa, sem færast í takt við umhverfisbreytingar á Norður Atlantshafi. Samspil og þróun loftslags, jökla og eldvirkni fyrir tíma samfelldra mælinga er margslungið og margt er enn á huldu um hvernig orsakasamhengi er háttað. Mikilvægt er að rýna betur í þessa ferla til að unnt verði að bæta spár um komandi umhverfis- og veðurfarsbreytingar. Þessi ritgerð greinir frá rannsóknum þar sem fjölþættum greiningaraðferðum er beitt í því skyni að betrumbæta skilning okkar á loftslagsbreytingum, útbreiðslu jökla og myndun gjóskulaga á Íslandi á Nútíma, með áherslu á Vestfirði og Drangajökul. Nákvæm greining á gjóskulögum, sem er að finna í seti vatna sem liggja að Drangajökli, var gerð til að ná fram áreiðanlegum aldursgreiningum á vatnasetinu og veðurvísum sem í því finnast, en þetta svæði hefur skort nákvæmt gjóskutímatal hingað til. Vitnisburður jökulframrása (stöðuvatnaset og aldursgreiningar á gróðri sem hefur komið í ljós undan hörfandi jökli) hafa að geyma nákvæm gögn um virkni Drangajökuls á Nútíma, studdur af veðurvísum (TOC, $\delta^{13}C$, C/N og lífrænn kísill) sem finnast í seti stöðuvatnanna. Að auki var með þessu verkefni í fyrsta skipti á Íslandi beitt rannsóknum á tveimur hitastigs- og rakanæmum lífmerkjum (alkenones and branched glycerol dialkyl glycerol tetraether, GDGTs) í seti eins stöðuvatnsins og í jarðvegssniði sem er að finna á upptakasvæði þess, í þeim tilgangi að ná fram þróun magnbundins sumarhita á Nútíma.

Svipað og rannsóknir á sögu og þróun annarra íslenskra jökla gefa til kynna, benda niðurstöður okkar til þess að hlýindi árla á Nútíma (á bilinu 2° til 5 °C yfir meðaltali síðustu áratuga) hafi leitt til hörfunar á forvera Drangajökuls. Fljótlega eftir að hámarki hlýnunar var náð, snemma á Nútíma, sýna veðurvísar í stöðuvatnaseti stigvaxandi hnignun í framleiðni vatnaþörunga og aukningu í jarðvegsrofi, sem svörun við hægfara lækkun sumarinngeislunar á norðurhveli jarðar. Drangajökull myndaðist á ný fyrir um 2300 árum, samhliða því að sumur tóku að kólna, og náði jökullinn hámarksútbreiðslu á litlu ísöldinni (fyrir 0,7-0,1 þúsund árum) þegar hitastig sumars er talið hafa verið ~1 °C undir meðalhita síðustu áratuga. Ástæður kaldra frávika á þessu tímabili eru tengdar minni sólarvirkni, aukinni eldvirkni (bæði sprengigosa og hraungosa) og innri breytileika veðurkerfa þar sem kólnun var viðhaldið af svörun hafs og hafíss.

Hitastigs- og rakanæma lífmerkið GDGT var að auki rannsakað í tveimur öðrum umhverfum; í jarðvegssniði frá Nútíma á hálendi Íslands, og í sjávarsetkjarna sem tekinn var af landgrunninu fyrir norðan Ísland. Fyrir sjávarsetskjarnann var að auki þróaður íslenskur GDGT-hitastigskvarði, sem byggir á yfirborðssýnum teknum af sjávarbotninum og sýna niðurstöður möguleika á að ná fram minni óvissu (±0,4 °C) með slíkri staðbundinni kvörðun samanborið við hnattræna kvörðun (±4,0 °C). Staðbundin kvörðun er sérstaklega mikilvæg fyrir svæði eins og Ísland, þar sem hitastigstengsl GDGT víkur frá heildar línulegri fylgni hnattrænna kvarða (þ.e. köld og heit svæði). Þó kólnun á litlu ísöldinni endurspeglist greinilega í hámarksstærð Drangajökuls og eðlisrænum veðurvísum, kemur kólnun Litlu ísaldarinnar ekki skýrt fram í hitastigsnæma lífmerkinu (GDGT) í þeim þremur umhverfum sem hér eru til umfjöllunar (vatnaseti, jarðvegi og sjávarseti). Í fyrstu tveim tilfellunum, (þ.e. vatnaseti og jarðvegssniði), er líklegasta ástæðan rof á eldri jarðvegi frá hlýrri tíma (þ.e eldri jarðvegur hefur fokið yfir yngri jarðveg og í stöðuvatnið á hámarki litlu ísaldar), næringarefni og GDGT hafa blandast yngra efni að einhverju leyti og gefa því til kynna hlýrra hitastig en var í raun á litlu ísöldinni. Í sjávarsetinu benda lífmerkin til þess að þykkur og samfelldur hafís hafi myndast á hámarki litlu ísaldarinnar og náð að einangra sjó undir yfirborðinu og þannig komið í veg fyrir hitastreymi frá undirlögum sjávar til

andrúmsloftsins. Þessi ritgerð bætir við nýjum og ítarlegum niðurstöðum sem eru mikilvægar fyrir gerð líkana sem miða að því að spá fyrir um þróun loftslags og hugsanlegar breytingar á næstu öldum.

To Mom

Table of Contents

List of Figures

List of Tables

Acknowledgements

First and foremost, I extend my most sincere gratitude to my advisors and mentors, Áslaug Geirsdóttir and Giff Miller, for providing me the opportunity to experience two incredible worlds, the freedom to take this dissertation's framework in a multitude of directions, and the collaborations and support to make it all happen. Second, were it not for my undergraduate advisor Bev Johnson's mentorship, guidance and ultimate connection to my current advisors, I'd be living out of a van somewhere in the desert or mountains chasing a very different dream. Thank you!

To Thor Thordarson – although nothing is formally written on any paperwork, I recognize your guidance and mentorship as equal to that of Áslaug and Giff and consider you as my third advisor. I am incredibly grateful for our numerous discussions, endless paper revisions, and time shared in the field. Your deep knowledge and interest in the tephra history of Iceland helped me uncover an academic interest in something I never would have expected. Aloha!

To my dissertation committee, Julio Sepúlveda, Tom Marchitto, and Bob Anderson – each of you has profoundly contributed to shaping this dissertation whether that was through inviting me into your lab and classroom, poking holes in my comprehensive exam, or collaborating on projects and papers. You are all part of an outstanding team of educators I have been so fortunate to learn from. Thank you for pushing me to create a dissertation I am incredibly proud of.

To Leif Anderson, John Andrews, Simon Belt, Lorelei Curtin and Billy D'Andrea – your interest and collaboration in my dissertation has brought it in new, exciting and unexpected directions. I am extraordinarily thankful to have had the pleasure of working with you all at some point over the last six years. Each of you has helped teach me the power of collaboration, and the greater amount of knowledge and fun that can be gained from that.

To my undergraduate assistants Eric Gunderson, Muugii Munkhbold, Wyatt Hansen – thank you for reaching out to me and allowing me to help you discover your own academic interests and career goals. I am grateful for your dedication and diligence to my lab work that allowed us to explore ever deeper questions, as well as for allowing me to learn as an advisor in terms of what and, and more importantly, what not to do.

To my friends and fellow graduate students on both sides of the Atlantic (Iceland and Colorado) – I am forever indebted to your company on our numerous mountain adventures and shenanigans and long hours in the office and lab. There are too many names to list here, so I hope you know who your are. In some way, shape or experience, you have all helped teach me the full meaning of *þetta reddast*, it will all work out okay. I love you all.

To my Family – words cannot not express my immense gratitude for your endless love, support and encouragement throughout the last six years. I know the distance has not been easy for any of us, so I appreciate your acceptance to let me roam free, pursue this chapter of my life, and become who I am. Mom, although it hurts more than anything that you cannot

be here to see me cross the finish line, I know you'd be incredibly proud. Thank you for teaching me the necessity of reading and writing outside the classroom, and for supporting me as I wandered by sinuous (and at times undesired) path towards college and graduate school. You always allowed us to make our own decisions and learn from them. I am beyond excited to have chosen this one. This dissertation is for you.

This dissertation has been graciously funded through the Icelandic Center of Research (RANNÍS): Grant #130775051, Grant-of-Excellence #141573052, and Doctoral Student Grant #163431051. Additional support has been provided through the University of Iceland Research Fund, University of Colorado Department of Geological Sciences, Beverly Sears Graduate Student Grants, and Columbia University's Chevron Student Initiative Fund.

1 Introduction

1.1 Introduction

The Arctic region is currently undergoing rapid climate changes – manifested in modern instrumental records of changing ocean circulation (Rahmstorf et al., 2015), reduced sea ice extent (Stroeve et al., 2007), glacier retreat (Gardner et al., 2013), hydrological change (Rawlins et al., 2010) and northward expansion of shrubs (Sweet et al., 2015). Amplification of global warming trends adversely affects the high latitudes (Miller et al., 2010), in response to strong positive feedbacks in both summer and winter (Serreze and Barry, 2011). However, the brevity of instrumental records makes it difficult to place these changes into the context of longer term climate variability. Developing high-resolution records of past changes in regional climate will help constrain climate models and improve our understanding of the global climate system (e.g., Braconnot et al., 2012), both of which are necessary for informed policy making.

Here the focus is Iceland, a North Atlantic landmass located within the periphery of the strongest projected warming (Fig. 1.1, IPCC AR5, 2013). As the North Atlantic is the region that exhibits the largest meridional heat flux in the Northern Hemisphere (Wunsch, 1990), and the area of deep-water formation that drives the Atlantic Meridional Overturning Circulation (Fig. 1.2), changes in local Icelandic climate have hemispheric relevance (Denton and Broecker, 2008; Buckley and Marshall, 2016). In this dissertation, I take advantage of Iceland's ideal geographic position, straddled by opposing Atlantic and Arctic ocean currents and proximal to the instrument sea ice edge (Fig. 1.2), to refine its glacier, climate and volcanic history during the Holocene. These datasets are available to constrain the forcings behind natural Holocene climate variability of the North Atlantic and improve models that strive to forecast our poorly-constrained future.

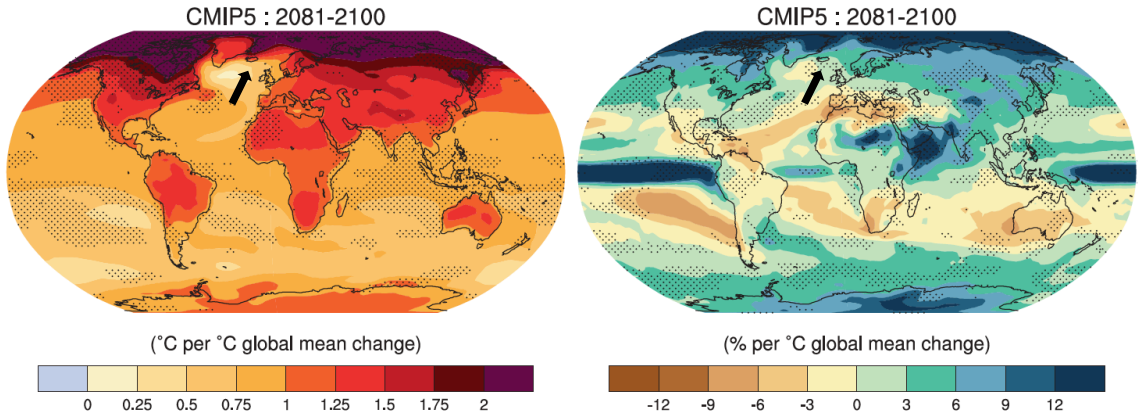

Figure 1.1. *Projected °C (left) and percent (right) temperature increases relative to global mean change per the Coupled Model Intercomparison Project 5 (CMIP5). Iceland's location along the periphery of strongest projected warming marked with a black arrow.*

1.2 Background on Iceland

Iceland is a small, isolated island located within the northern North Atlantic at the intersection of warm, saline Atlantic currents and cool, sea-ice bearing Arctic currents (Fig. 1.2). Due to its position astride the mid-Atlantic ridge, Iceland is volcanic in origin with the oldest subaerial sectors dating back to 15 Ma (northwest) and 12.5 Ma (east) and younging to Holocene age along the axial rift in central Iceland (Moorbath et al., 1968; Harðarson et al., 1997; Sinton et al., 2005; Jóhannesson, 2014). As a result, the bedrock is primarily composed of subaerial lava successions and subglacial hyaloclastites that are easily erodible and contribute to the relatively high sedimentation rates in lakes (Larsen et al., 2012; Geirsdóttir et al., 2013), and sandy soil accumulation in central and southern Iceland (Gísladóttir et al., 2005; Jackson et al., 2005; Arnalds, 2010). Repetitive Quaternary glaciations in Iceland (Geirsdóttir and Eiríksson, 1994; Geirsdóttir, 2004; Geirsdóttir et al., 2007) have sculpted a high density of bedrock-controlled, over-steepened lake basins (e.g., Principato and Johnson, 2009), which have been continuously accumulating sediment since regional deglaciation in the early Holocene (Larsen et al., 2012; Geirsdóttir et al., 2013; Harning et al., 2016b).

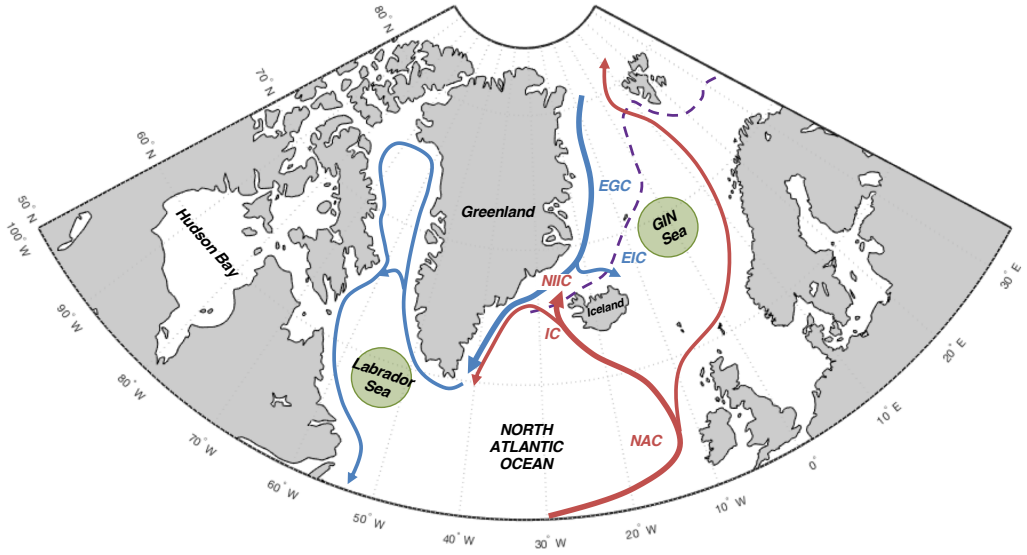

Figure 1.2. *Northern North Atlantic region, including simplified ocean surface currents and 1870-1920 CE sea ice edge position (dashed purple line, Divine and Dick, 2007). Green circles mark local regions of deep water formation in the Labrador and GIN (Greenland, Iceland, and Norway) Seas. Warm Atlantic currents are marked in red: NAC = North Atlantic Current, IC = Irminger Current, NIIC = North Iceland Irminger Current. Cold Arctic currents are marked in blue: EGC = East Greenland Current, EIC = East Iceland Current.*

The active and relic volcanic systems that speckle the Icelandic landscape represent a key variable that has shaped Iceland's regional environment in the past. The frequent production of thick tephra layers from these volcanos (Larsen and Eiríksson, 2008; Thordarson and Höskuldsson, 2008) periodically strips the landscape of vegetation and triggers intensified soil erosion (Arnalds, 2004; Geirsdóttir et al., 2009b; Larsen et al., 2011; Blair et al., 2015; Eddudóttir et al., 2017). If large enough, the impact of Icelandic volcanic emissions (e.g., sulfate) on local radiative balance as well as atmospheric properties and circulation can be significant (Guðlaugsdóttir et al., 2018), such as observed for the 1783-1784 CE Laki (Thordarson et al., 1996) and 934 CE Eldgjá eruptions (Thordarson et al., 2001), among

other Icelandic basaltic fissure eruptions (Thordarson et al., 2003). Emissions from even larger eruptions from equatorial volcanos can have greater geographical impact over the northern hemisphere, resulting in atmospheric cooling and cryosphere expansion feedbacks that maintain and amplify such cooling in the northern North Atlantic region (Miller et al., 2012; Slawinska and Robock, 2018).

In addition to the volcanic complexes, glaciers and ice caps also dominate Iceland's landscape (11% area, Björnsson and Pálsson, 2008). The geographic distribution of glaciers in Iceland is dictated by a combination of orography and precipitation receipts (Crochet et al., 2007; Björnsson and Pálsson, 2008), which translates to their presence where the equilibrium line altitude (ELA) intersects the underlying topography. As a result, most glaciers occupy high-elevation central volcanos in the southern and central highlands. Icelandic ice caps are primarily classified as warm-based, although some sectors of Drangajökull in northwest Iceland also exhibit cold-based characteristics (Harning et al., 2016, 2018), and all feature surge-type outlet glaciers (Ingólfsson et al., 2016). Although the mass balance of Icelandic ice caps is primarily driven by summer temperature (Björnsson and Pálsson, 2008), surging can complicate the extraction of paleoclimate information (Striberger et al., 2011; Brynjólfsson et al., 2015; Larsen et al., 2015), particularly if they are used to infer past climate variability over centennial timescales (e.g., Larsen et al., 2011). In a modern context, current global warming has resulted in Icelandic glaciers losing an average of 11 billion tons of ice a year since the mid-1990s (Björnsson et al., 2013; Compton et al., 2015), which when melted to completion will raise global sea levels by 1 cm (3600 km^3 ice, Björnsson and Pálsson, 2008).

A third, albeit anthropogenic, component of Iceland relevant to this dissertation is the long history of instrumental and historical weather/climate datasets. Since the arrival of Norse settlers around 870 CE, documentary records of past weather and climate conditions (Finnsson, 1796; Thoroddsen, 1916; Koch, 1945; Bergthórsson, 1969; Ogilvie and Jónsson, 2001) and volcanism (Thordarson and Larsen, 2007, and references therein) have been diligently maintained. In 1845 CE, the first weather station was erected in Stykkishólmur, west Iceland, which has been in continual operation ever since. The high correlation between instrumental sea surface temperature (Ólafsson, 1999; Hanna et al., 2006) and coastal temperature records such as those from Stykkishólmur have demonstrated the strong influence that the marine realm exerts on Iceland's terrestrial climate. Collectively, these rich documentary and instrumental archives provide valuable information to cross-validate climate proxies, such as qualitative temperatures from lake sediment cores (Geirsdóttir et al., 2009) and lipid biomarkers for sea ice off the north coast of Iceland (Massé et al., 2008).

1.3 Motivating Questions

This dissertation contributes to several outstanding questions, each of which are key to understanding Icelandic paleoclimate during the Holocene, and by extension the northern North Atlantic region. These questions span a range of disciplines from refining the glacier history of Iceland (glacial geology) to quantifying summer temperatures (organic geochemistry). Furthermore, this dissertation capitalizes on and merges a range of analytical techniques yet to be done before. Some are traditional, well-established tools, such as bulk physical and geochemical proxies and major oxide compositions of tephra in lake sediment, whereas others are rapidly emerging, such as the application of lipid biomarker distributions preserved in geologic archives to quantify temperatures in terrestrial and marine environments. Continued work through the acquisition of new records and improved

analytical methodologies will undoubtedly benefit this dissertation and the outstanding questions it targets. Hence, the questions below (and answers found in the following chapters) represent just a thin veneer of information that contributes the vast and continually growing body of knowledge centered around Iceland's Holocene paleoclimate history:

1) What was the Holocene history of Drangajökull, in northwest Iceland? Did it survive early Holocene warmth, or did it behave similarly to other Icelandic ice caps that melted to smaller than present dimensions before 9 ka? If the latter, when did it nucleate during the middle to late Holocene Neoglaciation, and how does this compare to other Icelandic ice cap reconstructions?
2) What was the Holocene climate history of the Vestfirðir peninsula, northwest Iceland? Was it non-linear as seen elsewhere in Iceland? And if so, can those punctuations be linked to known climate drivers and feedback amplifiers?
3) How has local and hemispheric volcanism impacted Icelandic paleoclimate?
4) Can we quantify the Holocene temperature history of Iceland with emerging organic geochemical toolsets to gain an appreciation for the glacier and climate sensitivity in Iceland during the Holocene?

This dissertation originally focused on reconstructing the Holocene glacier and climate evolution of the Vestfirðir peninsula. However, unforeseen obstacles and realizations has spurred it into several new directions. The first of which was age control and synchronization between paleoclimate records, which in Iceland has long presented itself as a central research challenge (e.g., Sveinbjörnsdóttir et al., 1998; Geirsdóttir et al., 2009). Paleomagnetic secular variation (PSV) synchronization has been used in other high-sedimentation rate Icelandic lakes (Ólafsdóttir et al., 2013), however, the sediment accumulation rates in the northwestern lakes proved to be too low to meaningfully extract PSV information (S. Ólafsdóttir, 2016, pers. comm.). Thus, I was motivated to rely on tephrochronology as one of the primary age control and correlation tools in this dissertation, which introduced new questions regarding the volcanic history of Iceland, Holocene tephra frequency and the potential influence from climate and glacier variability. Second to age control was the realization that the marine realm is one of the primary modulators of Iceland's terrestrial climate. My exploration into the existing paleoceanographic records revealed wide variability and remarkable inconsistency in the Holocene trends and temperatures estimates between proxy datasets. Although much of this variability may be related to the season and water depth that the biota occupies, improving our understanding of Icelandic paleoceanography developed as a secondary research motivation.

1.4 Research Methods and Goals

This dissertation primarily relies on lake sediment as sentinels of past climate change (e.g., Adrian et al., 2009), which continuously filter the regional climate through a wide range of physical, chemical and biological variables. Ultimately, the filtered climate signal is archived in proxies preserved in the sediment accumulation at the base of the lake, which can be used to reconstruct the regional paleoclimate of the lake and its catchment. To provide age constraint on these records, I use commonly employed Quaternary geochronometers, such as radiocarbon-dating of plant macrofossils (Libby et al., 1946; Reimer et al., 2013), tephrochronology (Thorarinsson, 1944; Lowe et al., 2011), and PSV synchronization to other well-dated archives (Stoner et al., 2007; Ólafsdóttir et al., 2013). Ice cap reconstructions

capitalize on methods developed elsewhere in the Arctic, such as the dating of threshold lake sediment records (Svendsen et al., 1987; Briner et al., 2010) and dead vegetation emerging from retreating ice margins (Anderson et al., 2008; Margreth et al., 2014; Miller et al., 2013, 2017; Pendleton et al., 2017, 2019; Schweinsberg et al., 2017, 2018), the latter of which had never been used in Iceland until now. High-resolution qualitative climate reconstructions are developed from well-established bulk proxies archived in lake (total organic carbon - TOC, $\delta^{13}C$, C/N, biogenic silica – BSi, Meyers, 2003) and marine sediment records (IP_{25}, calcite wt%, quartz wt%, Andrews et al.., 2001; Andrews, 2009; Belt, 2018). Finally, quantitative temperature proxies from terrestrial and marine sediment are derived from a novel variety of lipid biomarkers, such as branched and isoprenoid glycerol dialkyl glycerol tetraethers and alkenones (Castañeda and Schouten, 2011; Schouten et al., 2013). Detailed descriptions on the background of these proxies and their interpretation for this dissertation are provided where relevant in the chapters that follow.

The goals of this thesis are two-prong:

1) Evaluate and reconstruct climate and glacier history from new lake sediment archives to confirm the non-linear Holocene climate evolution of Iceland reflected in existing lake sediment climate records.
2) Apply emerging quantitative geochemical proxies to reliably quantify the Holocene temperature evolution in and around Iceland.

1.5 Dissertation Overview

The introduction presented here provides a brief overview of how this dissertation contributes to the highly relevant and broad area of paleoclimate research, some outstanding questions regarding the Holocene paleoclimate of Iceland, and the techniques employed to, at least partially, answer those questions. The following chapters are presented in manuscript form and organized in terms of topic, which generally follows the evolution of my doctoral research. Chapters 2 and 3 present a multidisciplinary approach to reconstructing the glacial evolution of Drangajökull during the Holocene. Chapter 4 develops a high-resolution qualitative climate reconstruction for the eastern Vestfirðir peninsula using two lake sediment records – one from a high-elevation, pro-glacial lake and the other from a low-elevation, non-glacial lake. Chapters 5 and 6 present tephrochronological frameworks for the Vestfirðir peninsula and west Iceland, respectively, which not only have implications for improved age control in Icelandic sedimentary records, but also for the synchronization between more distal paleoclimate datasets, and for Iceland's Holocene volcanic history. Chapter 7 aims to provide more reliable and continuous quantitative estimates of Holocene temperature than currently exist via the application of algal and bacterial lipid biomarker paleothermometers in Icelandic lake sediment and soils. Finally, Chapter 8 exits the terrestrial realm and ventures to the North Icelandic Shelf, where we employ archaeal lipid biomarkers to quantify winter subsurface ocean temperatures over the last millennium. I end with some concluding remarks that tie each of these chapters together and offer some suggestions for future work that would continue this research in beneficial and fruitful directions.

The records obtained and datasets generated under this dissertation have contributed to a wide variety of additional work. Alongside the alkenone and brGDGT temperature records developed from lake sediment, Lamont-Doherty Earth Observatory collaborators L.

Curtin and W.J. D'Andrea have constructed a Holocene δD record from plant wax alkanoic acids and are currently using 18S rRNA sequencing to understand the evolution of alkenone-producing haptophyte species during the Holocene. Unpublished datasets from this work will result in at least 2 co-authored peer-reviewed publications. Additionally, three published manuscripts and two theses, one Bachelor of Science and the other Master of Science, have had contributions from this dissertation's research. References to these publications are listed below:

Egilsson, K., 2015. Umhverfi Skorarvatns vestan Drangajökuls á nútíma: Rannsókn á veðurvísum úr setkjarna SKR14-5A-1N-01. B.S. thesis, University of Iceland, Reykjavík.

Anderson, L.S., Flowers, G.E., Jarosch, A.H., Aðalgeirsdóttir, G.Th., Geirsdóttir, Á., Miller, G.H., **Harning, D.J**., Þorsteinsson, Þ., Magnússon, E., Pálsson, F., 2018. Holocene glacier and climate variations in Vestfirðir, Iceland, from the modeling of Drangajökull ice cap. Quaternary Science Reviews 190, 39-56.

Gunnarsdóttir, S., 2018. Holocene environmental changes in the central highlands of Iceland as recorded in soils. M.S. thesis, University of Iceland, Reykjavík.

Harning, D.J., Geirsdóttir, Á., Thordarson, T., Miller, G.H., 2018. Climatic control on Icelandic volcanic activity during the mid-Holocene: COMMENT. Geology 46, e443.

Geirsdóttir, Á., Miller, G.H., Andrews, J.T., **Harning, D.J.**, Anderson, L.S., Larsen, D.J., Florian, C., Thordarson, T., 2019. The onset of Neoglaciation in Iceland and the 4.2 ka event. Climate of the Past Discussions 15, 25-40.

2 Early Holocene Deglaciation of Drangajökull, Vestfirðir, Iceland[1]

2.1 Abstract

The status of Icelandic ice caps during the early Holocene provides important constraints on North Atlantic climate and the mechanisms behind natural climate variability. A recent study postulates that Drangajökull on Vestfirðir, Iceland, persisted through the Holocene Thermal Maximum (HTM, 7.9-5.5 ka) and may be a relic from the last glacial period. We test this hypothesis with a suite of sediment cores from threshold lakes both proximal and distal to the ice cap's modern margin. Distal lakes document rapid early Holocene deglaciation from the coast and across the highlands south of the glacier. Sediment from Skorarvatn, a lake to the north of Drangajökull, shows that the northern margin of the ice cap reached a size comparable to its contemporary limit by ~10.3 ka. Two southeastern lakes with catchments extending well beneath modern Drangajökull confirm that by ~9.2 ka, the ice cap was reduced to ~20% of its current area. A continuous 10.3 ka record of biological productivity from Skorarvatn's sediment indicates local peak warmth occurred between 9 and 6.9 ka. The combination of warm and dry summers on Vestfirðir suggests that Drangajökull very likely melted completely shortly after 9.2 ka, similar to most other Icelandic ice caps.

2.2 Introduction

Constraining the early Holocene deglaciation of Icelandic ice caps provides valuable information about North Atlantic climate and the mechanisms behind natural climate variability. Lake sediment records and numerical modeling experiments have shown that most Icelandic glaciers were receding rapidly before 10.3 ka and likely melted completely or were reduced to small local residuals by the early-mid Holocene (Flowers et al., 2008; Geirsdóttir et al., 2009a; Larsen et al., 2012; Striberger, 2012). In contrast, Schomacker et al. (2016) employed basal dates from a network of lake sediment cores to conclude that Drangajökull in Vestfirðir, Iceland, probably survived the entire Holocene, in response to increased humidity during the HTM. If correct, this provides an important inference about precipitation gradients across Iceland during the Holocene and a vital parameter to be included in future numerical glacier models.

To test this hypothesis, we use a suite of threshold lake sediment cores both proximal and distal to Drangajökull's contemporary margin to more accurately constrain the ice cap's early Holocene deglaciation and to test the plausibility that the ice cap persisted through the Holocene. As supporting evidence, we provide a continuous lacustrine-based biogenic silica record to derive inferences about local Holocene summer temperature change. Collectively, these new data demonstrate that contrary to the conclusions of Schomacker et al. (2016)

[1] Harning, D.J., Geirsdóttir, Á., Miller, G.H., Zalzal, K., 2016. Early Holocene deglaciation of Drangajokull, Vestfirðir, Iceland. Quaternary Science Reviews 153, 192-198.

Drangajökull was already reduced to ~20% of its current area by 9.2 ka and very likely disappeared shortly thereafter.

2.3 Regional Setting

2.3.1 Vestfirðir Peninsula and Local Climate

Vestfirðir comprises Iceland's northwesternmost extension into the North Atlantic Ocean where the warm and saline Irminger Current (IC) flows along the west coast and the cooler, lower-salinity North Iceland Irminger Current (NIIC) and East Icelandic Current (EIC) dominate to the north and east (Fig. 2.1a). A multitude of over-deepened lake basins remnant from prior glaciations surround the region's local ice cap, Drangajökull (~142 km^2 area in 2011; Jóhannesson et al., 2013). Drangajökull's modern (2000-2015 CE) glacier-wide equilibrium line altitude (ELA, ~660 m asl; Harning et al., 2016) is considerably lower than other Icelandic ice caps such as Langjökull (~1080 m asl) and Vatnajökull (~1215 m asl) (Björnsson and Pálsson, 2008). This low ELA likely reflects the ice cap's proximity to the relatively low sea surface temperatures (SST) of the adjacent ocean resulting in relatively short, cool summers. A correlation between JJA SSTs and JJA air temperature over Drangajökull between 1950 and 2000 CE imply oceanic SSTs on the North Iceland Shelf impart the greatest influence on Vestfirðir summer temperatures (Harning et al., 2016). Mean annual precipitation (1961-1990 CE) over Drangajökull (~3000 mm) is considerably less than precipitation receipts for ice caps along the south coast of Iceland (e.g., 7000 mm over Vatnajökull) (Crochet et al., 2007; Björnsson and Pálsson, 2008). Drangajökull's low ELA and periods of positive or near-zero net mass balance between 1946 and 2011 CE (Magnússon et al., 2016) have led to speculation that the ice cap has behaved differently than other Icelandic ice caps during the Holocene.

2.4 Methods

2.4.1 Lake Sediment Cores

Seven lakes (elev. 42-463 m asl) were targeted for sediment cores to maximize the spatio-temporal constraint of the Icelandic Ice Sheet (IIS, henceforth referred to as proto-Drangajökull) during deglaciation of northeastern Vestfirðir (Table 2.1, Fig. 2.1b). Each lake serves as a threshold, documenting when proto-Drangajökull left the lake catchment and ice-erosional products ceased to dominate the sediment input (e.g., Briner et al., 2010). During field campaigns in 2010, 2012, 2014 and 2015, sediment cores were recovered using a percussion driven piston corer from each lake's deepest basin. The cores were subsequently split and lithology described. Magnetic susceptibility (MS), a proxy for the proportion of clastic sediment (e.g., Larsen et al., 2011, 2012), was measured at 0.5 cm intervals on each split core using a GeoTek Multi-Sensor Core Logger at the University of Iceland (UoI).

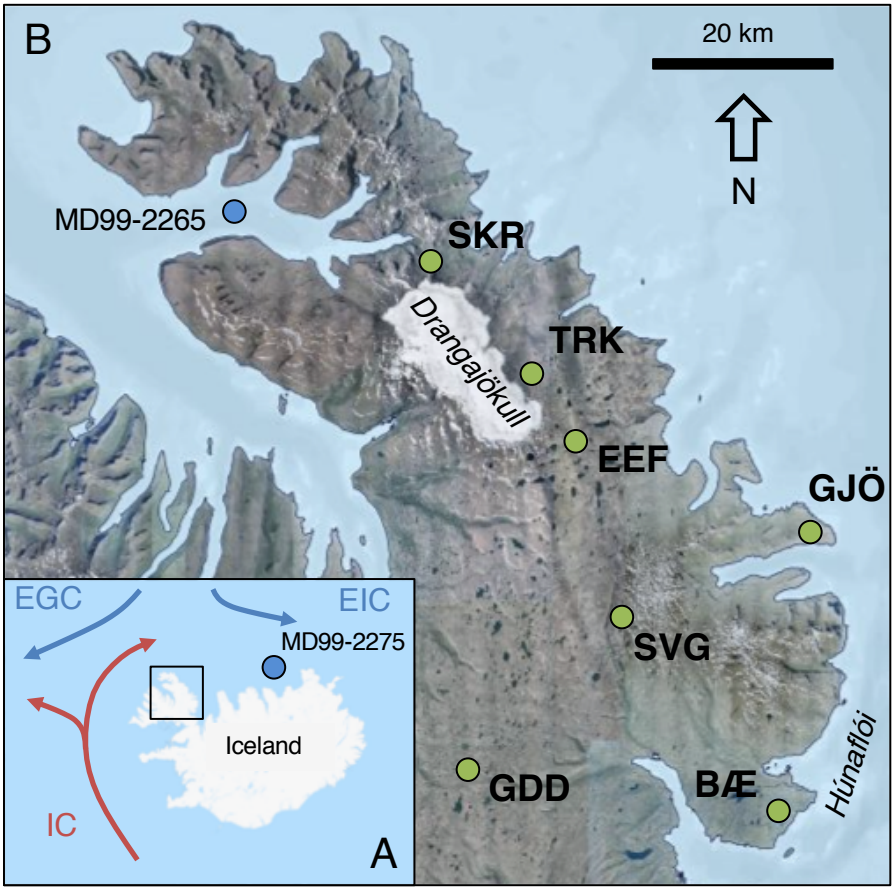

Figure 2.1. *A) Modern ocean currents around Iceland. Black box marks the location of B) Eastern Vestfirðir and this study's lakes (green circles). Blue circles mark locations of marine sediment cores referred to in the text. 2005 base image courtesy of Loftmyndir ehf.*

Table 2.1. *Lake Information.*

Lake	Core name	Sediment core coordinates	Elevation (m asl)	Saksunarvatn?	Sampler
Skorarvatn (SKR)	SKR14-6A/4A-1N	66° 15.376'N 22° 19.328'W	183	YES	D. Harning
Tröllkonuvatn (TRK)	TRK14-3A-2B	66° 8.551'N 22° 3.364'W	336	no	D. Harning
Efra-Eyvindarfjarðarvatn (EEF)	EEF14-3A	66° 4.668'N 21° 57.187'W	408	no	D. Harning
Svartárgilsvatn (SVG)	SVG10-1B-1N	65° 54.508'N 21° 49.318'W	430	YES	K. Zalzal
Bæjarvötn (BÆ)	BAE10-2B-1N	65° 43.266'N 21° 26.172'W	140	YES	K. Zalzal
Gedduvatn (GDD)	GDD10-1A-1B	65° 45.287'N 22° 10.810'W	409	YES	K. Zalzal
Gjögurvatn (GJÖ)	GJÖ15-2A-2B	65° 99.744'N 21° 36.289'W	42	YES	S. Gunnarson

2.4.2 Biogenic Silica, A Relative Summer Temperature Proxy in Skorarvatn Sediment

Skorarvatn (25 m deep) is a lake 3 km north of Drangajökull (Fig. 2.1b). Sediment subsamples (n=154) were taken at ~1.5 cm intervals from sediment core SKR14-6A, freeze-dried, then ground and homogenized at the UoI. Biogenic silica (BSi) was measured following the procedures of Florian (2016) via Fourier Transform Infrared Spectroscopy (FTIRS) at the University of Colorado Boulder (UCB). Since published calibrations are linear and do not influence the nature of the proxy curve, we report measured BSi values in FTIR absorbance units rather than %BSi.

2.4.3 Geochronology: Tephrochronology and Radiocarbon

Primary tephras located by visual inspection in lake sediment cores were extracted and sieved to isolate glass fragments between 150 and 250 μm, and then embedded in epoxy plugs. Elemental analysis of samples was performed on a JEOL JXA-8230 election microprobe at the UoI along with the international A99 standard to monitor instrumental drift. Tephra sources were identified via geochemical comparisons to diagnostic geochemical signatures of known-age Icelandic tephra (see Supplemental Information, Tables S2.1 and S2.2).

Fragments of plant macrofossils picked from sediment cores were gently rinsed with deionized water to remove sediment, and then freeze-dried at the UoI. Samples were given an acid-base-acid pretreatment and graphitized at UCB, then measured by AMS at the University of California-Irvine. Ages were calibrated using OxCal 6.0 and IntCal13 (Bronk Ramsey, 2009; Reimer et al., 2013) and are reported in calibrated years BP (Table 2.2).

An age-depth model was generated for Skorarvatn using all tephra and radiocarbon dates in the CLAM 2.2 package (Blaauw, 2010; Fig. 2.2). A smooth spline regression was applied with 1000 iterations resulting in a low goodness-of-fit value of 5.39 and a very low level of uncertainty for the early Holocene.

Table 2.2. *Radiocarbon information*.

Lake (sediment depth cm)	Lab ID	Material	^{14}C date ± σ	Cal age BP ± σ	Sampler
Skorarvatn (43)	CURL-21039	moss	3970 ± 20	4460 ± 50	D. Harning
Skorarvatn (59)	CURL-21034	moss	4760 ± 20	5530 ± 50	D. Harning
Skorarvatn (82)	CURL-21035	moss	5355 ± 20	6120 ± 90	D. Harning
Skorarvatn (140.5)	CURL-21036	moss	7205 ± 25	8000 ± 20	D. Harning
Skorarvatn (214.8)	CURL-19489	moss	8295 ± 25	9340 ± 60	D. Harning
Skorarvatn (222.5)	CURL-21041	moss	8905 ± 35	10060 ± 120	D. Harning
Skorarvatn (283.5)	CURL-21033	moss	9145 ± 35	10300 ± 70	D. Harning
Tröllkonuvatn (394)	CURL-19502	moss	7925 ± 25	8750 ± 100	D. Harning
Efra-Eyvindarfjarðarvatn (248)	CURL-19499	moss	8260 ± 30	9220 ± 80	D. Harning
Svartárgilsvatn (355.5)	CURL-12025	aquatic moss	3820 ± 15	4200 ± 40	K. Zalzal
Gedduvatn (417.8)	CURL-12031	aquatic moss	7945 ± 25	8820 ± 160	K. Zalzal

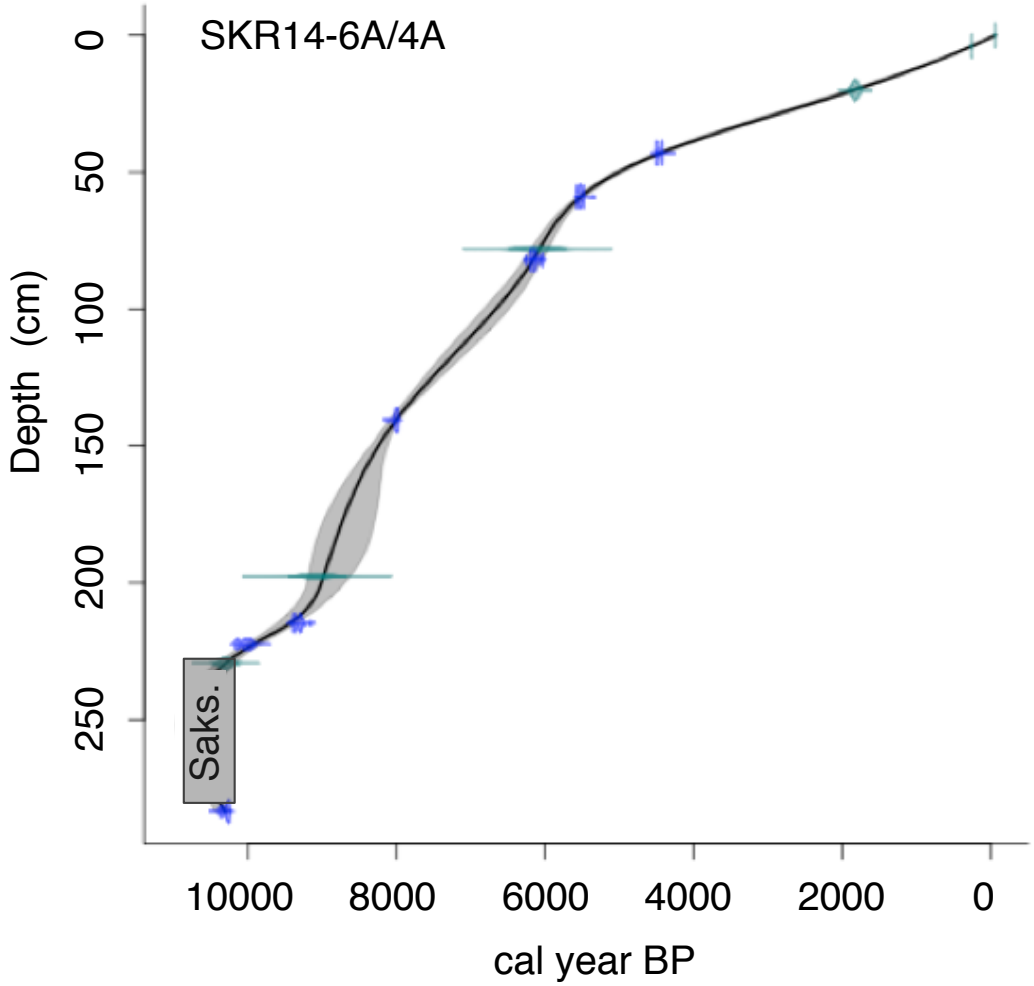

Figure 2.2. *Skorarvatn's smooth-spline regression age-depth model produced in CLAM version 2.2 (Blaauw, 2010). Gray shaded areas represent 95% confidence limit. Saksunarvatn tephra units and interbedded deglacial units represented by grey 'Saks.' box.*

2.5 Results and Interpretations

2.5.1 Lake Sediment Properties

All seven lake sediment cores record the transition between basal glaciolacustrine and overlying non-glacial sediment (Fig. 2.3). Glaciolacustrine units are blue-gray well-sorted silts and clays with high MS. Non-glacial units consist of olive-brown gyttja (low MS) with varying amounts of plant macrofossils and primary tephra horizons, which only began accumulating in the lakes following recession of proto-Drangajökull from their catchments. Minimum ages of deglaciation come from ^{14}C dates of basal plant macrofossils or identified tephras, such as Saksunarvatn (10.30 ± 0.09 ka, Rasmussen et al., 2006), close to or at the boundary of glaciolacustrine sediment packages.

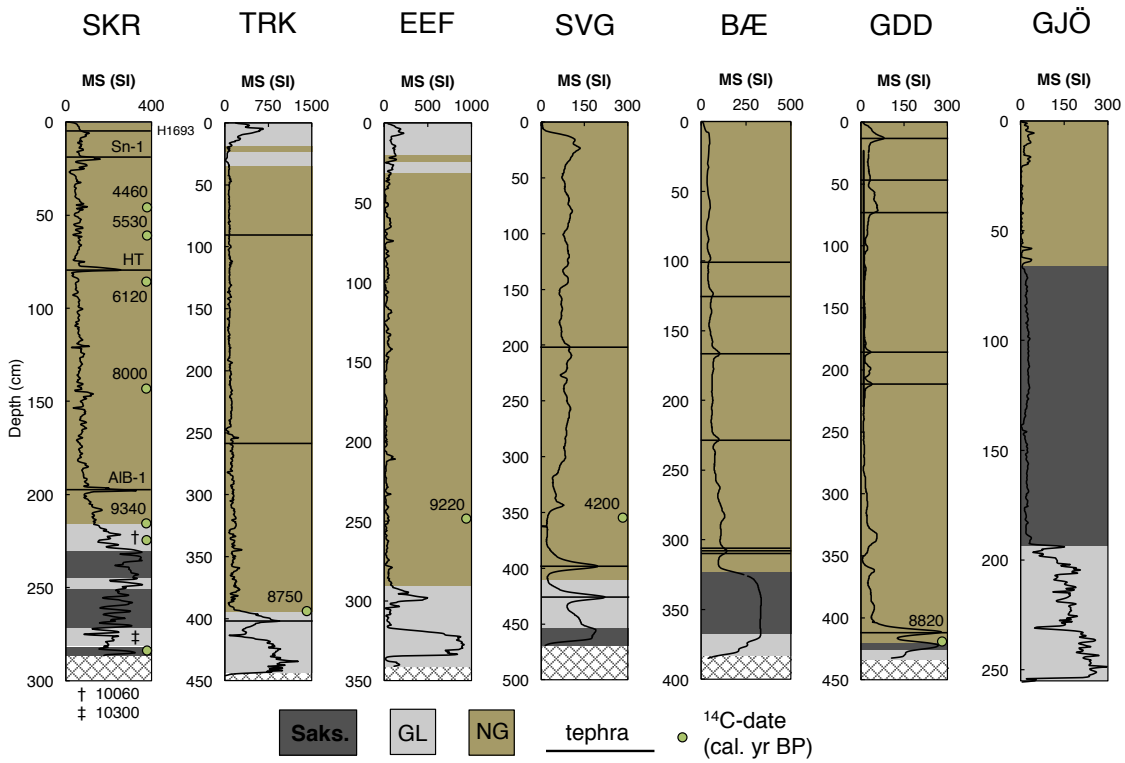

Figure 2.3. *Sediment lithologies and MS against depth (cm). Saks. = Saksunarvatn tephra, GL = glaciolacustrine sediment and NG = non-glacial sediment. Hatched boxes indicate end of sediment cores.*

Skorarvatn (SKR; 183 m asl, 66.25627°N, 22.32213°W) sits ~3 km north and outside the drainage of Drangajökull. SKR´s catchment terminates ~1 km closer to Drangajökull at 420 m asl, the threshold for receiving glacial sediment. A Holocene age model is based upon five primary tephras; H1693, Sn-1, Hekla T (Harning et al., 2016), and AlB-1 and Saksunarvatn (Tables S2.1 and S2.2), in addition to seven ^{14}C dates (Table 2.2). The basal moss fragment is dated to 10,300 ± 70 cal BP (CURL-21033) providing a minimum constraint on local deglaciation.

The rapid decrease in MS and rise in BSi defines the transition from a glacier-dominated to non-glacial catchment at 9.3 ka (Figs. 2.3 and 2.4b). The lack of subsequent non-tephra related high MS values indicates the glacier did not re-enter the catchment during the remainder of the Holocene. Maximum BSi values are reached between 9-8.4 ka and 7.9-6.9 ka with a significant reduction between 8.4-7.9 ka. The remainder of the record documents a first-order decrease in BSi towards present. We interpret the relative amount of BSi to track diatom productivity (e.g., Conley and Schelske, 2001). Changes in diatom relative abundance have been shown to be a function of spring/summer temperature in non-glacial Icelandic lakes (Geirsdóttir et al., 2009b) and in lakes from other Arctic regions (McKay et al., 2008).

Tröllkonuvatn (TRK, 336 m asl, 66.14252°N, 22.05607°W) resides ~1 km east of Drangajökull's margin (Fig. 2.1), and currently receives sediment-laden meltwater. TRK's catchment extends 2.5 kilometers underneath the ice cap's contemporary margin to a threshold elevation of ~700 m asl (Harning et al., 2016), based on recent subglacial topographic reconstructions (E. Magnússon, pers. comm.). A basal moss is ^{14}C-dated to 8750

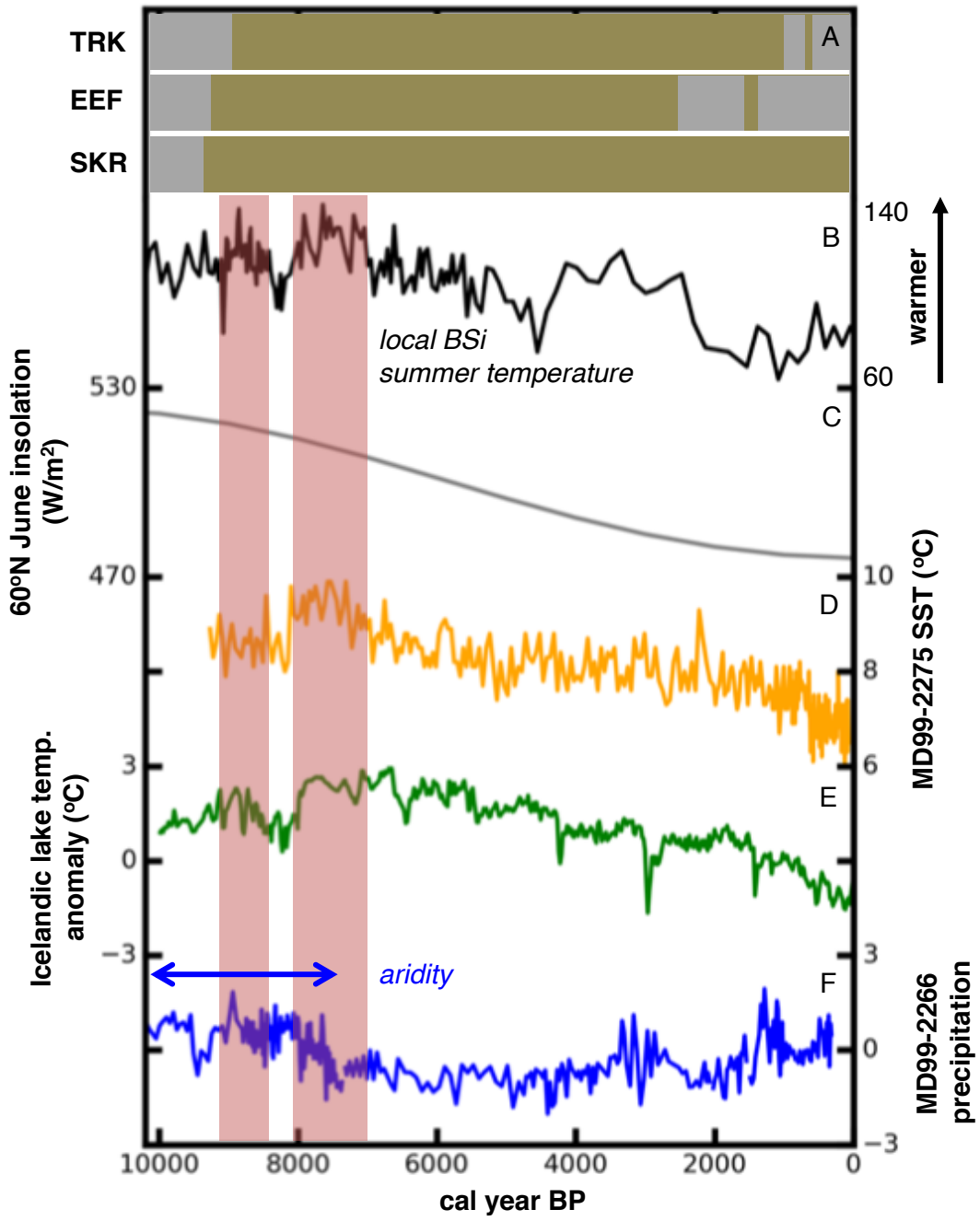

Figure 2.4. *Comparison of A) simplified sediment lithologies from threshold lakes TRK, EEF and SKR on their age models after Fig. 3 and Harning et al. (2016, in press), B) changes in BSi in lake SKR sediment (scaled in FTIR absorbance units), C) Northern Hemisphere summer (June) insolation (W/m2) at 60oN (Berger and Loutre, 1991), D) diatom-inferred SSTs from MD99-2275 (Jiang et al., 2015), E) Icelandic composite lake temperature anomaly record relative to today (Geirsdóttir et al., 2013) and F) normalized (mean/standard deviation) composite of average chain length variability of leaf wax derived n-alkanes (ACL25-35), soil pH and δDC29 illustrating precipitation variability from MD99-2266 (Moossen et al., 2015). Red bars mark peak warmth inferred from BSi in SKR.*

± 100 cal BP (CURL-19502), providing a minimum age on glacier recession from TRK's catchment.

Efra-Eyvindarfjarðarvatn (EEF, 408 m asl, 66° 4.668'N, 21° 57.187'W), ~4 km southeast of Drangajökull (Fig. 2.1) sits in a large catchment, which extends 1 kilometer underneath the ice cap's current limit to an elevation of ~740 m asl (Harning et al., 2016; E. Magnússon, pers. comm.). A moss macrofossil 40 cm above deglacial sediment is ^{14}C-dated to 9220 ± 80 cal BP (CURL-19499), which provides a minimum age on glacier recession from EEF's catchment.

Svartárgilsvatn (SVG, 430 m asl, 65.0778°N, 21.82197°W) sits ~22 km south of Drangajökull (Fig. 2.1). The Saksunarvatn tephra (16 cm thick) defines the base of the core (468-453 cm) and is overlain by glaciolacustrine silts and clays implying proto-Drangajökull was still within its catchment but not over the lake basin following the tephra deposition. An aquatic macrofossil 50 cm above the glaciolacustrine unit has a ^{14}C age of 4200 ± 40 cal BP (CURL-12025), which suggests that the sedimentation rate during the early Holocene was extremely low in SVG.

Bæjarvötn (BÆ, 140 m asl, 65.7211°N, 21.4362°W), ~32 km southeast of Drangajökull, sits ~1.9 km off the coast of Húnaflói (Fig. 2.1). The core contains a thick, 31 cm Saksunarvatn tephra separating non-glacial and glaciolacustrine units at 322 cm depth in the core. The stratigraphic position of Saksunarvatn tephra implies BÆ's catchment was already deglaciated at the time of the tephra's deposition.

Gedduvatn (GDD, 409 m asl, 65.75478°N, 22.18017°W) sits on a high mountain pass ~35 km south of Drangajökull (Fig. 2.1). The Saksunarvatn tephra separates glaciolacustrine and non-glacial sediment packages, and thus, indicates deglaciation of GDD's catchment occured prior to the deposition of the Saksunarvatn tephra.

Gjögurvatn (GJÖ, 42 m asl, 66.6624°N, 21.60482°W), ~49 km southeast of Drangajökull, sits ~0.8 km off the coast of Húnaflói. The core has a 128 cm thick Saksunarvatn tephra, below which lies the glaciolacustrine package demonstrating GJÖ's catchment was deglaciated prior to the Saksunarvatn deposition.

2.6 Discussion

2.6.1 Retreat of Proto-Drangajökull

The deposition of primary Saksunarvatn tephra in lakes SVG, BÆ, GDD, and GJÖ demonstrates that by 10.3 ka, proto-Drangajökull had retreated from the coastal sites along Húnaflói and the highland plateau south-southeast of the extant ice cap (Fig. 5a). Due to the nature of glaciolacustrine sediment overlying SVG's Saksunarvatn tephra, proto-Drangajökull still occupied SVG's catchment and, hence, this location defines a southern limit at 10.3 ka. SKR's Saksunarvatn tephra and the age of basal moss, both dated to ~10.3 ka, suggest that the northern extent of proto-Drangajökull was near the ice cap's contemporary limit at this time.

Our constraint on the ice cap's retreat from SKR's catchment at ~9.3 ka is in close agreement with the basal dates of lake TRK and EEF (~8.7 and 9.2 ka, respectively), implying the northern and southern limits of the ice cap receded in tandem. The catchments of both TRK and EEF rise to a topographic high (700-740 m asl) beneath Drangajökull's contemporary margin, which provides firm evidence that the southern margin melted behind those limits before 9.2 ka (Fig. 5c). A small residual of glacial ice may have also remained

above 700 m asl on the isolated subglacial rise ~3 km northwest of TRK and EEF's subglacial catchment terminations. The larger residual of ice to the north likely reached a lower elevation (~500 m asl), which is near the threshold catchment elevation of SKR (420 m asl). These constraints suggest that at ~9.2 ka there was a N-S elevation gradient for proto-Drangajökull's margin, where the southern margin was higher than the north. At this time the ice cap's area was ~20% smaller relative to 2011 CE (Jóhannesson et al., 2013; Fig. 5c).

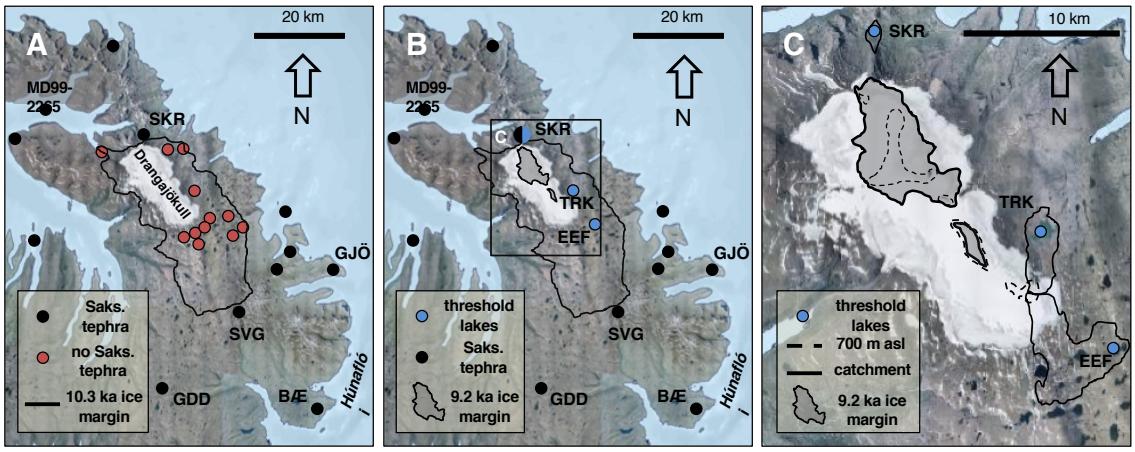

Figure 2.5. *A) Estimated extent of proto-Drangajökull at 10.3 ka. Black circles mark locations of sediment cores or soil sections containing undisturbed Saksunarvatn tephra, as described by Andrews et al. (2002), Geirsdóttir et al., (2002), Principato et al. (2006) and this study. Red circles mark locations of sediments cores containing no Saksunarvatn tephra, as described by Schomacker et al. (2016), Harning et al. (2016) and this study. B) Remnant ice cap margin at 9.2 ka with relevant threshold lakes marked by blue circles. C) Close-up of remnant ice margin shown at 9.2 ka. Subglacial lake catchments and 700 m asl bedrock contour were extracted from a subglacial topographic DEM by (E. Magnússon, pers. comm.). 2005 base image courtesy of Loftmyndir ehf.*

2.6.2 Aquatic Bioactivity Inferred from Skorarvatn

SKR's algal productivity (BSi) suggests peak warmth between 9-8.4 ka and 7.9-6.9 ka (Fig. 4b). The close agreement between our independent qualitative summer temperature record and glacial reconstruction provides supporting evidence that increasing summer air temperatures were a likely driving mechanism behind proto-Drangajökull's early Holocene recession.

2.6.3 Regional Comparisons

In NW Iceland, the cessation of ice-rafted debris in marine sediment cores after 11 ka shows that the waning ice sheet had become mostly grounded (Geirsdóttir et al., 2002). Considering the close correlation between regional SSTs and air temperatures over Drangajökull (Harning et al., 2016), the northward propagation of the warm Irminger Current likely accelerated ice melt as the current became fully established along the western and northern shelves by 10.2 ka (Ólafsdóttir et al., 2010). Changes in North Atlantic Ocean circulation and peak NH summer insolation contributed to elevated sea surface temperatures (SSTs, Castañeda et al., 2004; Jiang et al., 2015; Moossen et al., 2015) and terrestrial air temperatures (Caseldine et al., 2006; Axford et al., 2007; Langdon et al., 2010; Geirsdóttir et al., 2013) around Iceland which peaked between ~7.9 and 5.5 ka (Fig. 4c-e). The resultant

early Holocene warmth was the most likely driving mechanism for the retreat of Langjökull (Geirsdóttir et al., 2009a; Larsen et al., 2012) and Vatnajökull (Striberger et al., 2012) to locations behind their contemporary margins by 10.3 and 9 ka, respectively. Ice cap modeling experiments using simulated temperature increases through the HTM suggest that summer warmth was sufficient to completely melt most Icelandic ice caps prior to the mid-Holocene (e.g., Flowers et al., 2008).

Although widespread evidence exists across Iceland for the early Holocene recession of the Icelandic ice caps, Schomacker et al. (2016) postulate that Drangajökull retreated slowly and remained intact through the HTM as a result of elevated precipitation. However, three independent biomarker proxies from marine sediment core MD99-2266 just 40 km west of the ice cap record persistent aridity during the early Holocene (Fig. 4f; Moossen et al., 2015), as do pollen studies from north central Iceland (Caseldine et al., 2006). These relative precipitation records provide evidence against a potential for increased humidity as suggested by Schomacker et al. (2016). Existing marine and terrestrial temperature records (Fig. 4d-e), along with our BSi-inferred summer temperature record from Skorarvatn (Fig. 4b) all strongly support peak warmth between 9 and 6.9 ka. The evidence for conditions conducive to negative glacier mass balance (local aridity and warmth) by 9 ka is consistent with our lake records documenting a rapidly receding ice cap. Thus, it is highly likely that elevated NH summer insolation and sea surface temperatures led to the continued melt and eventual demise of the ice cap during the early Holocene and that similar to other Icelandic ice caps, Drangajökull did not persist through the Holocene.

2.7 Conclusions

Using a collection of threshold lake sediment records, we provide firm constraints on the early Holocene deglaciation of northeastern Vestfirðir, with supporting evidence from BSi, an independent qualitative summer temperature proxy. Proto-Drangajökull retreated from the coast to the southeastern highlands on Vestfirðir before 10.3 ka (Fig. 5a). Lake sediment records document the contraction of proto-Drangajökull to ~20% of its current area by ~9.2 ka (Figs. 5b and 5c) consistent with existing marine and terrestrial temperature records that indicate relatively dry and warm summers. Combined with our local BSi-inferred summer temperature reconstruction from Skorarvatn, we suggest a combination of high summer insolation and increasing regional sea surface temperatures were the driving mechanisms behind the ice cap's rapid early Holocene recession. Although we cannot constrain the date of the ice cap's final disappearance, based on rates of retreat between 10.3 and 9.2 ka, we speculate that all ice had likely melted shortly after 9 ka.

2.8 Acknowledgements

This project was supported by RANNIS (grant #130775051) and the RANNIS Grant-of-Excellence (grant #141573-052) awarded by the Icelandic Center for Research to Á. Geirsdóttir and G.H. Miller and a University of Iceland PhD grant awarded to K. Zalzal from 2010 to 2012. We thank Þorsteinn Jónsson, Sveinbjörn Steinþórsson, Chris Florian and Celene Blair for lake coring assistance. Sydney Gunnarson and Brynja Berndsen (UoI) helped analyze Gjögurvatn´s sediment and tephra record and Eric Gunderson (UCB) assisted in developing the BSi record, for which all of their help is greatly appreciated. Finally, we

thank the editor and one anonymous reviewer for constructive reviews which helped strengthen the manuscript.

2.9 Supplemental Information

Table S2.1. *Major elemental compositions of individual tephra grains from SKR sample (200 cm depth) in comparison to AlB-1 tephra samples from other locations in Hvítárvatn, Haukadalsvatn and Hestvatn (Jóhannsdóttir, 2007).*

Site	SiO_2	TiO_2	Al_2O_3	FeO	MnO	MgO	CaO	Na_2O	K_2O	P_2O_5	Total
SKR 200 cm (n=19)	**46.45**	**2.59**	**15.25**	**12.76**	**0.20**	**7.15**	**10.90**	**2.51**	**0.49**	**0.28**	**98.57**
σ	0.50	0.48	0.68	1.31	0.03	0.88	0.94	0.29	0.30	0.07	0.54
Hvítárvatn mean (n-6)	**46.93**	**2.85**	**15.40**	**13.78**	**0.19**	**6.73**	**10.47**	**2.63**	**0.52**	**0.33**	**99.81**
σ	0.41	0.18	0.32	0.87	0.03	0.33	0.57	0.25	0.12	0.04	0.87
Haukadalsvatn mean (n=31)	**46.42**	**2.62**	**15.36**	**12.89**	**0.19**	**7.26**	**11.39**	**2.46**	**0.42**	**0.22**	**99.24**
σ	0.53	0.34	0.69	1.16	0.03	0.79	0.90	0.20	0.06	0.05	0.69
Hestvatn mean (n=9)	**46.83**	**2.83**	**15.43**	**13.43**	**0.21**	**7.01**	**11.02**	**2.47**	**0.45**	**0.25**	**99.93**
σ	0.44	0.26	0.52	0.98	0.04	0.46	0.74	0.19	0.05	0.05	0.54

Table S2.2. *Major elemental compositions of individual tephra grains from SKR sample (235 cm depth), SVG sample (453 cm depth), BÆ sample (322 cm depth), GDD sample (434 sample depth) and GJÖ sample (84 cm depth) in comparison Saksunarvatn tephra samples from the type locality on the Faroe Islands (Mangerud et al., 1986).*

Site	SiO_2	TiO_2	Al_2O_3	FeO	MnO	MgO	CaO	Na_2O	K_2O	P_2O_5	Total
SKR 235 cm (n=19)	**48.93**	**2.89**	**13.16**	**14.24**	**0.24**	**5.57**	**9.70**	**2.65**	**0.44**	**0.33**	**98.15**
σ	0.20	0.06	0.07	0.18	0.03	0.13	0.16	0.08	0.01	0.02	0.36
SVG 453 cm mean (n=16)	**49.60**	**3.07**	**13.10**	**14.26**	**0.24**	**5.51**	**9.93**	**2.66**	**0.43**	**0.33**	**99.12**
σ	0.70	0.09	0.26	0.33	0.01	0.21	0.25	0.13	0.03	0.02	0.97
BÆ 343 cm mean (n-8)	**49.11**	**3.08**	**13.30**	**14.19**	**0.24**	**5.53**	**9.90**	**2.56**	**0.41**	**0.30**	**98.62**
σ	0.45	0.05	0.22	0.22	0.01	0.10	0.17	0.11	0.02	0.01	0.44
GDD 434 cm mean (n=15)	**48.36**	**3.10**	**12.94**	**14.36**	**0.24**	**5.63**	**9.89**	**2.74**	**0.41**	**0.32**	**98.00**
σ	0.39	0.16	0.35	0.44	0.01	0.24	0.30	0.11	0.04	0.02	0.67
GJÖ 84 cm mean (n=19)	**49.25**	**2.91**	**13.10**	**14.21**	**0.24**	**5.60**	**9.85**	**N/A**	**N/A**	**N/A**	**N/A**
σ	0.34	0.09	0.10	0.16	0.02	0.11	0.13				
Saksunarvatn, Faroe Islands mean (n=13)	**49.19**	**3.04**	**12.88**	**13.29**	**0.24**	**5.60**	**9.28**	**N/A**	**0.46**	**N/A**	**N/A**
σ	0.85	0.30	0.35	0.47	0.08	0.33	0.35		0.06		

3 Episodic Expansion of Drangajökull, Vestfirðir, Iceland, Over the Last 3 ka Culminating in its Maximum Dimension During the Little Ice Age[2]

3.1 Abstract

Non-linear climate change is often linked to rapid changes in ocean circulation, especially around the North Atlantic. As the Polar Front fluctuated its latitudinal position during the Holocene, Iceland's climate was influenced by both the warm Atlantic currents and cool, sea ice-bearing Arctic currents. Drangajökull is Iceland's fifth largest ice cap. Climate proxies in lake sediment cores, dead vegetation emerging from beneath the ice cap, and moraine segments identified in a new DEM constrain the episodic expansion of the ice cap over the past 3 ka. Collectively, our data show that Drangajökull was advancing at ~320 BCE, 180 CE, 560 CE, 950 CE and 1400 CE and in a state of recession at ~450 CE, 1250 CE and after 1850 CE. The Late Holocene maximum extent of Drangajökull occurred during the Little Ice Age (LIA), occupying 262 km^2, almost twice its area in 2011 CE and ~20% larger than recent estimates of its LIA dimensions. Biological proxies from the sediment fill in a high- and low-elevation lake suggest limited vegetation and soil cover at high elevations proximal to the ice cap, whereas thick soil cover persisted until ~750 CE at lower elevations near the coast. As Drangajökull expanded into the catchment of the high-elevation lake beginning at ~950 CE, aquatic productivity diminished, following a trend of regional cooling supported by proxy records elsewhere in Iceland. Correlations between episodes of Drangajökull's advance and the documented occurrence of drift ice on the North Icelandic Shelf suggest export and local production of sea ice influenced the evolution of NW Iceland's Late Holocene climate.

3.2 Introduction

Persistent and rapid anthropogenic warming is one of the most pressing global environmental issues. In the Arctic, this abrupt warming is manifested in glacier, sea ice, snow cover and permafrost contraction (IPCC AR5, 2013). However, recent warming follows a trend of natural cooling since the mid-Holocene driven by the monotonic decrease in Northern Hemisphere summer insolation (Berger and Loutre, 1991). In Iceland, a general decline in summer temperatures beginning ~5.5 ka was punctuated by step-wise cooling (Geirsdóttir et al., 2013) which culminated in the Little Ice Age (LIA, 1250-1850 CE), the coldest multi-centennial climate anomaly of the Holocene (Grove, 1988; Miller et al., 2012).

---

[2] Harning, D.J., Geirsdóttir, Á., Miller, G.H., Anderson, L., 2016. Episodic expansion of Drangajokull, Vestfirðir, Iceland over the last 3 ka culminating in its maximum dimension during the Little Ice Age. Quaternary Science Reviews 152, 118-131.

Some combination of reduced solar irradiance (Shindell et al., 2001), sustained volcanism (Zhong et al., 2010; Miller et al., 2012), expanded sea ice (Miller et al., 2012; Sicre et al., 2013) and changes in the internal modes of variability in the ocean-atmosphere system (Trouet et al., 2009; Olsen et al., 2012) are called upon to explain these transitions (Wanner et al., 2011), yet there is no clear consensus on which forcings were most responsible for or the spatial continuity and duration of these events.

Glacier and lacustrine climate records from across Iceland reveal a Late Holocene history punctuated by increased glacial extent (Stötter et al., 1999; Larsen et al., 2011), enhanced terrestrial erosion, and decreased summer temperature (Axford et al., 2009; Geirsdóttir et al., 2009, 2013; Holmes et al., 2016) with the most extensive glacial coverage occurring during the peak LIA, between 1700 and 1900 CE (Bradwell et al., 2006; Larsen et al., 2011, 2015). The similarities in timing and direction of changes imply uniform driving mechanisms, likely from ocean and atmospheric variability of the North Atlantic (Geirsdóttir et al., 2013). Although terrestrial glacial and paleoclimate records are dispersed across Iceland, the northwest (Vestfirðir) lacks Late Holocene climate records despite the presence of Drangajökull, a small ice cap situated within 10 km of the North Atlantic. Between 1950 and 2010, summer (JJA average) air temperature at Drangajökull is strongly correlated to JJA averaged SSTs off the northeastern coast of Iceland, implying a dependency of local air temperatures on SSTs from this region (Fig. 3.1). Considering glacier mass balance is mainly controlled by summer temperature, and to a lesser degree precipitation (Oerlemans, 2005; Björnsson and Pálsson, 2008), constraining Drangajökull's evolution may improve our understanding of the role of ocean and atmospheric circulation in explaining rapid climate change.

Numerous marine records from the North Icelandic Shelf document variable Late Holocene sea surface temperatures (Bendle and Rosell-Melé, 2007; Sicre et al., 2011; Jiang et al., 2015) and the import of drift ice (Moros et al., 2006; Massé et al., 2008; Andrews et al., 2009; Cabedo-Sanz et al., 2016). Evidence suggests that marine conditions, particularly sea ice, exert a strong influence on near-shore environments of Iceland (Dickson et al., 1988; Stötter et al., 1999; Andrews et al., 2001; Hanna et al., 2006). The high albedo of sea ice reflects much of the incoming solar radiation in summer and insulates the ambient

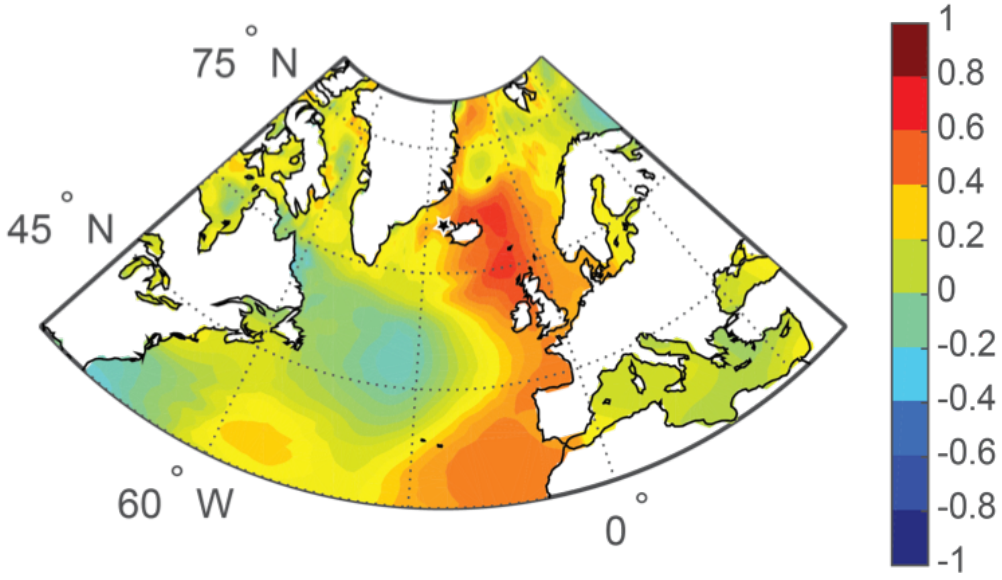

Figure 3.1. *Correlation of gridded JJA SSTs to JJA surface air temperature at Drangajökull (black star). See Supplemental Information for details on methodology.*

atmosphere from the relatively warm oceans during winter. Sea ice also limits the exchange of gases and moisture between the ocean and atmosphere (de Vernal et al., 2013). Due to its coastal setting, Drangajökull's mass balance is likely to have been strongly influenced by these ocean surface conditions.

In this paper, we provide a 3 ka multi-proxy record of Drangajökull's expansion and contraction. Historical accounts (Eythorsson, 1935; Grove, 1988) and previous mapping of ice-proximal surficial geology (Principato, 2008; Brynjólfsson et al., 2014, 2015) help to constrain the LIA areal extent of Drangajökull. However, previous maps of the glacier's LIA extent are largely limited to the three main outlet glaciers, which frequently surge and are not closely linked to climate change. Focusing on the non-surging margins, we better constrain Drangajökull's LIA margins and reconstruct its expansion over the last 3 ka by: 1) mapping LIA terminal moraines; 2) analyzing the sedimentary records of lakes proximal to the ice cap, which in some cases will define when Drangajökull was expanding; and 3) dating dead vegetation emerging from beneath the receding ice margin. By comparing our records with marine evidence from the North Icelandic Shelf, we test the dependence of Vestfirðir's past climate on local oceanic conditions.

3.3 Regional Setting

Vestfirðir is located near the modern Polar Front: the warm and saline Irminger Current (IC) dominates the west coast, whereas, the cooler, lower-salinity North Iceland Irminger Current (NIIC) and East Icelandic Current (EIC) dominate surface waters to the north and east (Fig. 3.2a). Regional bedrock is primarily composed of Tertiary basalts interbedded with thin sedimentary units (Harðarson et al., 2008). Upland surfaces are characterized by discontinuous andosols and vitrosols, low in organic content and sparsely covered with vegetation (Arnalds, 2004).

The highland plateau in eastern Vestfirðir hosts Iceland's fifth largest ice cap, Drangajökull (~142 km^2 area in 2011; Jóhannesson et al., 2013; Fig. 3.2b). Drangajökull is a polythermal ice cap, with surging outlet glaciers draining most of the east, north and west catchments. Based on our evidence of dead vegetation emerging from beneath the receding margin, the southern half of the ice cap, which mantles a high elevation, low relief landscape, is at least in part cold based. The ice cap's maximum elevation rises to 915 m asl with a 2000-2015 ice cap average equilibrium line altitude (ELA) at ~660 m asl, which is several hundred meters lower than Iceland's other ice caps (Björnsson and Pálsson, 2008). Drangajökull's low ELA likely reflects its proximity to the relatively low SST of the adjacent ocean resulting in short, cool summers. Mean sea level summer (JJA) air temperatures and annual precipitation are 6.9 ^{o}C and 1100 mm at Hornbjargsviti (1949-1994), 27 km north of the ice cap (Fig. 3.2b). In contrast, average conditions 17 km west of the ice cap on the island of Æðey are 8.9 ^{o}C and 580 mm (1954-2011; Veðurstofa Íslands, http://www.vedur.is). These records show that warmer and drier conditions persist to the west of the ice cap compared to those to the north. Northeasterly prevailing winds imply that most moisture is delivered to the glacier from the NE and that snow is redistributed by wind to the western side (Eythorsson, 1935; Magnússon et al., 2016).

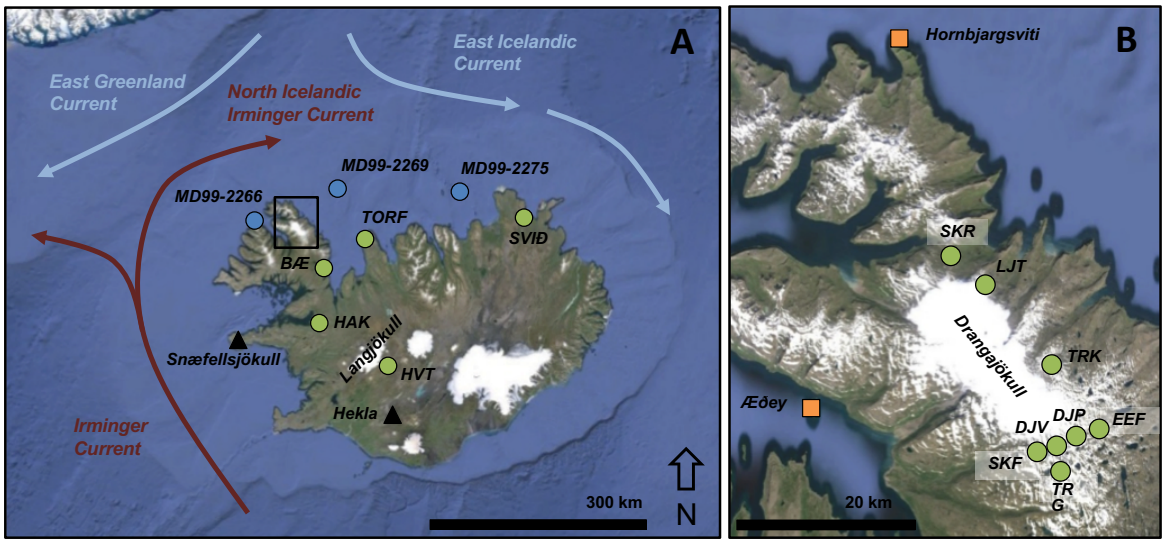

Figure 3.2. *A) Overview map of Iceland with locations of marine (blue) and terrestrial (green) sediment cores and tephra source volcanoes (black triangles) mentioned in text. Modern ocean currents after Hansen and Østerhus (2000). Black box highlights location of B) Eastern Vestfirðir with this study's lakes (green circles) surrounding Drangajökull and selected weather stations (orange squares). Base images are LANDSAT8 courtesy of USGS.*

3.4 Materials and Methods

3.4.1 Remote Imagery

Aerial imagery from 2005 (0.5 m resolution, Loftmyndir ehf., http://www.map.is) allowed identification of previously unrecognized moraines along Drangajökull's southern margin. Subsequently, a total of 23 stereoscopic aerial photographs from 1991 were acquired from the National Land Survey of Iceland (Landmælingar Íslands, LMÍ) in order to produce a DEM (5 m resolution) and a continuous orthoimage (50 cm resolution) of Drangajökull's southern margin (Fig. 3.3). Images were digitized by LMÍ, and processed using standard methods in ERDAS Imagine software. The 1991 images and DEM were examined to verify the moraine identifications from 2005 imagery. Lake catchments were extracted from this new DEM along with a 2011 LiDAR DEM of the ice cap and its vicinity (2 m resolution, Jóhannesson et al., 2013) and a 2014 subglacial bedrock DEM (50 m resolution, E. Magnússon, pers. comm.) in ESRI ArcMap 10 software.

3.4.2 Emerging Dead Vegetation

Samples of dead vegetation emerging from beneath receding ice margins along the northern and southern margins of the ice cap were collected in September of 2013 and 2014 following the protocol of Miller et al. (2013). Collection sites were selected along areas of high-elevation and low relief where cold-based conditions likely prevail (Fig. 3.4a). Ice catchments feeding these glacier margins are the smallest of the ice cap and are not associated with historically documented surges. Each sample was dated by radiocarbon as discussed in Section 5.4.4.

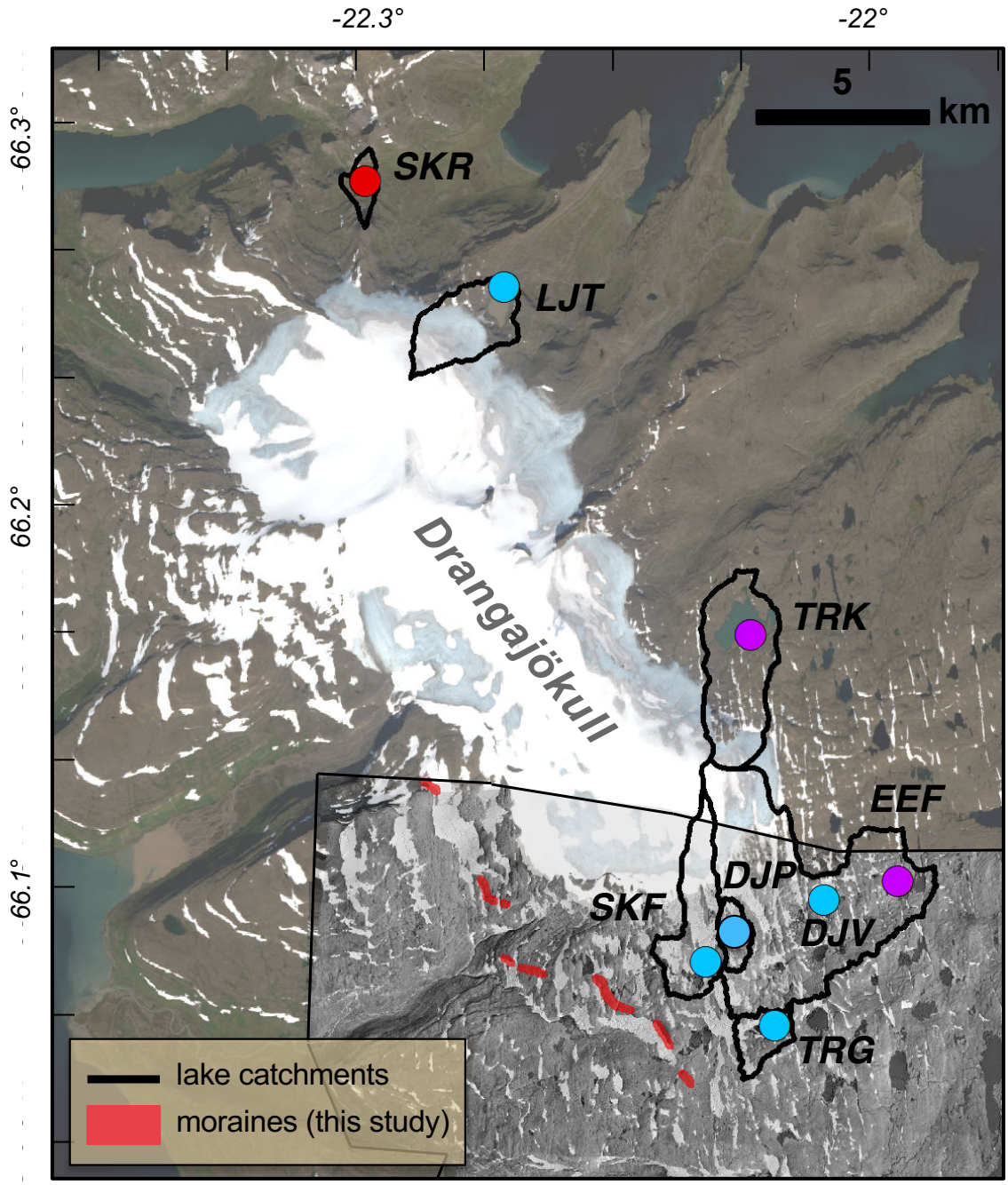

Figure 3.3. *Catchments of glacial (blue circles), threshold (purple circles) and non-glacial lakes (red circle). Southern margin of Drangajökull overlain with mosaic of 1991 LMI orthophotograph and DEM (grey scale). New terminal moraine segments highlighted in red (note: widths exaggerated for easier viewing). Base image is a product of LANDSAT8 courtesy of USGS from September 16, 2014.*

3.4.3 Lake Sediment Cores

Eight lakes were targeted for sediment cores to maximize spatio-temporal constraints of Drangajökull (Table 3.1, Fig. 3.2b). The catchments of higher elevation lakes (366-594 m asl) proximal to the ice cap serve as thresholds, which document if, when, and for how long

they were occupied by Drangajökull, with meltwater providing a distinctive sedimentary signal to the lake (e.g., Briner et al., 2010). Low-elevation Skorarvatn (183 m asl), a lake outside Drangajökull's drainage, was targeted to provide an independent record of local climate. Seismic surveys were performed on the two largest threshold lakes, Tröllkonuvatn and Ljótárvatn (Fig. 3.3), using a CHIRP 3.5 kHz system, to quantify lake sediment distribution. Sediment cores were recovered from each lake's deepest basin using a percussion driven piston corer: Skeifuvatn (SKF, 8.8 m), Djúpipollur (DJP, 34.5 m), Djúpavatn (DJV, 20.3 m), an un-named lake (TRG, 20.5 m), Efra-Eyvindarfjarðarvatn (EEF, 22.3 m), Tröllkonuvatn (TRK, 16.4 m), Ljótárvatn (LJT, 22.3 m) and Skorarvatn (SKR, 25 m) (Fig. 3.3, Table 3.1).

Magnetic susceptibility (MS) was measured on split cores at 0.5 cm intervals using a GeoTek Multi-Sensor Core Logger at the University of Iceland (UoI). MS is a physical proxy where higher (lower) MS indicates the transport of more (less) minerogenic, glacially eroded sediment to the lake (e.g., Larsen et al., 2011, 2012). For lakes TRK and SKR, sediment subsamples (~1 cm^3) taken at ~1 cm and ~0.5 cm intervals, respectively, were measured for total carbon (TC), total nitrogen (TN) and $\delta^{13}C$ (relative to VPDB) at the University of California Davis and computed for C/N. The local basalt bedrock has little or no carbon such that total carbon likely reflects total organic carbon (TOC). Percent TOC is a generic proxy for both autochthonous and allochthonous carbon sources, whereas C/N provides means to distinguish the two (algae = 4-10, vascular plants > 20; Meyers, 2003). $\delta^{13}C$ can reflect the input of organic carbon from aquatic macrophytes (~20 ‰), terrestrial vascular plants (~26 ‰) and algae (~30 ‰) (e.g., Geirsdóttir et al., 2013). Where algal productivity is the dominant signal, increased (decreased) productivity will enrich (deplete) bulk $\delta^{13}C$ (Meyers, 2003).

Table 3.1. *Lake data, where * indicates lakes with no sediment core proxy data.*

Lake	Core name	Elevation (masl)	Coordinates	Water depth (m)	Total core length (m)	Glacial sediment thickness (m)
Tröllkonuvatn (TRK)	TRK14-3A-2B	366	66° 8.551'N 22° 3.364'W	16.4	4.5	0.29
Efra-Eyvindarfjarðarvatn (EEF)	EEF14-3A-1B	408	66° 4.668'N 21° 57.187'W	22.3	4.0	0.27
Skeifuvatn (SKF)*	MLT12-1A-1N	594	66° 3.359'N 22° 4.765'W	8.8	1.0	1.0
Djúpipollur (DJP)*	n.a.	563	66° 3.774'N 22° 3.476'W	34.5	0	0
Djúpavatn (DJV)*	DJP12-1A-1N	513	66° 4.383'N 22° 0.287'W	20.3	0.29	0.29
Target (TRG)	TRG14-1A-1N	554	66° 2.366'N 22° 2.153'W	20.5	0.16	0.16
Ljótárvatn (LJT)	LJT14-6A-1N	454	66° 13.565'N 22° 13.918'W	22.3	1.42	1.42
Skorarvatn (SKR)	SKR14-6A-1N	183	66° 15.376'N 22° 19.328'W	25	2.5	0

3.4.4 Geochronology: Radiocarbon and Tephrochronology

Emerging dead vegetation and lacustrine sediment macrofossils were freeze-dried, gently rinsed with deionized water to remove sediment and freeze-dried again at the UoI. Plant

fragments were given an acid-base-acid pretreatment and graphitized at the University of Colorado-Boulder, then measured by AMS at the University of California Irvine. Radiocarbon ages were calibrated using OxCal 6.0 with the IntCal13 calibration curve (Bronk Ramsey, 2009; Reimer et al., 2013) and are reported in calibrated years BCE/CE (Tables 3.2 and 3.3).

Tephra visible in the lake sediment cores were extracted and sieved to isolate tephra glass between 150 to 250 μm, then embedded in epoxy plugs and analyzed on a JEOL JXA-8230 election microprobe at the UoI. The international A99 standard was analyzed every 10th sample to monitor instrument drift and maintain consistency between samples. Tephra source identifications were carried out by geochemical comparisons to previously published tephrochronologies from terrestrial and marine settings (Larsen et al., 2002; Dugmore et al., 2007; Jóhannsdóttir, 2007; Kristjánsdóttir et al., 2007).

Table 3.2. *Emerging dead vegetation sample informaton. See Figs. 3.5 and S3.1 for discussion on the calibration of these dates.*

Lab ID	Material	Latitude	Longitude	Elevation (masl)	$\delta^{13}C$ (‰)	Fraction modern	Conventional ^{14}C age ± 1σ
UCIAMS-134344	Terr. moss	66° 13.200'N	22° 20.468'W	685	N/A	0.7948	1845 ± 40
CURL-18795	Terr. moss	66° 5.047'N	22° 11.864'W	454	-26.9	0.9695	250 ± 20*
CURL-19491	Terr. moss	66° 4.512'N	22° 7.566'W	555	-22.0	0.9727	220 ± 20*
CURL-18798	Terr. moss	66° 5.077'N	22° 11.905'W	464	-24.2	0.9737	215 ± 20*
CURL-18810	Terr. moss	66° 4.810'N	22° 11.548'W	424	-23.5	0.9741	210 ± 20*
CURL-19485	Terr. moss	66° 4.532'N	22° 5.809'W	601	-22.4	0.9743	210 ± 20*
CURL-18814	Terr. moss	66° 4.463'N	22° 6.111'W	582	-26.6	0.9746	205 ± 25*
CURL-19487	Terr. moss	66° 4.532'N	22° 5.809'W	601	-19.9	0.9783	175 ± 20*
CURL-18809	Terr. moss	66° 5.663'N	22° 12.304'W	535	-28.8	0.9890	90 ± 20

Table 3.3. *Radiocarbon sample information from lake sediment. Calibrated using OxCal 6.0 and IntCal13 radiocarbon curve (Bronk Ramsey, 2009; Reimer et al., 2013).*

Lake (sediment depth)	Lab ID	Material	$\delta^{13}C$ (‰)	Fraction modern	Conventional ^{14}C age ± σ	Calibrated age BCE/CE ± σ
TRK (18 cm)	CURL-19503	Macrofossil	-22.2	0.9348	540 ± 15	1410 ± 10
TRK (30.5 cm)	UCIAMS-165968	Macrofossil	N/A	0.8686	1130 ± 20	930 ± 50
EEF (21 cm)	CURL-19492	Macrofossil	-20.2	0.8542	1265 ± 15	730 ± 50
EEF (30 cm)	UCIAMS-165967	Macrofossil	N/A	0.7324	2500 ± 25	660 ± 120
EEF (121 cm)	CURL-19504	Macrofossil	-23.0	0.38	7775 ± 25	6620 ± 20

3.5 Results

3.5.1 Moraine Segments and Lake Catchments

The combination of aerial imagery from 1991 and 2005 along with DEMs from this study and 2011 (Jóhannesson et al., 2013) allow new interpretations of Drangajökull's evolution during the Late Holocene. We identified a subdued terminal moraine complex along the ice cap's southern margin that defines a previously larger glacial extent (Fig. 3.3). These terminal moraines segments add to the inventory of ice margin indicators previously identified and described along the western, northern and eastern ice cap margins (Principato, 2008; Brynjólfsson et al., 2014). Based on a sub-glacial DEM (E. Magnússon, pers. comm.), the underlying topography of Drangajökull allows us to identify where and at what elevation the ice cap expanded into threshold lake catchments (Fig. 3.3). For EEF and TRK, these threshold elevations are 740 and 700 m asl, respectively.

3.5.2 Emerging Dead Vegetation

Nine dead vegetation samples were collected within one meter of Drangajökull's contemporary ice margin and dated by radiocarbon (Table 3.2, Fig. 3.4a). Individual dates and/or peaks in summed probability distribution functions (PDF) from the emerging dead vegetation define the onset of persistent snowline depression and subsequent glacial expansion at each site (e.g., Miller et al., 2013). The sample from the northern margin of the ice cap, UCIAMS-134344, records an expansion of Drangajökull over the site at 180 ± 50 CE. The eight samples collected along the southern margin all have radiocarbon ages <400 years that fall in a particularly variable portion of the calibration curve with large uncertainties (Reimer et al., 2013). Seven of the eight samples have similar radiocarbon concentrations, yielding a normalized cumulative PDF limited to three discrete peaks: 1664 ± 30 CE (39%), 1765 ± 40 CE (49%) or 1938 ± 10 CE (12%) (Fig. 3.5). Given the low probability of the mid-20th Century expansion of Drangajökull, we consider the two earlier dates as equally probably dates for a LIA expansion of the ice cap's southern margin.

3.5.3 Lake Types and Sediment Properties

3.5.3.1. Glaciated Lakes

Our glaciated lakes along the southern and northeastern margins of Drangajökull lack non-glacial sediment and contain either purely glacially derived sediment packages or no recoverable sediment.

Skeifuvatn (SKF; 66° 3.359'N, 22° 4.765'W), south of Drangajökull, has a lake catchment extending ~3 km north underneath the modern ice cap's margin (Fig. 3.3). The 1 m core collected from its central basin consists of a basal gravel-sized diamicton overlain by coarsely laminated silt and clay.

Djúpipollur (DJP; 66° 3.774'N, 22° 3.476'W), south of the ice cap's current drainage sits in a small catchment which is currently isolated from the ice cap (Fig. 3.3). The central basin contained no recoverable sediment and, thus, is assumed to be bare bedrock.

Djúpavatn (DJV; 66° 4.383'N, 22° 0.287'W), southeast of Drangajökull's modern southern margin, resides in a large catchment which currently extends ~2 km under the base

of the ice cap to the north (Fig. 3.3). The short, 29 cm core recovered from the lake, consists of diamicton with gravel-sized clasts overlain by glaciolacustrine silts and clay.

TRG (66° 2.366'N, 22° 2.153'W) sits outside the current drainage of Drangajökull's southern margin (Fig. 3.3). The short, 16 cm core consists of glaciolacustrine silt with a 6 cm diameter clast at its base. The uppermost cm is massive, non-glacial olive-brown sediment.

Ljótárvatn (LJT; 66° 13.565'N, 22° 13.918'W), on Drangajökull's northeast margin, currently resides within Drangajökull's drainage network receiving considerable amounts of rock-flour-laden meltwater (Fig. 3.3). The 1.42 m core consists of ~0.5 m of poorly-sorted diamicton with clasts up to 6 cm in diameter supported by a clay- to silt-sized matrix overlain by glaciolacustrine silt and clay.

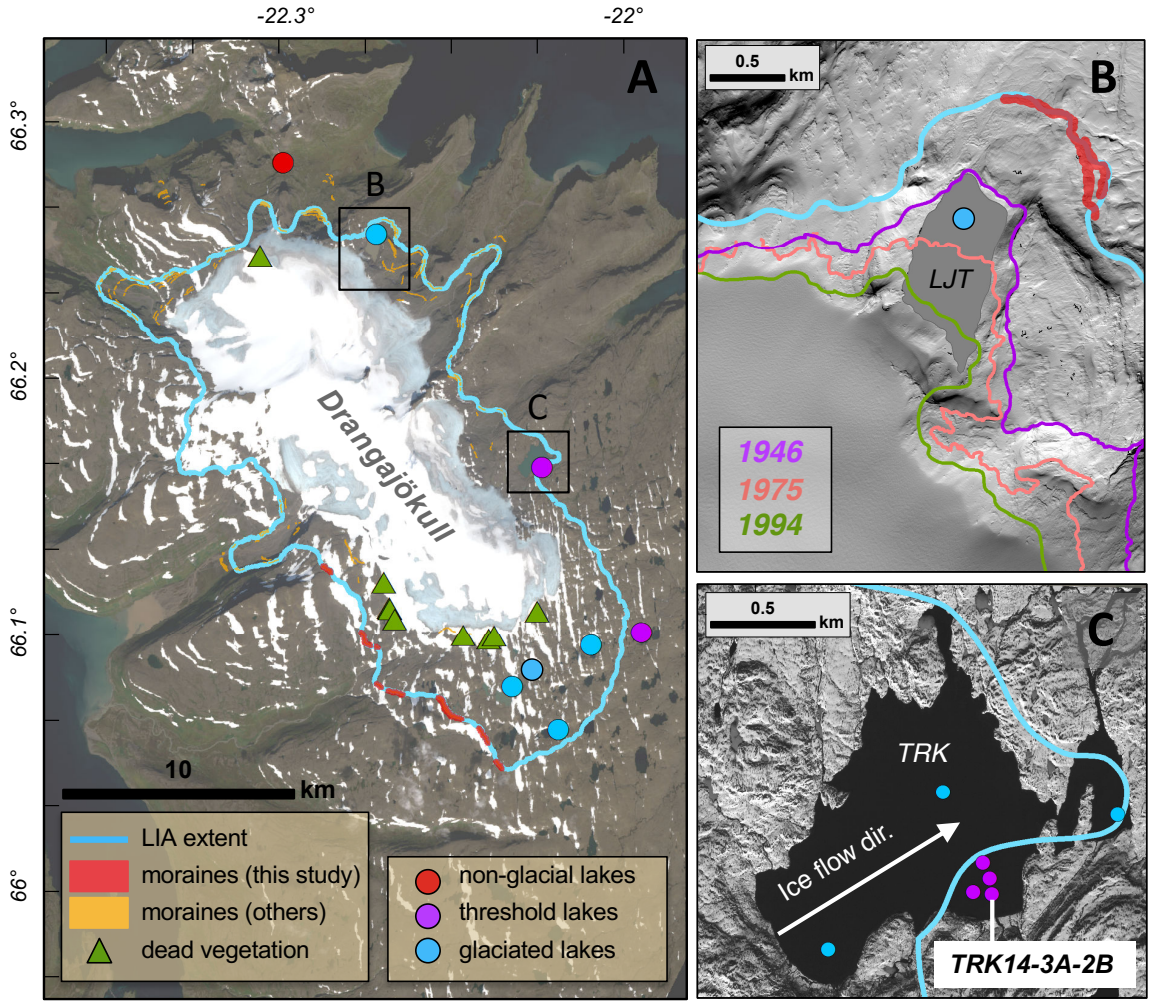

Figure 3.4. *A) Estimated LIA areal extent inferred from lakes and moraines identified in this study and others (Principato, 2008; Brynjólfsson et al., 2014). Base image is a product of LANDSAT8 courtesy of USGS. B) Ljótárvatn (LJT) and ice cap limits from 1946, 1975 and 1994 CE aerial imagery showing progressive retreat of Drangajokull from LIA moraine. Base image is a 2011 LiDAR DEM (Jóhannesson et al., 2013). C) Estimated LIA extent in TRK inferred from cores acquired in 2012 and 2014. 2013 base image courtesy of Digital Globe.*

3.5.3.2. Threshold Lakes

Our interpretation of changes in lithostratigraphy in threshold lakes is based on non-glacial facies being predominately dominated by OM, frequently including thick layers of macrofossils interbedded with thin olive-brown gyttja, and relatively low MS, reflecting the absence of Drangajökull within its catchment. Glaciolacustrine facies are light brown to gray silt and clay with higher MS and thus indicate the delivery of glacial sediment when Drangajökull's margin crossed the catchment threshold (e.g., Briner et al., 2010). The highest MS values occur during the latest Holocene between ~1400 and 1850 CE.

Efra-Eyvindarfjarðarvatn (EEF, 66° 4.668'N, 21° 57.187'W), southeast of Drangajökull, resides in the same catchment as DJV. Glacial meltwater that feeds EEF is first directed through lake DJV and, thus, EEF only receives fine-grained glacial sediment still in suspension after exiting DJV's eastern outlet. An age-depth model was generated for EEF using three ^{14}C-dated macrofossils (Table 3.3) and the CLAM 2.2 package (Blaauw, 2010; Fig. 3.6). A smooth spline regression was applied with 1000 iterations resulting in a low goodness-of-fit value of 4.98 and a low level of uncertainty over the last 3 ka. The resultant age model is nearly linear over the past 3 ka.

Tröllkonuvatn (TRK, 66° 8.551'N, 22° 3.364'W) resides on Drangajökull's eastern margin. A small portion of the TRK catchment still receives Drangajökull meltwater. A sediment core from the SE basin (TRK14-3A-2B; Fig. 3.4c) records a two-phase glaciolacustrine sequence in the upper 30.5 cm of sediment (Fig. 3.7). Age constraint is derived from two ^{14}C-dated macrofossils (Table 3.3) and two primary tephras diagnostic of specific eruptions (Tables S3.1 and S3.2). Unique major elemental compositions distinguish the presence of the rhyolitic Snæfellsjökull-1 (Sn-1, 1820 ± 90 cal BP; Larsen et al., 2002) and the basaltic Hekla-T (6100 ± 200 cal BP; Jóhannsdóttir, 2007) tephras. An age model was produced following the procedures for EEF resulting in a low goodness-of-fit value of 2.72 and a very low level of uncertainty over the last 3 ka (Fig. 3.6).

Because lakes EEF and TRK are both threshold lakes, transitions between sediment lithologies need not represent the precise timing of the ice cap's response to climate forcings as the margin may have initiated an advance prior to entering the lake catchment. However, the timings of transitions to glaciolacustrine units do provide maximum age estimates on periods of active glacier advance.

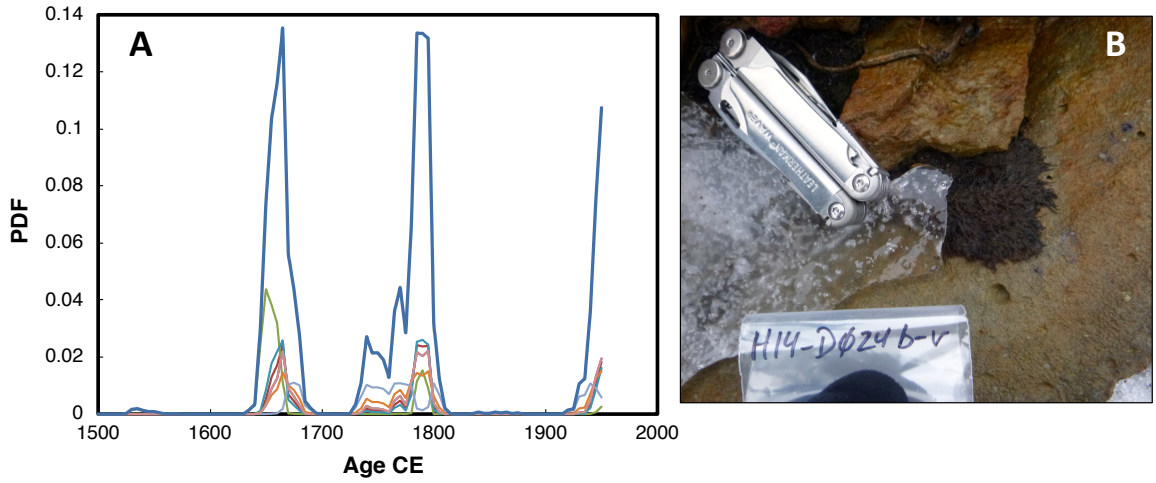

Figure 3.5. *Individual probability distribution functions (PDF) of the 7 emerging dead vegetation samples with ^{14}C dates between 250 and 175 BP. Ages calibrated in OxCal 6.0 with the IntCal13 calibration curve*

(Bronk Ramsey, 2009; Reimer et al., 2013). A normalized sum of the individual PDFs is shown by the bold blue line. B) Example of dead vegetation sample (CURL-18810) emerging from the southern margin prior to sampling.

3.5.3.3. Non-glacial Lake

Skorarvatn (SKR; 66° 15.376'N, 22° 19.328'W) and its catchment are not influenced by Drangajökull at its current dimensions or at its peak LIA dimension (Fig. 3.3). A 250 cm long sediment core, SKR14-6A-1N, was recovered from 25 m water depth. Following the procedures applied to lakes EEF and TRK, an age-depth model (Fig. 3.6) was generated (goodness-of-fit=3) using three primary tephra identifications; Hekla-1693 (1693 CE; Dugmore et al., 2007), Snæfellsjökull-1 and Hekla-T. The latest 3 ka (30 cm) is comprised of massive to weakly laminated olive-brown non-glacial sediment, interbedded with discrete tephra and macrofossil lenses. MS values are low and exhibit no trend. C/N ratios are relatively low yet variable between ~1000 BCE and 200 CE, steadily increasing from ~200 to 600 CE where they reach their highest values, followed by a modest decrease towards present (Fig. 3.7).

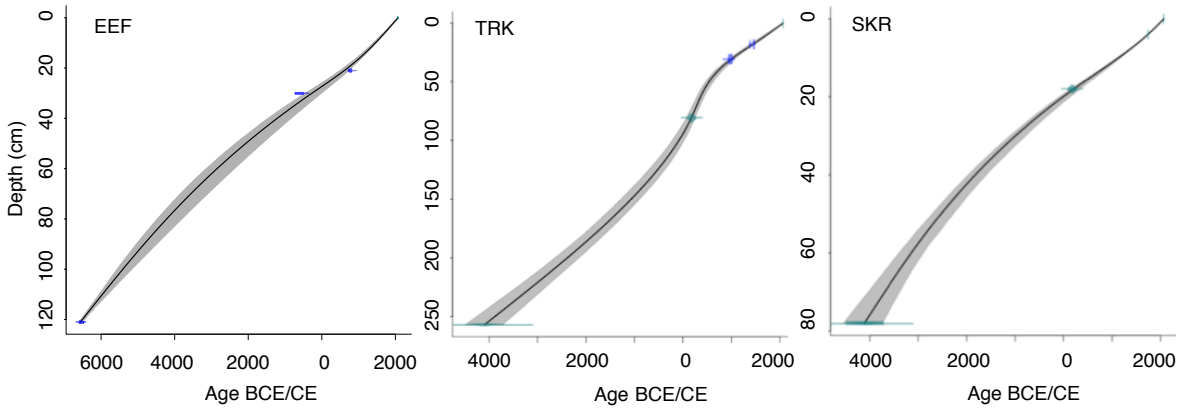

Figure 3.6. *Age-depth models for EEF (left), TRK (middle) and SKR (right) produced using smooth spline regression in CLAM version 2.2 (Blaauw, 2010). Gray shaded areas represent 95% confidence limit.*

3.6 Interpretation

3.6.1 1000 BCE – 950 CE

Evidence from threshold lakes and emerging dead vegetation permit the identification and dating of previously unknown expansions and contractions of Drangajökull's northern and southern margins during the Late Holocene and, thus, help constrain changes in summer temperature and precipitation. Non-glacial units in threshold lake sediment are characterized by low MS, and in the case of TRK also relatively high yet variable %TOC, $\delta^{13}C$ and C/N with no distinct trends. Increased MS in addition to lower %TOC, depleted $\delta^{13}C$ and lower C/N reflect greater contributions of glacially eroded minerogenic material relative to OM that dominates when the lake catchment is glaciated (Fig. 3.7).

Drangajökull first crossed into EEF's catchment (elev. 740 m asl) at ~320 BCE at the first transition to glaciolacustrine sediment. Although not reflected in the near linear age model (Fig. 3.6), we postulate that the sediment accumulation rate increased with the input

of comminuted silt and clay. During the earliest phase of glaciolacustrine sedimentation (30-23 cm; Fig. 3.7) Drangajökull did not likely reach DJV, which trapped a large fraction of the glacial sediment from reaching EEF. However, Drangajökull occupied DJV during some of the time that the upper glaciolacustrine sediment (21-0 cm; Fig. 3.7) was deposited permitting more direct delivery of glacial sediment to EEF. These constraints suggest the sedimentation accumulation rate was highest 0-21 cm, lowest during non-glacial deposition 21-23 cm, and intermediate during 23-30 cm. Lacking quantitative data to define these changes we provide large errors bars on the temporal boundaries between these units (Fig. 3.8). At 180 CE, emerging dead vegetation records persistent snowline depression and glacier expansion on the north side of the ice cap. A transition back to non-glacial sediment

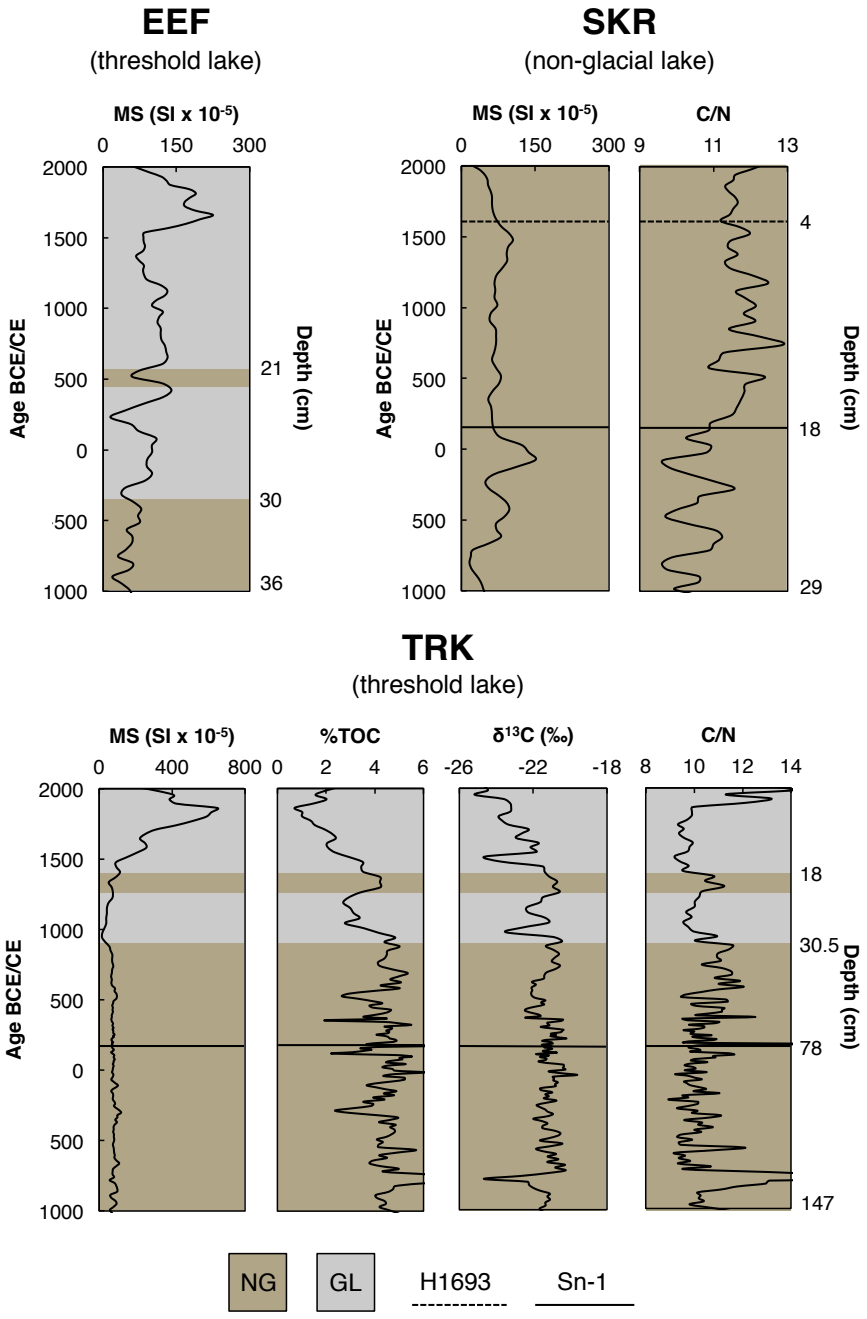

Figure 3.7. *Downcore physical and biological proxies with simplified sediment lithologies for the last 3 ka in threshold lakes EEF (top left) and TRK (bottom) and non-glacial lake SKR (top right). NG = non-glacial*

sediment and GL = glaciolacustrine unit deposited from sediment-laden meltwater. Black lines (dashed and bold) mark key tephras of known age.

at ~450 CE in EEF indicates Drangajökull retreated from EEF's catchment then. The southern margin subsequently readvanced into EEF's catchment at ~560 CE, the date for the final transition to glaciolacustrine sediment, and has remained within EEF's catchment through to the present.

Non-glacial lake SKR and threshold lake TRK (Figs. 3.2 and 3.3) support local climate variability inferred from Drangajökull's activity using independent biological proxies. TRK's OM is predominately derived from aquatic plants and algae (Fig. 3.9) implying that the surrounding catchment was limited in terrestrial vegetation and soils. Consequently down-core changes in MS, TOC, $\delta^{13}C$ and C/N primarily reflect aquatic bioactivity, where lower bioactivity is associated with cooler summer lake temperatures (e.g., Geirsdóttir et al., 2009, 2013). In contrast to TRK, SKR sits in a more vegetated catchment. Increases in C/N, reflecting a higher proportion of terrestrial OM result from increasing landscape destabilization and erosion of terrestrial vegetation and soils, which are a consequence of cooler, windier summers (Axford et al., 2007; Geirsdóttir et al., 2009; Larsen et al., 2011).

Between ~1000 BCE and 200 CE, TRK's aquatic bioactivity and SKR's catchment are relatively stable based on their respective composite and C/N records exhibiting no distinct trends (Fig. 3.10). However, at ~320 BCE, TRK and SKR document a short-term reduction in aquatic bioactivity and increase in catchment erosion. The temporal agreement between these two independent proxies with the first advance of Drangajökull based on EEF's transition to glaciolacustrine sediment lends strong support for an episode of summer cooling. Increasingly cooler summer temperatures between ~200 CE and 750 CE are supported by increased terrestrial erosion around lake SKR and two episodes (~180 CE and 560 CE) of reduced aquatic bioactivity in TRK and glacial expansions on the northern and southern margins of Drangajökull. The synchronicity and direction of independent climate proxies in multiple archives provides firm evidence for specific episodes of summer cooling. However, the warmth implied by Drangajökull's retreat at ~450 CE based on EEF lithofacies and proxies is not quite in agreement with the biological records from TRK and SKR. TRK's aquatic productivity remains fairly stable whereas SKR's C/N suggests elevated landscape erosion in its catchment (Fig. 3.10).

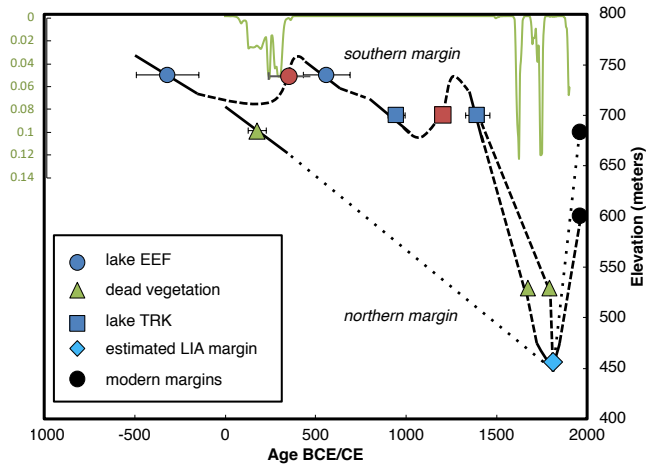

Figure 3.8. *Change in ice margin elevation over the last 3 ka on the northern (dotted) and southern margins (dashed). Blue (red) indicate advance (retreats) from lake catchment thresholds. LIA margin at 1850 CE*

estimated from Fig. 4 and is assumed to have an error of ± 100 meters. Error bars represent 95% confidence limit from lake age-depth models (Fig. 3.5). Cumulative PDF of southern margin emerging dead vegetation ^{14}C-dated inverted on top (see Fig. 3.5).

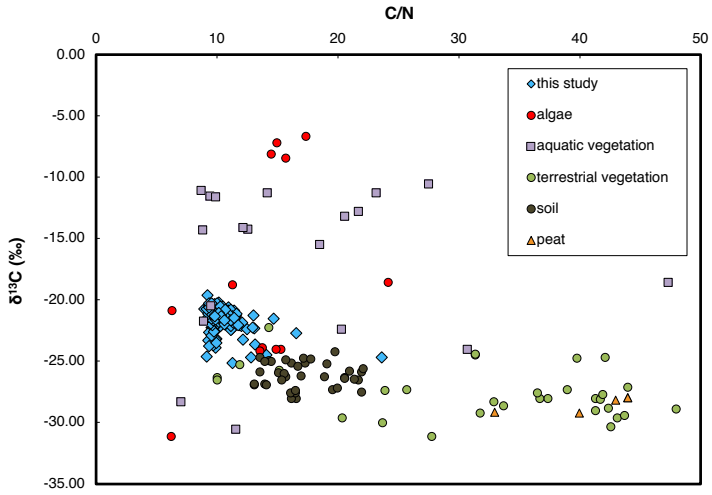

Figure 3.9. *Organic matter provenance of lake TRK sediment (blue diamonds) inferred from C/N and bulk δ^{13}C. End members are combined from modern Icelandic vegetation (Wang and Wooller, 2006; Skrzypek et al., 2008; Langdon et al., 2010; C. Florian, unpublished, pers. comm.). Note: C/N axis cut off at 50, however, terrestrial vegetation range up to 205 in these studies.*

3.6.2 950 CE – Present

Lake TRK's glaciolacustrine sediment records two episodes of Drangajökull's expansion into its catchment (elev. 700 m asl); the first at ~950 CE, then retreat from its catchment at ~1250 CE, and subsequently readvance of the ice cap into TRK's catchment at ~1400 CE (Fig. 3.8). Coincident with the two glacial advances, TRK's composite record shows persistent reduction in aquatic bioactivity, and hence, summer cooling (Fig. 3.10). Although slightly decreasing, the relative stability of lake SKR's C/N after ~950 CE implies a cessation of non-glacial terrestrial erosion, and at first glance, a stable climate. However, given the significant 1st order cooling inferred from proxies suggesting Drangajökull's growth we argue that stable C/N represents either 1) depletion of terrestrial soils and vegetation as documented in nearby Reykjarfjörður (Andrews et al., 2001) and/or 2) perennially frozen ground preventing the mobilization of vegetation and soils (Florian et al., 2015). The intermittent warmth implied by elevated bioactivity in lake TRK supports Drangajökull's retracted state between ~1250 and 1400 CE (Fig. 3.10).

The seven emerging dead vegetation dates from Drangajökull's southwestern margin provide two options for the ice cap's LIA expansion (Fig. 3.8). The likelihood that the combined ages reflect snowline depression during the 20th Century is very low (12%) and likely an artifact of the calibration curve. Due to the higher probability of peaks at ~1660 (39%) and ~1770 CE (49%), we argue that the snowline lowered or that a somewhat earlier snowline lowering resulted in subsequent ice expansions across these sites during one of these two intervals with persistent ice cover over the sites until 2014 CE, the year of their collection. The coolest summers inferred from the most reduced aquatic productivity in lake TRK (Fig. 3.10) support the expansion of Drangajökull at either ~1660 CE or ~1770 CE as it approached its maximum LIA extent.

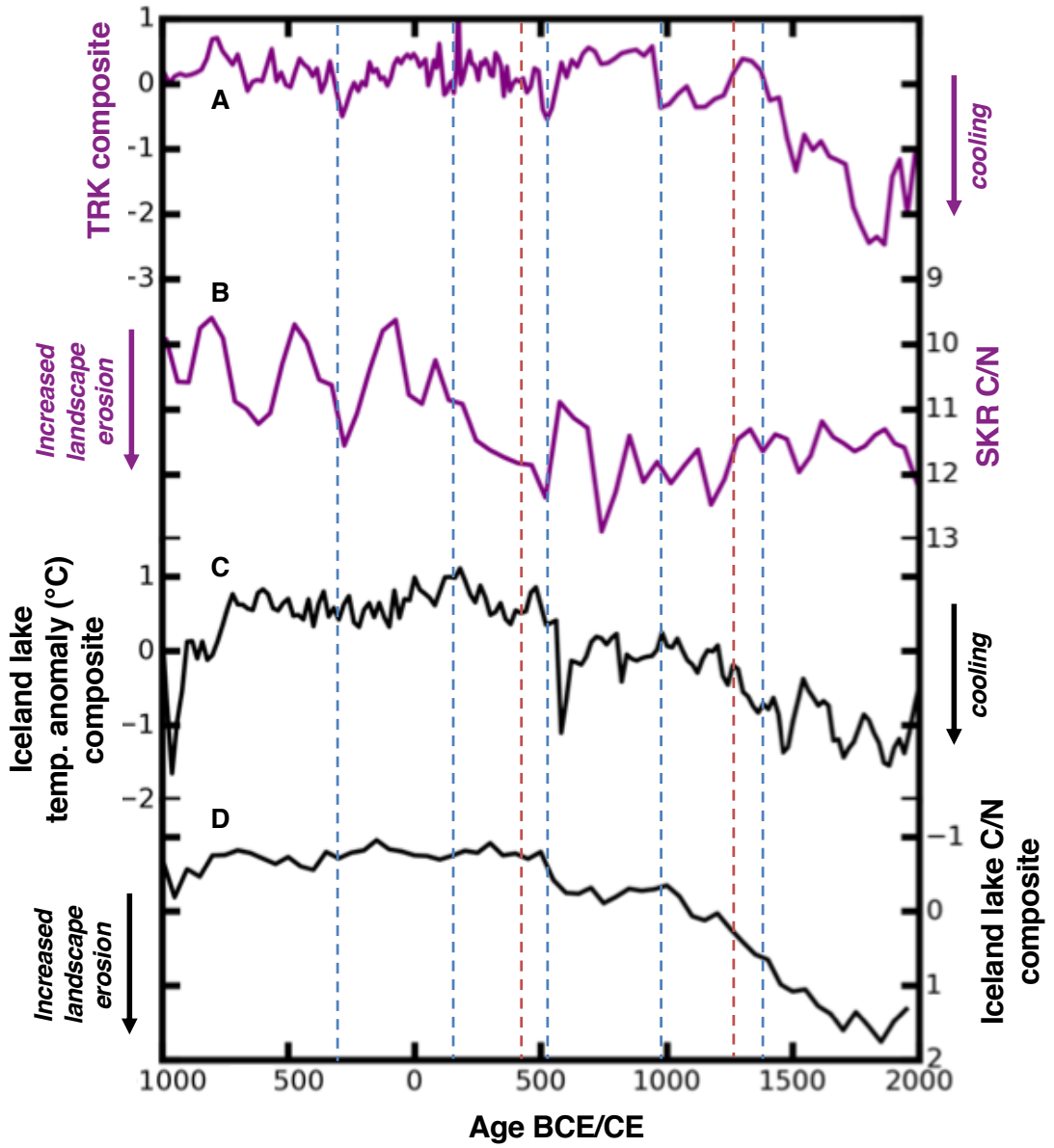

Figure 3.10. *Biological proxy record illustrated by A) lake TRK composite of MS, %TOC, $\delta^{13}C$ and C/N (following methods of Geirsdóttir et al., 2013), B) lake SKR C/N, C) Icelandic composite lake temperature anomaly record relative to modern (Geirsdóttir et al., 2013) and D) inverted Icelandic composite lake C/N record from Hvítárvatn (HVT; Larsen et al., 2011), Haukadalsvatn (HAK; Geirsdóttir et al., 2013), Bæjarvötn and Torfdalsvatn (BÆ and TORF; Florian et al., in review) and Stora Viðarvatn (SVIÐ; Axford et al., 2009). See Fig. 2A for lake locations. All records were resampled to a uniform interval of 50 years using AnalySeries (Paillard et al., 1996), normalized (mean/standard deviation) and averaged to illustrate increasing landscape destabilization during the Late Holocene. All proxies oriented down for cooler conditions. Blue (red) vertical lines represent episodes of Drangajökull advance (retreat).*

3.6.3 Reconstructing Drangajökull's Maximum LIA Extent

By combining information from southern margin moraine segments and the physical properties of all the lake sediment cores, we can constrain Drangajökull's LIA maximum areal extent (Fig. 3.4a), which local sources and lichenometry on moraines from Vestfirðir document at ~1850 CE (Principato, 2008; Brynjólfsson et al., 2015). We show that five lakes

proximal to Drangajökull were over-ridden and occupied by the ice cap during the LIA. When ice expanded across the plateau to the southwestern and northeastern moraines any previous non-glacial sediment was eroded out of the glaciated lakes, leaving only glacially derived sediment packages. The LIA moraine beyond LJT confirms that Drangajökull occupied this lake during the LIA (Fig. 3.4b). Aerial imagery captures the progressive retreat of Drangajökull from the lake basin between 1946 and 2013. Since lakes SKF and DJV have similar sediment lithologies and are also still within Drangajökull's catchment, LJT's scenario likely applies to these two lakes as well. Lake TRG also captures Drangajökull's occupation of the main basin (diamict) and subsequent retreat (silts). The 1-cm-thick gyttja cap on the sediment core from the main basin reflects the dominance of organic matter (OM) accumulation following the ice cap's recession from its catchment. Lake DJP has a small catchment (1.74 km^2) and its lack of sediment indicates a rapid recession of the ice cap from the lake and catchment limiting any significant deglacial sediment accumulation. Collectively, all of these lakes provide minimum estimates for the maximum LIA extent of Drangajökull.

For the threshold lakes (EEF and TRK), glaciolacustrine sediment implies that Drangajökull was present and actively eroding within both of the lakes' catchments. Since EEF contains underlying pre-LIA non-glacial sediment, the lake was not glaciated and, thus, the southeastern LIA limit must lie between EEF and lake DJV, a glaciated lake. Sediment cores from TRK indicate that during the LIA, it was both a glaciated and a threshold lake. Ice filled nearly the entire lake basin scouring out most non-glacial sediment (Fig. 3.4c). The ice occupying the main basin at the LIA maximum must have been thin, because the southeastern sub basin, orthogonal to the main ice-flow direction, contains a thick sequence of undisturbed stratified non-glacial sediment. SKR's non-glacial record confirms that Drangajökull did not advance into its catchment at any time over the latest 3ka, supporting previous LIA limits for the northern margin (Brynjólfsson et al., 2014). We estimate the dimensions of Drangajökull during the peak LIA (~1850 CE) to have been ~262 km^2, 1.2 times larger than the previous estimate of 216 km^2 (Brynjólfsson et al., 2015), with the major differences between the two reconstructions situated along the southern margin.

3.7 Regional Comparisons

Numerous marine and terrestrial studies manifest the Late Holocene climate of Iceland in decreasing summer temperatures (Axford et al., 2009; Jiang et al., 2015; Holmes et al., 2016), growth of glaciers (Stötter et al., 1999; Kirkbride and Dugmore, 2006, 2008; Larsen et al., 2011, 2012, 2015), increased landscape erosion (Axford et al., 2009; Geirsdóttir et al., 2009; 2013) and enhanced sea ice export from the Arctic Ocean (Moros et al., 2006; Massé et al., 2008; Cabedo-Sanz et al., 2016). First-order cooling represented by these various climate records is dominantly in response to the progressive reduction in Northern Hemisphere summer insolation (Berger and Loutre, 1991; Mayewski et al., 2004; Wanner et al., 2011). Although Drangajökull's record of Late Holocene expansion is punctuated by at least two periods of recession, the general evolution from restricted glacial conditions 3 ka ago to maximum areal coverage during the LIA is consistent with orbitally induced cooling. However, the episodic nature of Drangajökull's expansion (Fig. 3.8) suggests factors other than insolation modulated the overall trend toward cooler summers.

3.7.1 Sub-Atlantic Period (SA, 600 BCE – 100 BCE)

At ~320 BCE, Drangajökull advanced. Other Iceland glaciers expanded at about the same time: Langjökull, in central Iceland (Larsen et al., 2011), small mountain glaciers in south and central Iceland (Kirkbride and Dugmore, 2006, 2008) and alpine glaciers in nearby Tröllaskagi, North Iceland (Stötter et al., 1999) (Fig. 3.11). Evidence from the marine realm reveals a cooler NIIC (Castañeda et al., 2004; Ólafsdóttir et al., 2010), and increased IP_{25} suggests greater transport of sea ice onto the North Icelandic Shelf (Fig. 3.11g; Cabedo-Sanz et al., 2016). The evidence of cooler summers from Drangajökull, its proximal lakes and the other existing climate records from Iceland highlights Vestfirðir's capacity to document periods of North Atlantic cooling likely related to nearby ocean surface conditions at this time.

3.7.2 Roman Warm Period (RWP, 100 BCE – 600 CE)

At 180 CE, emerging dead vegetation records Drangajökull's expansion during the Roman Warm Period (RWP), when lake temperatures are the warmest of the last 3 ka in Haukadalsvatn and Hvítárvatn (Fig. 3.10c; Geirsdóttir et al., 2013), glaciers are not known to be expanding elsewhere in Iceland and oceanic conditions on the North Icelandic Shelf are dominated by a relatively warm IC (Giraudeau et al., 2004; Sicre et al., 2011) with less sea ice cover (Fig. 3.11g; Cabedo-Sanz et al., 2016). Farther north into the Arctic (~79ºN latitude), intervals of less pervasive sea ice on oceanic water sources (Müller et al., 2012) have provided sufficient moisture supply to drive glacier growth (Nesje et al., 2008; D'Andrea et al., 2012). A local marine biomarker record from MD99-2266 just west of Drangajökull records increased moisture availability during the RWP (Moossen et al., 2015) potentially related to reduced local sea ice coverage (Fig. 3.11g). Therefore, a precipitation driven advance is a plausible explanation for expansion of Drangajökull at this time. As this episode is currently based on only a single date, replication from additional dead vegetation samples would strengthen our argument. Several centuries later, at ~450 CE, Drangajökull's southern margin retreated, at a time when SSTs were elevated and there was less sea-ice over the North Icelandic Shelf (Fig. 3.11g). We argue that this recession or standstill at ~450 CE was forced by elevated air temperatures likely related to higher regional SSTs and less pervasive sea ice.

3.7.3 Dark Ages Cold Period (DACP, 600 CE – 950 CE)

Drangajökull's two advances at ~560 CE and ~950 CE correspond to the Dark Ages Cold Period (DACP). During this period, terrestrial sites elsewhere in Iceland document rapidly decreasing lake temperatures and enhanced terrestrial soil erosion at Haukadalsvatn and Hvítárvatn (Fig. 3.10d-d; Geirsdóttir et al., 2013), enhanced glacial erosion of Langjökull (Fig. 3.11d; Larsen et al., 2011) and moraines reflecting enhanced glacial activity to the east on Tröllaskagi (Fig. 3.11f; Stötter et al., 1999). Both episodes of terrestrial cooling in Vestfirðir are also supported by evidence from the marine realm indicating a cooler NIIC (Castañeda et al., 2004; Ólafsdóttir et al., 2010), and increased IP_{25} implying greater transport of sea ice onto the North Icelandic Shelf (Fig. 3.11g; Cabedo-Sanz et al., 2016). The advance at ~560 CE may be synchronous with a cold period (~536-600 CE) documented in Eurasia likely driven by radiative forcing linked to large volcanic eruptions and sustained by ocean and sea-ice feedbacks (Büntgen et al., 2016). The latter episode of Drangajökull's

advance at ~950 CE correlates with glacial advances across the Northern Hemisphere (Solomina et al., 2016).

3.7.4 Medieval Warm Period (MWP, 950 CE – 1250 CE) and LIA (1250 – 1850 CE)

The retreat of Drangajökull at ~1250 CE is anomalous considering Icelandic composite lake records (Fig. 3.10c-d), chironomid-based lake temperatures (Axford et al., 2009; Holmes et al., 2016) and marine SSTs (Sicre et al., 2011; Moossen et al., 2015) documenting widespread cooling and enhanced terrestrial erosion across Iceland and the adjacent North Icelandic Shelf. During the Medieval Warm Period (MWP), higher SSTs west (Moossen et al., 2015) and east (Sicre et al., 2011) of the ice cap were likely associated with higher air temperatures and, hence, glacial recession as reflected by lower MS in lakes EEF and TRK (Fig. 3.11a-b). However, in contrast to Drangajökull's recession, Langjökull initiated its LIA expansion at ~1250 CE (Larsen et al., 2011), likely as a response to multi-decadal volcanism and subsequent sea ice expansion (Zhong et al., 2010; Miller et al., 2012). As regional cooling progressed, abrupt increases in Hvítárvatn's varve thickness at ~1400 CE indicate intensified growth of Langjökull, which coincides with Drangajökull's LIA expansion (Fig. 3.11). The synchronicity between the 1400 CE advances of both ice caps and the rapid increase in sea ice across the North Icelandic Shelf implies ocean surface conditions influenced mass balances of both ice caps, consistent with the findings of Miller et al. (2012). The lack of evidence for expansion of Drangajökull at ~1250 CE may be due to catchment thresholds. Hvítárvatn, which receives meltwater from Langjökull, was already under the influence of the ice cap as early as 5.5 ka and, thus, registered modest increases in glacial sediment at ~1250 CE (Larsen et al., 2012). In contrast, TRK, which currently receives meltwater from Drangajökull, is a threshold lake, and the expansion of Drangajökull into TRK's catchment may not have occurred until after 1400 CE; hence a ~1250 CE expansion would not be recorded.

3.7.5 Role of Sea Ice in Regional Climate Variability

In Iceland, the dependency of coastal summer air temperature on local ocean surface conditions is well documented through the instrumental period (Fig. 3.1; Dickson et al., 1988; Hanna et al., 2006). Considering that most episodes of Drangajökull´s expansion, and hence summer air temperature, align with increases in sea ice abundance on the North Icelandic Shelf (Fig. 3.11), statistical covariance between the two should highlight the degree to which sea ice export impacts the mass balance of the ice cap over the last 3 ka. Seasonal sea ice concentrations exhibit a strong positive correlation with TRK's MS ($R^2 = 0.70$), demonstrating a strong coevolution between growth in seasonal sea ice concentrations and the marginal expansion of Drangajökull, particularly during the LIA (Fig. 3.11). In terms of the coevolution preceding the LIA, EEF's glacial record correlates moderately strong with North Icelandic Shelf sea ice ($R^2 = 0.51$). The statistical evidence presented here suggests that the import of sea ice north of Iceland is coeval to the growth of Drangajökull through the latest 3 ka. Even though relative moisture availability from sea ice's presence may impact glacier growth on the centennial scale, this is strong evidence that colder temperatures either related to the existence of sea ice or partially caused by sea ice helped the glacier expand. As local ice cap activity is the strongest yet available record for Vestfirðir's climate, regional ocean surface conditions appear to exert a significant impact on its state.

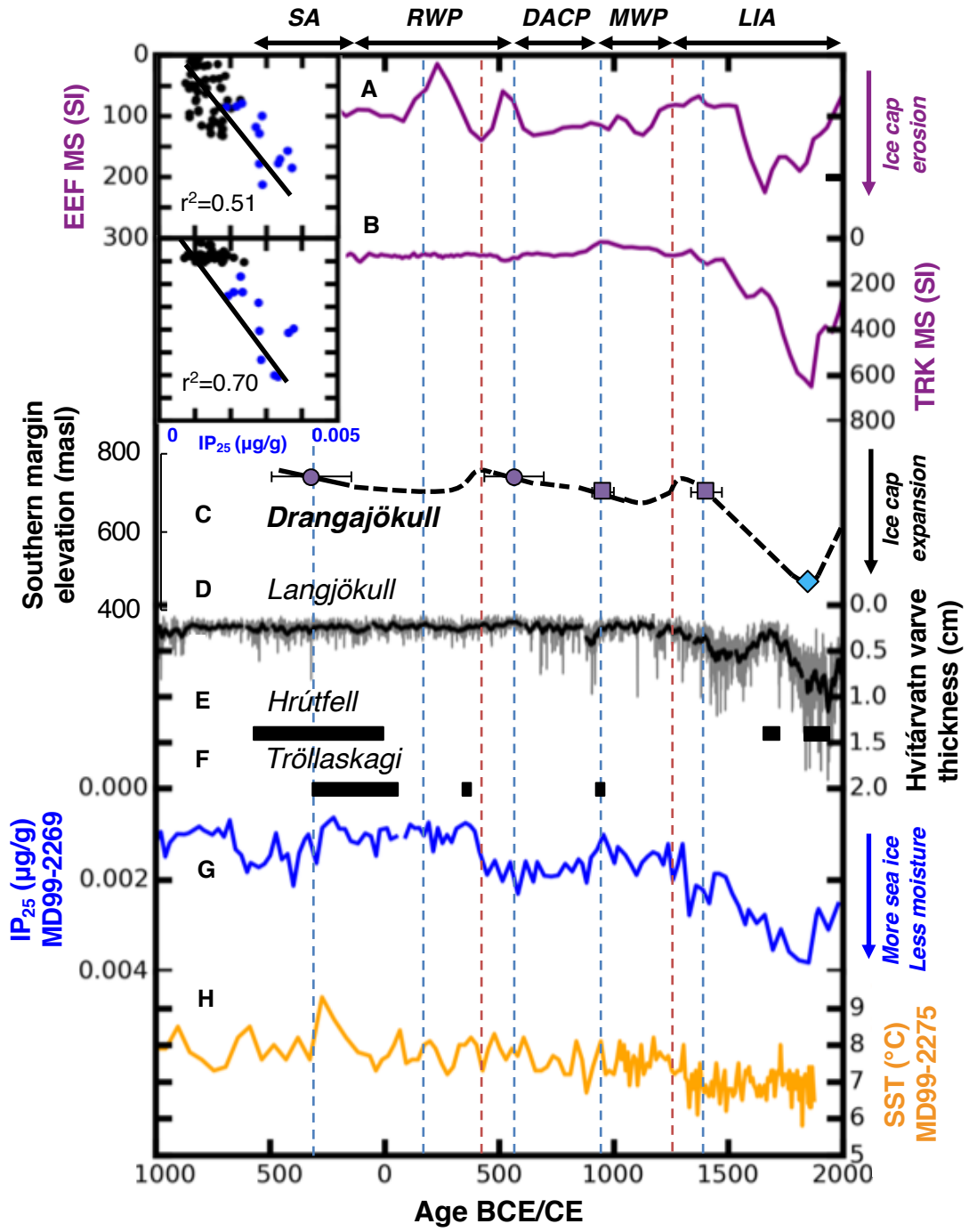

Figure 3.11. *Glacial proxy records illustrated by inverted MS records from A) EEF and B) TRK, C) south margin elevation change, D) inverted Hvítárvatn varve thickness record (Larsen et al., 2011), E) Hrútfell moraine ages (Kirkbride and Dugmore, 2006), Tröllaskagi moraines (Stötter et al., 1999), G) inverted IP_{25} sea ice record from MD99-2269 on the North Icelandic Shelf (Cabedo-Sanz et al., 2016) and H) diatom-inferred SST record from MD99-2275 on the North Icelandic Shelf (Jiang et al., 2015). All records oriented down for cooler conditions. Blue (red) vertical lines represent episodes of Drangajökull advance (retreat). Insets (upper left): Biplots of MD99-2269 IP_{25} versus MS records from lakes EEF and TRK over the last 3 ka. All records were resampled to a common and uniform interval of 51 and 43 years, for EEF and TRK respectively, using the AnalySeries software package (n = 69, Paillard et al., 1996). Blue points highlight LIA conditions (1400 – 1850 CE) and black points for pre-LIA conditions (1000 BCE – 1400 CE).*

3.8 Conclusions

Newly identified moraines, radiocarbon/tephra-constrained lake sediment records and dead vegetation emerging from beneath Drangajökull, Vestfirðir, Iceland, provide new constraints on the episodic expansion of the ice cap during the last 3 ka. Episodes of glacier advance occur at ~320 BCE, 180 CE, 560 CE, 950 CE and 1400 CE (LIA) and intervals of recession at 450 CE, 1250 CE and 1850 CE. The final expansion to its peak LIA dimensions most likely occurred at either 1665 ± 30 CE or 1765 ± 40 CE. The close temporal agreement between Drangajökull's expansion and independently dated, biological proxy records indicating colder summers at these times strengthens our paleoclimate reconstructions. Our network of lake sediment cores and remotely sensed moraines refine the maximum marginal extent of Drangajökull during the LIA to a peak area of ~262 km^2, 1.8 times larger than its areal extent in 2011 (142 km^2, Jóhannesson et al., 2013) and 1.2 times larger than previous estimates by Brynjólfsson et al. (2014). The similarities between Drangajökull's glacial and environmental record and other glacial, lacustrine and sea ice records elsewhere in Iceland suggests that Drangajökull's evolution reflects regional variability of both temperature and precipitation. Furthermore, the local climate of eastern Vestfirðir, most clearly manifested in local ice cap activity, appears to be strongly influenced by nearby ocean surface conditions, SST and sea ice coverage, which are linked to large-scale changes in North Atlantic circulation in response to some combination of orbital changes, explosive volcanism and/or reduced solar irradiance.

3.9 Acknowledgements

This project was supported by RANNIS (grant #130775051) and the ANATILS RANNIS Grant-of-Excellence (grant #141573-052) awarded by the Icelandic Center for Research to ÁG and GHM. We thank Brian Harning for assistance in dead vegetation collection, Devin Hougardy and the University of Minnesota Duluth for lake seismic surveys, and Þorsteinn Jónsson and Sveinbjörn Steinþórsson for diligent lake coring. Siggi and Áslaug are thanked for their warm hospitality during fieldwork at the road's end in Dalbær, west of the ice cap. Joaquín M.C. Belart constructed the southern margin DEM, for which his help is greatly appreciated. The manuscript benefitted from fruitful discussions with John Andrews, Sarah Crump, Chris Florian, Sydney Gunnarson, Steffen Mischke, Simon Pendleton, Tayo van Boeckel, Þorvaldur Þórðarson and the rest of the ANATILS working group. We also thank two anonymous reviewers for their constructive comments, which helped strengthen the manuscript.

3.10 Supplemental Information

Figure 3.1 Methodology: We calculated the co-variance of summer (JJA average) screen-level air temperature (Legates and Willmott, 1990) over Drangajökull to summer sea-surface temperatures (JMA, 2006) across the North Atlantic from 1950 to 2010. Temperatures at each pixel were de-trended to remove correlations associated with linear trends in the data (due to global warming). Pixels where the correlation is positive indicate that warm (cold) sea-surface temperature years were associated with warm (cold) air temperature years near Drangajökull. Pixels where the correlation is negative indicate that warm (cold) summer sea-

surface temperatures were associated with cold (warm) summer air temperatures near Drangajökull. The location of highest positive correlation to the northeast of Drangajökull corresponds with the location of core MD99-2275 (Jiang et al., 2015).

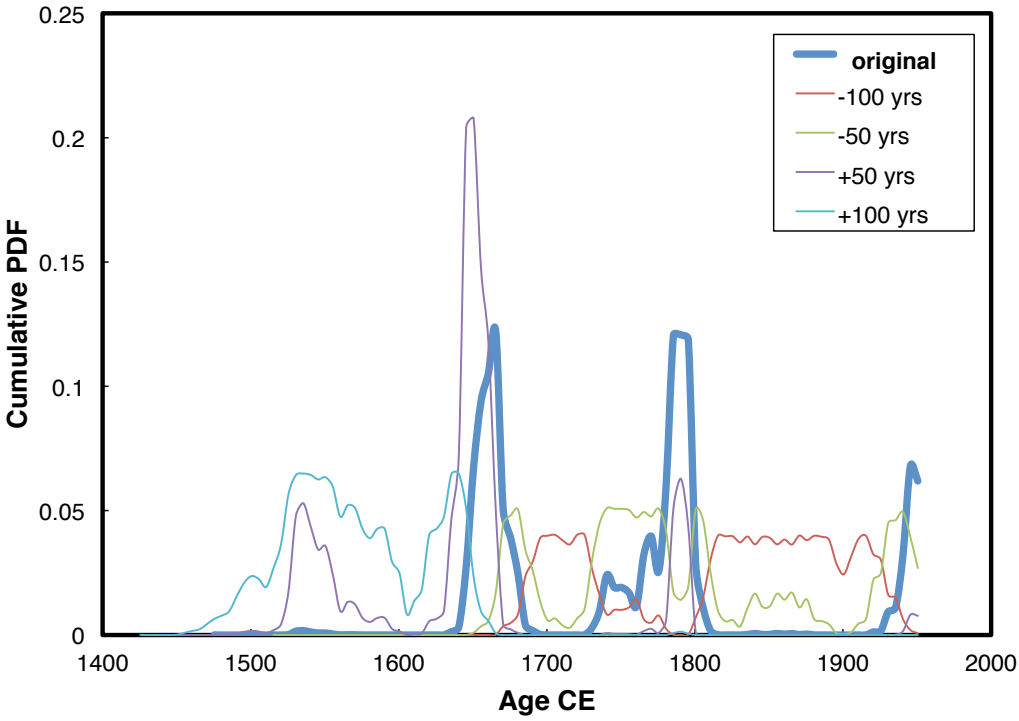

Figure S3.12: *Plot of the original calibrated cumulative PDF (bold blue line) for the 7 emerging dead vegetation samples with ^{14}C dates between 250 and 175 BP. By altering the original ^{14}C dates by -100, -50, +50 and +100 years and summing the new individual PDFs from recalibrated ages, we show that the three peaks revealed in the original cumulative PDF are unique and not an artifact of the Late Holocene's variable calibration curve.*

4 Punctuated Holocene Climate of Vestfirðir, Iceland, Linked to Internal/External Variables and Oceanographic Conditions[3]

4.1 Abstract

Emerging Holocene paleoclimate datasets point to a non-linear response of Icelandic climate against a background of steady orbital cooling. The Vestfirðir peninsula (NW Iceland) is an ideal target for continued climate reconstructions due to the presence of a small ice cap (Drangajökull) and numerous lakes, which provide two independent means to evaluate existing Icelandic climate records and to constrain the forcing mechanisms behind centennial-scale cold anomalies. Here, we present new evidence for Holocene expansions of Drangajökull based on ^{14}C dates from entombed dead vegetation as well as two continuous Holocene lake sediment records. Lake sediments were analyzed for both bulk physical (MS) and biological (%TOC, $\delta^{13}C$, C/N, and BSi) parameters. Composite BSi and C/N records from the two lakes yield a sub-centennial qualitative perspective on algal (diatom) productivity and terrestrial landscape stability, respectively. The Vestfirðir lake proxies suggest initiation of the Holocene Thermal Maximum by ~8.8 ka with subsequent and pronounced cooling not apparent until ~3 ka. Synchronous periods of reduced algal productivity and accelerated landscape instability point to cold anomalies centered at ~8.2, 6.6, 4.2, 3.3, 2.3, 1.8, 1, and 0.25 ka. Triggers for cold anomalies are linked to variable combinations of freshwater pulses, low total solar irradiance, explosive and effusive volcanism, and internal modes of climate variability, with cooling likely sustained by ocean/sea-ice feedbacks. The climate evolution reflected by our glacial and organic proxy records corresponds closely to marine records from the North Iceland Shelf.

4.2 Introduction

Spatially distributed and temporally accurate paleoclimate records are required to both disentangle natural variations in Earth's climate from anthropogenic change (Masson-Delmotte et al., 2013), and to evaluate the performance of climate models (Braconnot et al., 2012). Due to the amplification and sensitivity of climate change inherent to the cryosphere (Serreze and Barry, 2011), targeting the higher latitudes for such reconstructions is essential. Iceland's geographic location within the North Atlantic is ideally situated for high-latitude Holocene climate reconstructions due to its position at the confluence of major oceanic and atmospheric circulation patterns integral to global heat distribution (Fig. 4.1). As these circulation patterns change, the resultant climate evolution influences the status of Icelandic ice caps and leaves continuous archives of past terrestrial and marine environments in sedimentary records (Geirsdóttir et al., 2009a). Marine records are complicated by the

[3] Harning, D.J., Geirsdóttir, Á., Miller, G.H., 2018. Punctuated Holocene climate of Vestfirðir, Iceland, linked to interal/external variables and oceanographic conditions. Quaternary Science Reviews 189, 31-42.

integration of climate signals over various portions of the water column (e.g., Kristjánsdóttir et al., 2016), salinity and relative sea level changes (e.g., Quillmann et al., 2010) and dating problems due to variable ^{14}C reservoir corrections (e.g., Eiríksson et al., 2004). Thus, Iceland's terrestrial realm can provide valuable insight into the nature and causes of northern North Atlantic Holocene climate variability.

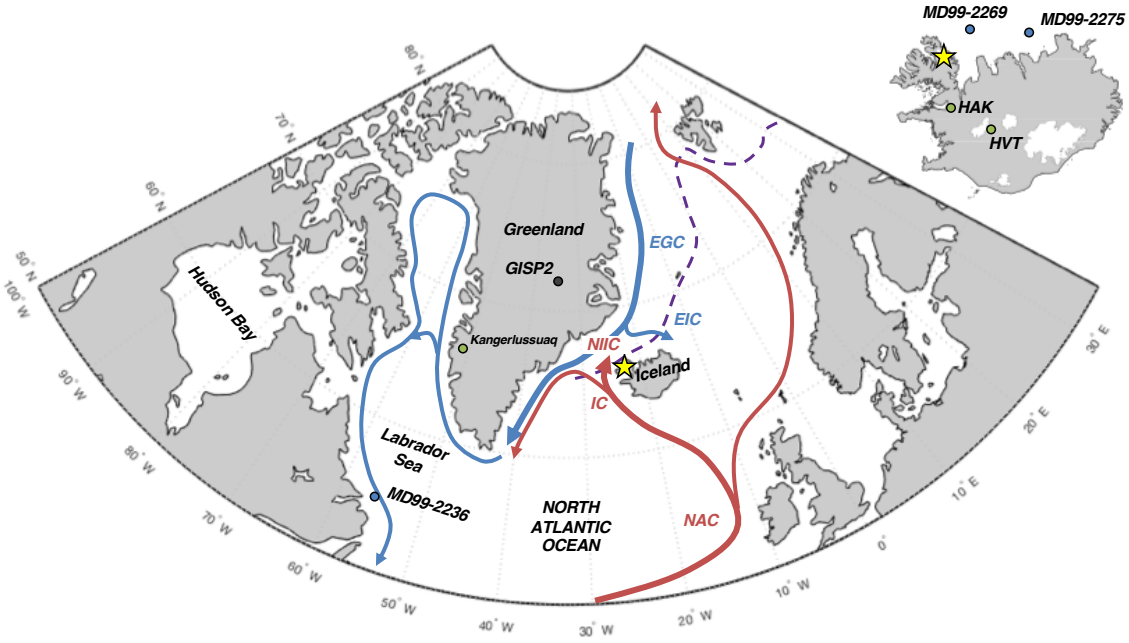

Figure 4.1. *Northern North Atlantic region, including simplified ocean surface currents and 1870-1920 CE sea ice edge position (dashed purple line, Divine and Dick, 2007). Key sites mentioned in text are labeled (blue marine sediment cores and green lake sediment cores), as well as the location of Vestfirðir (yellow star). HAK = Haukadalsvatn, HVT = Hvítárvatn.*

During the Holocene, the orbitally driven reduction of Northern Hemisphere (NH) summer insolation has been the predominate control over Iceland's climate over millennial timescales (Larsen et al., 2012; Geirsdóttir et al., 2013; Jiang et al., 2015). Along Iceland's insular shelves, the insolation forcing is recorded by general cooling of surface currents through the Holocene (Andersen et al., 2004; Castañeda et al., 2004; Giraudeau et al., 2004; Smith et al., 2005; Solignac et al., 2006; Bendle and Rosell-Melé, 2007; Justwan et al., 2008; Ólafsdóttir et al., 2010; Jiang et al., 2015; Moossen et al., 2015; Kristjánsdóttir et al., 2016) and by increases in sea ice during the late Holocene (Moros et al., 2006; Cabedo-Sanz et al., 2016). However, emerging datasets point to a non-linear response of Icelandic climate to a first-order cooling trend (Larsen et al., 2012; Geirsdóttir et al., 2013). Notable cold perturbations include the '8.2 ka event' (Castañeda et al., 2004; Larsen et al., 2012; Quillmann et al., 2012; Geirsdóttir et al., 2013; Jiang et al., 2015), likely induced by meltwater floods from the waning Laurentide Ice Sheet (Alley and Ágústdóttir, 2005; Rohling and Pälike, 2005), and the Little Ice Age (LIA, 1250-1850 CE), linked to sustained volcanism and subsequent sea ice expansion (Miller et al., 2012; Sicre et al., 2013). The mechanisms behind other Holocene perturbations however remain ambiguous (Larsen et al., 2012; Geirsdóttir et al., 2013).

In this study, we focus on the Vestfirðir peninsula, where recent studies have constrained the Holocene evolution of the region's local ice cap, Drangajökull (Brynjólfsson

et al., 2015a; Harning et al., 2016a, b). We expand upon these studies by presenting new evidence for the timing of Drangajökull expansions based on ^{14}C-dated in situ dead vegetation revealed from beneath the receding ice margins and in the physical characteristics of nearby lake sediment. Second, we develop a series of continuous and qualitative lacustrine-based Holocene climate records to make inferences about past spring/summer temperature and validate the glacier record. Ultimately, our new Vestfirðir climate records are employed to evaluate the nature of and further constrain the causes of Icelandic climate variability. Considering the vulnerability of Iceland's terrestrial climate to dynamic ocean currents, Vestfirðir is an ideal target for assessing the marine influence on Icelandic climate during the Holocene.

4.3 Regional Setting

4.3.1 Vestfirðir Peninsula

Vestfirðir comprises Iceland's northwesternmost extension into Denmark Strait and, as such, is the closest sector to the instrumental (post 1870 CE) sea ice edge (Fig. 4.1, Divine and Dick, 2007). The warm and saline Irminger Current (IC) branches off the North Atlantic Current (NAC) and flows north along the west coast of Iceland until it reaches Vestfirðir where it turns east along the North Iceland Shelf as the cooler, lower-salinity North Iceland Irminger Current (NIIC). The East Icelandic Current (EIC) branches off the East Greenland Current (EGC) and flows eastward along the north coast of Iceland (Fig. 4.1). Sea ice rarely forms along the insular shelves, but sea ice exported from the Arctic Ocean via the EGC is commonly transported along north Iceland's coastline via the EIC.

Regional bedrock on Vestfirðir is primarily composed of Neogene tholeiitic lava successions separated by thin sedimentary units of fluvial and aeolian origin (Harðarson et al., 2008). On eastern Vestfirðir, the northeastern highland plateau hosts the polythermal ice cap, Drangajökull (~142 km^2 area in 2011 CE; Jóhannesson et al., 2013). Three surging outlet glaciers drain most of the east, north and west catchments through deeply incised valleys (Fig. 4.2b). Each surging outlet glacier occupies a cirque-like bowl whereas the non-surging southern half of the ice cap mantles a relatively low-relief high plateau (Magnússon et al., 2016). Drangajökull's modern glacier-wide equilibrium line altitude (ELA) is considerably lower than other Icelandic ice caps with a 2000-2015 ELA at ~660 m asl. This low ELA likely reflects the ice cap's proximity to the relatively low SST of the adjacent ocean resulting in short, cool summers (www.vedur.is) and high snow accumulation (Belart et al., 2017).

4.3.2 Selected lakes (Table 4.1)

Non-glacial lake Skorarvatn (Fig., 4.2c, SKR; 66.25627°N, 22.32213°W) is situated in a low mountain pass (183 m asl) ~3 km north of Drangajökull and ~4 km from the sea. The threshold for receiving glacier meltwater terminates ~1 km closer to Drangajökull at ~420 m asl. Skorarvatn reaches a maximum depth of 25 m with a lake surface area of ~0.2 km^2 and catchment area of ~1.2 km^2. Modern catchment vegetation is sparse and dominated by a variety of moss species, which tend to clump on small tussocks. The only apparent aquatic vegetation is algae and moss.

Pro-glacial lake Tröllkonuvatn (Fig. 4.2d, TRK; 66.14252°N, 22.05607°W) is a higher-elevation (366 m asl) lake on Drangajökull's eastern periphery. Total lake surface area is ~1.3 km^2 and the catchment area, including that beneath the extant ice cap, is ~9.4 km^2. The catchment is composed primarily of exposed bedrock and block fields with negligible accompanying vegetation, although isolated pockets exist near river inlets. Tröllkonuvatn currently receives sediment-laden glacial meltwater through an inlet located along the southwestern shoreline in addition to a second inlet into the lake's small southeastern sub-basin. During the LIA, Drangajökull occupied Tröllkonuvatn (Fig. 4.2d), eroding sediment from most of the lake, but left undisturbed sediment in the small southeastern basin (16.4 m depth), preserving a continuous sedimentary sequence since local deglaciation ~9 ka (Harning et al. 2016a, b).

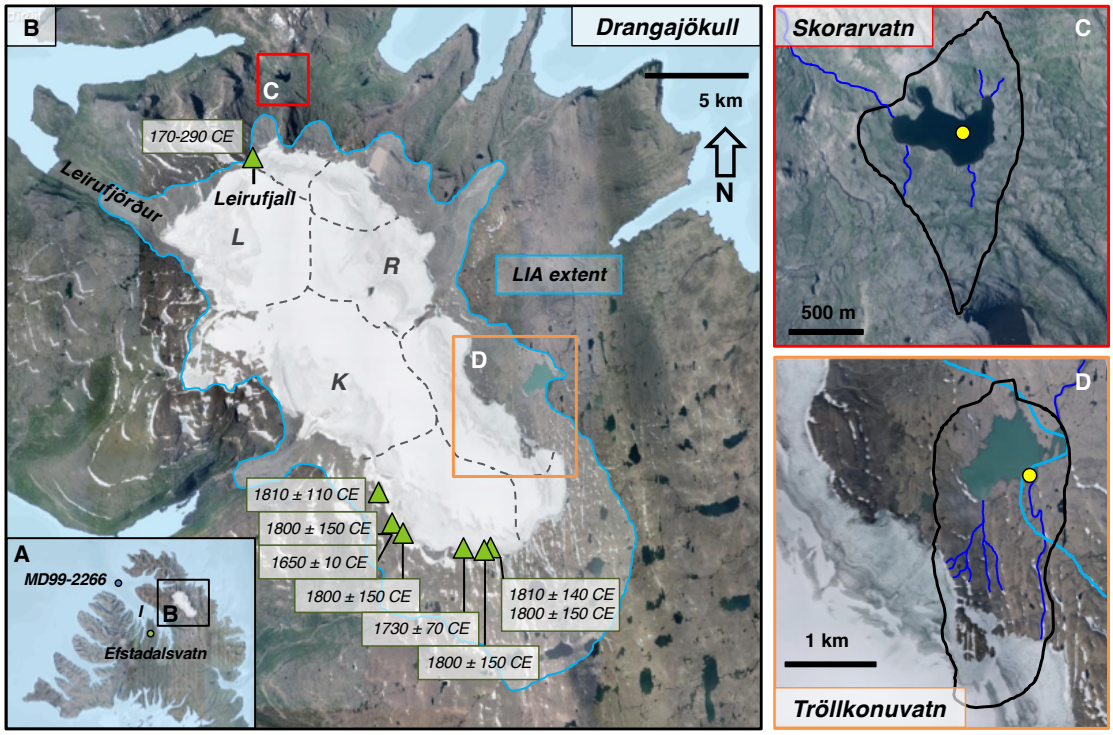

Figure 4.2. *Overview map of study area. A) Vestfirðir peninsula, I=Ísafjarðardjúp, B) Drangajökull and emerging dead vegetation sampling sites (green triangles, Harning et al., 2016a, this study). Ice catchments delineated with dashed gray lines after Magnússon et al. (2016). Little Ice Age (LIA) extent after Harning et al. (2016a). The three surging outlet glaciers labeled as K (Kaldalónsjökull), L (Leirufjarðarjökull) and R (Reykjarfjarðarjökull). C and D) location of this study's two lakes, their sediment core sites (yellow circles) and lake catchments (black lines after Harning et al. (2016a)). 2005 base images courtesy of Loftmyndir ehf.*

Table 4.1. *Lake information.*

Lake	Lake type	Core name	Elevation (m asl)	Coordinates	Water depth (m)	Total core length (m)
Skorarvatn	Non-glacial	SKR14-6A/4A-1N	183	66° 15.376'N 22° 19.328'W	25	2.86
Tröllkonuvatn	Threshold	TRK14-3A-2B	366	66° 8.551'N 22° 3.364'W	16.4	4.5

4.4 Methods

4.4.1 Entombed Dead Vegetation

Harning et al. (2016a) reported one ^{14}C date from an in situ dead vegetation sample from Leirufjall (Fig. 4.2b), which demonstrated the nature of non-erosive ice occupying this low relief ice divide. In late August 2016, six additional in situ dead vegetation samples were collected from the same location, each <1 m from the receding ice margin. The new specimens span a horizontal distance of 23 m and elevational range of 3 m. The ice catchment feeding this sector of Drangajökull is the smallest of the ice cap (Fig. 4.2b) and is not associated with historically documented surges (Brynjólfsson et al., 2015b). Samples were prepared and dated by radiocarbon after Miller et al. (2017) (Table 4.2). Ages of these seven samples, in addition to eight samples collected from the southern margin (Harning et al., 2016a), are reported as a single cumulative probability density function (PDF) in calibrated years CE, using OxCal 6.0 (Bronk Ramsey, 2009) and the IntCal13 calibration curve (Reimer et al., 2013).

Table 4.2. *Emerging dead vegetation radiocarbon information.*

Lab ID	Material	Latitude	Longitude	Elevation (m asl)	$\delta^{13}C$ (‰)	Fraction modern	Conventional ^{14}C age ± σ	Calibrated age CE (BP ± σ)
UCIAMS-134344*	Terr. moss	66° 13.200'N	22° 20.468'W	685	N/A	0.7948	1845 ± 40	180 (1770 ± 50)
CURL-21571	Terr. moss	66° 13.151'N	22° 20.411'W	724	-22.2	0.7956	1835 ± 20	170 (1780 ± 40)
CURL-21582	Terr. moss	66° 13.149'N	22° 20.405'W	722	-22.0	0.8022	1770 ± 15	280 (1670 ± 40)
CURL-21556	Terr. moss	66° 13.147'N	22° 20.401'W	721	-25.0	0.8051	1740 ± 20	290 (1660 ± 40)
CURL-21561	Terr. moss	66° 13.145'N	22° 20.398'W	722	-24.5	0.8031	1760 ± 15	280 (1670 ± 40)
CURL-21547	Terr. moss	66° 13.145'N	22° 20.396'W	722	-24.5	0.7951	1840 ± 15	170 (1780 ± 40)
CURL-21558	Terr. moss	66° 13.141'N	22° 20.393'W	724	-24.9	0.8031	1760 ± 15	280 (1670 ± 40)
CURL-18795*	Terr. moss	66° 5.047'N	22° 11.864'W	454	-26.9	0.9695	250 ± 20	1650 (300 ± 10)
CURL-19491*	Terr. moss	66° 4.512'N	22° 7.566'W	555	-22.0	0.9727	220 ± 20	1730 (220 ± 70)
CURL-18798*	Terr. moss	66° 5.077'N	22° 11.905'W	464	-24.2	0.9737	215 ± 20	1800 (150 ± 150)
CURL-18810*	Terr. moss	66° 4.810'N	22° 11.548'W	424	-23.5	0.9741	210 ± 20	1800 (150 ± 150)
CURL-19485*	Terr. moss	66° 4.532'N	22° 5.809'W	601	-22.4	0.9743	210 ± 20	1800 (150 ± 150)
CURL-18814*	Terr. moss	66° 4.463'N	22° 6.111'W	582	-26.6	0.9746	205 ± 25	1800 (150 ± 150)
CURL-19487*	Terr. moss	66° 4.532'N	22° 5.809'W	601	-19.9	0.9783	175 ± 20	1810 (140 ± 140)
CURL-18809*	Terr. moss	66° 5.663'N	22° 12.304'W	535	-28.8	0.9890	90 ± 20	1810 (140 ± 110)

*Previously published in Harning et al. (2016a)

4.4.2 Physical and Biological Climate Proxies from Lake Sediment

In 2014, sediment cores were recovered from each lake's deepest basin using a percussion driven piston corer in 3 m-long sections. To capture a continuous sedimentary sequence, metal casings were emplaced to guide the piston corer into the same hole for the second and final drive. Magnetic susceptibility (MS) was measured at 0.5 cm intervals on split cores from each lake using a GeoTek Multi-Sensor Core Logger at the University of Iceland. Sediment subsamples (~1 cm^3) taken at ~0.5 cm and ~1 cm intervals from Skorarvatn and Tröllkonuvatn, respectively, were measured for total carbon (TC), total nitrogen (TN), and $\delta^{13}C$ (relative to VPDB) following standard procedures on an elemental analyzer at the

University of California-Davis. Biogenic silica (BSi) was measured in triplicates at the University of Colorado-Boulder via Fourier Transform Infrared Spectroscopy (c.f., Florian, 2016), resulting in low instrumental error (0.087-4.334 absorbance units). Skorarvatn's BSi record was previously reported in Harning et al. (2016b) and we have since completed a complimentary BSi record from Tröllkonuvatn.

4.4.3 Lake Sediment Chronology: Tephra and ^{14}C

Age models using diagnostic tephra of known age and ^{14}C ages of plant macrofossils (Table 4.3) are detailed in Harning et al. (2018) and presented in Fig. 4.3. Maximum age uncertainty, calculated in the CLAM age modeling software (95% confidence of 1000 iterations, Blaauw, 2010), is highest for both lakes from the earliest Holocene to ~8 ka (±200 years). For the remainder of the Holocene, age uncertainty rarely exceeds 100 years and is typically below 50 years for the interval corresponding to the Neoglacial.

Table 4.3. *Lake sediment radiocarbon information.*

Lake (sediment depth, cm)	Lab ID	Material	$\delta^{13}C$ (‰)	Fraction modern	Conventional ^{14}C date ± σ	Calibrated age BP ± σ	Reference
Skorarvatn (43)	CURL-21039	moss	-24.3	0.6102	3970 ± 20	4460 ± 50	Harning et al. (2016b)
Skorarvatn (59)	CURL-21034	moss	-25.3	0.5529	4760 ± 20	5530 ± 50	Harning et al. (2016b)
Skorarvatn (82)	CURL-21035	moss	-26.3	0.5136	5355 ± 20	6120 ± 90	Harning et al. (2016b)
Skorarvatn (140.5)	CURL-21036	moss	-29.7	0.4079	7205 ± 25	8000 ± 20	Harning et al. (2016b)
Skorarvatn (214.8)	CURL-19489	moss	-23.9	0.356	8295 ± 25	9340 ± 60	Harning et al. (2016b)
Skorarvatn (222.5)	CURL-21041	moss	-23.3	0.33	8905 ± 35	10060 ± 120	Harning et al. (2016b)
Skorarvatn (283.5)	CURL-21033	moss	-25.0	0.3203	9145 ± 35	10300 ± 70	Harning et al. (2016b)
Tröllkonuvatn (18)	CURL-19503	moss	-22.2	0.9348	540 ± 15	540 ± 10	Harning et al. (2016a)
Tröllkonuvatn (30.5)	UCIAMS-165968	moss	N/A	0.8686	1130 ± 20	1020 ± 50	Harning et al. (2016a)
Tröllkonuvatn (165.5)	CURL-21038	moss	-21.6	0.6333	3670 ± 15	4020 ± 50	Harning et al. (2018)
Tröllkonuvatn (285.5)	CURL-21037	moss	-23.1	0.4858	5800 ± 20	6610 ± 40	Harning et al. (2018)
Tröllkonuvatn (394)	CURL-19502	moss	-24.4	0.3729	7925 ± 25	8750 ± 100	Harning et al. (2016b)

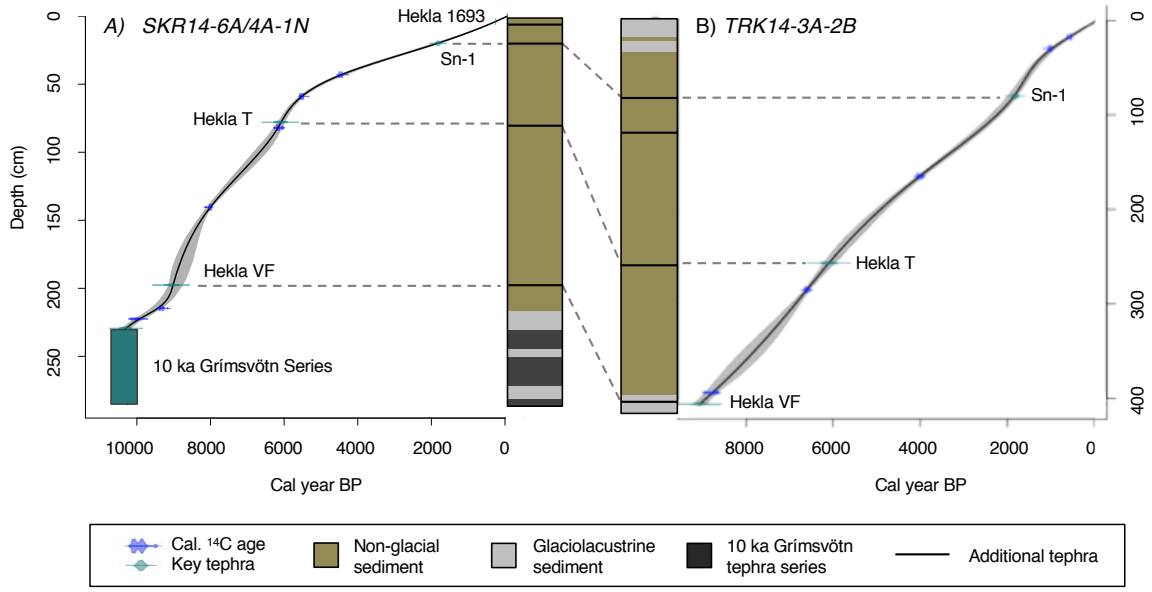

Figure 4.3. *CLAM age models and simplified stratigraphy for A) Skorarvatn and B) Tröllkonuvatn. Gray shaded areas denote the 95% confidence envelope (Blaauw, 2010). Radiocarbon information provided in Table 4.3.*

4.5 Results and Interpretations

4.5.1 Entombed Dead Vegetation

Radiocarbon dates on dead vegetation exposed by recent ice cap recession define the death of the plant due to persistent expansion of the cryosphere. This results from either the immediate transformation of new snow to ice or expansion of non-erosive ice at each collection site following persistently cooler summers (e.g., Miller et al., 2013). Based on a single ^{14}C-dated emerging dead vegetation sample from atop Leirufjall (Table 4.2, UCIARMS-134344), Harning et al. (2016a) proposed an expansion of Drangajökull's northern margin at ~180 CE. Previously published emerging dead vegetation samples from the low-relief southwestern margin (Fig. 4.2b, n=8) suggest that the ice cap expanded across these sites during the LIA, at either ~1660 or 1770 CE (Fig. 4.4d, Harning et al., 2016a).

Our six new samples from the northern margin support the interpretation of Drangajökull's expansion early in the first millennium CE, at 150-200 CE. However, the expanded dataset also reveals a second, slightly younger PDF peak, at 250-300 CE (Fig. 4.4d). We suggest that the initial 150-200 CE snowline depression killed several of our samples, but was followed by a brief warming, re-exposing Leirufjall's marginal landscape, before Drangajökull expanded again, killing the younger plants at 250-300 CE. For the dead plants from the earlier expansion to remain preserved, the warm interval is required to be short with very little marginal meltwater, the most effective erosive agent. Plants that recolonized that newly re-exposed margin, were killed by the second snowline depression, and remained continually beneath ice until the recent warming. The difference in emerging dead vegetation ^{14}C ages from the northern (average elev. 717 m asl) versus southern margin samples (average elev. 527 m asl) likely reflects general snowline depression associated with Neoglacial cooling (e.g., Harning et al., 2016a; Miller et al., 2017).

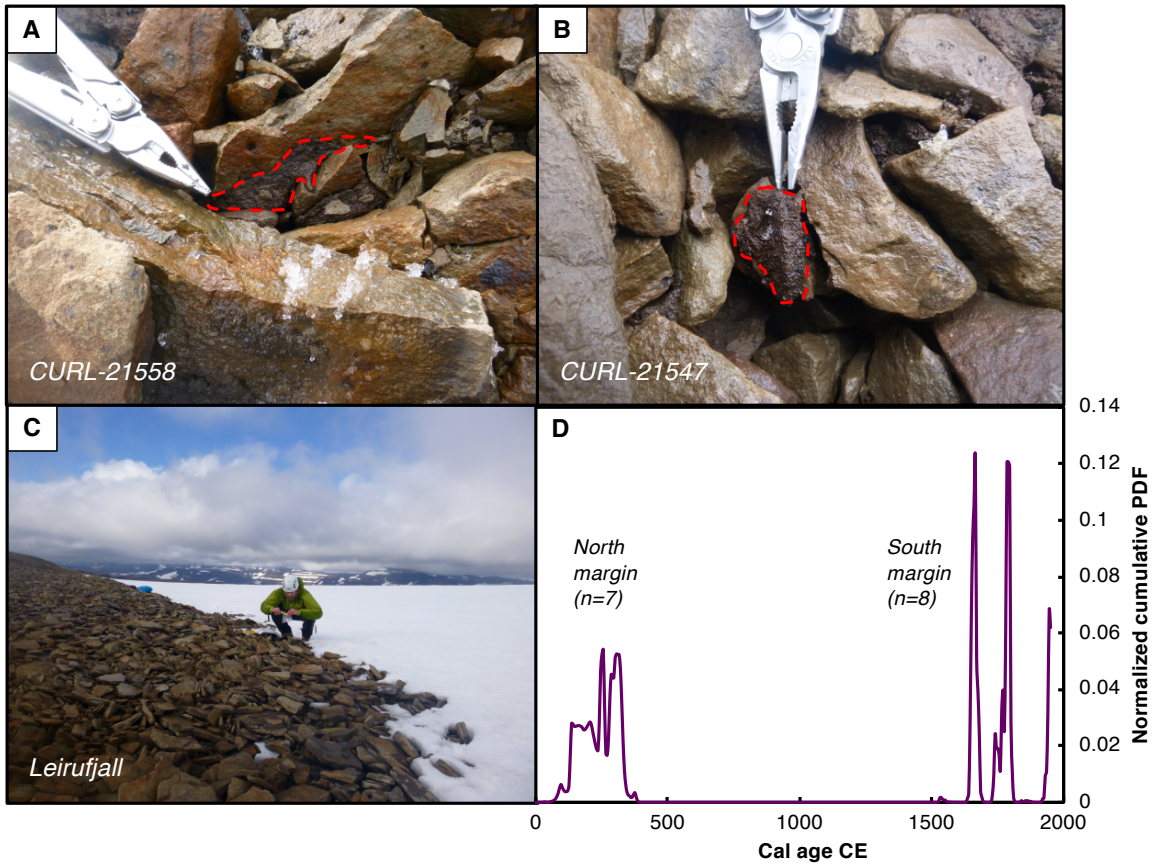

Figure 4.4. *Cumulative PDF, and photos of in situ emerging dead vegetation (dashed red outlines) from the northern margin atop Leirufjall. A) sample CURL-21558, B) sample CURL-21547, C) collecting samples along the low-relief glacier margin, D) cumulative PDF of calibrated ages from emerging dead vegetation (Harning et al., 2016a, this study). Photos taken in August 2016.*

4.5.2 Lake Sediment Proxy Records

Physical proxies (i.e., MS, density) provide information about the contribution of minerogenic sediment relative to organic sediment in the lake. Subglacial erosion of the basaltic bedrock produces minerogenic rock flour with relatively high MS in downstream lake sediment records. Thus, during glacial occupation of a lake catchment, MS can be used to make inferences about past glacier erosion rates (Larsen et al., 2012). When ice caps are absent from Icelandic lake catchments, discrete MS peaks are generally indicative of minerogenic tephra deposits (Christensen, 2013). However, in some lakes, particularly those with high topographic relief, MS tracks landscape destabilization of soil by wind and water (e.g., Gathorne-Hardy et al., 2009).

Iceland's basaltic bedrock has negligible amounts of carbon such that the total carbon measured in lake sediment generally reflects total organic carbon (TOC). Percent TOC is a generic proxy for both autochthonous and allochthonous carbon sources, whereas C/N can distinguish the two (algae=4 to10, vascular plants >20; Meyers, 2003). For Icelandic lakes, we interpret increasing C/N to represent a larger contribution of soil carbon eroded during colder summers with dry/windy winters (Geirsdóttir et al., 2009b). The $\delta^{13}C$ value can reflect the relative input of carbon from algae (-17.0±8.3‰), aquatic macrophytes (-16.6±6.0‰),

terrestrial plants (-27.4±1.9‰), soil (-26.1±1.0‰) and peat (-28.5±0.6‰) (Skrzypek et al., 2008; Wang and Wooller, 2008; Langdon et al., 2010; Florian, 2016). If organic matter source is constant, and algal communities are instead the dominant influence on $\delta^{13}C$, then increased (decreased) algal productivity will increase (decrease) bulk $\delta^{13}C$ values (Meyers, 2003). BSi tracks the concentration of biogenic silica, a proxy for algal (diatom) productivity (Conley and Schelske, 2001). Assuming little change in the overall sedimentation rate, changes in BSi reflect qualitative changes of spring/summer lake temperature in Iceland (Geirsdóttir et al., 2009b), as seen elsewhere in the Arctic (McKay et al., 2008).

4.5.2.1. Low-Elevation, Non-Glacial Lake Skorarvatn

Based on multiple layers of the 10 ka Grímsvötn tephra series (Harning et al., 2018), proto-Drangajökull retreated from Skorarvatn's central basin before 10.3 ka (Harning et al., 2016b). However, the waning ice cap occupied a portion of the catchment until ~9.3 ka, as indicated by glaciolacustrine sediment with high MS and low %TOC (Fig. 4.5). At ~9.4 ka, MS increases, which we interpret to reflect increased discharge of glacial sediment resulting from a minor readvance of the glacier's northern margin. Following lake catchment deglaciation at 9.3 ka, Drangajökull never advanced into Skorarvatn's catchment during the remainder of the Holocene, as shown by low and stable MS levels and elevated %TOC (Fig. 4.5).

The organic matter in the remainder of the sediment core originates from variable contributions of catchment soil, algae and terrestrial and aquatic vegetation (Fig. 4.6). Between ~9.3 and 7.9 ka, C/N is lowest of the record and $\delta^{13}C$ is the highest, reflecting the dominance of aquatic contributions to TOC (Fig. 4.5). This could be interpreted as either little terrestrial soil and vegetation erosion and/or a predominance of aquatic algal productivity, as indicated by high BSi values during this time (Fig. 4.5). A notable perturbation in this trend is evident between ~8.2 and 8 ka, when C/N sharply rises with an accompanying low $\delta^{13}C$ and BSi values. Together, these proxies suggest increased contributions of terrestrial plants and soils along with significant reductions in algal productivity peaking at ~8.2 ka. Except for the 8.2-8.0 ka perturbation, Skorarvatn's catchment was relatively stable between ~9.3 and 7.9 ka, with little catchment erosion (low C/N). In conjunction with elevated algal productivity (high BSi), these data point to generally warm springs/summers.

After ~7.9 ka, C/N increases, $\delta^{13}C$ decreases and BSi begins an irregular decline. This first-order trend continues until ~3 ka, which reflects progressively greater contributions of terrestrial plants and soils relative to algae (Fig. 4.5). Superimposed on this trend are notable excursions in C/N, $\delta^{13}C$ and BSi (at ~7, 6.5, 6.2-6, 5.2-4.7 and 4.2-4 ka), which likely reflect accelerated terrestrial influx and/or reduced algal productivity in and around Skorarvatn. The first-order trend suggests decreasing local spring/summer temperatures whereas the perturbations record transient times of further cooling.

Between ~3 and 1 ka, Skorarvatn's C/N values increase. However, in contrast to the earlier portions of the record that show an inverse relationship between C/N and $\delta^{13}C$, $\delta^{13}C$ only briefly follows this trend (Fig. 4.5). At ~2.4 ka, $\delta^{13}C$ abruptly increases as C/N continues to gradually increase. Higher C/N indicates increasing relative contributions from vascular plants (terrestrial and aquatic). Although the abrupt shift toward heavy $\delta^{13}C$ values can signify either a change in organic matter source or elevated algal productivity, the corresponding decline in BSi suggests a changing organic matter source. Based on Icelandic

vegetation studies (Skrzypek et al., 2008; Wang and Wooller, 2008; Langdon et al., 2010; Florian, 2016), the vegetation group most enriched in ^{13}C is aquatic plants (Fig. 5.6). Therefore, we suggest that at ~2.4 ka, there was a shift in the local ecosystem where contributions from aquatic vegetation (high C/N, high $\delta^{13}C$) began to dominate over terrestrial vegetation and soils (high C/N, low $\delta^{13}C$). This may have resulted from either 1) depletion of soils and terrestrial vegetation and/or 2) perennially frozen ground preventing the mobilization of terrestrial vegetation and soils. In either case, a transition toward cooler springs/summers at ~2.4 ka is suggested.

At ~1 ka, C/N plateaus and then gradually declines toward present values whereas $\delta^{13}C$ step shifts toward lower values. Both records are still indicative of some terrestrial contribution to the lake. However, the shift from a positive to slightly negative C/N slope may suggest relatively less influx of terrestrial material (Fig. 4.5), likely reflecting similar conditions to those previously suggested for the changes observed at ~2.4 ka. After 1 ka BSi remains low, consistent with other Icelandic lake records documenting the lowest algal productivity of the Holocene during the last millennium (Axford et al., 2007; Geirsdóttir et al., 2009b; Larsen et al., 2012; Blair et al., 2015; Florian, 2016).

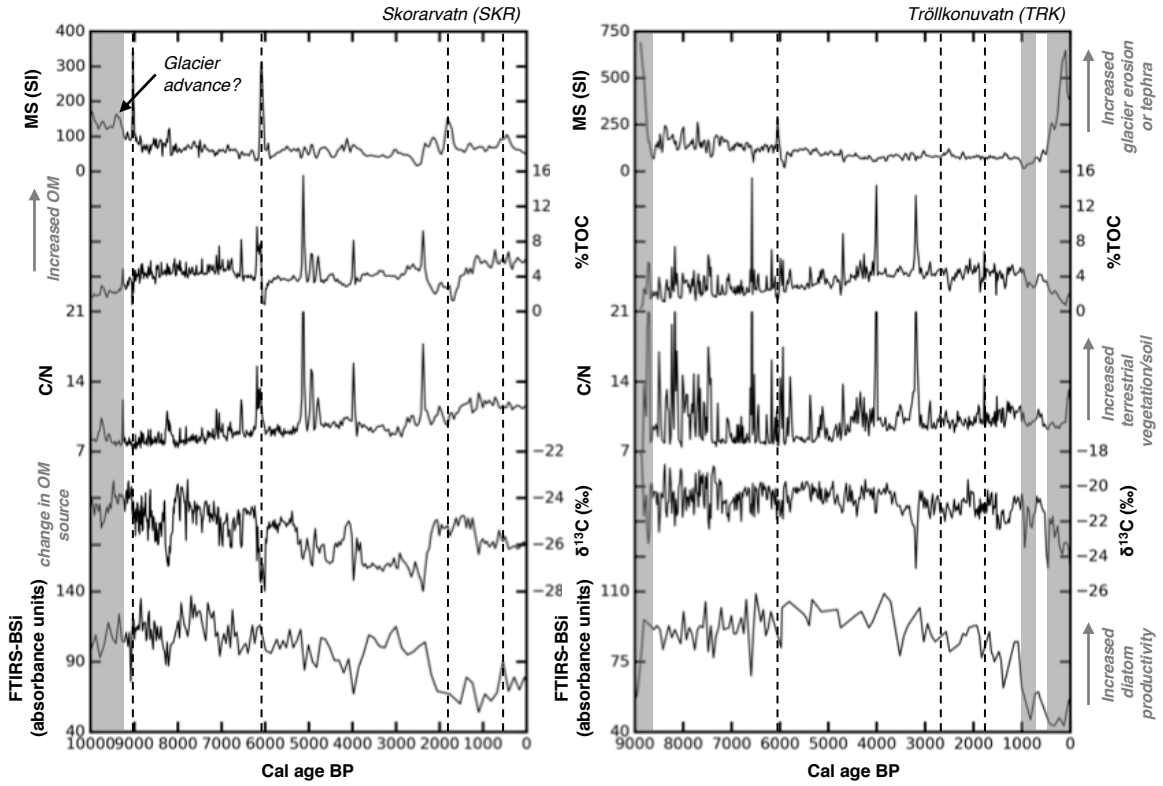

Figure 4.5. *Physical and biological proxies from Skorarvatn and Tröllkonuvatn sediment cores. Gray bars denote glaciolacustrine sediment and dashed black lines demarcate visible tephra detailed in Harning et al. (2018). Gray text provides generalized proxy interpretations.*

4.5.2.2. High-Elevation, Glacial Lake Tröllkonuvatn

Based on a ^{14}C-dated macrofossil at the base of Tröllkonuvatn's organic sediment package, proto-Drangajökull receded from its catchment by ~8.8 ka (Harning et al., 2016b). The low MS through most of the remaining record indicates sedimentation was dominated by non-glacial sources until Drangajökull expanded into Tröllkonuvatn's catchment during the late Holocene (Harning et al., 2016a), evident by two steps of higher MS and/or lower %TOC beginning ~1 ka (Fig. 4.5).

Organic matter archived in Tröllkonuvatn's sediment is predominately sourced from aquatic plants and algae, as indicated by higher δ^{13}C values relative to Skorarvatn throughout the Holocene (Figs. 4.5 and 4.6). Between ~8.8 ka and 5.5 ka, the baselines for C/N (low) and δ^{13}C (high) are suggestive of an algal dominated environment. The periodically high C/N coupled with relatively heavy δ^{13}C indicates the development of larger amounts of aquatic plants relative to terrestrial plants and soils within the newly deglaciated catchment (Fig. 4.5). Notably, C/N and δ^{13}C show values most consistent with terrestrial source, at ~8.2 ka, suggesting that the landscape was the least stable at this time. Tröllkonuvatn's BSi record depicts a gradual increase in algal productivity from ~8.8 to 6.5 ka. The suppressed productivity relative to Skorarvatn may be a result of its higher elevation and associative lower water temperature.

Between ~5.5 and 4 ka, the C/N baseline transitions from flat to a first-order positive slope (Fig. 4.5). Because BSi is relatively stable over this period (constant algal productivity), increasing C/N likely indicates increased terrestrial erosion into the lake. Accordingly, δ^{13}C values exhibit negative departures at ~4.7, 4.4 and 4 ka. From ~3.8-3 ka, 1.8-1.7, and 1.5-1 ka there are notable increases in C/N and decreases in δ^{13}C and BSi values. These episodes likely represent some degree of spring/summer cooling unrelated to glacial occupation of the catchment, which ensued shortly thereafter. Harning et al. (2016a) provide a more detailed discussion on the last 3 ka of Tröllkonuvatn's sedimentary record with emphasis on Drangajökull's expansion during the last 1 ka, which exerted significant influence on the aquatic environment and its sediment.

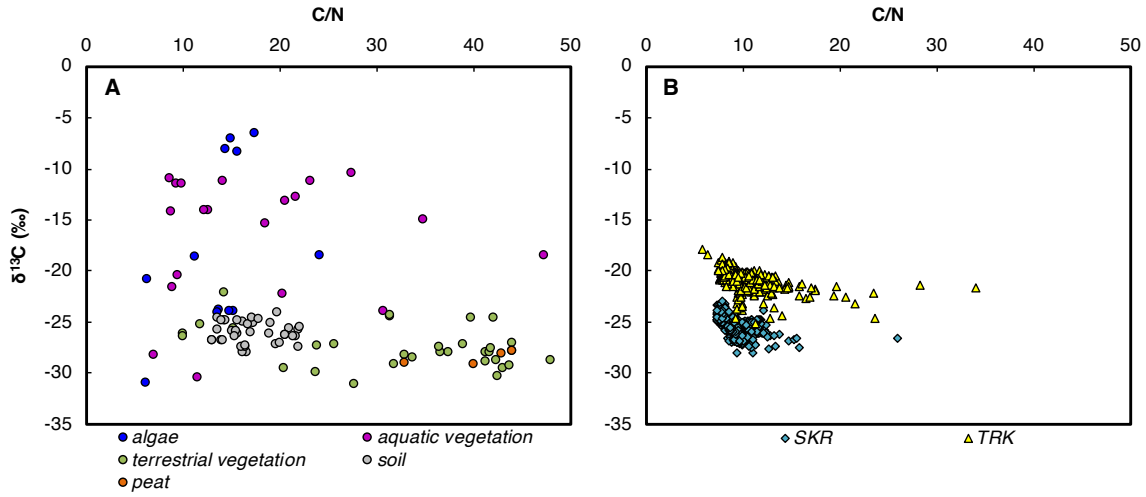

Figure 4.6. *Organic matter provenance biplots. A) End members synthesized from modern Icelandic vegetation datasets (Wang and Wooller, 2008; Skrzypek et al., 2008; Langdon et al., 2010; Florian, 2016). B) Skorarvatn (SKR) and Tröllkonuvatn (TRK) bulk lake sediment. Note: C/N axis terminated at a value of 50, but terrestrial vegetation from the modern end member studies range up to 205.*

4.5.3 Vestfirðir Composite Records

To extract a generalized Holocene climate record for Vestfirðir, we focus on two of our organic proxies, BSi and C/N. By generating a composite of each proxy record from Skorarvatn (low elevation, non-glacial) and Tröllkonuvatn (high elevation, proglacial), we reduce uncommon signals between the lakes (catchment-specific processes) and amplify those that are shared (climate variability) (e.g., Geirsdóttir et al., 2013). Each record was resampled to a uniform 20-year resolution in the AnalySeries software (Paillard et al., 1996), normalized (mean/standard deviation), then averaged with the other lake's corresponding proxy record to construct BSi and C/N composites. The composite BSi and C/N records (Fig. 4.7j-k) reveal peak algal productivity and landscape stability following deglaciation at ~8.8 ka, with negligible first-order changes through the middle Holocene. Subsequently, pronounced cooling, most evident in the BSi composite, initiates at ~3 ka. Superimposed on these general trends are "cold events" centered at ~8.2, 6.6, 4.2, 3.3, 2.3, 1.8, 1, and 0.25 ka (Fig. 4.7j-k). We define "cold events" as synchronous departures in 100-year running averages of BSi (lower algal productivity) and C/N (enhanced terrestrial erosion) proxy composite records. During the Neoglacial, the steady decline of the BSi composite may mask more pronounced changes associated with some "cold events" (e.g., 2.3 ka, Fig. 4.7j). However, the clear punctuations in the C/N composite indicate that the local environment is indeed being perturbed at these times (Fig. 4.7k). Based on our age models (Fig. 4.3), the "cold events" primarily occur within the window of least age uncertainty (<50 years), and thus, are temporally well-constrained.

Comparison to records of Drangajökull expansions (Harning et al., 2016a, b, this study) offers a mostly independent avenue to validate the trends and cold events apparent in the composite lake records. We hypothesize that if there are centennial scale cold anomalies, which suppress local algal productivity and induce terrestrial erosion, then glacier advances of the local ice cap are likely to be concurrent. The first four cold events from the composite lake records (8.2, 6.6, 4 and 3.3 ka) are not observed in Drangajökull's record (Fig. 4.7i). At these times, the ice cap had receded to considerably smaller dimensions than present (Harning et al., 2016b) such that any potential residual ice never breached local lake catchment thresholds. During the late Holocene, Drangajökull was actively expanding into two threshold lake catchments on the southeastern margin (Harning et al., 2016a). The threshold lake records combined with ^{14}C-dated emerging dead vegetation define five periods of increasing ice cap dimensions at ~2.3, 1.8, 1.4, 1 and 0.5 ka. The four most recent lake-composite cold events (2.3, 1.8, 1 and 0.5 ka) are closely aligned with these times of Drangajökull expansion (Fig. 4.7). The final two ice margin advances (1 and 0.5 ka) are interpreted from Tröllkonuvatn's sediment record, when abundant clastic sediment was deposited into the lake. Because algal productivity can be hindered under glacial occupation of the lake, the Tröllkonuvatn organic proxy record is not fully independent from the corresponding Drangajökull advances.

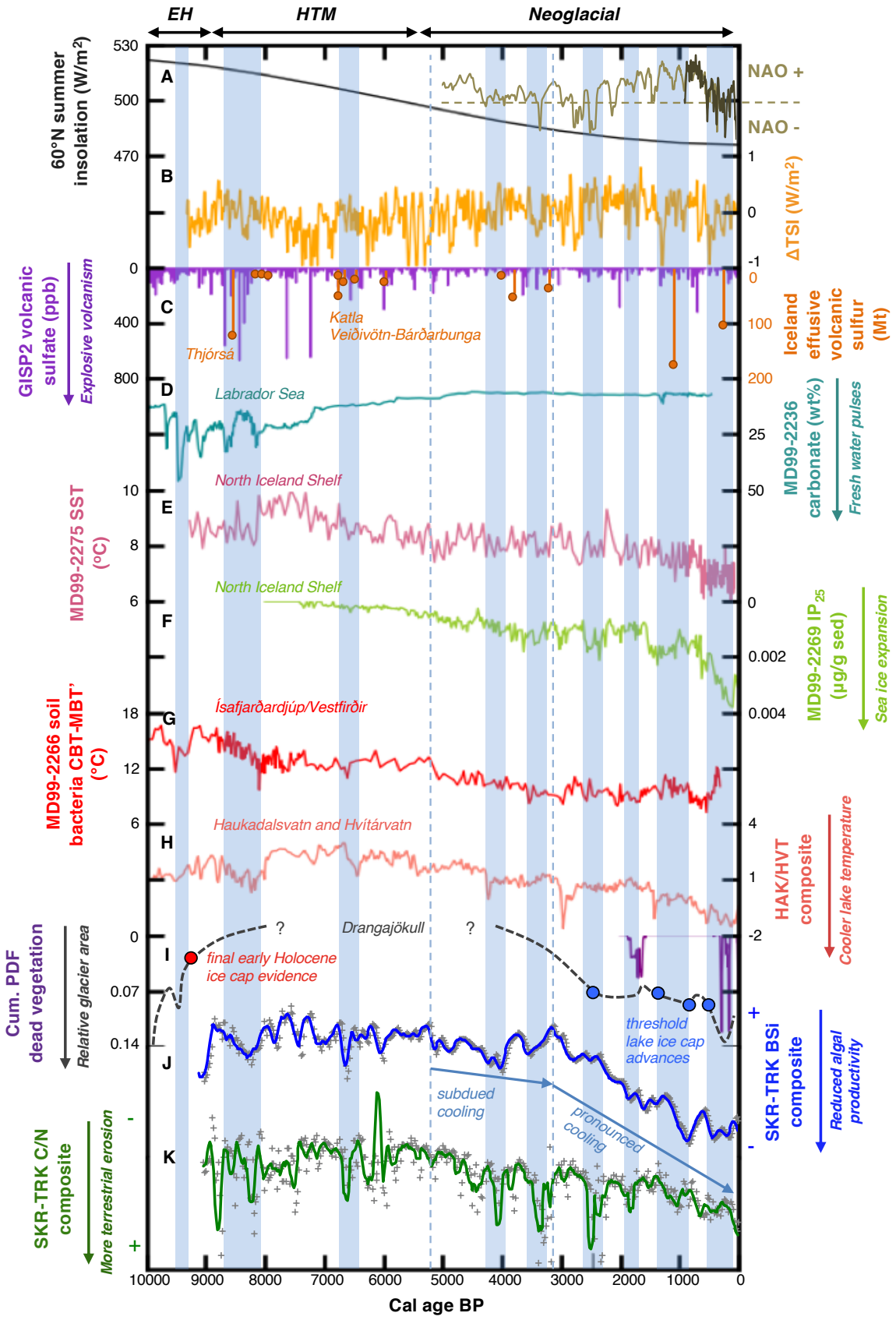

Figure.4.7. *Comparison of potential climate forcings to northern North Atlantic, Icelandic and Vestfirðir climate records. A) 60°N summer insolation (W/m², Berger and Loutre, 1991), and NAO variability*

reconstructed from SW Greenland (light brown, Olsen et al., 2012) and Morocco-Scotland (dark brown, Trouet et al., 2009), B) ΔTSI derived from ice core ^{10}Be (Steinhilber et al., 2009), C) GISP2 volcanic sulfate, based on empirical orthogonal function analysis of total sulfate (Zielinski et al., 1996) and atmospheric sulfur loading from Icelandic fissure vent eruptions (Thordarson et al., 2003), D) Labrador Shelf detrital carbonate wt% (MD99-2236, Jennings et al., 2015), E) North Iceland Shelf diatom-inferred SST (MD99-2275, Jiang et al., 2015), F) North Iceland Shelf IP_{25}-inferred seasonal sea ice (MD99-2269, Cabedo-Sanz et al., 2016), G) Vestfirðir MBT'-CBT MAT derived from terrestrial soil bacteria (MD99-2266, Moossen et al., 2015) H) qualitative spring/summer temperature lake proxy composite from Iceland (Geirsdóttir et al., 2013), I) relative area of Drangajökull based on threshold lake sediment records (Harning et al., 2016a, b) and ice margin advances inferred from ^{14}C-dated emerging dead vegetation (Harning et al. 2016a, this study), J) and K) SKR-TRK BSi and C/N composites with 100-yr running averages. All records oriented down toward cooler conditions. Blue boxes highlight "cold events" inferred from Vestfirðir proxy composite records.

4.6 Regional Comparisons and Climate Forcing Mechanisms

4.6.1 Early Holocene (10-8.8 ka)

Although NH summer insolation reached its Holocene zenith at ~11 ka (Berger and Loutre, 1991), peak warmth over Iceland appears to have been delayed by the retreat of the Icelandic Ice Sheet (Geirsdóttir et al., 2009a), and by the release of fresh water into the North Atlantic from the waning Laurentide Ice Sheet, slowing the Atlantic Meridional Overturning Current (AMOC) and driving pervasive, short-term cooling events (Barber et al., 1999; Alley and Ágústdóttir, 2005; Jennings et al., 2015). Two of these events at 9.4 and 8.2 ka (Fig. 4.7d), are coincident with a slight readvance of proto-Drangajökull within Skorarvatn's catchment and cold climate proxies at ~8.2 ka in the composite lake records (Fig. 4.7i-k).

Independent evidence for an early Holocene readvance of proto-Drangajökull's northern margin comes from a moraine at the mouth of Leirufjörður, with an average ^{36}Cl age of 9.3 ± 0.8 ka (n=4) obtained from exposed boulders (Brynjólfsson et al., 2015a). Considering the uncertainty in the ^{36}Cl age estimate (± 0.8 ka), the moraine may correlate to our 9.4 ka advance. In support of this correlation, the lowermost ^{14}C age from a lake sediment record near the mouth of Leirufjörður, suggests that the Leirufjarðarjökull readvance/standstill likely occurred during the older side of the ^{36}Cl range (Schomacker et al., 2016). At this time elsewhere in Iceland, cooler and drier conditions are inferred from pollen and chironomid head capsules on nearby Tröllaskagi (Caseldine et al. 2006; Langdon et al., 2010), reduced δ^{18}O-SST in Ísafjardardjúp (Quillmann et al., 2010) and on the North Iceland Shelf (Castañeda et al., 2004), and depressed mean annual air temperature derived from a Vestfirðir soil bacteria MBT'-CBT index (Fig. 4.7g, Moossen et al., 2015). High plagioclase/basalt ratios offshore of Vestfirðir also suggest increased ice rafting between ~9.6 and 9.4 ka (Andresen et al., 2005). Collectively, these lines of evidence point to oceanographic and terrestrial environmental change in Iceland that is consistent with a meltwater forcing mechanism from the Laurentide Ice Sheet.

4.6.2 Holocene Thermal Maximum (HTM, 8.8-5.5 ka)

Iceland's terrestrial HTM has previously been constrained to ~7.9 to 5.5 ka based on qualitative lake sediment proxies (Fig. 4.7h, Larsen et al., 2012; Geirsdóttir et al., 2013), likely in association with progressive strengthening and warming of the Irminger Current (Castañeda et al., 2004; Smith et al., 2005; Ólafsdóttir et al., 2010). Numerical modeling

experiments for Drangajökull suggest that peak air temperatures were 2.5-3 °C warmer at this time relative to the 1961-1990 CE average (Anderson et al., 2018). In contrast to the findings of Geirsdóttir et al. (2013), Drangajökull's significant areal reduction (Harning et al., 2016b), peak algal productivity, and relatively stable terrestrial environments on Vestfirðir point to peak Holocene warmth initiating earlier than 7.9 ka, by at least 8.8 ka (Fig. 4.7i-k). Peak Holocene mean annual air temperatures inferred from soil bacteria biomarkers between ~10.5 and 8.5 ka (Fig. 4.7g, Moossen et al., 2015) and the arrival of thermophilic birch trees on Vestfirðir (Caseldine et al., 2003) and around Tröllaskagi, north Iceland (Wastl et al., 2001; Eddudóttir et al., 2015) by ~9 ka, further support an earlier terrestrial HTM at this time.

We suggest the delayed warmth reflected in other Icelandic lake records may be related to additional confounding variables. During the early Holocene, Haukadalsvatn was transitioning from a fjord to terrestrial environment (Geirsdóttir et al., 2013), and thus, may partially incorporate a cooler marine signal and/or freshwater input from meltwater associated with the lingering Pleistocene ice sheets. At the same time, Hvítárvatn may have been under the influence of the waning Icelandic Ice Sheet in the central highlands (Larsen et al., 2012), which would likely hinder local biological productivity and catchment stabilization. Intense volcanism induced from decompression of the mantle following recession of the Icelandic Ice Sheet (Sigvaldason et al., 1992; Sinton et al., 2005) may also have played a role. Considering Haukadalsvatn and Hvítárvatn are more proximal to the active volcanic zones relative to Vestfirðir, ecosystem disturbance and soil erosion from tephra fallout (Christensen, 2013) may have masked the warmth observed in Vestfirðir. In the marine realm, cooler SST along the North Iceland Shelf during the early Holocene may be linked to a more stratified water column characterized by a nutrient-depleted, freshwater cap, which could result in artifically lower SST reconstructions as the biological SST proxies respond to these secondary variables (e.g., Kristjánsdóttir et al., 2016).

Between ~8.7 and 7.9 ka, multi-centennial cooling on Vestfirðir is reflected by a gradual reduction in algal productivity and increase in terrestrial erosion (Fig. 4.7j-k). Peak cooling at this time is constrained to ~8.2 ka, coincident with the widespread 8.2 ka event (Alley and Ágústdóttir, 2005; Rohling and Pälike, 2005). Although geologic evidence is lacking, recent numerical modeling experiments suggest a transient formation of <1 km^3 of ice where Drangajökull is currently situated at 8.2 ka (Anderson et al., 2018), similar to Langjökull, central Iceland (Flowers et al., 2008). In marine core MD99-2266 from Ísafjarðardjúp, Quillmann et al. (2012) measured paired $\delta^{18}O$ and Mg/Ca in benthic foraminifera through the 8.2 ka event, providing evidence for local surface water freshening and a SST depression of 3 to 5 ^{o}C. Based on diatom assemblages, Jiang et al. (2015) suggest a more modest summer SST reduction of ~0.8 °C farther east at MD99-2275 (Fig. 4.7E). On Iceland's terrestrial realm, a composite lake sediment proxy record from Haukadalsvatn and Hvítárvatn (HAK/HVT composite) suggests lower qualitative spring/summer temperatures between ~8.7 and 7.9 ka, similar to Vestfirðir (Fig. 4.7h, Geirsdóttir et al., 2013). The extended cooling reflected across lake records beginning at ~8.7 ka indicates that additional mechanisms influenced Iceland's climate prior to the release of freshwater from the Laurentide Ice Sheet at ~8.2 ka. Geirsdóttir et al. (2013) proposed atmospheric sulfate injection from explosive NH volcanism as a likely forcing, which begins at ~8.7 ka, as interpreted from Greenland ice core sulfate records (Fig. 4.7c). In contrast to the short-lived atmospheric mass-loading of sulfur from explosive eruptions, Icelandic effusive fissure eruptions can last for years and generate substantially more sulfate locally than their explosive counterparts (Thordarson et al., 1996, 2001). The prodigious sulfur release (121 Mt) from the Thjórsá effusive fissure eruption at ~8.6 ka may have contributed to Iceland's

prolonged cooling (Fig. 4.7c, Thordarson et al., 2003), in addition to another meltwater pulse through the Hudson Strait at ~8.6 ka (Fig. 4.7d, Jennings et al., 2015), and synchronous reduction of sunspot numbers (Solanki et al., 2004).

At ~6.6 ka, Vestfirðir's composite proxy records mark another period of cooling reflected in Icelandic lake and marine records (Fig. 4.7e-k). Between 6.8 and 6.5 ka, a series of four fissure vent eruptions were generated from the Katla and Veiðivötn volcanic systems in Iceland, which may have driven the observed local cooling through sustained atmospheric sulfur loading (Fig. 4.7c, Thordarson et al., 2003), in addition to separate NH explosive eruptions indicated by elevated sulfate concentrations in Greenland ice core records (Fig. 4.7c).

4.6.3 Neoglaciation (5.5 ka to Present)

Existing lacustrine proxy records indicate the initiation of Iceland's Neoglaciation at ~5.5 ka, with subsequent and persistent step-wise cooling through to the present (Fig. 4.7h, Larsen et al., 2012; Geirsdóttir et al., 2013). However, along Iceland's northern coastline, three lakes show relatively stable conditions until 3-2 ka, after which the climate enters a pronounced cooling trend (Axford et al., 2007; Florian, 2016).

A first-order cooling trend is apparent in Vestfirðir's BSi and C/N composite records beginning at ~5.3 ka, consistent with the Vestfirðir soil bacteria CBT-MBT' MAT and the HAK/HVT composite (Fig. 4.7g-h). But similar to elsewhere in north Iceland, more persistent cooling is delayed until ~3 ka (Fig. 4.7j). Marine records spanning the North Iceland Shelf indicate relatively stable summer SST during the middle Holocene (Giraudeau et al., 2004; Bendle and Rosell-Melé, 2007; Jiang et al., 2015), with a regime shift toward cooler conditions between ~3.4 and 3 ka (Andersen et al., 2004; Moossen et al., 2015; Kristjánsdóttir et al., 2016). These records suggest that during the late Holocene the thermal inertia of the North Iceland Shelf's sea surface was a more important modulator of Vestfirðir and north Iceland's coastal climate (Axford et al., 2007; Florian, 2016) relative to that of the interior, where summer insolation decline was more influential (Larsen et al., 2012; Geirsdóttir et al., 2013).

Coincident with Vestfirðir's cold event between 4.2 and 4 ka, as inferred from the BSi and C/N composites, there is a notable cooling on the North Iceland Shelf inferred from the $\delta^{18}O$ of benthic and planktonic foraminifera (Castañeda et al., 2004) as well as diatom assemblages (Fig. 4.7e). Changes in IP_{25} concentrations off north Iceland suggest a gradual increase of sea ice after 4 ka (Fig. 4.7f). The HAK/HVT composite also documents cooling at ~4.2 ka (Fig. 4.7h). This cold event coincides with a period of lower TSI (Fig. 4.7b), which has previously been proposed as a driving mechanism for this North Atlantic centennial-scale cooling event (e.g., Bond et al., 2001).

At ~3.3 ka, there is a decrease in MD99-2275 SST and a sea ice increase at MD99-2269, coincident with Vestfirðir's cold event (Fig. 4.7e-f). Although this cold anomaly is not reflected in the HAK/HVT composite (Fig. 4.7h), there is a concurrent BSi reduction in Haukadalsvatn (Geirsdóttir et al., 2013), as well as some of the lowest Holocene temperatures inferred from the soil bacteria CBT-MBT' index in Ísafjarðardjúp (Fig. 4.7g, Moossen et al., 2015). At the same time on nearby Tröllaskagi, north Iceland, birch pollen reached the lowest concentrations of the past 9.2 ka (Wastl et al., 2001). This interval is characterized by below average TSI and moderate explosive volcanism (Fig. 4.7b-c), as well as weakening of the AMOC south of Iceland (Hall et al., 2004). Additionally, changes may relate to atmospheric (Trouet et al., 2009; Olsen et al., 2012) and/or oceanic (Knudsen et al., 2011) modes of internal climate variability. A North Atlantic Oscillation (NAO) proxy

record constructed from lake sediment collected near Kangerlussuaq, SW Greenland, reveals a shift toward a negative mode (NAO-) at ~3.3 ka (Fig. 4.7a, Olsen et al., 2012). In the North Atlantic, the NAO- pushes the prevailing westerlies southward, which then allows colder, northerly winds to dominate (Hurrell et al., 2003). These changes in wind structure may strengthen the southward flowing Arctic ocean currents, weaken the strength of the warmer IC carried around Iceland (Blindheim and Malmberg, 2005) as well as transport more sea ice to Iceland's coastline.

At ~2.4 ka, Vestfirðir's third cold event and the first recorded expansion of Drangajökull (Fig. 4.7i) are contemporaneous with advances of other glaciers in Iceland (Stötter et al., 1999; Geirsdóttir et al., 2009a; Larsen et al., 2011), cooler SST (Fig. 4.7e, Jiang et al., 2015) and abrupt sea ice expansion on the North Iceland Shelf (Fig. 4.7f, Cabedo-Sanz et al., 2016). This cold period aligns with a NAO- mode (Fig. 4.7a) in addition to a tropical volcanic eruption with the largest radiative forcing of the last 2.5 ka (Sigl et al., 2015), offering triggers for the observed changes. The multi-centennial duration observed in the marine and terrestrial records suggests then that the initial cooling may have been sustained by additional mechanisms, such as ocean/sea-ice feedbacks (e.g., Miller et al., 2012).

At 1.8 ka, Drangajökull's northern margin expanded and the Vestfirðir lake composites suggest cooler local conditions, particularly with respect to elevated terrestrial erosion. Elsewhere in Iceland, intensified cooling is interpreted from BSi records, in north (Florian, 2016) and west Iceland (Geirsdóttir et al., 2009b). In contrast to the observed Icelandic cooling, there exist no significant changes in North Iceland Shelf SST and seasonal sea ice is relatively reduced at this time (Fig. 4.7e-f). Although an explosive NH volcanic event is recorded at ~ 2ka in Greenland ice cores, there is little evidence for explosive volcanism during the 1.8 ka cool event (Fig. 4.7c). However, TSI does exhibit a short-term reduction to below average values at ~1.8 ka (Fig. 4.7b). Due to the steadily diminishing NH summer insolation, the climate system in Iceland was perhaps more vulnerable to slight changes in climate forcings, such as TSI, at this time.

At ~1.3 ka, the cooling on Vestfirðir indicated by Drangajökull advances (Harning et al., 2016a) and the lake proxy composites is supported by a step shift toward lower spring/summers inferred from the HAK/HVT composite (Fig. 4.7h) and synchronous expansion of Langjökull (Larsen et al., 2011) and glaciers across the NH (Solomina et al., 2016). South of Iceland, reduced sortable silt sizes from marine sediment reflect a weakened AMOC, which would lead to reduced northward heat transport (Hall et al., 2004). We suggest that these oceanographic circulation changes may have driven the concurrent reduction in SST and expansion of sea ice reflected on the North Iceland Shelf (Fig. 4.7e-f). Albeit with a potentially different trigger, we propose that similar to the LIA (Miller et al., 2012), pronounced reduction of TSI (Steinhilber et al., 2009) and/or a series of large volcanic eruptions (Sigl et al., 2015; Büntgen et al., 2016) likely led to the observed changes in ocean circulation and sea surface conditions around Iceland.

During the Little Ice Age (LIA, 1250-1850 CE), the Vestfirðir region entered the lowest multi-centennial spring/summer temperature anomalies of the last 9 ka. Based on recent numerical modeling simulations, this anomaly is estimated to be 0.6-0.8 ºC below the 1950-2015 average on Vestfirðir (Anderson et al., 2018). The LIA witnessed the maximum Neoglacial dimensions of Drangajökull (Brynjólfsson et al., 2014; Harning et al., 2016a) as well as other Icelandic ice caps (Geirsdóttir et al., 2009a; Larsen et al., 2011; Striberger et al., 2012) and those throughout the NH (Solomina et al., 2016). At this time, the North Iceland Shelf is characterized by the coldest summer SST and most extensive sea ice of the Holocene (Fig. 4.7a-f), yet with minimal changes in NH summer insolation (Fig. 4.7a,

Berger and Loutre, 1991). Recent modeling efforts constrained by data-based observations point to a feedback forcing mechanism where initially a series of explosive volcanic eruptions induced persistent NH cooling, allowing subsequent expansion of sea ice, slowing of the northward heat transfer in the North Atlantic and reduction of SST (Miller et al., 2012; Sicre et al., 2013). Changes in atmospheric modes of internal climate variability (NAO-) likely contributed to the state of the LIA (Trouet et al., 2009) as well as TSI minima (Shindell et al., 2001).

4.7 Conclusions

We present the first continuous climate reconstruction since deglaciation based on lake sediment proxies from Vestfirðir, Iceland. The composite proxy records for spring/summer temperature (BSi) and organic matter source (C/N) from two lakes provide a sub-centennial qualitative perspective on local climate and help verify new and previously constrained activity of Drangajökull. The HTM initiates ~1ka earlier than in other terrestrial Icelandic records, in line with the rapid deglaciation of proto-Drangajökull and elevated NH summer insolation. Although Neoglacial cooling initiates at ~5.3 ka elsewhere in Iceland, pronounced cooling on Vestfirðir is delayed, likely due to its proximity to the SST along the adjacent North Iceland Shelf. In addition to the monotonic reduction of NH summer insolation, forcing mechanisms/feedbacks likely responsible for Vestfirðir's punctuated Holocene climate history include early Holocene freshwater pulses from the decaying Laurentide Ice Sheet and local effusive volcanism. Late Holocene stepped cooling is likely driven by variable combinations of low TSI, explosive and effusive volcanism, internal modes of climate variability, and sustained by ocean/sea-ice feedbacks. The strong similarities between climate proxy records from Vestfirðir lake sediment records and North Iceland Shelf oceanographic records reinforce the growing conception that Iceland may be representative of climate evolution across the northern North Atlantic region.

4.8 Acknowledgements

This work was supported by the Icelandic Center for Research through grants awarded to DJH (#163431051) and to ÁG and GHM (#130775051, Grant-of-Excellence #141573052) as well as the University of Iceland Research Fund. A CU Geological Sciences Department Mentor Grant supported Eric Gunderson, who assisted in developing both FTIR-BSi records. We thank Siggi and others from West Tours, Ísafjörður, for facilitating boat transportation to Hrafnsfjörður in August 2016. Þorsteinn Jónsson, Sveinbjörn Steinþórsson and Sydney Gunnarson are kindly thanked for exceptional assistance and company in the field. We appreciate the constructive comments provided by two anonymous reviewers, which contributed to the overall improvement of this manuscript.

5 Provenance, Stratigraphy, and Chronology of Holocene Tephra from Vestfirðir, Iceland[4]

5.1 Abstract

Tephrochronology facilitates the interpretation and correlation of terrestrial and marine paleoclimate records in and around Iceland. The Holocene tephra record on the Vestfirðir peninsula has until now been poorly known. Based on detailed analysis of major element chemistry, we present a holistic tephra stratigraphy and chronology (n=30) generated from four lakes located on northeastern Vestfirðir. Key markers are Tv-3, the 10 ka Grímsvötn tephra series along with the Hekla VF, Katla EG, Hekla T, Hekla 4 (intermediate component) and Hekla 3 (intermediate component), Snæfellsjökull-1, Landnám (basalt and rhyolite), Katla 920, Hekla 1693 and Bárðarbunga 1716 tephra layers. Notably, we also document two early Holocene intermediate tephra from the Hekla volcano, the oldest yet identified. Imperfections in the continuity of tephra records between lakes indicate gaps produced by either variable ash plume trajectories or periodic ice coverage (glacier or seasonal) of the lakes. The northernmost lake, Skorarvatn, archives three tephra layers consistent with the 10 ka Grímsvötn tephra layer series formed by eruptions in the same time frame as the well-known Saksunarvatn tephra from the Faroe Islands. Radiocarbon-dated macrofossils bounding Skorarvatn's upper and basal tephra layers from the 10 ka series indicate that they were produced by at least three large, successive eruptions from Grímsvötn over ~240 years. The composite Vestfirðir tephra stratigraphy and chronology presented here will enable better age control and synchronization between paleoclimate records in the northern North Atlantic.

5.2 Introduction

Tephrochronology has evolved into a highly valuable tool for the temporal constraint of various Icelandic sedimentary records (i.e., climatology, oceanography and archeology) since the seminal work of Thorarinsson (1944). The deposition of tephra layers is instantaneous on geologic timescales making them valuable stratigraphic isochrons (Haflidason et al., 2000; Larsen and Eiríksson, 2008), and diagnostic geochemical fingerprints of tephra allow the identification of their respective source (e.g., Larsen et al., 1999; Óladóttir et al., 2011a). Other traditional methods for dating sedimentary records, such as radiocarbon, are commonly less reliable in Iceland due to the mobilization of older organic material into lake environments (Sveinbjörnsdóttir et al., 1998; Geirsdóttir et al., 2009). As such, detailed tephrochronologies from numerous marine and terrestrial sedimentary archives in Iceland have demonstrated the efficacy of providing or aiding in secure age control (Eiríksson et al., 2000a; Jóhannsdóttir, 2007; Kristjánsdóttir et al., 2007;

[4] Harning, D.J., Thordarson, T., Geirsdóttir, Á, Zalzal, K., Miller, G.H., 2018. Provenance, stratigraphy, and chronology of Holocene tephra from Vestfirðir, Iceland. Quaternary Geochronology 46, 59-76.

Gudmundsdóttir et al., 2012; Larsen et al., 2011, 2012; Geirsdóttir et al., 2013; Blair et al., 2015). The wealth of known age tephra layers in the marine realm also allows direct correlation between marine and lacustrine records (Larsen et al., 2002; Eiríksson et al., 2004; Gudmundsdóttir et al., 2016) and better synchronization between paleoclimate proxy datasets (Ólafsdóttir et al. 2013).

The goal of this paper is to improve the current Icelandic tephra record by constraining the provenance, stratigraphy and chronology of Holocene age tephra from Vestfirðir lake sediment. Various studies have identified key tephra markers from lake and soil sections on Vestfirðir (Hjort et al., 1985; Caseldine et al., 2003; Principato et al., 2006; Thordarson and Höskuldsson, 2008; Langdon et al., 2011; Schomacker et al., 2016; Harning et al., 2016a, b; Brader et al., 2017), yet none have been presented in a holistic stratigraphic framework. We expand upon these previous studies by systematically identifying additional tephra horizons and detailing the Holocene chemistry and chronology of all currently known tephra on Vestfirðir. This record will be available for future application in dating and correlating between sedimentary archives in Iceland and throughout the northern North Atlantic.

5.3 Regional Setting

5.3.1 Vestfirðir Peninsula

Vestfirðir comprises Iceland's northwesternmost extension into the North Atlantic Ocean. The peninsula is the oldest subaerial sector of Iceland dating back to over 15 Ma and lies outside the current active volcanic zones and belts (Fig. 5.1a, Moorbath et al., 1968; McDougall et al., 1984; Harðarson et al., 1997). Regional bedrock is primarily composed of Neogene basaltic lava successions intercalated with relatively thin sedimentary horizons of mostly aeolian and fluvial origin. Rhyolite outcrops indicate the presence of relic central volcanoes near the local ice cap, Drangajökull (Harðarson et al., 2008). Upland surfaces on the plateau surrounding Drangajökull are characterized by discontinuous andosols and vitrosols, low in organic content and sparsely covered with vegetation (Arnalds, 2004). At lower elevations, low-lying heath vegetation prevails but it is scattered and tends to clump in small tussocks atop soil patches.

The prevailing westerlies in the upper troposphere and lower stratosphere are the main control on ash plume trajectories in Iceland (Lacasse, 2001), which commonly results in net north to eastward dispersal of the plumes produced by explosive eruptions in Iceland. This, in conjunction with the location of volcanic zones and belts in Iceland in relation to Vestfirðir (Fig. 5.1a), implies that relatively few tephra plumes reach the Vestfirðir peninsula (e.g., Thordarson and Höskuldsson, 2008). Thus, only explosive eruptions that are large and/or take place during spring/summer when the prevailing westerlies shift toward weak easterlies (Lacasse, 2001) have the potential to deposit primary tephra into Vestfirðir's lakes.

5.3.2 Study Lakes

The Vestfirðir peninsula hosts a multitude of over-deepened lake basins remnant from prior glaciations (Principato and Johnson, 2009). The continuous sedimentation in most of these lakes since the last deglaciation has allowed the preservation of organic matter interspersed with discrete Icelandic tephra (Caseldine et al., 2003; Thordarson and Höskuldsson, 2008; Langdon et al., 2011; Schomacker et al., 2016; Harning et al., 2016a, b). Four lakes ranging

in elevation from 140 to 470 m asl on northeastern Vestfirðir were selected for this study (Fig. 5.1b). Bæjarvötn and Gedduvatn are located over 30 kilometers from Drangajökull's extant margin, whereas Tröllkonuvatn and Skorarvatn are located within 3 kilometers of the ice cap. Thus, the distribution of sampled lakes includes vegetated low-elevation coastal locations, sparsely vegetated highlands, and lakes currently influenced by Drangajökull.

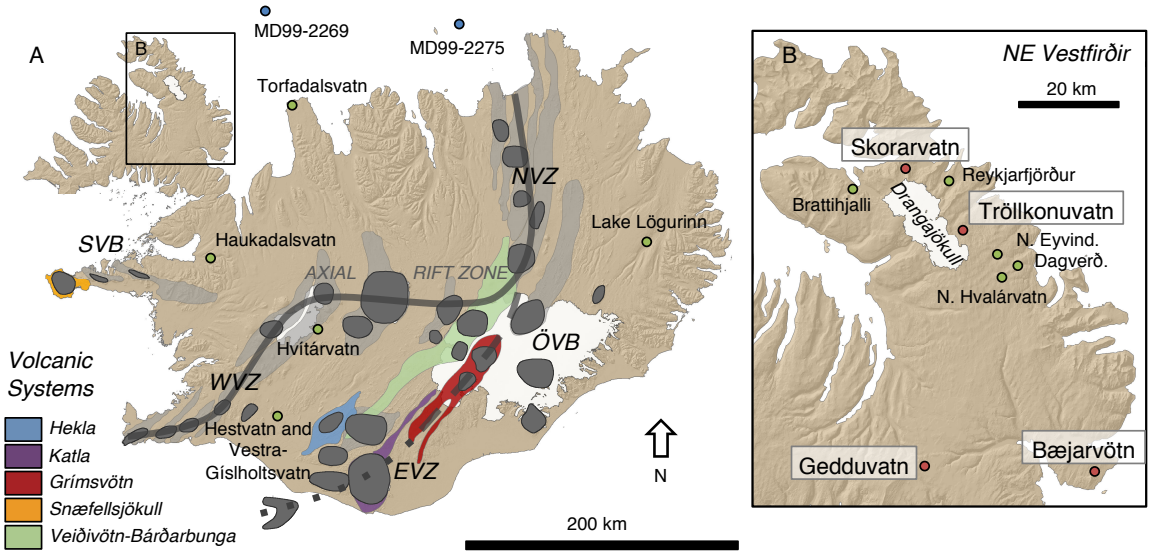

Figure 5.1. *Location maps. A) Overview of Iceland showing the volcanic systems and central volcanoes (dark grey, Catalogue of Icelandic Volcanoes). Colored volcanic systems reflect those that generated tephra found on Vestfirðir. Solid gray line delineates the axial rift. Dashed gray line marks the tholeiitic portion of the propagating rift, whereas the dotted gray line marks the alkalic/transitional portion of the propagating rift. Also labeled are key lake (green circles) and marine sites (blue circles) mentioned in text. B) Locations of this study's lakes (red circles) and other key lake sites (green circles, Schomacker et al., 2016) on northeastern Vestfirðir.*

5.4 Methods

5.4.1 Lake Sediment Coring and Inspection

Bæjarvötn, Gedduvatn, Tröllkonuvatn and Skorarvatn (Fig. 5.1b) were cored during the winter of 2010 and 2014. Sediment cores were recovered from each lake's deepest basin(s) using a percussion driven piston corer. The presence of deglacial sediment at the base of each core confirms that the entire sedimentary sequence since local deglaciation of proto-Drangajökull was captured from each lake (Fig. 5.2; Harning et al., 2016b). All cores were subsequently split, sedimentology described, and visually inspected for pristine tephra horizons at the University of Minnesota's LacCore facility (2010 cores) and the University of Iceland (2014 cores).

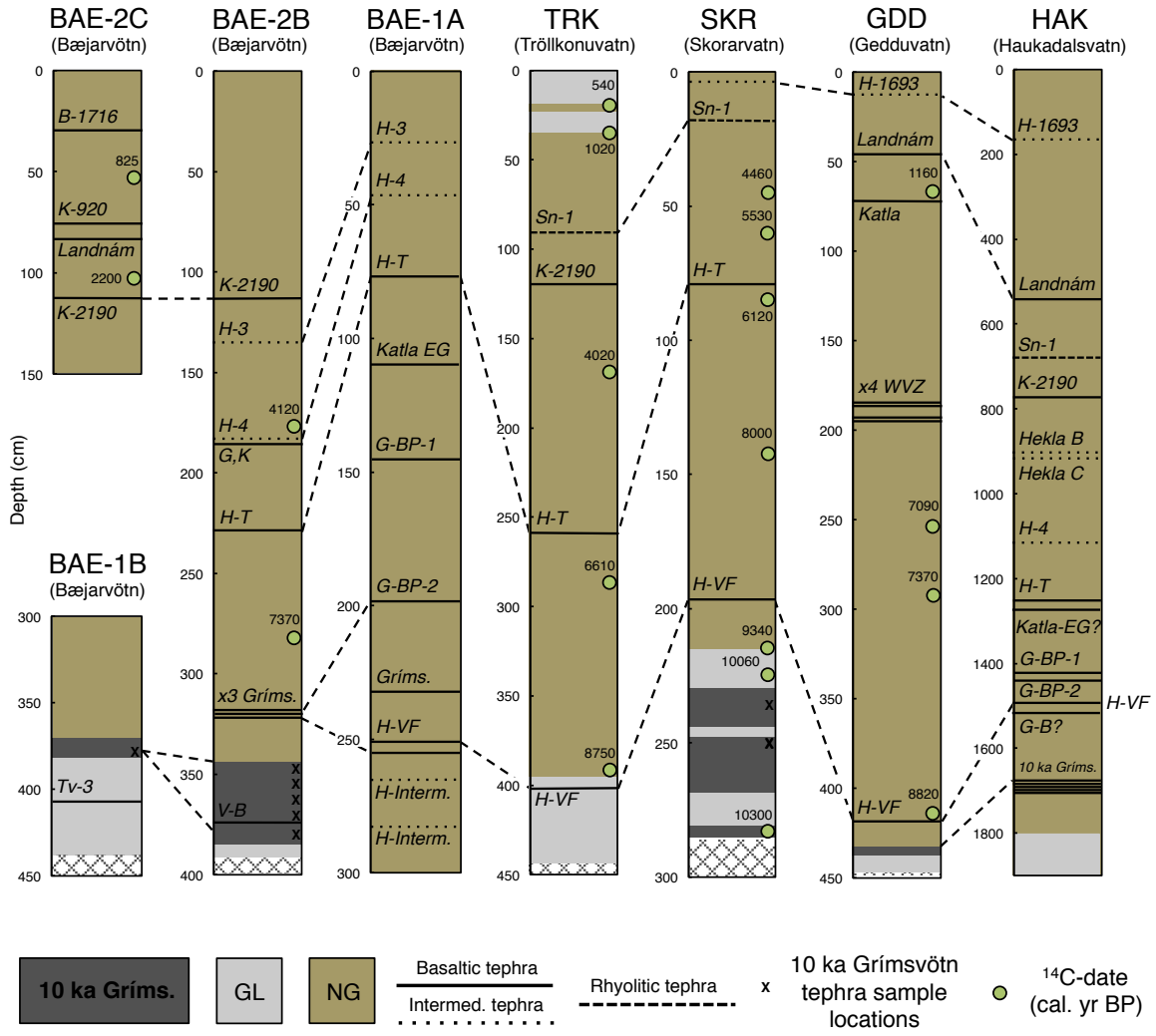

Figure 5.2. *Simplified lithologies and location of visible tephra in lake sediment cores. GL = glaciolacustrine sediment and NG = non-glacial sediment. Hatched boxes indicate the bottom of sediment cores. Dashed lines represent tephra correlations between cores. Simplified lithology and key tephra from Haukadalsvatn (HAK)'s GLAD4-HAK-03-1B sediment core are shown on far right (Jóhannsdóttir, 2007; Geirsdóttir et al., 2009, 2013).*

5.4.2 Major-Elemental Analysis of Pristine Tephra

Tephra layers located by visual inspection in split cores halves (Figs. 5.2 and 5.3) are fine to medium ash comprised of glassy tephra grains (>98% grain population) in addition to a trace of accidental lithics. These layers are clean and do not include any of the surrounding sediments or any other foreign material indicative of reworking (Fig. 5.3a-c). Hence, each of the tephra layers is pristine (i.e., primary and not reworked) and deposited directly from ash plumes overhead. The fact that the tephra shards feature small and delicate protrusions (Fig. 5.3d), which would not survive fluvial transport, underpins the above assertion. Each tephra sample was sieved to isolate glass fragments between 63 and 250 μm and then embedded in epoxy plugs, exposing 100s-1000s of grains (depending on the exact grain size distribution of the tephra separates), from which ~20 randomly selected grains were subject to microprobe analysis. Hence, in layers that feature a compositionally coherent range of two or more distinct chemical compositions, there is always the chance the one

compositional type is represented by a single analysis, although many more tephra of that composition may be present in significantly greater concentrations within the tephra's sedimentary horizon. Thus, singularity only implies a minority type in the sample. Consequently, the basic premises we take are that (i) a layer with uniform composition throughout represents a single eruption event, (ii) a layer with a range of composition, yet conforming to the geochemical characteristics of a single volcanic system, represent a tephra erupted from a compositionally layered storage zone, and (iii) a tephra comprised of two or more distinct compositions (indicating origin from two or more volcanic systems) indicates deposition from separate eruptions closely spaced in time. The latter occurrence is expected to be more common in relatively low sediment accumulation areas, like Vestfirðir (e.g. Harning et al., 2016b), compared to areas close to the active volcanic zones that are typified by high sedimentation rates.

Tephra layers sampled from the 2010 cores were analyzed at the University of Edinburgh on a Cameca SX100 electron microprobe, using an acceleration voltage of 15 kV, beam current of 8 nA and beam diameter of 10 µm. For tephra collected from the 2014 lake sediment cores, elemental point analysis of samples was performed at the University of Iceland on a JEOL JXA-8230 election microprobe using an acceleration voltage of 15 kV, beam current of 10 nA and beam diameter of 10 µm. Lipari (rhyolitic obsidian) and BHV02G (basaltic glass) international standards were run periodically between samples at the University of Edinburgh, whereas the international A99 standard was used at the University of Iceland, to monitor for instrumental drift and maintain consistency between measurements. Geochemical anomalies from point analyses are reflective of lithic mineral contamination or impurities in the glass. These outliers and any analyses with elemental sums >100% were removed from the final dataset but retained in Supplemental Information of published text.

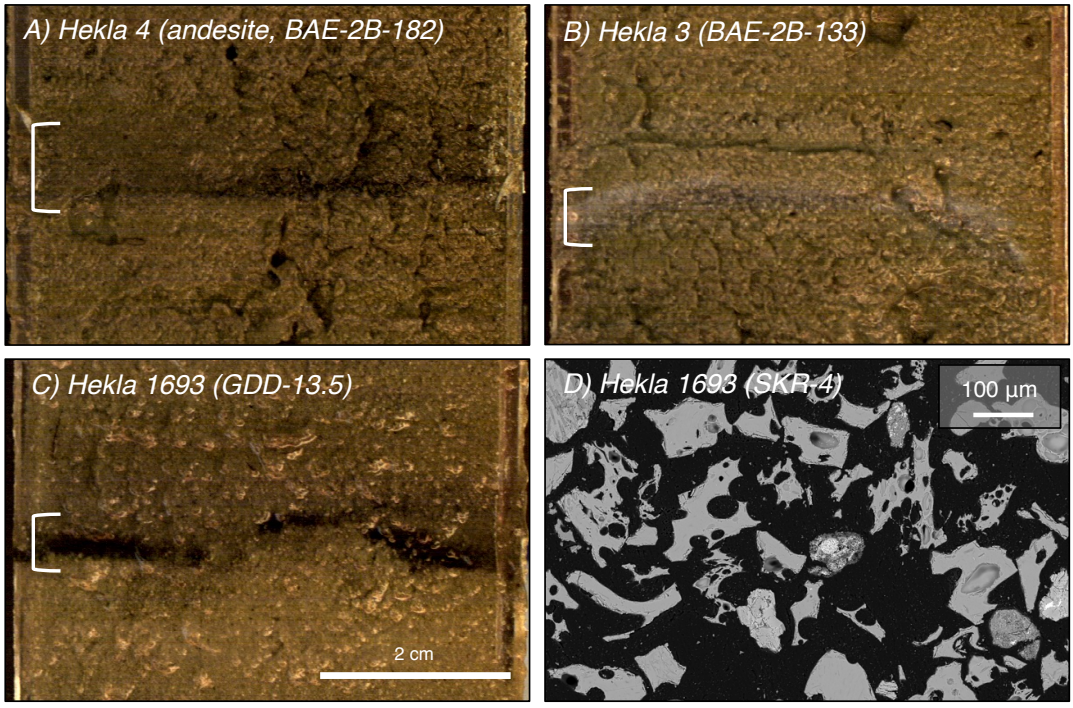

Figure 5.3. *Examples of tephra visible in lake sediment cores. A) Hekla 4 from Bæjarvötn, B) Hekla 3 from Bæjarvötn, C) Hekla 1693 from Gedduvatn, and D) electron microprobe backscatter image of Hekla 1693*

tephra glass from Skoravatn. Photos A, B and C courtesy of LacCore, University of Minnesota. Photo D by S. Gunnarson.

5.4.3 Macrofossil Radiocarbon Dating

Plant macrofossils were identified visually and picked to provide additional age control and to help constrain tephra where the geochemistry was enigmatic of a particular eruption. Samples were given an acid-base-acid pretreatment and graphitized at University of Colorado-Boulder, then measured by AMS at the University of California-Irvine. Conventional radiocarbon ages were calibrated in OxCal 6.0 using the IntCal13 calibration curve (Bronk Ramsey, 2009; Reimer et al., 2013) and are reported in calibrated years BP (cal BP, Table 5.1).

Table 5.1. *Radiocarbon information.*

Lake (sediment depth cm)	Lab ID	Material	$\delta^{13}C$ (‰)	Fraction modern	^{14}C date ± σ	Cal. age BP ± σ	Reference
Bæjarvötn-2C (53)	CURL-16695	moss	-29.6	0.8938	900 ± 25	825 ± 85	This study
Bæjarvötn-2C (106.5)	CURL-16691	moss	-31.4	0.7643	2160 ± 25	2200 ± 110	This study
Bæjarvötn-2B (173)	CURL-12004	bark fragment	-29.0	0.6263	3760 ± 15	4120 ± 30	This study
Bæjarvötn-2B (280.5)	CURL-12023	bark fragment	-26.2	0.4495	6425 ± 20	7370 ± 50	This study
Gedduvatn (64)	CURL-12689	aquatic moss	-30.5	0.8584	1225 ± 15	1160 ± 70	This study
Gedduvatn (255.5)	CURL-12006	aquatic moss	-26.0	0.4636	6175 ± 20	7090 ± 70	This study
Gedduvatn (292.5)	CURL-12018	aquatic moss	-22.9	0.4489	6435 ± 20	7370 ± 50	This study
Gedduvatn (417.8)	CURL-12031	aquatic moss	-27.7	0.372	7945 ± 25	8820 ± 160	Harning et al. (2016b)
Skorarvatn (43)	CURL-21039	moss	-24.3	0.6102	3970 ± 20	4460 ± 50	Harning et al. (2016b)
Skorarvatn (59)	CURL-21034	moss	-25.3	0.5529	4760 ± 20	5530 ± 50	Harning et al. (2016b)
Skorarvatn (82)	CURL-21035	moss	-26.3	0.5136	5355 ± 20	6120 ± 90	Harning et al. (2016b)
Skorarvatn (140.5)	CURL-21036	moss	-29.7	0.4079	7205 ± 25	8000 ± 20	Harning et al. (2016b)
Skorarvatn (214.8)	CURL-19489	moss	-23.9	0.356	8295 ± 25	9340 ± 60	Harning et al. (2016b)
Skorarvatn (222.5)	CURL-21041	moss	-23.3	0.33	8905 ± 35	10060 ± 120	Harning et al. (2016b)
Skorarvatn (283.5)	CURL-21033	moss	-25.0	0.3203	9145 ± 35	10300 ± 70	Harning et al. (2016b)
Tröllkonuvatn (18)	CURL-19503	moss	-22.2	0.9348	540 ± 15	540 ± 10	Harning et al. (2016a)
Tröllkonuvatn (30.5)	UCIAMS-165968	moss	N/A	0.8686	1130 ± 20	1020 ± 50	Harning et al. (2016a)
Tröllkonuvatn (165.5)	CURL-21038	moss	-21.6	0.6333	3670 ± 15	4020 ± 50	This study
Tröllkonuvatn (285.5)	CURL-21037	moss	-23.1	0.4858	5800 ± 20	6610 ± 40	This study
Tröllkonuvatn (394)	CURL-19502	moss	-24.4	0.3729	7925 ± 25	8750 ± 100	Harning et al. (2016b)

5.5 Results and Interpretations

The major elemental composition of Icelandic tephra generally allows the correlation back to their source volcanic system (Larsen, 1982; Óladóttir et al., 2011a). During the Late Pleistocene and Holocene, Icelandic volcanic systems have produced three distinct magma suites: alkaline, transitional-alkaline and tholeiitic (Jakobsson, 1979; Sigmarsson and Steinþórsson, 2007; Jakobsson et al., 2008). The tholeiitic suite is distinguished by the lowest total alkalis (Na_2O+K_2O); plotting below the Kuno line (Kuno, 1968) on total alkali vs. silica (TAS) plots (Fig. 5.4a) and below the MacDonald-Katsura line (MacDonald and Katsura, 1964) on the basalt confined TAS plots (Fig. 5.4b-d). The alkaline suite has high total alkali content and plots above the Kuno and MacDonald-Katsura lines on TAS plots (Fig. 5.4a-d). The transitional-alkaline suite typifies the magma production at two Icelandic volcanoes, namely Hekla and Katla. It takes its name from the fact that the basalt from these volcanoes plot in the alkali field (i.e., above the Kuno line) while intermediate Katla and intermediate to silicic Hekla magmas plot in the tholeiitic field (i.e., below the Kuno line).

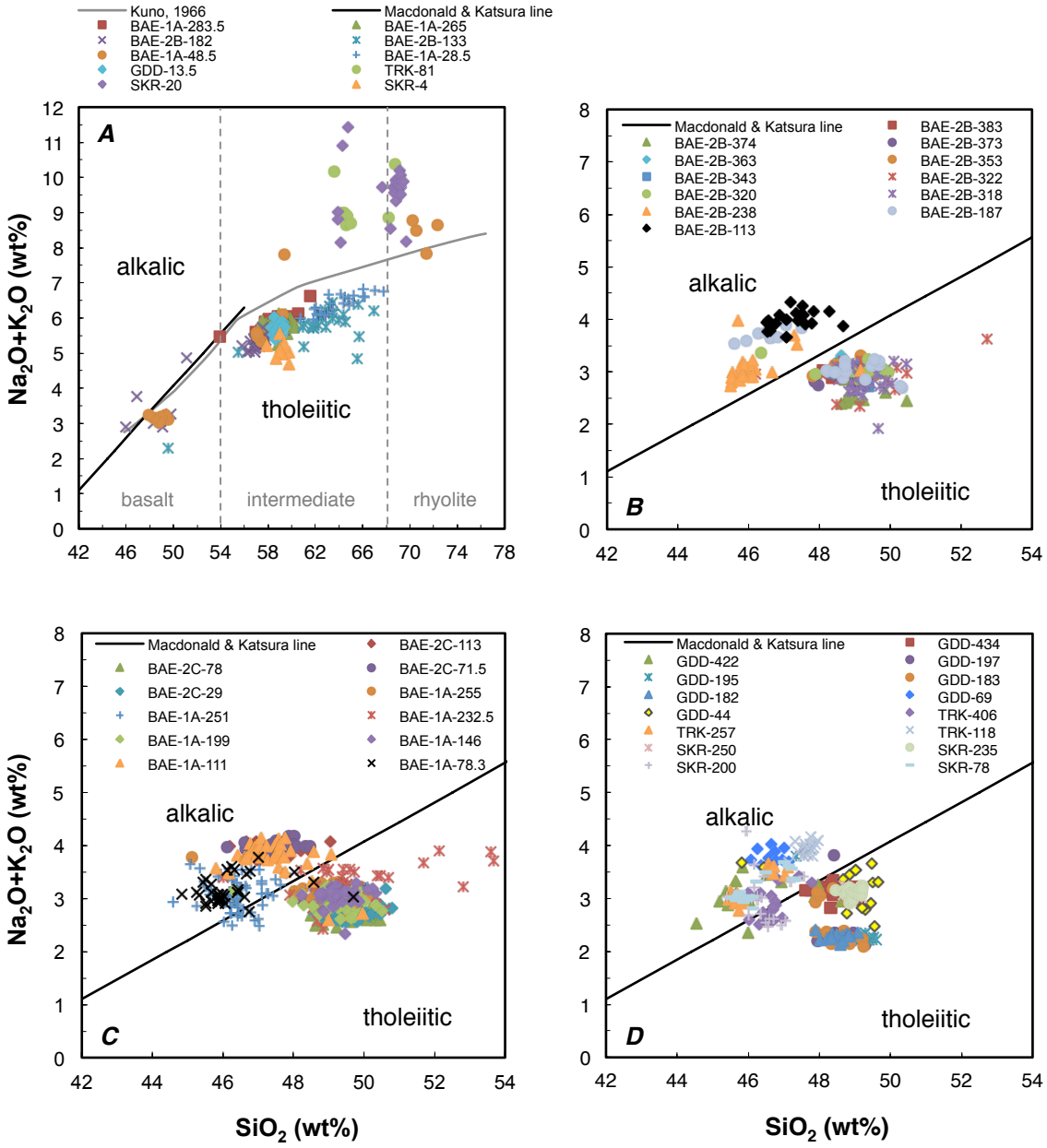

Figure 5.4. *All Vestfirðir tephra plotted on TAS plots (A) and basalt confined TAS plots (B-D). The M-K (MacDonald and Katsura, 1964) and Kuno lines (Kuno, 1968) separate alkalic from tholeiitic tephra. A) Predominately intermediate tephra from Bæjarvötn, Gedduvatn, Tröllkonuvatn and Skorarvatn, B) Basaltic tephra from Bæjarvötn's BAE10-2B-1N sediment core, C) Basaltic tephra from Bæjarvötn's BAE10-2C-1N and BAE10-1A-1N sediment cores, and D) Basaltic tephra from Gedduvatn, Tröllkonuvatn and Skorarvatn.*

These three magma suites have distinct distributions. The tholeiitic magma suite characterizes the axial rift along the North (NVZ), West (WVZ) and East (EVZ) volcanic zones (Fig. 5.1a). The alkaline magma suite typifies the intraplate volcanic belts of Snæfellsnes (SVB) and Öræfajökull (ÖVB) (Fig. 5.1a). The EVZ is an axial rift in the making, formed by propagation to the southwest through older crust and, therefore, it exhibits distinct spatial variability in terms of the magma suites produced. The northern sector, where the Grímsvötn and Veiðivötn-Bárðarbunga volcanic systems are located (Fig. 5.1a), is typified by tholeiitic magma suites, which contain higher FeO, TiO_2, K_2O and P_2O_5

at similar MgO values when compared to the mid-ocean ridge tholeiites typifying the far northern and southwestern segments of the axial rift in Iceland (Sigmarsson and Steinþórsson, 2007). The volcanic systems Vestmannaeyjar, Torfajökull, Tindfjöll and Eyjafjöll in the southern sector of the EVZ produce alkalic magmas (Jakobsson, 1979; MacDonald, 1990; Larsen et al., 1999) and as stated above, the Katla and Hekla systems of the EVZ feature the transitional magma suite, which is characterized by higher FeO and TiO_2 content and FeO/TiO_2 values compared to the tholeiitic and alkali suites (Lacasse et al., 1995; Larsen et al., 2001; Thordarson et al., 2003).

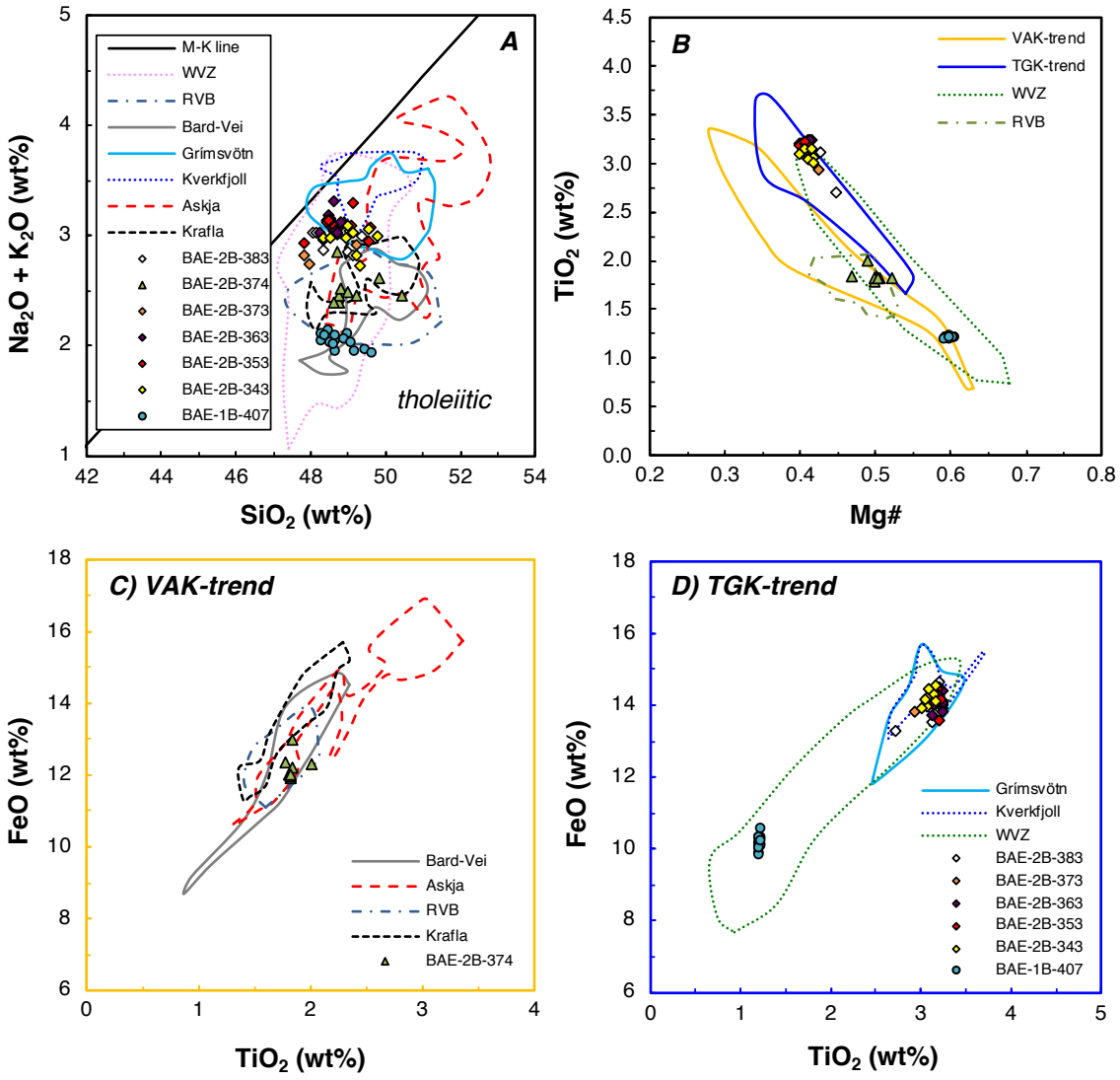

Figure 5.5. *Examples of tholeiitic basalt tephra discrimination from Bæjarvötn. Panel B enables further discrimination of tephra based on their affinity to either the VAK-trend volcanic systems (C) or the TGK-trend volcanic systems (D). Mg# = (MgOwt%/40.3)/((FeOwt%/71.8)+(MgOwt%/40.3)). BAE-2B-374 originated from the Bárðarbunga-Veiðivötn volcanic system, BAE-1B-407 from the WVZ and BAE-2B-383, -373, -363, -353, and -343 from Grímsvötn.*

5.5.1 Tephra Discrimination in Lake Sediment Cores

Tephra microprobe datasets were analyzed using an approach similar to that outlined in Jennings et al. (2014). This approach provides a robust and systematic procedure of identification of the source volcanic system for each tephra layer (see Section 5.9. Supplemental Information for complete dataset), and then the source eruption via direct comparison with composition of tephra layers from the same volcanic system and the relevant stratigraphical interval. Most importantly, this approach significantly reduces the potential bias that is introduced when the original data is compared to data from a set of tephra layers handpicked by an operator from the published literature.

Each tephra was first categorized as alkali, transitional-alkaline or tholeiitic basalt on the basis of TAS plots, as illustrated in Fig. 5.4. Subsequently, the source volcanic system was systematically verified through a series of bi-elemental plots. In Figs. 5.5-5.8, we provide examples of this tephra discrimination process with a subset of tephra representative of basaltic (alkali and tholeiite), intermediate and rhyolitic classes (see Supplemental Information of published text for complete data set). The bi-elemental plots contain the compositional domains of relevant tholeiitic or alkalic/transitional volcanic systems as implied by the TAS plots (Fig. 5.4). Correlation to tephra of known age was carried out first by estimation of the tephra's age based on its stratigraphic position and any supporting radiocarbon ages, followed by comparison to established tephra composition for the volcanic systems as well as individual tephra layers. This identification procedure was corroborated by comparison to Haukadalsvatn's detailed Holocene tephra stratigraphy (Fig. 5.2, Geirsdóttir et al., 2009, 2013) because both sites are located northwest of the primary volcanic zones (Fig. 5.1a) and, therefore, should share similar tephra sequences. Furthermore, Haukadalsvatn's age model (Ólafsdóttir et al., 2013), which is derived from paleomagnetic secular variation synchronization to a well-dated (^{14}C) marine core on the North Iceland Shelf (MD99-2269, Fig. 5.1a, Kristjánsdóttir et al., 2007; Stoner et al., 2007), underpins the high-resolution age estimates for the core. Where correlations were not possible, Vestfirðir lake age models (Fig. 5.9) were employed to provide estimates for the time of tephra deposition.

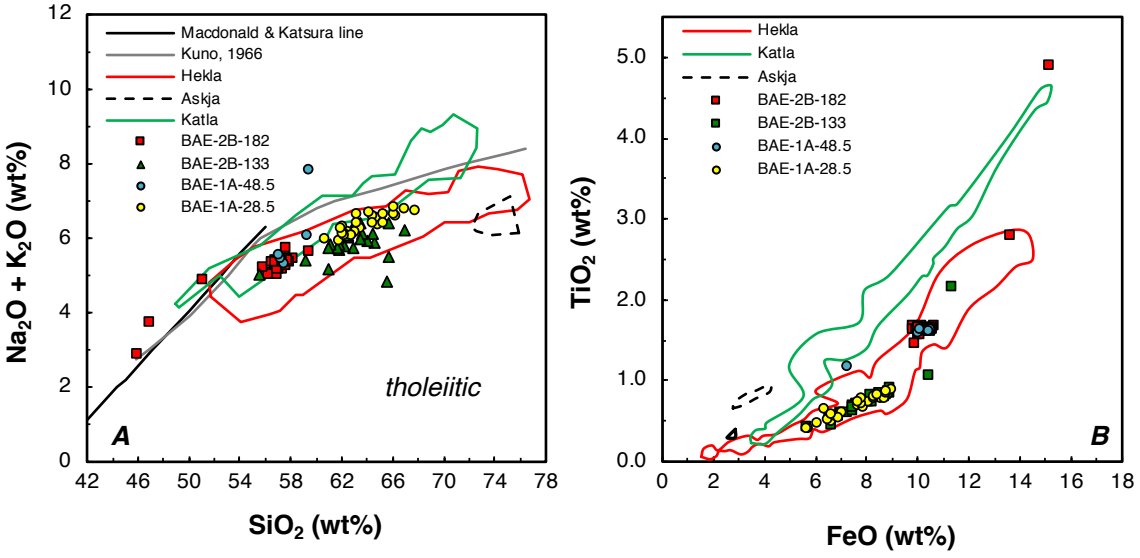

Figure 5.6. *Examples of intermediate tephra discrimination from Bæjarvötn. All four tephra are tholeiitic and clearly originate from the Hekla volcanic system.*

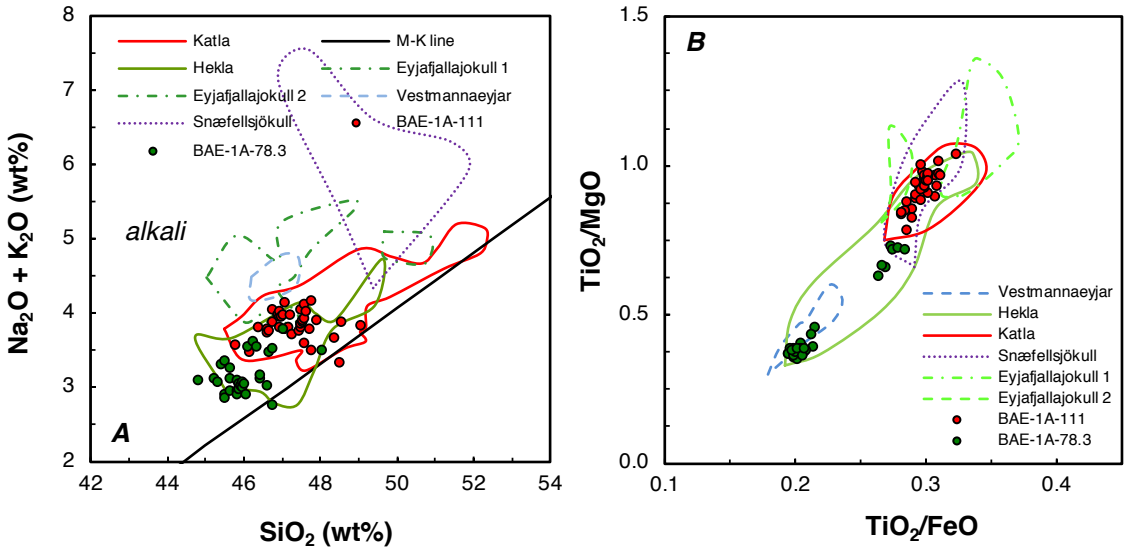

Figure 5.7. *Examples of alkali basalt tephra discrimination from Bæjarvötn. BAE-1A-111 originates from Katla whereas BAE-1A-78.3 is from Hekla.*

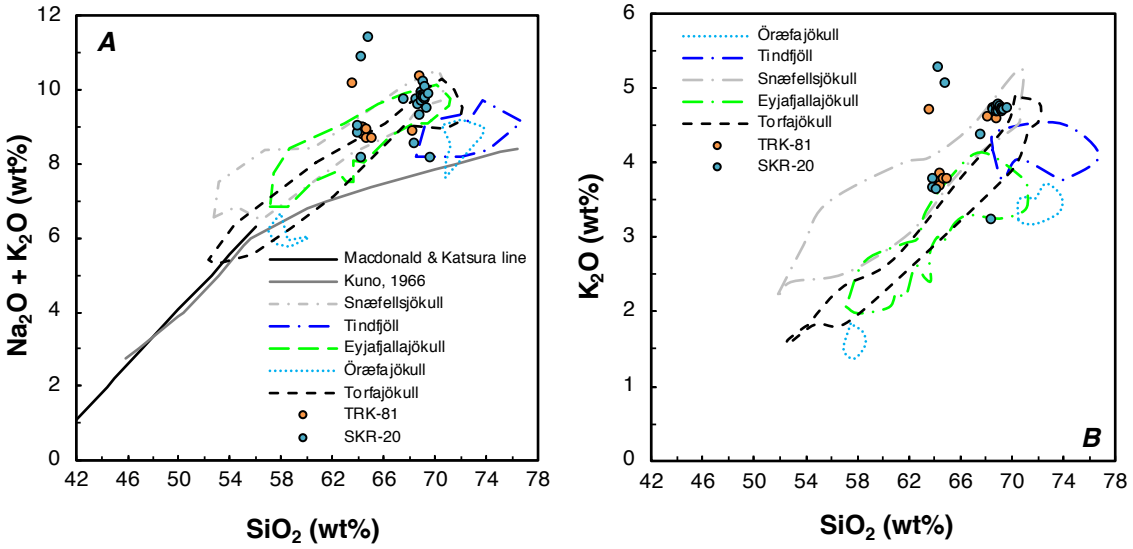

Figure 5.8. *Examples of silicic tephra discrimination from Tröllkonuvatn and Skorarvatn. Both tephra are clearly alkalic and likely originated from Snæfellsjökull.*

5.5.1.1. Bæjarvötn

Bæjarvötn (BAE, 140 m asl, 65.7211°N, 21.4362°W) sits ~32 km south of Drangajökull and ~1.9 km west of Vestfirðir's eastern coastline (Fig. 5.1b). Bæjarvötn's catchment was deglaciated in the early Holocene prior to the deposition of the 10 ka Grímsvötn tephra series (Harning et al., 2016b). Sedimentation for the remainder of the Holocene has been non-

glacial with 28 total tephra horizons visible in four separate lake sediment cores; BAE10-2B-1N, BAE10-2C-1N, BAE10-1B-1N and BAE10-1A-1N (Fig. 5.2). Six of these tephra are intermediate and 25 are mafic. Furthermore, four tephra are alkaline, four are transitional-alkaline, one is a mixture of alkaline and tholeiitic, and 22 are tholeiitic (Fig. 5.4a-c, Tables S5.1 and S5.2). Below, the tephra are described as they were found in specific depth intervals in one or more sediment cores from Bæjarvötn.

BAE-1B 407 cm. Lake sediment core BAE10-1B-1N penetrated the deepest into Bæjarvötn's sedimentary sequence and archived one tephra (407 cm depth) not recovered in the longest Holocene core BAE-2B-1N from Bæjarvötn (Fig. 5.2). This basal tephra reveals a major elemental composition consistent with tholeiitic basalt from the West Volcanic Zone (WVZ) (Fig. 5.5d, Table S5.1). In the lake Torfadalsvatn, ~60 km northeast of Bæjarvötn (Fig. 5.1a), a compositionally identical tephra layer (Tv-3, Supplemental U) to BAE-1B-407 is situated between the well-known Vedde Ash and the so-called Saksunarvatn ash (Björck et al., 1992). Björck et al. (1992) correlated the Tv-3 tephra to the early Holocene I-THOL-I tephra, which was previously suggested to originate from the Veiðivötn-Bárðarbunga volcanic system based on major element compositional similarities (Kvamme et al., 1989), yet we now note that it was likely generated from the WVZ instead. Elsewhere in Iceland, four WVZ eruptive lava units surrounding the extant Langjökull ice cap in central Iceland were generated during the earliest Holocene based on evidence indicating interaction with shallow ice or meltwater from the retreating Icelandic Ice Sheet (Sinton et al., 2005). Lacking better age control for these four lava flows we do not draw specific correlations to any of these at this time, but maintain them as probable sources for the Tv-3 tephra. In terms of the Tv-3 tephra's age, Björck et al. (1992) constrained it to 9200 ^{14}C years BP (calibrated to ~8900 cal BP following methods in Section 3.3) based on radiocarbon dates. Recent work from the Greenland ice cores has produced revised age estimates for the so-called Saksunarvatn ash (10300 cal BP) and the Vedde Ash (12120 cal BP) (Rasmussen et al., 2006), which bound the Tv-3 tephra in Torfadalsvatn (Björck et al., 1992). If these revised ages are applied to the stratigraphic depths of the Saksunarvatn ash (10.52 m) and Vedde Ash (11.05 m) in Torfadalsvatn, and we assume a linear sedimentation rate, the age of the Tv-3 tephra (10.67 m) is now estimated to be ~10800 cal BP.

BAE-1B 384 cm. A 12 cm-thick tephra horizon occurs above the Tv-3 tephra starting at 384 cm depth (Fig. 5.2). Major elemental composition of this tephra reveals tholeiitic characteristics consistent with the Grímsvötn volcanic system (Table S5.1). Furthermore, its deep stratigraphic position within the core, large sand-sized tephra grains and thickness indicate that this is correlative to the one of the westward-dispersed 10 ka Grímsvötn tephra series layers (Supplemental U), which are separate tephra layers that share indistinguishable chemical attributes to that of the Saksunarvatn tephra from the Faroe Islands (Mangerud et al., 1986). As many as seven 10 ka Grímsvötn tephra series layers are now known to have been dispersed westward from the Grímsvötn volcanic system between 10400 and 9900 cal BP (Jóhannsdóttir, 2007; Jennings et al., 2014; Thordarson, 2014).

BAE-2B 383, 374, 373, 363, 353, and 343 cm. The basal tephra unit(s) in core BAE-2B-1N was analyzed at six intervals: 383, 374, 373, 363, 353 and 343 cm (Fig. 5.2). Five of the six intervals have major element compositions typical for the Grímsvötn volcano (Fig. 5.5), which in conjunction with their deep stratigraphic position, thickness, and coarse nature are all diagnostic of the 10 ka Grímsvötn tephra series. The 1 cm-thick tephra horizon at 374 cm depth has a major elemental composition consistent with Veiðivötn-Bárðarbunga's tholeiitic magma suite (Fig. 5.5). The formation of three distinct horizons (i.e., lower 10 ka Grímsvötn tephra, middle Veiðivötn-Bárðarbunga tephra and upper 10 ka Grímsvötn tephra) indicates at least three successive eruptions. Considering age constraint on individual 10 ka

Grímsvötn series tephra is currently unavailable and that one or more of these bounds the Veiðivötn-Bárðarbunga tephra, we assign an age estimate of 10400-9900 cal BP to the Veiðivötn-Bárðarbunga tephra.

BAE-2B 322, 320, and 318 cm. We identified three closely spaced basaltic tephra at 322, 320 and 318 cm depths in core BAE-2B-1N, which are all predominately tholeiitic (Fig. 5.4b) and whose major element compositions are compatible with origin within the Grímsvötn volcanic system. The BAE-2B-322 tephra also contains one alkalic grain from Hekla and two other tholeiitic grains; one with origin from Askja and the other from Veiðivötn-Bárðarbunga. The BAE-2B-320 tephra also contains one alkalic grain originating from the Katla system. The BAE-2B-318 tephra is characterized by moderately high MgO wt% (6.49 ± 0.69%, i.e., "primitive basalt"), which has not been produced by the Grímsvötn system in historic time (i.e., within the last 1140 years), but is a well-known feature within the prehistoric tephra record (Óladóttir et al., 2011).

The deep stratigraphic position of these tephra indicates early Holocene deposition (Fig. 5.2). In marine core MD99-2269, ~105 km northeast of Bæjarvötn (Fig. 5.1a), Kristjánsdóttir et al. (2007) developed a well-constrained Holocene cryptotephra record via a combination of calibrated radiocarbon dates (ΔR=0) and paleomagnetic secular variation. An early Holocene Grímsvötn cryptotephra constrained to 9890 ± 120 cal BP exhibits similar chemical attributes to the BAE-2B-322 and -320 tephra (G2-2269, Supplemental U, Kristjánsdóttir et al., 2007). Bæjarvötn's age model, based on key tephra and radiocarbon, suggests that the tephra were deposited at 9380 ± 260 cal BP and 9370 ± 250 cal BP, respectively (Fig. 5.9a). Owing to the fact that the marine reservoir corrections (ΔR) may be as much as 150 years (Eiríksson et al., 2004), the cryptotephra from MD99-2269 may be the same as the tephra from Bæjarvötn. In terms of correlations for BAE-2B-318, primitive basalts of similar composition identified elsewhere on Iceland during the early Holocene include the ThB-1 tephra (8560 cal BP) found in Haukadalsvatn, Hvítárvatn, and Hestvatn, and the ThB-2 tephra (8700 cal BP) from Haukadalsvatn and Hestvatn (Jóhannsdóttir, 2007) (Grímsvötn BP-2, Supplemental U). Due to the older age of the ThB-2 tephra, and the identification of a slightly younger primitive basalt in another Bæjarvötn core (see BAE-1A 232.5-246 cm) we suggest the ThB-2 as a likely correlation. Hence, we provide an estimated age of 8700 cal BP to the BAE-2B-318 tephra and hereafter refer to this as the Grímsvötn BP-2 ("Bæjarvötn Primitive 2") tephra.

BAE-2B 238 cm. A dark colored tephra at 238 cm depth originated from the Hekla transitional-alkaline magma suite. Based on the stratigraphic position 42.5 cm above bark dated to 7370 ± 50 cal BP (CURL-12023, Fig. 5.2, Table 5.1), we suggest a time of deposition during the middle Holocene (Fig. 5.2). The age and distinct basaltic Hekla chemistry indicates that this is the Hekla T regional marker tephra identified in other northeastern Vestfirðir (Harning et al, 2016a, b) and west Iceland lake sediments (Harðardóttir et al., 2001; Jóhannsdóttir, 2007). Thus, we assign an age of 6100 ± 100 cal BP to this tephra (Jóhannsdóttir, 2007).

BAE-2B 187 cm. Major elemental composition of the tephra layer visible at 187 cm depth in Bæjarvötn reveals tephra grains with alkalic and others with tholeiitic affinities (Fig. 5.4b). The composition of the 14 tholeiitic grains reveals Grímsvötn as their source, whereas the 9 alkalic grains are compatible with the Katla system. Kristjánsdóttir et al. (2007) identified several tephra of similar mixed Grímsvötn and Katla origin in marine core MD99-2269 between 5892 and 4599 cal BP. If Bæjarvötn's tephra correlates to one of MD99-2269's, it cannot be determined given the several possibilities in MD99-2269 and lack of more direct age control from Bæjarvötn's sediment surrounding this tephra. Bæjarvötn's

age-depth model estimates a time of deposition at 4530 ± 80 cal BP for the BAE-2B-187 tephra (Fig. 5.9a).

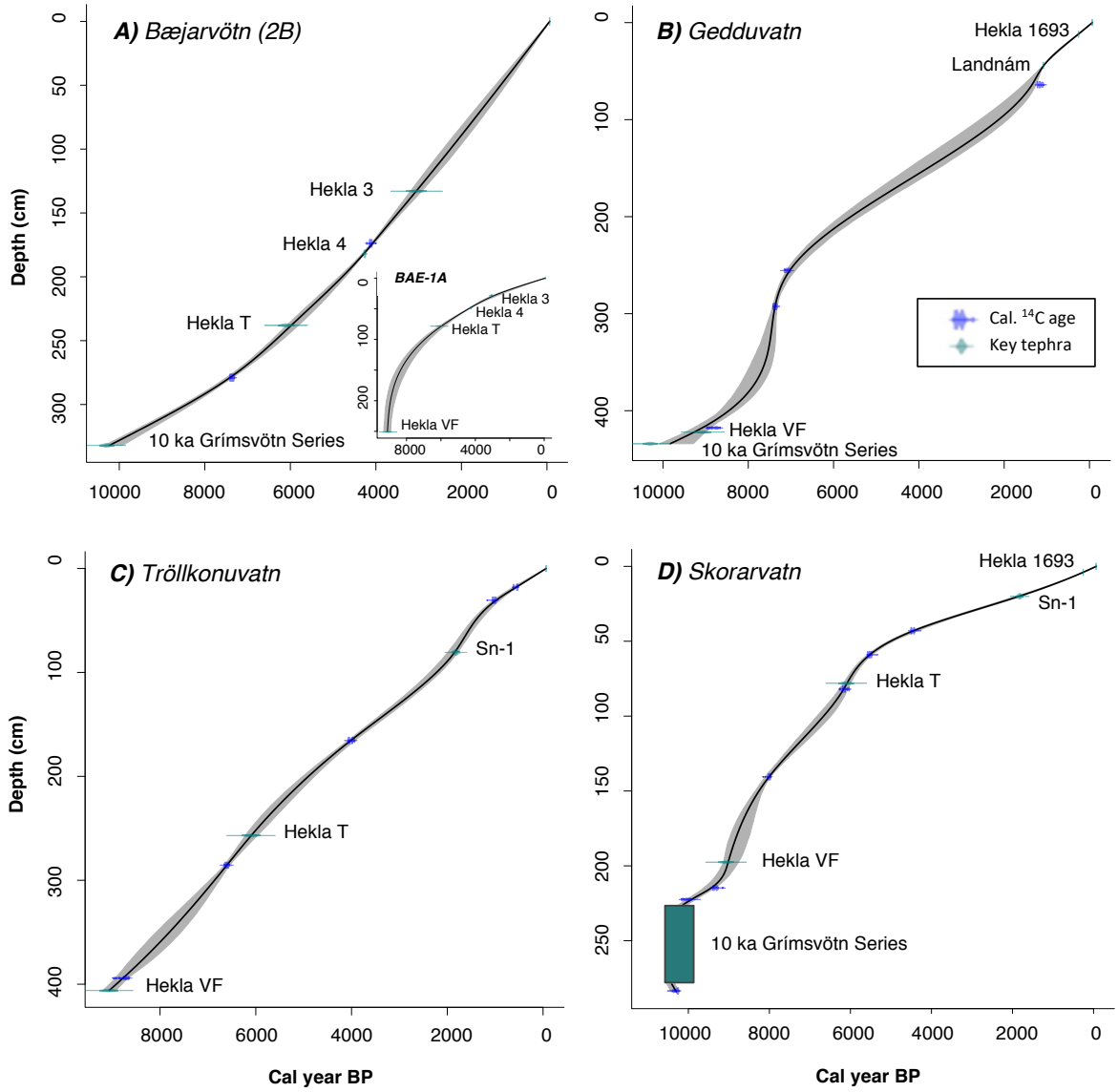

Figure 5.9. *CLAM age models for A) Bæjarvötn 2B and 1A (inset), B) Gedduvatn, C) Tröllkonuvatn and D) Skorarvatn based on calibrated ^{14}C ages (blue) and key tephra of known age (green). Gray shaded areas denote the 95% confidence limit. Detailed ^{14}C information provided in Table 5.1.*

BAE-2B 182 cm. The tephra layer at 182 cm depth is of intermediate composition with SiO_2 content of 56.97 ± 1.39 wt% (n=26) and tholeiitic (i.e., "sub-calcic") in character (Fig. 5.4a). It also contains a minor amount of basaltic tephras, two alkalic grains and four grains of tholeiitic affinity (Fig. 5.4a). The tephra layer is black-brown in color (Fig. 5.3a) and the composition of the intermediate fraction originates from the Hekla volcanic system (Fig. 5.6). Its stratigraphic position implies deposition during the middle Holocene. This age estimate is further supported by a radiocarbon age of 4120 ± 30 cal BP on bark situated 9 cm above the layer (CURL-12004, Table 5.1, Fig. 5.2). In Haukadalsvatn, an intermediate tephra (n=34, HAK-03-27) with similar SiO_2 contents of 57.46 ± 0.71 wt% is constrained to ~4200 cal BP. Detailed comparisons of additional major elements suggests that the BAE-

2B-182 tephra correlates to the HAK-03-27 tephra (Supplemental U) and is consistent with intermediate fractions of the Hekla 4 tephra (4260 ± 10 cal BP, Dugmore et al., 1995), which was dispersed over western Iceland after the cessation of the dominant NNE-trending rhyolitic phase (Larsen and Thorarinsson, 1977). Based on the previous identification of the Hekla 4 in several nearby lake sediment records (Brattihjalli, Reykjarfjörður and Neðra Eyvindarfjarðarvatn, Fig. 5.1b, Schomacker et al., 2016), and its presence in other west Iceland lake sites (e.g., Haukadalsvatn), the Hekla 4 tephra stands as a key marker throughout this region.

BAE-2B 133 cm. The majority of light colored tephra glass at 133 cm depth (Fig. 5.3b) reveals an intermediate composition typified by SiO_2 contents of 62.75 ± 2.38 wt% (Fig. 5.4a), consistent with origin from Hekla's volcanic system (Fig. 5.6). A single basaltic glass shard also reveals source from the Veiðivötn-Bárðarbunga system. The widepread Hekla 3 tephra (3050 ± 120 cal BP, Dugmore et al., 1995) is well expressed throughout Iceland, including Hestvatn (Harðardóttir et al., 2001), Hvítárvatn (Jagan, 2010; Larsen et al., 2011), Neðra Eyvindarfjarðarvatn (Schomacker et al., 2016), as well as marine cores MD99-2269 (Kristjánsdóttir et al., 2007) and MD99-2275 (Larsen et al., 2002). This and the strong chemical similarities to reference data make Hekla 3 the most likely candidate (Supplemental U). Because Vestfirðir's Hekla 3 tephra has an intermediate composition, the tephra here is likely from the middle to latter phase of the eruption (Larsen and Thorarinsson, 1977).

BAE-2B 113 cm. The tephra visible at 113 cm depth is alkaline (Fig. 5.4b) and has major element composition consistent with the Katla volcanic system. The major element composition is nearly identical to that of a tephra at the same depth from Bæjarvötn's short companion core (BAE-2C-113, Fig. 5.2, Supplemental U). Analyses on tephra from Haukadalsvatn have identified a compositionally indistinguishable Katla layer (Katla 2190, 2190 cal BP, Supplemental U), strongly supporting a correlation. Kristjánsdóttir et al. (2007) report two compositionally similar Katla tephra layers in marine core MD99-2269 (Katla K2-2269; 2440 ± 100 cal BP and Katla K1-2269; 1400 ± 60 cal BP). Bæjarvötn's age model indicates deposition at 2120 ± 40 cal BP for the BAE-2B-113 tephra (Fig. 5.9a). The similar age of the BAE-2B-113 tephra and MD99-2269's K2-2269 tephra provide a tentative correlation to the North Iceland Shelf.

BAE-2C 113 cm. A short companion core from Bæjarvötn (BAE10-2C-1N) captures four late Holocene tephra, of which three are obscured in the longer BAE-2B-1N core (Fig. 5.2). Major elemental composition of the tephra at 113 cm depth is consistent with Katla's alkaline magma suite. Identical depth within sediment cores and major elemental chemistry suggest that this tephra correlates to the BAE-2C-113 tephra and the Katla 2190 tephra from Haukadalsvatn (Supplemental U), and potentially, the K2-2269 tephra from marine core MD99-2269.

BAE-2C 78 cm. A younger tephra at 78 cm depth has major element composition that indicates a tholeiitic origin (Fig. 5.4c) from the Veiðivötn-Bárðarbunga system. The tephra has a composition similar to the basaltic component of the Landnám tephra (Larsen et al., 2002, Supplemental U), which was deposited at 1080 cal BP (Haflidason et al., 2000) as well as a slightly younger Veiðivötn tephra from the 10th century (Lawson et al., 2007). Although evidence suggests the silicic component of the Landnám tephra was only dispersed across southern (Larsen et al., 2002) and western Iceland (Jennings et al., 2014), the basaltic component has been documented throughout Iceland (Larsen et al., 2002). The dispersal pattern of the basaltic Landnám component, the similar major elemental composition and the stratigraphic position above the Katla 2190 supports the correlation of this tephra to the Landnám marker.

BAE-2C 71.5 cm. A slightly younger tephra at 71.5 cm depth has major elemental composition demonstrating alkalic affinities (Fig. 5.4c) from the Katla system. The tephra's stratigraphic position above the Landnám tephra (Fig. 5.2) allows correlation to any number of Iceland's historic eruptions recorded since Norse settlement (Thordarson and Larsen, 2007). Notable eruptions with similar major elemental compositions include the Katla 920 and Eldgjá 934 eruptions (Supplemental U). However, traits such as relatively higher K_2O and P_2O_5 of the BAE-2C-71.5 tephra (Table S5.1) are more consistent with the Katla 920 tephra rather than the Eldgjá 934 tephra (Haflidason et al., 1992, 2000; Thordarson, et al., 2001; Óladóttir et al., 2007).

BAE-2C 29 cm. The uppermost tephra in core BAE10-2C-1N (29 cm depth) has a tholeiitic composition (Fig. 5.4c) consistent with the Veiðivötn-Bárðarbunga volcanic system. BAE-2C-29 shares strong chemical attributes to the Veiðivötn 1410, Veiðivötn 1477 and Bárðarbunga 1717 CE tephra found in north Iceland, all of which are virtually indistinguishable (Supplemental U, Haflidason et al., 2000; Larsen et al., 2002, Lawson et al., 2007). Geographical evidence suggests these tephra are restricted to northern and eastern Iceland (Larsen et al., 2002; Lawson et al., 2007) and thus, are unlikely to be archived on the Vestfirðir peninsula. However, documentary evidence suggests that another eruption from the Veiðivötn-Bárðarbunga volcanic system preceded the Bárðarbunga 1717 eruption in the year 1716 CE, and had an ash dispersal trajectory toward northwest Iceland (Jónsson, 1945). Due to the rather uniform major elemental compositions of tephra generated from the Veiðivötn-Bárðarbunga volcanic system during the Late Holocene (Supplemental U), we are unable to discriminate specific eruptions based on chemistry. Therefore, we suggest that this tephra was generated in the Bárðarbunga 1716 eruption based on the observational evidence from Jónsson (1945).

BAE-1A 283.5 and 265 cm. The two deepest tephra (283.5 and 265 cm depths) in Bæjarvötn core BAE10-1A-1N exhibit tholeiitic characteristics (Fig. 5.4a). As their SiO_2 contents range from 58.74 ± 1.13 to 58.93 ± 0.60 wt%, they are intermediate tephras (Fig. 5.4a) with compositions consistent with the Hekla volcanic system. Although neither the 10 ka Grímsvötn tephra series nor deglacial sediment were recovered in this sediment core, the corresponding depths in the BAE-2B-1N core and position below the Hekla VF tephra (Fig. 5.2) indicate an early Holocene age. As no Hekla tephra layers of intermediate composition are known in the current early Holocene tephra stratigraphy to draw correlations to, we employ the age model based on key tephra to constrain potential ages (Fig. 5.9a, inset). By extrapolating the basal sedimentation rate (17.2 yr cm^{-1}), we estimate ages of at least 9600 and 9400 cal BP for the two tephra. To the best of our knowledge, these two tephra represent the oldest intermediate Hekla tephra yet recorded in Iceland.

BAE-1A 255 cm. A basaltic tephra layer of tholeiitic affinity (Fig. 5.4c), at 255 cm depth, has a composition that points to Grímsvötn as the source system. Its stratigraphic position and nearly identical chemical attributes to the BAE-2B-320 (9370 cal BP) tephra from Grímsvötn (Supplemental U) suggests they are correlative. Furthermore, these two Grímsvötn tephra from Bæjarvötn exhibit chemical similarities to a tephra from Haukadalsvatn (HAK-01-10, Supplemental U) constrained to 9280 cal BP. Although the correlation to Haukadalsvatn remains tentative due to some compositional inconsistencies, the tephra correlation between the two Bæjarvötn sediment cores is much stronger. Hence, we provide the formal name Grímsvötn B ("Bæjarvötn") to this tephra in Bæjarvötn.

BAE-1A 251 cm. The major elemental compositions of 60 out of 75 grains analyzed in the basaltic tephra layer at 251 cm depth indicate alkalic affinities (Fig. 5.4c) and origin from the Hekla system. Compositions of the remaining 15 basalt grains exhibit tholeiitic affinities (Fig. 5.4c) consistent with Grímsvötn. Proximity to the tephra at 255 cm indicates

BAE-1A-251 is also of early Holocene age (Fig. 5.2). The identification of only one other early Holocene basaltic Hekla tephra (AlB-1, 9070 cal BP) of identical chemistry in a number of lake sites throughout west Iceland (Jóhannsdóttir, 2007) and on Vestfirðir (see Section 5.6.3) supports the Hekla "AlB-1" tephra as a correlation (Supplemental U). The widespread regional presence of this basaltic Hekla tephra demonstrates its utility as a key regional marker. Hence, we formally provide the new Hekla VF ("Vestfirðir") name to this tephra.

BAE-1A 232.5, 199, and 146 cm. Three tephra at 232.5, 199 and 146 cm depths have major element compositions that reveal tholeiitic affinities (Fig. 5.4c) from Grímsvötn. Furthermore, the moderately high MgO wt% (6.32 ± 0.49 and 6.12 ± 0.45) for the tephra at 199 and 146 cm depths is consistent with the relatively primitive Grímsvötn compositions of Óladóttir et al. (2011). As discussed for the moderately primitive Grímsvötn tephra in Bæjarvötn sediment core BAE10-2B-1N, primitive early Holocene basalts of similar chemistry identified elsewhere in western Iceland include the ThB-2 tephra (8700 cal BP, Jóhannsdóttir, 2007), now referred to as the Grímsvötn BP-2 tephra, and the ThB-1 tephra (8560 cal BP, Jóhannsdóttir, 2007). The stratigraphic positions and similar chemistries of BAE-1A-199 to the BAE-2B-318 tephra support a Grímsvötn BP-2 tephra correlation (Supplemental U). The stratigraphic positions and similar compositions of BAE-1A-146 and the ThB-1 tephra point to a tentative correlation between these tephra as well (Supplemental U). However, we do note that there are offsets between the elemental compositions of the BAE-1A-199, -146 tephra and the ThB-2 and ThB-1 reference compositions. In addition to the similar stratigraphic positions and elemental compositions noted, the geographic locations of all lakes are northwest of Grímsvötn, which further supports these correlations at this time. Hence, we term this younger tephra the Grímsvötn BP-1 ("Bæjarvötn Primitive 1") tephra, with an age assignment of 8560 cal BP.

BAE-1A 111 cm. Major elemental composition of the tephra at 111 cm depth demonstrates predominately alkalic affinities (Fig. 5.4c) consistent with Katla (Fig. 5.7). Two additional grains are tholeiitic (Fig. 5.4c) with affinities to the Grímsvötn system. Stratigraphic position implies deposition during the early to middle Holocene (Fig. 5.2). A Katla tephra of identical major elemental composition is found in Haukadalsvatn and dated to 6400 cal BP (HAK-2-9, Geirsdóttir et al., 2009, Supplemental U). The frequency in basaltic tephra peaks and elemental composition of tephra glass from several marine sediment cores southeast of Greenland also indicate that there is only one Katla basalt tephra ("Katla EG") that dispersed westward during the early to middle Holocene (Jennings et al., 2014). Due to the distinct major elemental composition (Supplemental U), in conjunction with the tephra's stratigraphic position suggesting a middle Holocene age, we correlate the BAE-1A-111 tephra to the Katla EG tephra marker and assign the corresponding age of 6400 cal BP from Haukadalsvatn.

BAE-1A 78.3 cm. The basaltic tephra at 78.3 cm depth is transitional-alkaline (Fig. 5.4c) and has composition consistent with Hekla as the source system (Fig. 5.6). Its major element composition along with stratigraphic position indicates this is the Hekla T tephra and correlates with BAE-2B-238 as well as the Hekla T tephra found in Tröllkonuvatn and Skorarvatn (Supplemental U, Harning et al, 2016a, b). Thus, we assign an age of 6100 ± 100 cal BP (Jóhannsdóttir, 2007).

BAE-1A 48.5 cm. Major elemental composition of the tephra at 48.5 cm depth reveal three distinct compositions. The largest fraction of grains (n=6) has composition consistent with an origin from the tholeiitic Grímsvötn volcanic system (Fig. 5.4c). Five grains have tholeiitic and intermediate composition, corresponding to Hekla (Figs. 5.4c and 5.6), and four silicic grains have an unusual alkalic composition (Fig. 5.4c and 5.10). Stratigraphic

position above the Hekla T tephra suggests deposition during the middle Holocene. The SiO_2 contents of 58.05 ± 1.18 wt%, and high CaO, MgO, FeO and low K_2O of the Hekla component are diagnostic of Hekla 4's late stage intermediate tephra (Supplemental U). Based on the bi-elemental discrimination plots, the tightly clustered chemistry of the four silicic alkaline tephra shards reveals no coherency with other silicic tephras analyzed thus far in Iceland, although the elemental composition, particularly the unusually high K_2O content, is more in line with that of the Torfajökull volcanic system (Fig. 5.10). The glass shards also register very low MgO, CaO and P_2O_5 and low TiO_2 and FeO values revealing a very evolved composition. Further discrimination on a ternary plot indicates a domestic (ocean island rhyolite) origin with affinities to Hekla, in particular Hekla 4 (Fig. 5.10c). Jennings et al. (2014) noted that many Hekla layers found on the SE Greenland Shelf feature a minor component of silicic grains with compositions akin to Torfajökull and Katla, which we suggest is also reflected in our Hekla 4 data.

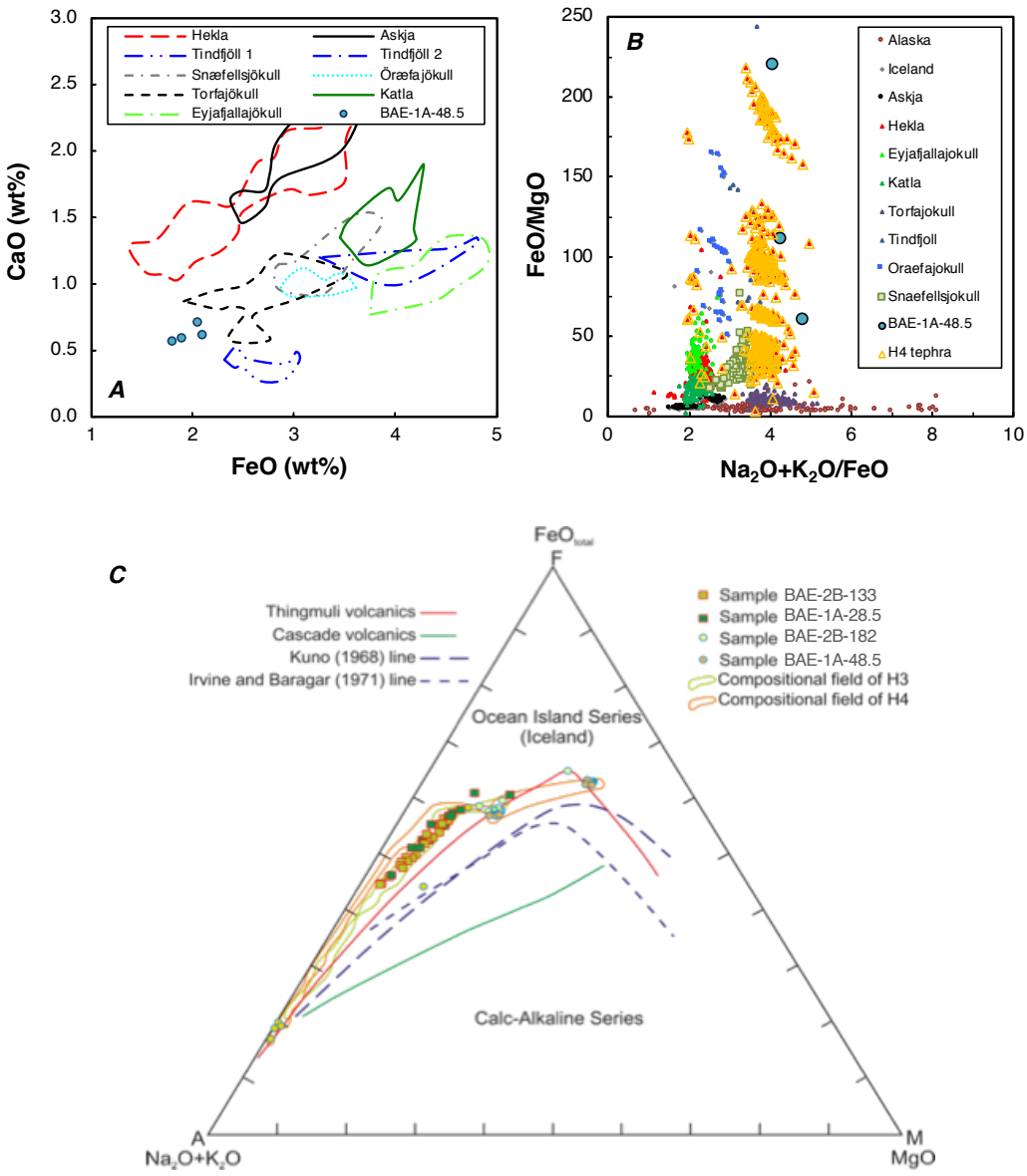

Figure 5.10. *Elemental biplots of the silicic component from tephra sample BAE-1A-48.5. A) Comparison against established Icelandic compositional fields. B) More discriminatory plots including compositional fields from Alaska (Riehle et al., 1999) and the Hekla 4 tephra. C) AFM ternary plot displaying the magma series*

and volcanic environments of Bæjarvötn's Hekla 3 and Hekla 4 tephra. Although similar to Cascadian tephra, the silicic portion of the BAE-1A-48.5 tephra maintains an ocean island affinity consistent with Iceland.

BAE-1A 28.5 cm. A light-colored tephra at 28.5 cm depth has an intermediate composition (Fig. 5.4a, 63.84 ± 1.81 wt% SiO_2) consistent with origin from Hekla (Fig. 5.6). The stratigraphic position of the tephra and the identical chemical composition to the BAE-2B-133 tephra (Fig. 5.6, Supplemental U) confirms the presence of the intermediate component of the Hekla 3 tephra in Bæjarvötn and on eastern Vestfirðir. Thus, we assign an age of 3050 ± 120 cal BP to this tephra (Dugmore et al., 1995).

5.5.1.2. Gedduvatn

Gedduvatn (GDD, 470 m asl, 65.71822°N, 22.18880°W) sits on a high mountain pass ~35 km south of Drangajökull's southern margin (Fig. 5.1b). The lake was deglaciated by the time of at least one eruption corresponding to the 10 ka Grímsvötn Series (Harning et al., 2016b). Subsequent sedimentation in GDD10-1A-1B was dominated by organic gyttja with eight additional, visible tephra (Fig. 5.2). Of the nine, one tephra can be categorized as intermediate whereas the other eight are mafic. Furthermore, one is comprised of mixture of alkaline and tephra grains, two are strictly alkaline and the remaining six are tholeiitic (Table S4.3).

GDD 434 cm. The basal tephra from Gedduvatn at 434 cm depth was previously reported in Harning et al. (2016b) and linked to the "Saksunarvatn tephra" based on its composition and large grain size. However, because the tephra in Gedduvatn was clearly dispersed to the west of Grímsvötn, we highlight that is likely not the same tephra layer as the one in Saksunarvatn, Faroe Islands (Mangerud et al., 1986), which was dispersed eastward from Iceland. As such, the GDD-434 tephra is hereafter referred to as one of seven (or more) tephra from the 10 ka Grímsvötn eruptions that dispersed westward (Supplemental U, Jóhannsdóttir, 2007; Jennings et al., 2014; Thordarson, 2014).

GDD 422 cm. Major element composition of the basaltic tephra at a depth of 422 cm is transitional-alkaline (Fig. 5.4d) and consistent with the Hekla system (Supplemental K). A macrofossil just above the tephra has an age of 8820 ± 160 cal BP (CURL-12031, Fig. 5.2, Table 5.1), providing a minimum age on tephra deposition. This age constraint and the presence of only one early Holocene Hekla basalt tephra layer on Vestfirðir (Harning et al., 2016b) strongly indicate that this is the Hekla VF tephra (Supplemental U, Jóhannsdóttir, 2007).

GDD 197, 195, 193, and 182 cm. Four tightly spaced basaltic tephra (197, 195, 183 and 182 cm depth), share similar major element composition for the majority of grains analyzed and all exhibit tholeiitic affinities (Fig. 5.4d). Despite their placement along the boundary of the VAK and TGK trends (e.g. Fig. 5.5b), the consistent placement of the data within the WVZ compositional field on bi-elemental plots indicates that these tephra layers were produced by eruptions from the WVZ. However, each layer contains minor abundances of grains with different compositions. In addition to the 12 grains of WVZ composition, the GDD-197 dataset features a tholeiitic grain of Grímsvötn affinity, an alkalic basalt grain of Katla affinity and an intermediate grain of Hekla system affinity. Besides the 13 grains of WVZ affinity, the GDD-195 tephra contains one grain with Grímsvötn and one with Katla attributes. The GDD-183 dataset contains 11 grains of WVZ and 4 of Grímsvötn affinity,

while GDD-182 has 14 WVZ grains and one dacitic Katla grain. The stratigraphic position of these tephra suggests that they are of middle Holocene age (Fig. 5.2). A series of both central vent and fissure eruptions took place in the immediate vicinity of Langjökull between the Hekla 5 and Hekla 4 eruptions (~6100 and 4200 cal BP, Sinton et al., 2005). At this stage it is difficult to correlate the Gedduvatn tephra directly to these events. Gedduvatn's age model constrains the deposition of these WVZ tephra to 5530 ± 210, 5470 ± 220, 5070 ± 250, and 5040 ± 260 cal BP, respectively (Fig. 5.9b).

GDD 69 cm. The tephra at 69 cm depth in the Gedduvatn core reveals alkali affinities (Fig. 5.4d) consistent with Katla's volcanic system. Stratigraphic position implies deposition during the late Holocene, which is supported by a macrofossil at 64 cm depth radiocarbon-dated to 1160 ± 70 cal BP (CURL-12689, Fig. 5.2, Table 5.1). Three Katla tephra constrained to this age window in Haukadalsvatn demonstrate virtually indistinguishable major element compositions in comparison to the GDD-69 tephra (Supplemental U). Because these Haukadalsvatn Katla tephra only span ~25 years (1270, 1260 and 1245 cal BP) and the Gedduvatn core lacks precise age control within this window, we assign an average of the Haukadalsvatn ages (~1260 cal BP) to the GDD-69 tephra.

GDD 44 cm. Seven of the analyzed tephra grains are tholeiitic basalt (Fig. 5.4d) with affinities consistent with origin from Grímsvötn, whereas five tholeiitic basalts are from the Veiðivötn-Bárðarbunga system. Two grains are alkalic (Fig. 5.4d) and have Katla affinities and one is an alkalic silicic grain consistent with Torfajökull. The radiocarbon date beneath the tephra suggests late Holocene deposition after 1160 ± 70 cal BP (CURL-12689, Fig. 5.2, Table 5.1). There exist two main components of the Landnám tephra (1080 cal BP) generated by simultaneous eruptions from the Veiðivötn (basaltic) and Torfajökull (rhyolitic) volcanic systems (Larsen et al., 1984, 1999), both of which are present in Haukadalsvatn's sedimentary record (HAK-01-02 and HAK-01-03, Supplemental U). Gedduvatn's five Veiðivötn glass shards (49.25 ± 0.30 wt% SiO_2) are consistent with Landnám's basaltic compositional field (Supplemental U), while the composition of the single Torfajökull grain (70.64 wt% SiO_2 and 4.41 wt% K_2O) is consistent with the rhyolitic component (Supplemental U, Larsen et al., 1999, 2002). Despite the fact that both components of the Landnám tephra have been found in Greenland ice cores (Grönvold et al., 1995; Zielinski et al. 1997), as well as the SE Greenland Shelf (Jennings et al., 2014), the rhyolitic component on Vestfirðir has until now only been documented in the southwestern corner of the peninsula from the lake Vatndalsvatn (Jennings et al., 2014). The presence of Grímsvötn and Katla tephra likely reflects known eruptions from these volcanic systems, which occured in the centuries preceding the "Landnám" eruptions (e.g., Wastegård et al., 2003; Sigurgeirsson et al., 2013).

GDD 13.5 cm. A 0.5 cm-thick tephra (Fig. 5.3c) at 13.5 cm depth is intermediate (e.g., 58.89 ± 0.35 wt% SiO_2) with tholeiitic composition (Fig. 5.4a) and affinities for the Hekla volcanic system. Stratigraphic position implies deposition during historical time or within the last 1140 years (Fig. 5.2). The major element composition is identical to chemical attributes of the Hekla 1693 tephra found in Skorarvatn (59.15 ± 0.47 wt% SiO_2, Harning et al., 2016a). The Hekla 1693 tephra is the only known intermediate tephra with significant thickness (0.1-0.5 cm) to have been dispersed to Vestfirðir during the Late Holocene (Thorarinsson, 1967; Janebo et al., 2016). Thus, we conclude that Gedduvatn also archives the Hekla 1693 tephra.

5.5.1.3. Tröllkonuvatn

Tröllkonuvatn (TRK, 366 m asl, 66.14252°N, 22.05607°W) sits ~1 km east of Drangajökull (Fig. 5.1b). Organic, non-glacial sedimentation began at ~8.7 ka, following the retreat of proto-Drangajökull from the lake catchment, and prevailed until the Late Holocene when Drangajökull episodically expanded into Tröllkonuvatn's catchment at ~950 CE and ~1450 CE, delivering abundant clastic sediment. Four tephra are visible in the sediment core (Fig. 5.2), one of which is silicic whereas the remaining three are mafic. Furthermore, two tephra are alkaline and the other two are transitional-alkaline (Table S5.4). Harning et al. (2016a) previously identified the Hekla T (6100 cal BP) and Snæfellsjökull-1 (Sn-1, 1820 cal BP) tephra in Tröllkonuvatn's sediment record.

TRK 406 cm. Near the top of the basal glaciolacustrine sediment package, we identify a tephra layer at 406 cm depth (Fig. 5.2). Major elemental composition of the basaltic TRK-406 tephra exhibits a transitional-alkaline nature (Fig. 5.4d) and its relatively low TiO_2 and high MgO contents are consistent with origin from the Hekla volcanic system. Stratigraphic position of this tephra below a moss layer with a radiocarbon age of 8750 ± 100 cal BP (CURL-19502, Fig. 5.2, Table 5.1) and strong chemical similarities to the Hekla VF in Bæjarvötn, Gedduvatn and Skorarvatn (Supplemental U) supports this as the Hekla VF tephra.

TRK 257 cm. Above the Hekla VF tephra is another basaltic tephra at 257 cm depth, exhibiting transitional-alkaline characteristics (Fig. 5.4d) consistent with the Hekla volcanic system. Stratigraphic position above a moss layer at 285.5 cm dated to 6610 ± 40 (CURL-21037, Fig. 5.2, Table 5.1) suggests deposition during the middle Holocene. The indistinguishable chemical attributes compared to the Hekla T tephra (Supplemental U), the only known middle Holocene basaltic Hekla tephra on Vestfirðir during this time, supports this as the most likely correlation, with an age of 6100 cal BP (Jóhannsdóttir, 2007).

TRK 118 cm. The chemical composition of a tephra at 118 cm depth verifies mildly alkalic affinities (Fig. 5.4d) from the Katla system. The stratigraphic position implies deposition during the middle-late Holocene (Fig. 5.2). The chemistry is indistinguishable from the Katla 2190 tephra identified in Bæjarvötn (BAE-2C-113 and -2B-113) and Haukadalsvatn (Supplemental U). Using Tröllkonuvatn's age model (Fig. 5.9c), we estimate the age of TRK-118 to be 2690 ± 100 cal BP. The similar stratigraphic position and estimated age to the tephra from Bæjarvötn may suggest a correlation to the Katla 2190 tephra.

TRK 81 cm. The tephra in Tröllkonuvatn at 81 cm depth is alkalic and predominately rhyolitic (Fig. 5.4a). The major elemental composition is similar to the Snæfellsjökull-1 tephra (Sn-1, 1820 ± 90 cal BP, Larsen et al., 2002) identified in marine core MD99-2275 (Supplemental U, Larsen et al., 2002) and Haukadalsvatn (Supplemental U), supporting this as a correlation.

5.5.1.4. Skorarvatn

Skorarvatn (SKR; 183 m asl, 66.25627°N, 22.32213°W) sits ~3 km north of Drangajökull (Fig. 5.1b), but has not received glacier meltwater since ~9.3 ka (Harning et al., 2016b). Thus, subsequent lake sediment consists of organic gyttja interspersed with discrete tephra layers. The composite sediment core (SKR14-6A/4A-1N) contains seven, fairly evenly spaced tephra (Fig. 5.2), of which one is silicic, one is intermediate and the remaining four are mafic. Furthermore, one is alkaline, two are transitional-alkaline and three are tholeiitic in character (Table S4.5). Harning et al. (2016a, b) showed that the following tephra layers

in Skorarvatn have been preserved: a layer from the 10 ka Grímsvötn series (originally referred to as the "Saksunarvatn tephra"), Hekla VF (9070 cal BP, formerly "AlB-1"), Hekla T (6100 cal BP), Sn-1 (1820 cal BP) and Hekla 1693.

SKR 284-235 cm. Within Skorarvatn's basal glaciolacustrine sediment package are tephra at 284-278, 266-246 and 242-230 cm depths (Fig. 5.2). Major elemental compositions from tephra subsampled at 235 cm depth (Harning et al., 2016b) and 250 cm depth have similar physical and chemical attributes. Both of these tephra layers show no evidence of reworking and are tholeiitic in character (Fig. 5.4d). They both plot within the Grímsvötn compositional field as well as within the 10 ka Grímsvötn tephra series domain (Supplemental U). Hence, we take these layers to represent two of the seven 10 ka Grímsvötn tephra series layers dispersed westward (Jóhannsdóttir, 2007; Jennings et al., 2014; Thordarson, 2014).

SKR 200 cm. At basaltic tephra at 200 cm depth is transitional-alkaline (Fig. 5.4d) with major element composition consistent with the Hekla volcanic system. Stratigraphic position near the base of the non-glacial sediment and ~15 cm above a radiocarbon age of 9340 ± 60 cal BP (CURL-19489, Fig. 5.2, Table 5.1) demonstrates an early Holocene time of deposition. The strong chemical similarities to the only other known basaltic Hekla tephra found on Vestfirðir during this window of the Holocene underpins this as the Hekla VF tephra (9070 ± 100 cal BP, Jóhannsdóttir, 2007, Supplemental U).

SKR 78 cm. Harning et al. (2016a) previously documented the tephra located at 78 cm depth in Skorarvatn. The major elemental composition of all analyzed glass shards reveals a transitional-alkaline nature (Fig. 5.4d) and Hekla affinities. The stratigraphic position 1 cm above a radiocarbon date of 6120 ± 90 cal BP (CURL-21035, Fig. 5.2, Table 5.1) and close chemical correspondence to the basaltic Hekla T tephra (6100 cal BP) identified in other lakes from Vestfirðir and elsewhere across western Iceland (Jóhannsdóttir, 2007) strongly point to the Hekla T tephra as the most likely correlation (Supplemental U).

SKR 20 cm. Skorarvatn's tephra at 20 cm depth is alkalic, predominately rhyolitic (Fig. 5.4a) and demonstrates an origin from the Snæfellsjökull central volcano (Fig. 5.8). The tephra's upper stratigraphic position indicates a late Holocene age (Fig. 5.2). Comparison of SKR-20's major element composition to the Sn-1 tephra identified in nearby Tröllkonuvatn (TRK-81), marine core MD99-2275 (Larsen et al., 2002) and Haukadalsvatn support the Sn-1 as the most likely correlation (Supplemental U).

SKR 4 cm. The 0.25-cm thick tephra (Fig. 4.3a-b) at 4 cm depth in Skorarvatn is intermediate (e.g., 59.15 ± 0.47 wt% SiO_2), tholeiitic in composition (Fig. 5.4a) and demonstrates affinities for the Hekla volcanic system. Stratigraphic position above the Sn-1 tephra suggests deposition during the latest Holocene (Fig. 5.2), and likely within historic time (last 1140 years). Major element composition is identical to chemical attributes of the Hekla 1693 tephra found in Gedduvatn (Supplemental U). The estimated age, chemical correlation, and thickness compared to the revised isopach maps of Janebo et al. (2016), further supports this as the Hekla 1963 tephra.

5.6 Discussion

5.6.1 Composite Vestfirðir Tephra Stratigraphy and Chronology

We present geochemical, stratigraphical and chronological evidence supporting the identification of 30 tephra from Vestfirðir lake sediment (Table 5.2). The highest density of

tephra are found during the early Holocene (Fig. 5.11), in line with studies suggesting intensified volcanism as a result of decompression melting of the mantle following deglaciation of the Icelandic Ice Sheet (Sigvaldason et al., 1992; Sinton et al., 2005). The relative scarcity of tephra in the composite Vestfirðir stratigraphy (n=30) compared to the

Table 5.2. *Composite Vestfirðir tephra stratigraphy and chronology. Thicknesses are typical for all sites unless range given.*

Tephra ID	Composition	Thickness (cm)	Inferred Age (cal BP) **Estimated from age model*	Lakes (This study; Harning et al., 2016b; Schomacker et al., 2016)
Bárðarbunga 1716	Basalt; tholeiitic	0.4	233	Bæjarvötn
Hekla 1693	Intermediate	0.25-0.5	257	Gedduvatn, Tröllkonuvatn, Brattihjalli
Katla 920	Basalt; alkalic	0.5	1030	Bæjarvötn
Landnám (*V-B*)	Basalt; tholeiitic	0.4	1080	Bæjarvötn, Gedduvatn
Landnám (*Torfajökull*)	Rhyolite; alkalic	0.4	1080	Gedduvatn
Katla 1260	Basalt; alkalic	0.5	1270-1245	Gedduvatn
Snæfellsjökull-1	Rhyolite; alkalic	0.3	1820 ± 90	Tröllkonuvatn, Skorarvatn, Reykjarfjörður, Neðra Eyvindarfjarðarvatn, Dagverðardalur, Neðra Hválárvatn
Katla 2190	Basalt; alkalic	0.5	2190	Bæjarvötn, Tröllkonuvatn
Hekla 3	Intermediate	0.5	3050 ± 120	Bæjarvötn, Neðra Eyvindarfjarðarvatn
Hekla 4	Intermediate	0.5	4260 ± 10	Bæjarvötn, Brattihjalli, Reykjarfjörður, Neðra Eyvindarfjarðarvatn
Grímsvötn/Katla mix	Basalt; tholeiitic/alkalic	0.5	**4530 ± 80*	Bæjarvötn
WVZ	Basalt; tholeiitic (high MgO)	0.2	**5040 ± 260*	Gedduvatn
WVZ	Basalt; tholeiitic (high MgO)	0.2	**5070 ± 250*	Gedduvatn
WVZ	Basalt; tholeiitic (high MgO)	0.4	**5470 ± 220*	Gedduvatn
WVZ	Basalt; tholeiitic (high MgO)	0.5	**5530 ± 210*	Gedduvatn
Hekla T	Basalt; transitional-alkaline	1.75	6100 ± 100	Bæjarvötn, Tröllkonuvatn, Skorarvatn, Brattihjalli
Katla EG	Basalt; alkalic	1.0	6400	Bæjarvötn
Grímsvötn BP-1	Primitive basalt; tholeiitic	0.3	8560 ± 100	Bæjarvötn
Grímsvötn BP-2	Primitive basalt; tholeiitic	0.2	8700 ± 100	Bæjarvötn
Grímsvötn	Basalt; tholeiitic	0.2		Bæjarvötn
Hekla VF	Basalt; transitional-alkaline	0.4	9070 ± 100	Bæjarvötn, Gedduvatn, Tröllkonuvatn, Skorarvatn, Reykjarfjörður, Neðra Eyvindarfjarðarvatn, Neðra Hválárvatn, Dagverðardalur?
Grímsvötn B	Basalt; tholeiitic	0.4	**9370 ± 250*	Bæjarvötn
Grímsvötn	Basalt; tholeiitic	0.5	**9380 ± 260*	Bæjarvötn
Hekla	Intermediate	0.5	**~9400*	Bæjarvötn
Hekla	Intermediate	0.5	**~9600*	Bæjarvötn
10 ka Grímsvötn Series (3 layers)	Basalt; tholeiitic	12-128	10400-9900	Bæjarvötn, Gedduvatn, Skorarvatn, Gjögurvatn, Svartárgilsvatn
Veiðivötn-Bárðarbunga	Basalt; tholeiitic	1.0	10400-9900	Bæjarvötn
Tv-3	Basalt; tholeiitic		**~10800*	Bæjarvötn

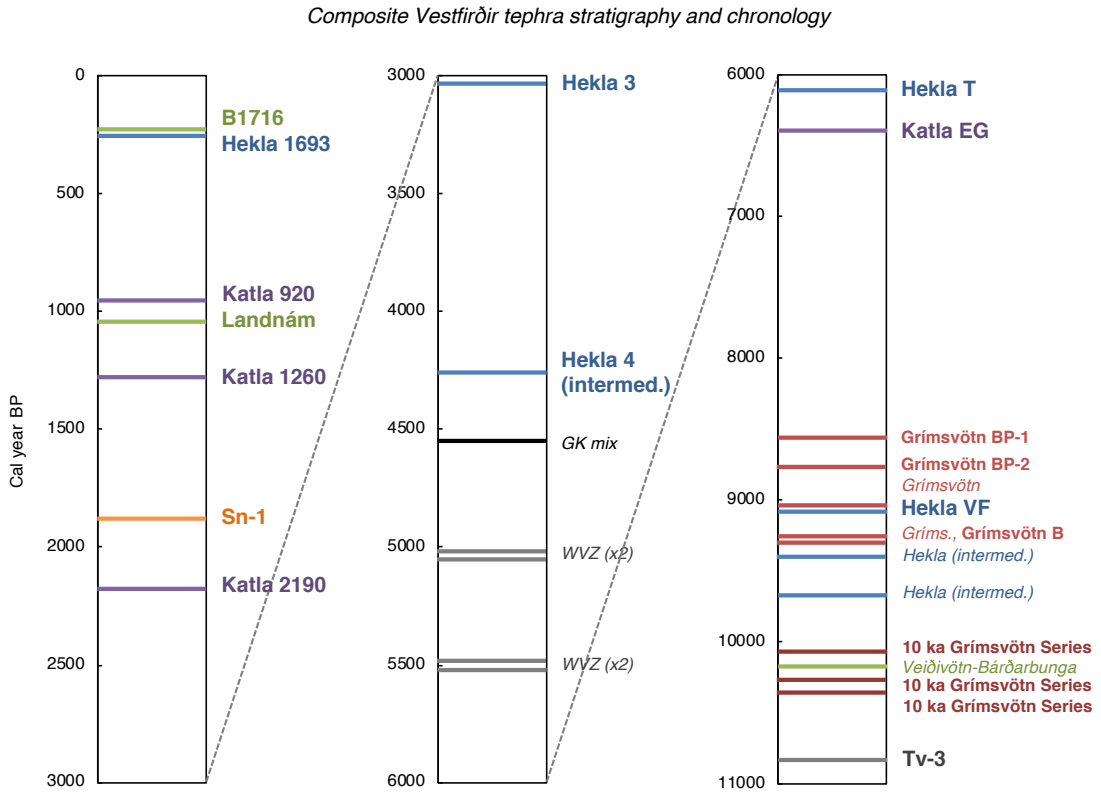

Figure 5.11. *Composite Vestfirðir tephra stratigraphy and chronology. Bold key tephra are of known age whereas italicized tephra are constrained with lake age models. Tephra colors correspond to source volcanic system, as shown in Fig. 5.1a. Note: the second 10 ka Grímsvötn Series layer and the overlying Veiðivötn tephra are only relatively constrained. They are separated for clarity between the upper and lower 10 ka Grímsvötn series tephra, which are constrained by* ^{14}C *ages.*

more abundant tephra archived in Haukadalsvatn, west Iceland (n=40, Geirsdóttir et al., 2009, 2013; Thordarson, 2017, unpublished data), Hvítárvatn, central Iceland (n=76, Jóhannsdóttir, 2007; Jagan, 2010; Thordarson, 2017, unpublished data), Hestvatn, south Iceland (n=118, Harðardóttir et al., 2001; Thordarson, 2017, unpublished data), Vestra Gíslholtsvatn, south Iceland (n=109, Blair et al., 2015; Thordarson, 2017, unpublished data), or Lake Lögurinn, east Iceland (n=157, Gudmundsdóttir et al., 2016), is likely due to Vestfirðir's distance from the active volcanic zones and belts, compounded by the prevailing wind directions which most frequently carry ash plumes northeastward (Lacasse, 2001).

Not one of the Vestfirðir lakes archives the complete stratigraphy. As such, our composite was only obtainable through the analysis of multiple lake sediment cores, which underscores the necessity of using multiple archives when constructing tephra stratigraphic records. Because the tephra exhibit no evidence for remobilization (e.g., Boygle, 1999), several other processes were likely dictating where tephra were archived. During the early Holocene, the absence of the 10 ka Grímsvötn tephra series in Tröllkonuvatn was controlled by more extensive glacial ice covering the lake at the time of the eruption (Fig. 5.12b, Harning et el., 2016b). After proto-Drangajökull receded to smaller than present dimensions by ~9.2 ka (Harning et el., 2016b), the variability of subsequent tephra between lake sites on Vestfirðir may provide constraint on ash plume boundaries (Fig. 5.12). As an example, the four middle Holocene WVZ tephra were only found in Gedduvatn, suggesting a restricted dispersal trajectory toward Vestfirðir, whereas the Hekla VF, Hekla T and Hekla 1693 tephra covered substantially larger areas, evidenced by their preservation in lake records throughout

west Iceland (Fig. 5.12a). Other factors, such as summer lake ice cover, are likely to be less influential at this time as local summer temperatures were rising to their early-middle Holocene maximum in response to elevated northern hemisphere summer insolation (Harning et el., 2016b). However, this period was also matched by reduced northern hemisphere winter insolation (Berger and Loutre, 1991). Hence, if eruptions took place during the winter, then lake ice cover cannot be ruled out as a factor governing tephra deposition during the early-middle Holocene.

As northeastern Vestfirðir's summer temperature decreased during the middle-late Holocene (Harning et al., 2016a, b) lake ice cover likely became a more important influence on the presence/absence of tephra in Vestfirðir lake sediment. The lower spring/summer temperatures would shorten the ice-free season allowing limited or no opportunity for tephra to be deposited in open lake water, at times of the year when the prevailing winds are most likely to shift toward easterlies (Lacasse, 2001). Furthermore, the greatest influence of ice cover would likely be felt at higher elevation lake sites where temperatures are lower due to the elevational lapse rate. As an example, the Hekla 3 tephra (~3050 cal BP) is archived in Neðra Eyvindarfjarðaravatn (NE, 300 m asl, Schomacker et al. 2016) and Bæjarvötn (140 m asl), but not in higher-elevation Tröllkonuvatn (366 m asl). Either Tröllkonuvatn was covered by lake ice at ~3050 cal BP (option 1) or the ash plume steered south of the lake catchment (option 2, Fig. 5.12b), both of which would prevent the direct deposition of the tephra into the lake. However, we cannot rule out the possibility of tephra incorporation into winter lake ice, and subsequent deposition into lake sediment after ice out during the following spring/summer. On the other hand, entrapment of tephra in snow patches (e.g., Davies et al., 2007) is an unlikely scenario. If this were to occur, tephra horizons would likely include abraded tephra fragments along with foreign debris, none of which were observed. A second example occurs during the Little Ice Age (1250-1850 CE), when Tröllkonuvatn was largely filled with glacial ice leaving a small, unoccupied basin where the sediment core was recovered (Harning et al. 2016a). The documentation of the Hekla 1693 tephra over much of Vestfirðir (Fig. 4.12b) but not in Tröllkonuvatn would suggest that the non-glaciated sub-basin was covered by lake ice at the time of the Hekla 1693 eruption on February 13th, 1693 CE (Thorarinsson, 1967). Despite the low temperatures induced by the winter season as well as orbital parameters at the time of the Hekla 1693 eruption, Gedduvatn and Skorarvatn must have remained at least partially ice free due to the presence of the primary tephra in their sedimentary sequences.

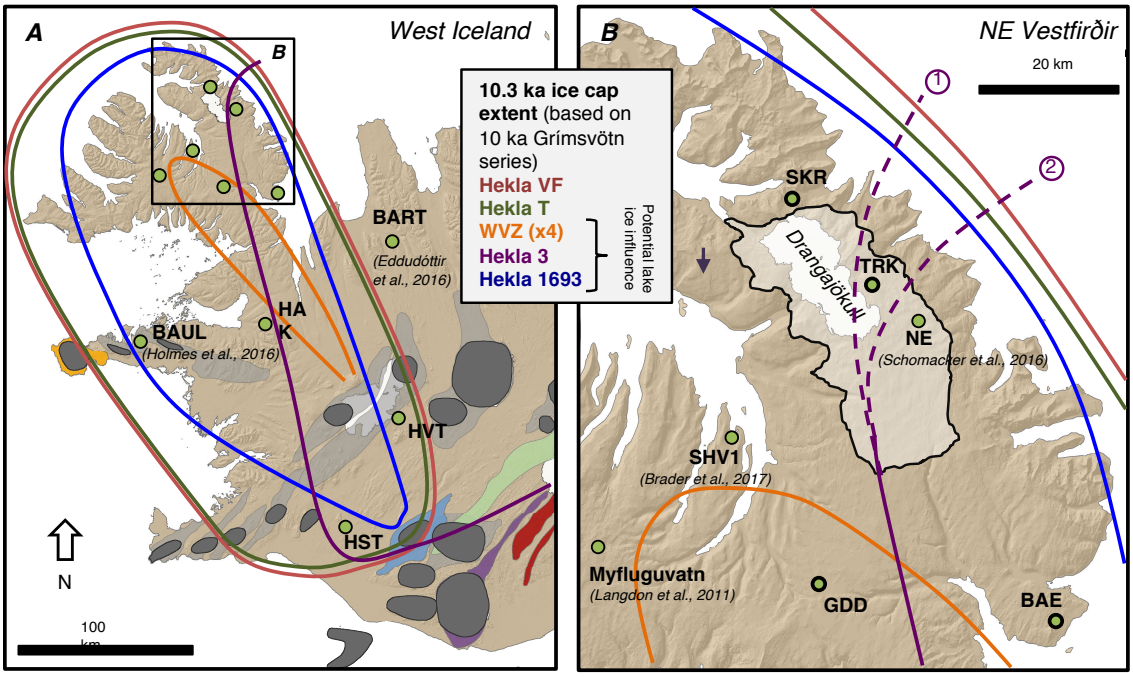

Figure 5.12. *Estimated dispersal boundaries of select tephra. Limits based on the presence/absence of tephra in A) west Iceland lake sediment records and B) Vestfirðir lake sediment records and soils sites (green circles, Harðardóttir et al., 2001; Jóhannsdóttir, 2007; Langdon et al., 2011; Eddudóttir et al., 2016; Harning et al., 2016a, 2016b; Holmes et al., 2016; Schomacker et al., 2016; Brader et al., 2017; this study). HAK = Haukadalsvatn, HVT = Hvítárvatn, HST = Hestvatn. 10.3 ka extent of proto-Drangajökull delineation based on the presence/absence of the 10 ka Grímsvötn tephra series in a network of lake sediment and soil sites (Harning et al., 2016b).*

5.6.2 10 ka Grímsvötn Tephra Series

The so-called "Saksunarvatn tephra" is generally found as a single horizon in Iceland (Björck et al., 1992; Eiríksson et al., 2000b; Andrews et al., 2002; Geirsdóttir et al., 2002; Caseldine et al., 2003; 2006; Principato et al., 2006; Blair et al., 2015; Gudmundsdóttir et al., 2016) and across the broader northern North Atlantic (Mangerud et al., 1986; Merkt et al., 1993; Grönvold et al., 1995; Birks et al., 1996). Thus, the tephra deposit has been attributed to be the product of one Grímsvötn eruption at ~10300 cal BP. However, Jóhannsdóttir (2007) described three discrete units of nearly identical "Saksunarvatn tephra" composition and grain morphology in Haukadalsvatn, Hestvatn and Hvítárvatn. Based on sediment accumulation rates of laminated sediment separating each tephra layer in Hvítárvatn, Jóhannsdóttir (2007) concluded that this Grímsvötn tephra sequence was formed over the course of ~120 years from three large phreatoplinian eruptions. More recent studies of Haukadalsvatn, Hestvatn and Hvítárvatn lake sediment and soil profiles in Iceland (Thordarson, 2014) in addition to marine sediment cores from the SE Greenland Shelf (Jennings et al., 2014) have revealed as many as seven indistinguishable tephra layers (i.e., 10 ka Grímsvötn tephra series) correlative to the "Saksunarvatn tephra", dated between 10400 and 9900 cal BP, that were dispersed to the west of Grímsvötn.

Our sediment record from Skorarvatn reveals three distinct Saksunarvatn-like tephra units. The chemical attributes and large, sand-sized grains of the upper two tephra suggest that they are correlative to the 10 ka Grímsvötn tephra series. The third basal layer likely correlates to the 10 ka Grímsvötn tephra series as well based on its large grain size and

deeper stratigraphic position. The radiocarbon date of the moss macrofossil within the basal tephra layer (CURL-21033) is calibrated to 10300 cal BP and the macrofossil above the upper tephra layer (CURL-21041) is calibrated to 10060 cal BP (Fig. 5.2, Harning et al., 2016b). The former date is consistent with that in the Greenland (NGRIP and GRIP) ice cores (10300 ± 90 cal BP, Rasmussen et al., 2006), which may suggest that the "Saksunarvatn tephra" found in the Greenland Ice Sheet correlates to the oldest of the three units found in Skorarvatn. The timespan (~240 years) between Skorarvatn's two radiocarbon dates bounding the 10 ka Grímsvötn tephra series is greater than the results from Hvítárvatn (Jóhannsdóttir, 2007), which is unsurprising given that the latter were based on sedimentation rates and likely reflect minimum values. Due to indistinguishable chemical and morphological compositions and lacking better age control, we cannot confirm that the three tephra in Skorarvatn are the same as those in Hvítárvatn at this time. However, we do suggest that the 10 ka Grímsvötn tephra series in Skorarvatn was formed by at least three large, explosive and successive eruptions over ~240 years.

5.6.3 Reevaluation of Previous Vestfirðir Tephra Identifications and Paleoclimate Implications

In a recent study, Schomacker et al. (2016) presented major elemental chemistry of a Holocene Hekla tephra, termed the "Brattihjalli" tephra, from six lake sites on northeastern Vestfirðir; Brattihjalli, Skorarvatn, Reykjarfjörður, Neðra Eyvindarfjarðarvatn, Dagverðardalur and Neðra Hvalárvatn (Fig. 5.1b). The basaltic component of this tephra exhibits strong chemical similarites to the middle Holocene Hekla T tephra (Fig. 5.13). However, each of the lake's analyzed tephra contains at least one glass shard exhibiting silicic characteristics, suggesting that the "Brattihjalli" tephra may have other potential correlations, such as the predominately silicic Hekla DH (6600 cal BP, Gudmundsdóttir et al., 2011) or Hekla Ö tephra (6060 cal BP, Gudmundsdóttir et al., 2011), consistent with a middle Holocene age (Schomacker et al., 2016). Because the "Brattihjalli" tephra is located near the glaciolacustrine/non-glacial sediment interface in Neðra Eyvindarfjarðarvatn, and Neðra Hvalárvatn, the tephra's age has important implications for the timing of proto-Drangajökull's deglaciation (e.g., Harning et al., 2016b). The middle Holocene age assignment to this tephra, in combination with the lowermost radiocarbon ages in these two sediment cores, ultimately led Schomacker et al. (2016) to conclude that Drangajökull persisted within these two lake catchments until 7.8 to 7.2 ka, and perhaps, survived the entire Holocene.

However, our datasets demonstrate that the chemical attributes of the middle Holocene Hekla T tephra (6100 cal BP) are difficult to distinguish from the early Holocene Hekla VF tephra (9070 cal BP, Fig. 5.13a-b). Examination of the age models for Skorarvatn, Reykjarfjörður, Neðra Eyvindarfjarðarvatn, and Neðra Hvalárvatn as presented by Schomacker et al. (2016) reveals relatively older radiocarbon ages from macrofossils/humic acids stratigraphically above the presumably younger "Brattihjalli" tephra (e.g., Fig. 5.13c). If the Hekla VF tephra, which is ~3 ka older than the "Brattihjalli" tephra, is substituted as an age control point in these lake age models then the age reversals are eliminated (e.g., Fig. 5.13d). This implies that the correlation of the basaltic "Brattihjalli" tephra in Skorarvatn, Reykjarfjörður, Neðra Hvalárvatn, Neðra Eyvindarfjarðarvatn is misguided and that the tephra Schomacker et al. (2016) are referring to in these lakes is more likely to be the early Holocene Hekla VF tephra. Consequently, the timing of deglaciation in these lake records is pushed back by a couple millennia. This reevalutation agrees well with the conclusions of Harning et al. (2016b) that proto-Drangajökull receded to a smaller than present

configuration by ~9.2 ka. We, therefore, stress that carefully crafted tephra correlations are vital for accurate chronologies employed in paleoclimate and glacier reconstructions. Ultimately, this has important ramifications for addressing forcing mechanisms as well as for numerical modeling studies relying on such targets.

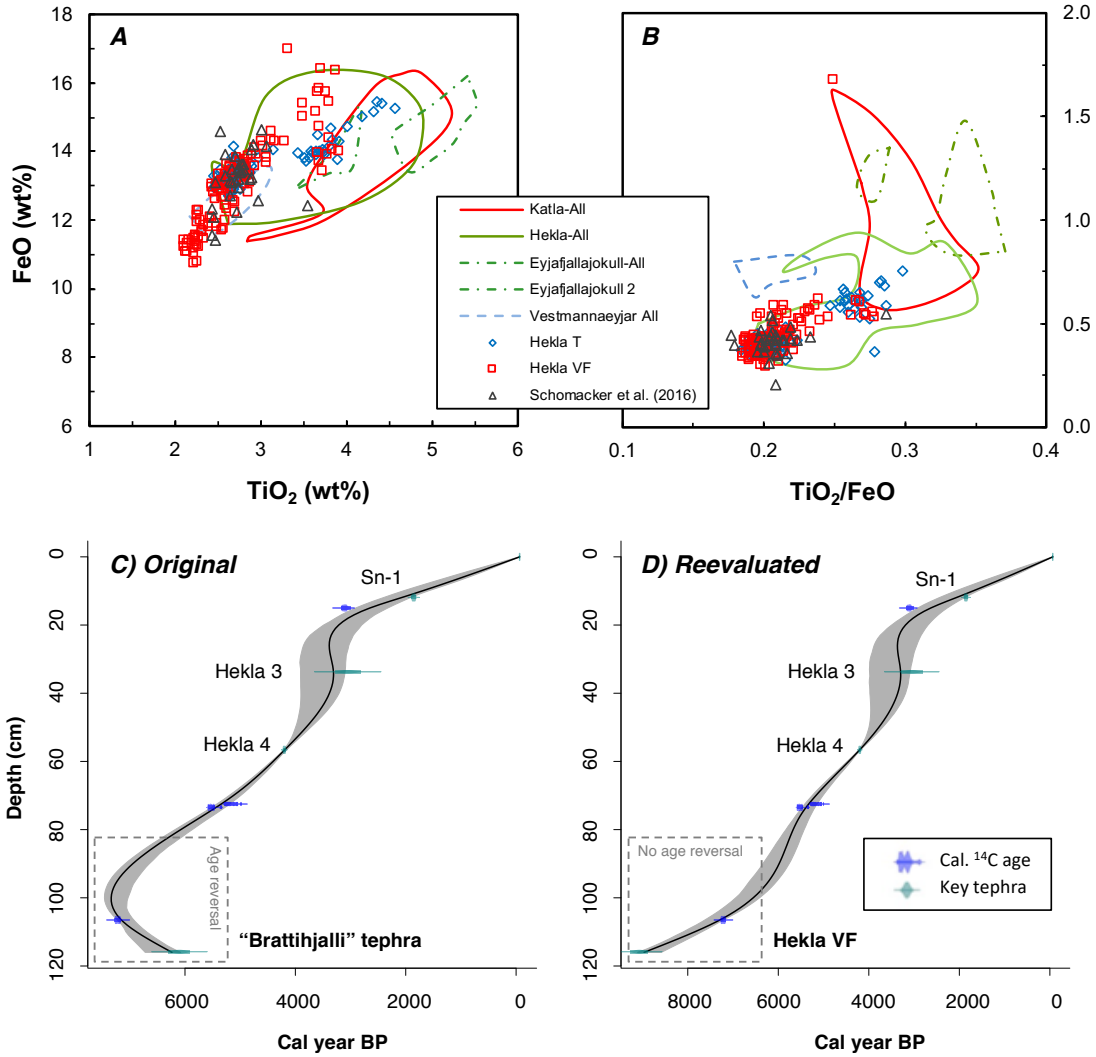

Figure 5.13. *Reevaluation of previous Vestfirðir tephra identifications. A and B) comparison of basaltic Hekla T and Hekla VF found on Vestfirðir (this study) against the basaltic components of the "Brattahjalli" tephra found on Vestfirðir (Schomacker et al., 2016), which all plot over each other, C) example age model from Neðra Eyvindarfjarðarvatn demonstrating the age reversal at the base of the sediment core when using the middle Holocene "Brattihjalli" tephra (Schomacker et al., 2016) and D) our suggested age model for Neðra Eyvindarfjarðarvatn with the Hekla VF tephra (9070 cal BP) substituted for the "Brattihjalli" tephra. Both age models were generated in the CLAM 2.2 software package using a smooth spline regression with 1000 iterations (Blaauw, 2010).*

5.7 Conclusions

Electron microprobe analyses of visible tephra (n=30) from four lakes on Vestfirðir provide the first detailed, composite tephra stratigraphy and chronology for northwest Iceland. Key tephra include Tv-3, the 10 ka Grímsvötn tephra series, Hekla VF, Katla EG, Hekla T, Hekla

4 (intermediate), Hekla 3 (intermediate), Snæfellsjökull-1, Landnám, Katla 920, Hekla 1693 and Bárðarbunga 1716. We identify the two oldest Holocene Hekla intermediate tephra in Iceland's tephra stratigraphy. Disparities in tephras recorded between lakes suggest variable ash plume trajectories and/or the occurrence of glacier/ice cover on some lakes during tephra fallout. The northernmost lake, Skorarvatn, archives three tephra layers correlative to the 10 ka Grímsvötn tephra series found across Iceland and the broader northern North Atlantic. Radiocarbon-dated macrofossils bounding the tephra units suggest that these tephra were the product of at least three large, successive eruptions from Grímsvötn over ~240 years. The tephra stratigraphy and chronology presented here expands the current Icelandic tephrochronology and provides an index to facilitate improved age control in Vestfirðir sedimentary records as well as correlations between paleoclimate records from Iceland and across the northern North Atlantic.

5.8 Acknowledgements

This work was supported by the Icelandic Center for Research (RANNÍS) through grants awarded to DJH (#163431051) and ÁG and GHM (Grant-of-Excellence # 070272011, #130775051, Grant-of-Excellence #141573052) as well as a University of Iceland PhD grant (2010-2012) awarded to KZ. Þorsteinn Jónsson and Sveinbjörn Steinþórsson are thanked for exceptional lake coring assistance over several winter field campaigns. We gratefully acknowledge Christopher Hayward (University of Edinburgh) as well as Sigurður Jakobsson, Guðmundur Guðfinnsson, Sydney Gunnarson and Bergrún Óladóttir (University of Iceland) for their assistance with tephra prep and microprobe analyses. Thorough and constructive reviews from the editor and two anonymous reviewers have substantially improved the manuscript.

6 Holocene Tephrochronology of West Iceland[5]

6.1 Abstract

Emerging lake sediment records are rapidly improving Iceland‘s Holocene tephra stratigraphy and chronology. Here, we expand upon these recent developments with a securely-dated tephrochronological record from the lake Haukadalsvatn in West Iceland. We capitalize on the existing paleomagnetic secular variation (PSV) age model, which uses 54 ties points to synchronize Haukadalsvatn‘s high-resolution lake sediment record to a well-dated PSV master chronology from marine core MD99-2269 on the North Iceland Shelf. Major element composition permits the identification of 38 tephra layers over the last 10500 years. Of these total 38 tephra, 13 can be traced to tephra found on the Vestfirðir peninsula and represent a series of well-dated marker tephra for West and Northwest Iceland. Despite their close geographical location, comparison of Haukadalsvatn‘s tephra layer frequency record to that of Northwest Iceland‘s reveals a striking amount of asychronicity. This regional disparity is likely the result of predominately small eruptions that featured narrow ash plumes. We argue that Haukadalsvatn serves as an important template for the tephrochronology of West Iceland and for future studies investigating the tephra records in more distal regions of the Northwest North Atlantic.

6.2 Introduction

High-resolution sedimentary archives require precise and accurate age control that enable absolute dating of their proxy-derived records. When independently dated, tephra are favorable due to their diagnostic geochemical fingerprints, instantaneous deposition over geologic timescales and vast geographical distribution (e.g., Lowe et al., 2011; Óladóttir et al., 2011a). In Iceland, the rich history of tephra-producing eruptions throughout the Holocene has aided in the temporal constraint of paleoclimate records (Eiríksson et al., 2000; Geirsdóttir et al., 2009a, 2013, 2019; Larsen et al., 2011, 2012; Blair et al., 2015; Eddudóttir et al., 2015, 2016; Harning et al., 2016a, 2018a; Gunnarson, 2017), past glacier dimensions (Larsen et al., 2012; Striberger et al., 2012; Harning et al., 2016b), and human settlement (e.g., Vésteinsson and McGovern, 2012; Schmid et al., 2017). Tephra records can also provide insight into the evolution of subsurface magma plumbing (Óladóttir et al., 2008, 2011b, 2018), frequency and magnitudes of past explosive eruptions (e.g., Thordarson and Larsen, 2007; Thordarson and Höskuldsson, 2008) and assessment of the transport of fine ash and its potential health and safety hazards to modern society (e.g., Janebo et al., 2016; Horwell et al., 2013; Damby et al., 2017).

---

[5] Harning, D.J., Thordarson, T., Geirsdóttir, Á., Miller, G.H., Ólafsdóttir, S. Holocene tephrochronology of West Iceland, *in prep*.

Establishing local and regional tephra stratigraphies is also vital for robust correlation to other regions. This is becoming increasingly pertinent as more sophisticated analytical techniques (see review by Davies, 2015) enable the identification of Icelandic-sourced (crypto)tephra in more distal locations across the northern hemisphere (Abbott and Davies, 2012; D'Andrea et al., 2012; Davies et al., 2014; Plunkett and Pilcher, 2018; Wastegård et al., 2018; Kalliokoski et al., 2019), which has recently been extended to >4000 km away in the Siberian Arctic (Haflidason et al., 2018). Hence, working towards an Icelandic master tephra stratigraphy and chronology that serves as a template for future cryptotephra investigations will facilitate better synchronization between proxy datasets (e.g., Ólafsdóttir et al., 2013) and assessment of lead and lags in the climate system (e.g., Lane et al., 2013). Key to these efforts, however, is the identification of marker tephra that feature firmly established chemical compositions and age estimates. A critical first step in establishing marker tephra requires stepwise correlation of the given marker tephra from its location proximal to the volcanic source to increasingly more distal locations in the same region. This systematic approach helps eliminate false correlations based on chemical composition alone, as tephra layers from any one volcano may be too similar in composition for secure marker tephra identifications (e.g., Lane et al., 2012).

In this study, we expand upon the known Icelandic tephra stratigraphy by detailing the chemical composition of tephra archived in the lake sediment of Haukadalsvatn, West Iceland. Due to the prevailing west-east flowing jet stream in the lower stratosphere (Lacasse, 2001) and injection of most ash plumes at this height (7-15 km), most tephra are carried eastward from their volcanic source and do not reach West Iceland. As such, many tephra stratigraphic studies have naturally focused on regions to the east of Iceland's major active volcanos (e.g., Thorarinsson, 1967; Óladóttir et al., 2005, 2008, 2011b; Gudmundsdóttir et al., 2012; 2016). However, if the explosive eruptions are large enough to reach the upper stratosphere (>15 km) or occur during the spring/summer when the prevailing westerlies shift towards weak easterlies (Lacasse, 2001), tephra can indeed fall over portions of West Iceland. A recent study by Harning et al. (2018b) demonstrated that 30 tephra were deposited in Vestfirðir, Northwest Iceland during the Holocene, which laid a framework for tephra-based studies in West Iceland. A similar study by Gudmundsdóttir et al. (2018) shortly followed, and at times, presented conflicting evidence for age estimates as well as chemical compositions of marker tephra proposed by Harning et al. (2018b). As Haukadalsvatn and Vestfirðir are both situated west of Iceland's primary volcanic zones, the two locations should share similar Holocene tephra sequences. Hence, a secondary goal of this paper is to use Haukadalsvatn's securely-dated tephra record to help evaluate and rectify some of these inconsistencies and better characterize key marker tephra found throughout West and Northwest Iceland.

6.3 Study Site

The lake Haukadalsvatn (3.3 km^2, elevation 32 m asl, 42 m depth) occupies a narrow, elongated glacially-eroded basin at the head of Hvammsfjörður, west Iceland, outside of the active volcanic zones and belts (Fig. 6.1a). During the earliest Holocene, Haukadalsvatn was situated in a fjord environment as a combined result of glacio-isostatic suppression and high relative sea level (70 m asl). Around 10600 cal yr BP, the basin became isolated from the sea as reflected by the transition from deglacial, IRD-rich marine sediment (12 m-thick) to lacustrine sediment (18 m-thick) that preserves primary tephra layers (Geirsdóttir et al., 2009a, 2009b). The surrounding bedrock is composed of Neogene basaltic lava successions

intercalated with relatively thin sedimentary horizons of mostly aeolian and fluvial origin (Harðarson et al., 2008). Soils within the lake catchment are predominately composed of andosols, with a minor organic component (Arnalds and Gretarsson, 2001). The largest portion of the catchment (172 m^2) lies above 500 m asl and has remained ice free since local deglaciation during the early Holocene.

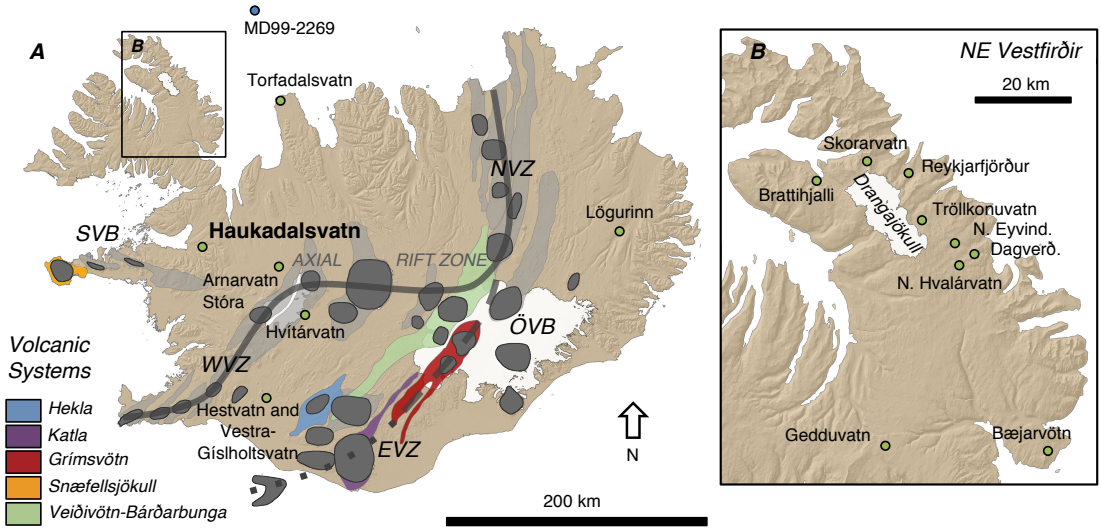

Figure 6.1. *Location maps. A) Overview of Iceland showing the volcanic systems and central volcanoes (dark grey, Catalogue of Icelandic Volcanoes). Colored volcanic systems reflect those that generated tephra found in Haukadalsvatn. Solid gray line delineates the axial rift. Dashed gray line marks the tholeiitic portion of the propagating rift, whereas the dotted gray line marks the alkalic/transitional portion of the propagating rift. Also labeled are key lake (green circles) and marine sites (blue circles) mentioned in text. B) Close up of other key lake sites on northeastern Vestfirðir, Northwest Iceland.*

6.4 Methods

6.4.1 Tephra sampling and compositional analysis

Paired sediment cores (HAK03-1A and HAK03-1B) were recovered from 38.3 m depth using a DOSECC GLAD-200 core rig to ensure complete sediment sequence retrieval (Geirsdóttir et al., 2009a). At the National Lacustrine Core Facility (LacCore), University of Minnesota, cores were split and examined, in addition to the visual identification of tephra and measurement of their thickness (Table 6.1). Further tephra characteristics (i.e., color, grainsize, fabric and depositional structure) are provided for tephra older than 4000 cal yr BP in Jóhannsdóttir (2007). Samples were collected from each layer for analysis of their major element composition. All tephra compositions presented in this study are from primary glassy tephra featuring delicate protrusions and void of any foreign material indicative of reworking. Furthermore, the upper and lower contacts between the tephra and lake sediment are sharply delineated. Hence, they represent original tephra fallout from an ash plume directly into the lake. Each sample was sieved to isolate glass fragments between 63 and 250 μm and embedded in epoxy plugs. Tephra layers were analyzed at both the University of

Edinburgh and the University of Hawaii at Manoa in accordance to the procedures described in Hayward (2012).

Major element composition datasets were assessed following the approach in Jennings et al. (2014) and Harning et al. (2018b). This method relies on all available compositional data of Icelandic tephra found in the literature (see Harning et al., 2018b). From this, we can systematically identify the source volcanic system through a series of bi-elemental plots, and then through direct compositional comparison alongside relevant stratigraphic information, identify the source eruption. In contrast, tephra studies have traditionally used select compositional datasets to derive tephra source information. Our objective approach in identifying tephra source is critical as the potential bias introduced in these cases is eliminated.

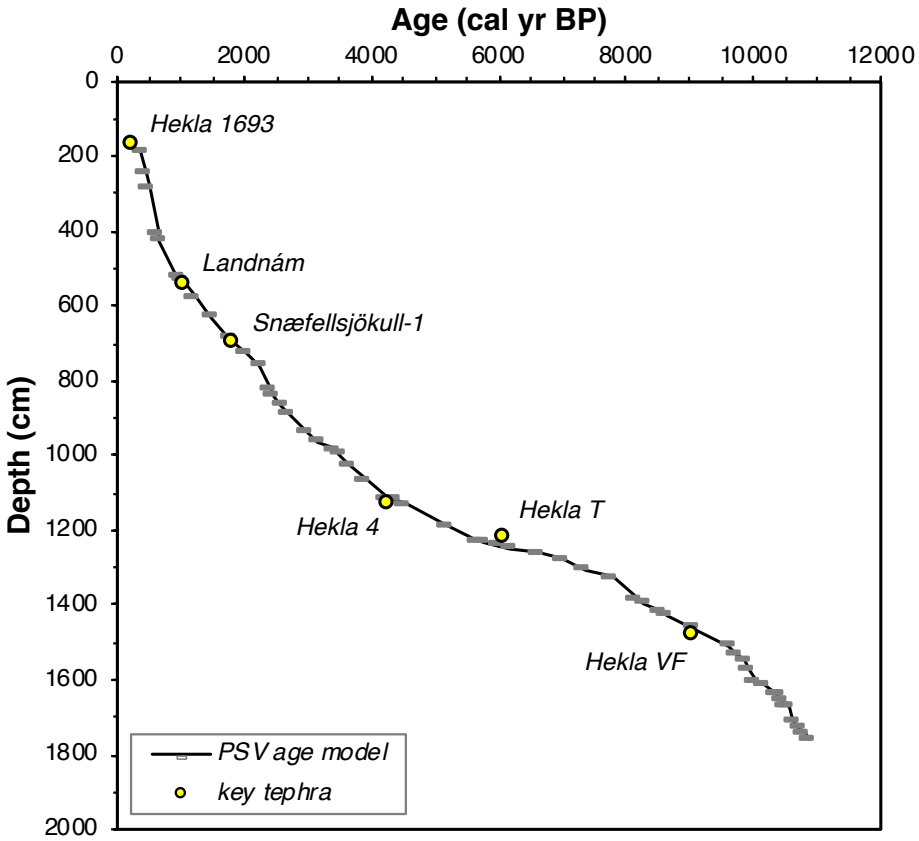

Figure 6.2. *PSV age model derived from 54 tie points to marine core MD99-2269 (grey ticks, Ólafsdóttir et al., 2013). Marker tephra, with ages independently constrained via ^{14}C dates from other locations, are marked in yellow.*

6.4.2 Chronology

Several ages models based on different toolsets currently exist for Haukadalsvatn's lake sediment record. Geirsdóttir et al. (2009a) first investigated a combination of ^{210}Pb, ^{237}Cs, ^{14}C-dated humic acids, and tephra of known age independently dated elsewhere (Jóhannsdóttir, 2007). The older calibrated humic acid ages were inconsistent with the tephra-derived age model, and the offset was interpreted as reflecting the variable intensity of soil erosion and delivery of old carbon to the lake. Hence, ^{14}C-dated humic acids were

deemed unreliable as secure age control points for Haukadalsvatn (Geirsdóttir et al., 2009a). Subsequently, Ólafsdóttir et al. (2013) generated a high-resolution (1 cm) paleomagnetic secular variation (PSV) record based on the natural remanent magnetization of the undisturbed lake sediment. An age model was derived from 54 tie points that link Haukadalsvatn's PSV record to the MD99-2269 (Fig. 6.1a) master PSV chronology (Fig. 6.2) resulting in low decadal-scale uncertainty throughout the record (Geirsdóttir et al., 2013). The latter MD99-2269 chronology is based on 44 ^{14}C dates derived from 2 PSV-synchronized marine sediment cores (Stoner et al., 2007), in addition to key tephra markers that account for the local Holocene evolution of the ΔR correction factor on the North Iceland Shelf (Kristjánsdóttir et al., 2007). A recent re-evaluation of these PSV records confirms that the close proximity of MD99-2269 to Icelandic lakes produces inclination and declination records that feature insignificant differences in direction and magnitude vital for robust correlation (Korte et al., 2019).

6.5 Results and Interpretations

6.5.1 Identification of tephra to its source system via major element composition

During the Late Pleistocene and Holocene, Icelandic volcanic systems have produced three distinct magma suites: alkaline, transitional-alkaline and tholeiitic (Jakobsson, 1979; Sigmarsson and Steinþórsson, 2007; Jakobsson et al., 2008), all of which have distinct distributions. The alkaline magma suite typifies the intraplate volcanic belts of Snæfellsnes (SVB) and Öræfajökull (ÖVB) (Fig. 6.1a). The tholeiitic magma suite characterizes the axial rift along the North (NVZ), West (WVZ) and East (EVZ) volcanic zones (Fig. 6.1a). Because the EVZ is an axial rift in the making, formed by gradual propagation to the southwest through older crust, it exhibits distinct spatial and compositional variability. The northern sector, where the Grímsvötn and Veiðivötn-Bárðarbunga volcanic systems are located (Fig. 6.1a), is typified by tholeiitic magma suites, which contain higher FeO, TiO_2, K_2O and P_2O_5 at similar MgO values when compared to the mid-ocean ridge tholeiites typifying the far northern and southwestern segments of the axial rift in Iceland (Sigmarsson and Steinþórsson, 2007). The volcanic systems Vestmannaeyjar, Torfajökull, Tindfjöll and Eyjafjöll in the southern sector of the EVZ all produce alkalic magmas (Jakobsson, 1979; MacDonald, 1990; Larsen et al., 1999). The Katla and Hekla systems of the EVZ feature the transitional-alkaline magma suite, which is characterized by higher FeO and TiO_2 content and FeO/TiO_2 values compared to the tholeiitic and alkali suites (Lacasse et al., 1995; Larsen et al., 2001; Thordarson et al., 2003).

Given the known spatial distribution of magma composition in Iceland, a tephra's source volcanic system can typically be traced back using its major oxide chemistry (Larsen, 1982; Óladóttir et al., 2011a). The tholeiitic suite is characterized by the lowest total alkalis ($Na_2O + K_2O$); plotting below the MacDonald and Katsura line (MacDonald and Katsura, 1964) on the basalt spectrum and below the Kuno line (Kuno, 1966) for the intermediate and rhyolitic type tephra on total alkali vs silica (TAS) plots (Fig. 6.3). In contrast, the alkaline suite has high total alkali content and plots above the MacDonald-Katsura and Kuna lines on TAS plots (Fig. 6.3). For the transitional-alkaline suite characterizing the magma of Hekla and Katla, basaltic magma plot in the alkali field (i.e., above the Kuno line) while intermediate Katla and intermediate to silicic Hekla magmas plot in the tholeiitic field (i.e.,

below the Kuno line). Subsequently, by using a series of bi-elemental plots, a single likely volcanic source can be identified among those within the same magma suite (e.g., Figs. 6.4-6.8).

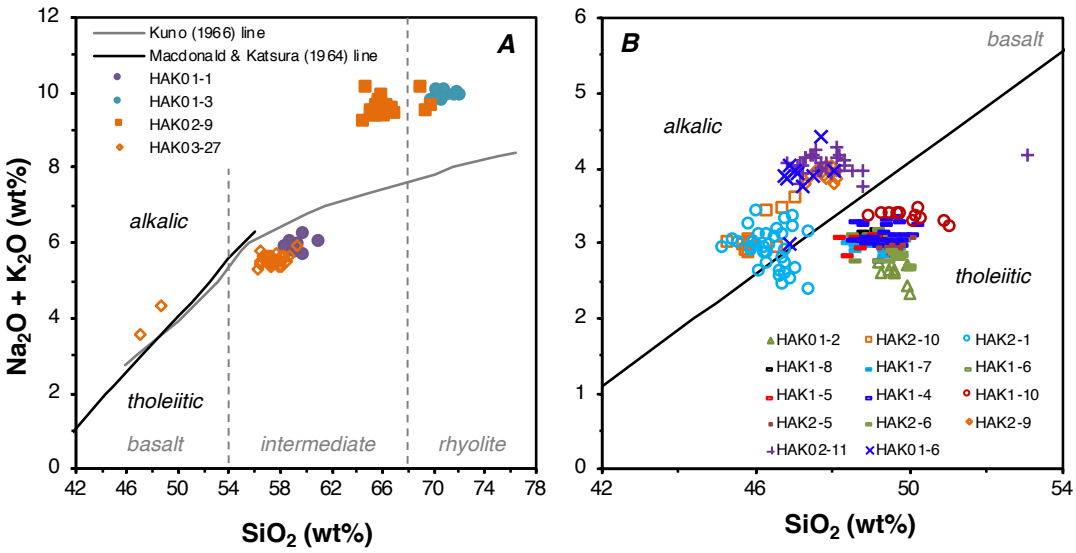

Figure 6.3. *Marker tephra from Haukadalsvatn plotted on a total alkali vs silica (TAS) plot, where B) is a basalt confined TAS plot.. The MacDonald and Katsura (1964) and Kuno (1966) lines separate alkalic from tholeiitic tephra.*

6.5.2 Description of key tephra marker layers in Haukadalsvatn

6.5.2.1. Grímsvötn 10 ka Series tephra

The basal tephra layers (HAK1-4, HAK1-5, HAK1-6, HAK1-7, HAK1-8) are identified deep in the sediment core at the following depth intervals: 1696.7, 1695.8, 1688, 1687.5, and 1685.6 cm. These tephra layers are charactertized by thicknesses ranging from 0.2 to 1 cm (Table 6.1) and are comprised of very fine to medium grey to black ash (Jóhannsdóttir, 2007). All five tephra layers are tholeiitc (Fig. 6.3) and exhibit major element compositions typical of the Grímsvötn volcanic system (Fig. 6.4a, 6.4b and 6.4d). These characteristics, in conjunction with their deep stratigraphic position, indicate that they are part of the widespread Grímsvötn 10 ka Series tephra. PSV-derived age contraints place the time of deposition for each horizon at 10400, 10395, 10320, 10315 and 10300 cal yr BP (Fig. 6.2), respectively.

6.5.2.2. Grímsvötn B

A 0.5-cm thick, dark gray to brown tephra layer of very fine ash (HAK1-10) is located at 1540.5 cm depth. All 11 grains analyzed indicate a tholeiitic basalt composition (50.03 ± 0.64 wt% SiO_2, 3.17 ± 0.29 wt% TiO_2, 4.99 ± 0.30 wt% MgO) consistent with origin from the Grímsvötn volcanic system (Figs. 6.3, 6.4a, 6.4b, and 6.4d). The deep stratigraphic position lying above and proximal to the Grímsvötn 10 ka Series implies an early Holocene age, which is supported by a PSV age estimate of 9280 cal yr BP (Fig. 6.2). This tephra layer exhibits strong chemical similarities, and hence, likely correlative to the Grímsvötn B tephra

identified in two sediment cores from the lake Bæjarvötn, in Northwest Iceland (Harning et al., 2018b).

6.5.2.3. Hekla VF

A 1.3-cm thick, black, fine to medium ash tephra (HAK2-1) was located at 1528.3 cm depth. All 34 grains analyzed indicate a basaltic trans-alkaline magma source (46.4 ± 0.5 wt% SiO_2, Fig. 6.3) from the Hekla volcanic system (Fig. 6.5). The relative deep stratigraphic position and proximity to the underlying Grímsvötn 10 ka Series tephra imply an early Holocene age, which is further supported by a PSV-derived age estimate of ~9100 cal yr BP (Fig. 6.2). This tephra has previously been correlated to a marker tephra found throughout a number of lakes on northeastern Vestfirðir, termed Hekla VF (VF=Vestfirðir, Harning et al., 2018b).

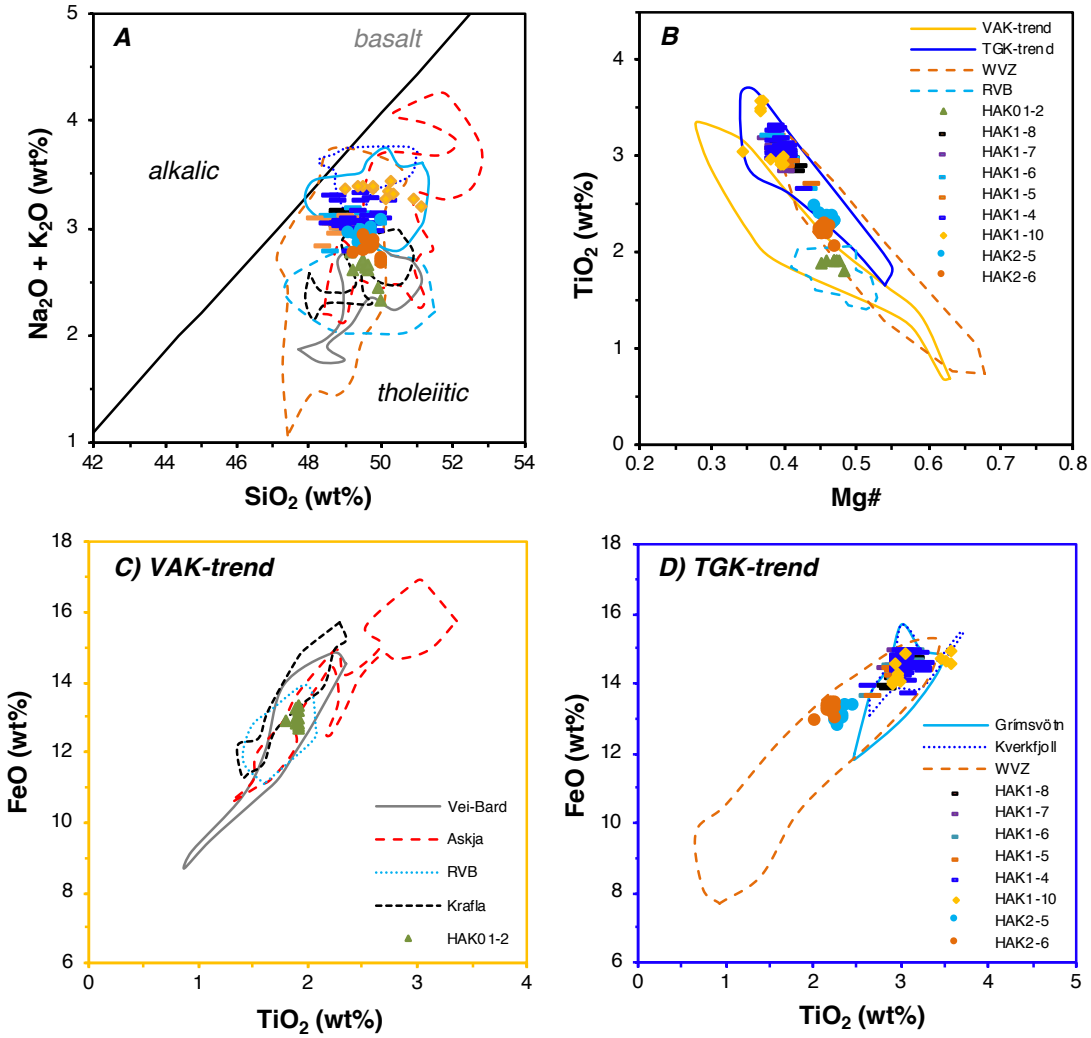

Figure 6.4. *Examples of tholeiitic basalt tephra discrimination from Haukadalsvatn. Panel B enables further discrimination of tephra based on their affinity to either the VAK (Veiðivötn, Askja, Krafla) volcanic systems (C) or the TGK (Thordarhyrna, Grímsvötn, Kverkfjöll) volcanic systems (D). Mg# = (MgOwt%/40.3)/((FeOwt%/71.8)+(MgOwt%/40.3)).*

6.5.2.4. Grímsvötn BP-2

A 0.25-cm thick, blackish gray tephra layer of very fine ash (HAK2-5) is located at 1441.9 cm depth. Analyses of the 12 grains indicate a primitive tholeiitic basaltic magma source (49.6 ± 0.23 wt% SiO_2, 2.34 ± 0.05 wt% TiO_2, 6.37 ± 0.13 wt% MgO), consistent with the Grímsvötn volcanic system‘s compositonal domain (Figs. 6.3, 6.4a, 6.4b, and 6.4d). The relatively deep stratigraphic position and proximity to the underlying Hekla VF tephra layer imply an early Holocene age, which is further supported by a PSV-derived age estimate of 8700 cal yr BP (Fig. 6.2). This primitive tephra layer has previously been identified in and correlated to a tephra layer (Grímsvötn BP-2) in two lake sediment cores from Bæjarvötn (Harning et al., 2018b) and in a lake sediment core from Hestvatn, south central Iceland (formerly ThB-2, Jóhannsdóttir, 2007).

6.5.2.5. Grímsvötn BP-1

A 0.2-cm thick, dark grey tephra layer of fine ash (HAK2-6) is located at 1425.5 cm depth. Analyses of the 12 grains indicate a primitive tholeiitic basaltic magma source (49.8 ± 0.24 wt% SiO_2, 2.21 ± 0.06 wt% TiO_2, 6.30 ± 0.09 wt% MgO), consistent with the Grímsvötn volcanic system‘s compositonal domain (Figs. 6.3, 6.4a, 6.4b, and 6.4d). The relatively deep stratigraphic position and proximity to the underlying Hekla VF tephra layer imply an early Holocene age, which is further supported by a PSV-derived age estimate of 8560 cal yr BP (Fig. 6.2). This primitive tephra layer has previously been identified in and correlated to a tephra layer (Grímsvötn BP-1) in a lake sediment cores from Bæjarvötn (Harning et al., 2018b) and in lake sediment cores from Hestvatn, south central Iceland and Hvítárvatn, west central Iceland (formerly ThB-1, Jóhannsdóttir, 2007).

6.5.2.6. Katla EG

A 0.2-cm thick, dark gray tephra layer of fine to medium ash (HAK2-9) is located at 1265.6 cm depth. All 12 grains analyzed indicate an alkalic basalt composition (47.8 ± 0.26 wt% SiO_2, 4.31 ± 0.11 wt% TiO_2, 4.77 ± 0.14 wt% MgO) consistent with origin from the Katla volcanic complex (Figs. 6.3 and 6.5). The moderately deep location within the sediment core suggests an early to middle Holocene age, which is supported by a PSV age estimate of 6240 cal yr BP (Fig. 6.2). The frequency in basaltic tephra peaks and elemental composition of tephra glass from several marine sediment cores southeast of Greenland also indicate that there is only one Katla basalt tephra (“Katla EG”) that dispersed westward during the early to middle Holocene (Jennings et al., 2014), consistent with tephra identified in a lake sediment core from Bæjarvötn, Northwest Iceland (Harning et al., 2018b) and in lake sediment cores from Hestvatn, Southcentral Iceland and Hvítárvatn, west central Iceland (formerly AlA-1, Jóhannsdóttir, 2007).

6.5.2.7. Hekla T

A 0.4-cm thick, black tephra layer of fine to medium ash (HAK02-10) is located at 1245.8 cm depth. The 12 grains that were analyzed are of mildly alkaline basalt (46.1 ± 0.5 wt% SiO_2, 2.94 ± 0.52 wt% TiO_2, 6.90 ± 0.73 wt% MgO), with composition consistent with origin from the Hekla volcanic system (Figs. 6.3 and 6.5). Its major element composition along with its mid-section stratigraphic position suggest that this is the Hekla T tephra (Jóhannsdóttir, 2007). This is consistent with the recent study on northeastern Vestfirðir,

which collectively indicates a west to northwest ash plume trajectory from Hekla after tracing the tephra through more proximal lake sites at Hestvatn and Hvítárvatn (Harning et al., 2018b). The original age estimate (6100 cal yr BP) derived from sedimentation rates interpolated from well-dated bounding tephra (Harðardóttir et al., 2001; Jóhannsdóttir, 2007) is supported by identical estimates from the high-resolution PSV age model (Fig. 6.2).

6.5.2.8. Hekla 4

A 0.85-cm thick, blackish-grey to greyish-white tephra of very fine to medium ash (HAK03-27) is located at 112.3 cm depth. Of the 36 grains analyzed, 34 are of intermediate composition with SiO_2 content of 57.5 ± 0.7 wt% characteristic of the Hekla volcanic system (Fig. 6.3, 6.6a, 6.6b and 6.6c). The remaining two grains are basaltic-icelandite (Fig. 6.3), also consistent with origin from the Hekla volcanic system. Its stratigraphic position implies deposition during the late middle Holocene, which led previous studies to conclude this as the Hekla 4 tephra (Jóhannsdóttir, 2007). Hence, an age of 4260 cal yr BP was assigned (Table 6.1, Dugmore et al., 1995), which was incorporated as a tie point into the original PSV age model (Fig. 6.2, Ólafsdóttir et al., 2013). The documentation of the intermediate chemistry here in Haukadalsvatn and on northeastern Vestfirðir (Harning et al., 2018b), as well as in Hestvatn and Hvítárvatn (Harðardóttir et al., 2001; Johannsdóttir, 2007), is important as the dominant composition of Hekla 4 further east in Iceland and throughout mainland Europe is typically rhyolitic (e.g., Davies et al., 2010; Lawson et al., 2012; Gudmundsdóttir et al., 2016), yet both compositions were generated during the same volcanic eruption (Larsen and Thorarinsson, 1977). The icelandite tephra identified in West Iceland reflects the tail end of the Hekla 4 eruption, which produced tephra of intermediate composition that had a more northwesterly dispersal than the preceding NNE-trending Plinian rhyolitic phase (Fig. 6.9, see Larsen and Thorarinsson, 1977 for details).

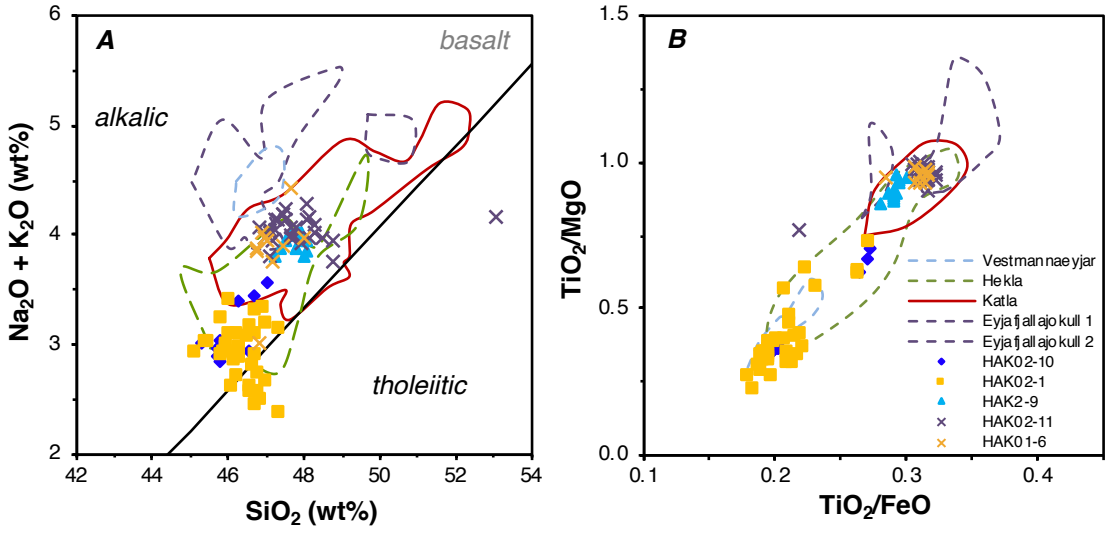

Figure 6.5. *Examples of alkali basalt tephra discrimination from Haukadalsvatn. HAK02-1 and HAK02-10 originate from the Hekla volcanic system, whereas HAK2-9, HAK02-11 and HAK01-6 are sourced from Katla.*

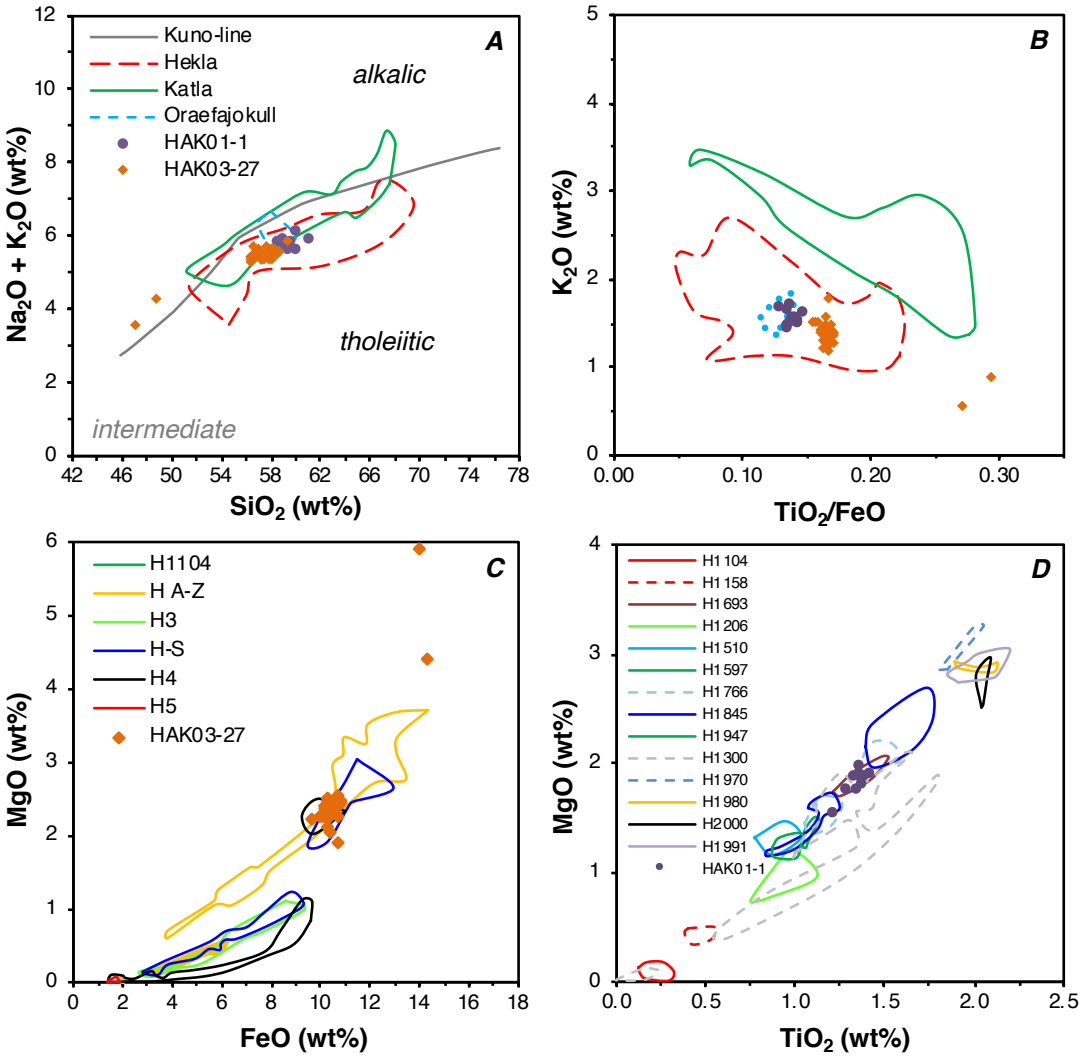

Figure 6.6. *Examples of intermediate key tephra discrimination from Haukadalsvatn to the Hekla volcanic system (A-B). C) HAK03-27 is the Hekla 4 tephra, and D) HAK01-1 is the Hekla 1693 tephra.*

6.5.2.9. Katla 2190

A 0.15-cm thick, black tephra layer of fine to medium ash (HAK02-11) is located at 753.7 cm depth. Of the 29 grains analyzed, 28 indicate an alkalic basalt composition (47.7 ± 0.53 wt% SiO_2, 4.60 ± 0.05 wt% TiO_2, 4.77 ± 0.10 wt% MgO) originating from the Katla volcanic system (Figs. 6.3 and 6.5). The other grain analyzed revealed an intermediate icelandite composition (Fig. 6.5a, 53.05 wt% SiO_2) consistent with the Hekla volcanic system. The stratigraphic position implies deposition during the middle-late Holocene, which is supported by a PSV age estimates of 2190 cal yr BP (Fig. 6.2). The major element composition of Haukadalsvatn's Katla 2190 tephra layer is indistinguishable from a Katla tephra layer of similar age identified in lake sediment cores from Bæjarvötn and Tröllkonuvatn, Northwest Iceland (Harning et al., 2018b), underpinning its use as a marker tephra across West Iceland.

6.5.2.10. Snæfellsjökull-1

A 0.5-cm thick, whitish gray tephra layer (HAK02-9) is located at 678 cm depth. The major element composition of the 25 grains analyzed are all alkalic and in the trachydacite (n=22) to rhyolite (n=3) compositional range (66.3 ± 1.3 wt% SiO_2, 5.46 ± 0.25 wt% Na_2O, 4.09 ± 0.30 wt% K_2O). Furthermore, they all plot within the compositional field of the Snæfellsjökull volcanic system (Figs. 6.3 and 6.7). Thordarson et al. (2012) has identified this as the marker layer Snæfellsjökull-1 (Sn-1, 1820 ± 90 cal BP, Larsen et al., 2002), which provided an age control tie point in the PSV age model (Fig. 6.2, Ólafsdóttir et al., 2013). The Snæfellsjökull-1 marker is widely distributed throughout the Vestfirðir peninsula (Gudmundsdóttir et al., 2018; Harning et al., 2018b) and represents one of the few Holocene rhyolitic tephras identified thus far in the region.

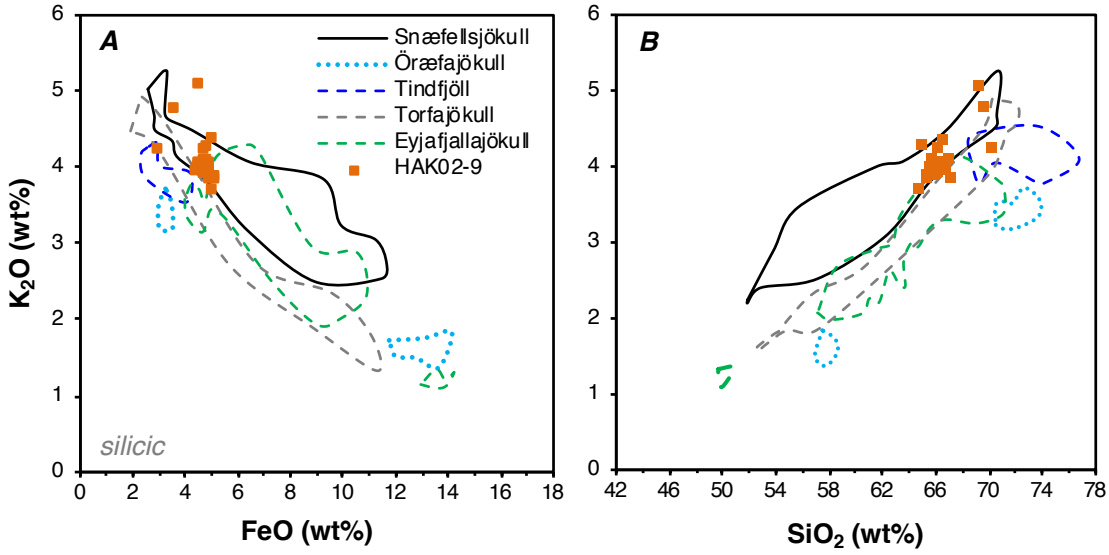

Figure 6.7. *Examples of silicic tephra discrimination from Haukadalsvatn to the Snæfellsjökull volcanic system. HAK02-9 is the Snæfellsjökull-1 tephra.*

6.5.2.11. Katla 1260

A 0.3-cm thick, black tephra layer of fine to medium ash (HAK01-6) is located at 574.9 cm depth. All 10 grains analyzed indicate an alkalic basalt magma source (47.2 ± 0.43 wt% SiO_2, 4.67 ± 0.04 wt% TiO_2, 4.89 ± 0.09 wt% MgO) consistent with origin from the Katla volcanic system (Figs. 6.3 and 6.5). Stratigraphic position implies deposition during the late Holocene, which is supported by an PSV age estimates of 1260 cal yr BP (Fig. 6.2). Indistinguishable chemical similarities with a Katla tephra layer of similar age link the Katla 1260 tephra layer to another identified in a lake sediment core from Gedduvatn, Northwest Iceland (Harning et al., 2018b).

6.5.2.12. The Settlement Layer

A 0.6-cm thick, tephra layer (HAK01-2 and HAK01-3) is located at 537.6 cm depth. It features a 0.25-cm thick light colored (silicic) lower component and a 0.3-cm thick darker (basaltic) upper component. Ten tephra grains from the upper dark portion (HAK01-2) revealed a tholeiitic basalt composition (49.6 ± 0.3 wt% SiO_2, 1.90 ± 0.03 wt% TiO_2, 6.46 ± 0.19 wt% MgO) that have affinities with basaltic magma originating from Veiðivötn-Bárðarbunga (Figs. 6.3, 6.4a and 6.4c). On the other hand, ten grains (HAK01-3) from the lower silicic part exhibit an alkalic rhyolite composition (71.0 ± 0.7 wt% SiO_2, 5.22 ± 0.10 wt% Na_2O, 4.64 ± 0.10 wt% K_2O) consistent with origin from the Torfajökull volcanic system (Figs. 6.3 and 6.8). The position of the tephra with the upper portion of the sediment core implies a late Holocene deposition (Fig. 6.2). The two identified components and stratigraphic position are consistent with the Settlement Layer (recently revised to 1073 cal yr BP, Schmid et al., 2017) that was generated by simultaneous eruptions from the Veiðivötn and Torfajökull volcanic systems (Larsen et al., 1984, 1999). Both components of the Settlement Layer have now been identified on the Vestfirðir peninsula (Jennings et al., 2014; Harning et al., 2018b) and as far as the SE Greenland Shelf (Jennings et al., 2014) and Greenland ice cores (Grönvold et al., 1995; Zielinski et al. 1997).

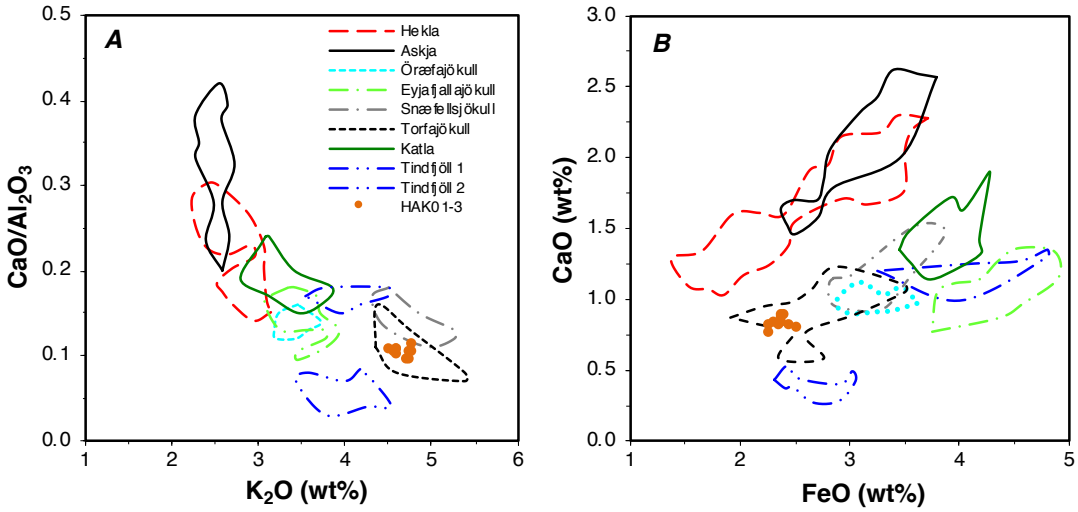

Figure 6.8. *Plots of the rhyolitic component of the Settlement Layer marker tephra demonstrating its origin from the Torfajökull volcanic system.*

6.5.2.13. Hekla 1693

A 0.4-cm thick, dark brown to black tephra layer (HAK01-1) is located at 189.2 cm depth. Major element composition demonstrates that the tephra has an intermediate magma source (59.4 ± 0.7 wt% SiO2, 1.83 ± 0.11 wt% MgO) from the Hekla volcanic system (Figs. 6.3, 6.6a, 6.6b and 6.6d). Stratigraphic position above the Settlement Layer and near the sediment core top suggests deposition during the latest Holocene within historic time (last 1140 years) (Fig. 6.2). The Hekla 1693 tephra is the only known intermediate tephra with significant thickness (0.1-0.5 cm) to have been dispersed this far west in Iceland during the late Holocene (Thorarinsson, 1967; Brynjólfsson et al., 2015; Janebo et al., 2016; Brader et al., 2017; Harning et al., 2018b), underpinning the identification of the Hekla 1693 tephra at this depth in Haukadalsvatn.

6.5.3 Tephrochronology in Haukadalsvatn lake sediment

Including the key tephra described above, a total of 38 tephra layers are identified in Haukadalsvatn's lake sediment. Of these, 31 were identified as basaltic, 5 as intermediate, 1 as rhyolitic and 1 featured a mixed composition of both basalt and rhyolite. Furthermore, 20 can be classified as alkalic, 13 as tholeiitic, 2 as transitional-alkaline and 2 were comprised about both alkalic and tholeiitic tephra grains (Table 6.1). By employing the systematic discrimination procedure briefly outlined in Section 6.5.1 (see also Jennings et al., 2014 and Harning et al., 2018b), we identified the source volcanic system for each tephra (Table 6.1). Tephra products are dominantly sourced from Katla (n=16) and Grímsvötn (n=11), then Hekla (n=7). A smaller proportion of tephra (n=1-2) were also present from Snæfellsjökull, the WVZ, Veiðivötn-Barðárbunga, Torfajökull, and potentially, Kverkfjöll.

Secure age estimates for Haukadalsvatn's tephra were obtained from the PSV age model (Fig. 6.2, Ólafsdóttir et al., 2013). Of the marker tephra layers identified in this study, Hekla 4, Snæfellsjökull-1 and the Settlement Layer were previously identified and incorporated into the MD99-2269 PSV record in order to account for marine ΔR variations (Kristjánsdóttir et al., 2007). Given that these three tephra are age control tie points, their age-depth relationship in Haukadalsvatn naturally fits with the PSV model (Fig. 6.2). Other key tephra dated through lake sedimentation rates (Jóhannsdóttir, 2007) and historical records (Thorarinsson, 1967), such as Hekla VF, Hekla T and Hekla 1693, also conform to the PSV-derived age model within uncertainty (Fig. 6.2), underpinning the accuracy of age estimates achieved for the remaining tephra identified in Haukadalsvatn's sedimentary record (Table 6.1).

Based on major elemental composition (e.g., Fig 6.10, Supplemental Information), stratigraphic position, and PSV-supported age estimates, at least 13 tephra layers are identified in Haukadalsvatn and in the network of lakes on Vestfirðir's northeastern peninsula in Northwest Iceland (Table 6.1, Harning et al., 2018b). These are at least two of the five layers corresponding to the Grímsvötn 10 ka Series tephra (10400-9900 cal yr BP), Grímsvötn B (9280 cal yr BP), Hekla VF (9100 cal yr BP), Grímsvötn BP-2 (8700 cal yr BP), Grímsvötn BP-1 (8560 cal yr BP), Katla EG (6400 cal yr BP), Hekla T (6100 cal yr BP), Hekla 4 (4260 cal yr BP), Katla 2190 (2190 cal yr BP), Snæfellsjökull-1 (1820 cal yr BP), Katla 1260 (1260 cal yr BP), the Settlement Layer (1073 cal yr BP) and Hekla 1693 (257 cal yr BP). As a combined result of their correlation across multiple lake sites and robust age estimates, we suggest that these 13 tephra layers serve as marker tephra for West and Northwest Iceland.

Table 6.1. *Haukadalsvatn tephra stratigraphy and chronology.*

Tephra ID	Lab ID	Composition	Thickness (cm)	PSV-derived age (cal BP)	Present on Vestfirðir
Hekla 1693	HAK01-1	Intermediate	0.4	257	X
Landnám (V-B/Torfajökull)	HAK01-2/HAK01-3	Basalt/Rhyolite; tholeiitic/alkalic	0.6	1073	X
Katla	HAK01-5	Basalt; alkalic	0.5	1245	
Katla 1260	HAK01-6	Basalt; alkalic	0.3	1260	X
Katla	HAK01-7	Basalt; alkalic	0.3	1270	
Grímsvötn	HAK02-8	Basalt; tholeiitic	0.3	1765	
Snæfellsjökull-1	HAK02-9	Dacite-rhyolite; alkalic	0.5	1820	X
Katla 2190	HAK02-11	Basalt; alkalic	0.15	2190	X
Hekla	HAK02-13	Intermediate	0.2	2145	
Katla	HAK03-14	Basalt; alkalic	0.6	2215	
Katla	HAK03-16	Basalt; alkalic	0.2	2515	
Katla	HAK03-18	Basalt; alkalic	0.3	2705	
Hekla B	HAK03-19	Intermediate	0.7	2765	
Hekla C	HAK03-20	Intermediate	0.3	2870	
Veiðivötn-Bárðarbunga	HAK03-21	Basalt; tholeiitic	0.3	2950	
Katla	HAK03-22	Basalt; alkalic	0.25	3090	
Katla	HAK03-23	Basalt; alkalic	0.35	3495	
Katla	HAK03-24	Basalt; alkalic	0.15	3745	
Katla	HAK03-25	Basalt; alkalic	0.3	3750	
Katla	HAK03-26	Basalt; alkalic	0.15	3995	
Hekla 4	HAK03-27	Intermediate	0.85	4260	X
Katla	HAK03-29	Basalt; alkalic	0.3	4275	
Hekla T	HAK2-10	Basalt; transitional-alkaline	0.4	6100	X
Katla EG	HAK2-9	Basalt; alkalic	0.2	6290	X
Grímsvötn	HAK2-8	Basalt; tholeiitic	0.2	6370	
WVZ/Katla mix	HAK2-7	Basalt; tholeiitic/alkalic	0.6	7135	
Grímsvötn BP-1	HAK2-6	Primitive basalt; tholeiitic	0.2	8560	X
Grímsvötn BP-2	HAK2-5	Primitive basalt; tholeiitic	0.25	8700	X
Kverkfjöll?	HAK2-4	Basalt; tholeiitic	0.1	8850	
Katla	HAK2-3	Basalt; alkalic	0.25	8940	
Hekla VF	HAK2-1	Basalt; transitional-alkaline	1.3	9100	X
Grímsvötn B	HAK1-10	Basalt; tholeiitic	0.5	9280	X
Grímsvötn	HAK1-9	Basalt; tholeiitic	0.2	9400	
Grímsvötn 10 ka Series	HAK1-8	Basalt; tholeiitic	0.3	10300	X
Grímsvötn 10 ka Series	HAK1-7	Basalt; tholeiitic	0.25	10315	
Grímsvötn 10 ka Series	HAK1-6	Basalt; tholeiitic	0.15	10320	
Grímsvötn 10 ka Series	HAK1-5	Basalt; tholeiitic	0.2	10395	
Grímsvötn 10 ka Series	HAK1-4	Basalt; tholeiitic	1	10400	X

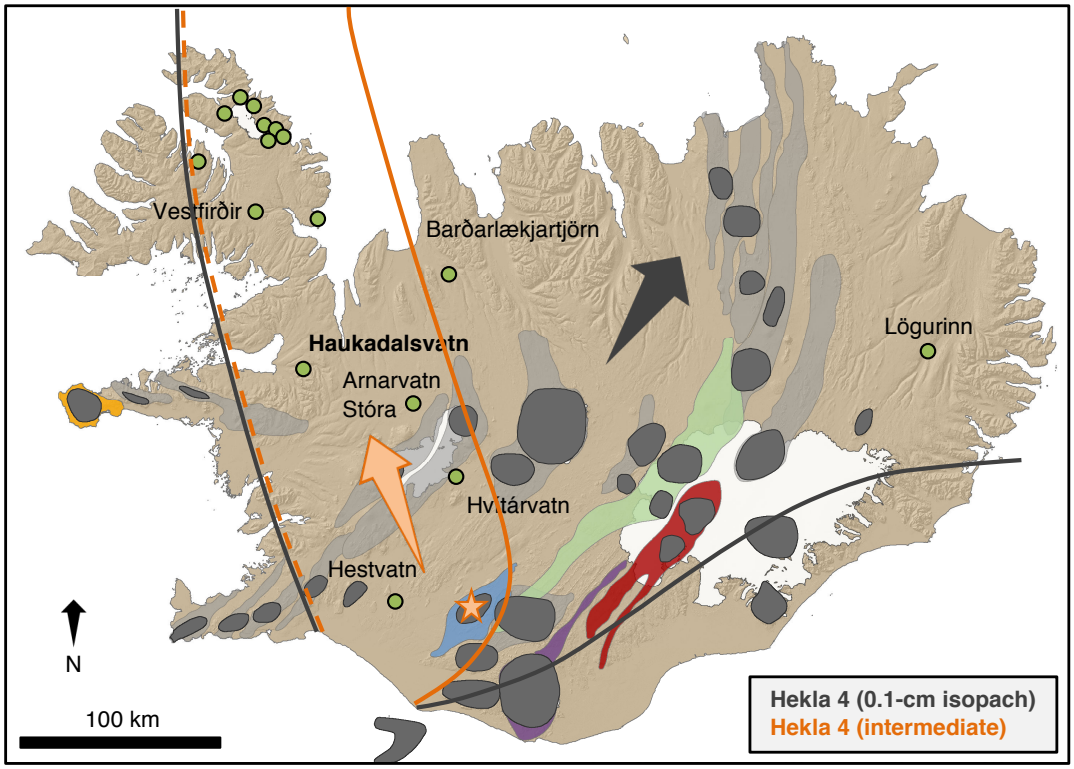

Figure 6.9. *Hekla 4 0.1-cm isopach map modified after Larsen and Thorarinsson (1977). Hekla 4 intermediate distribution corresponds to what is described as the "brownish-black pumice" that followed the cessation of the NNE-trending Plinian phase (Larsen and Thorarinsson, 1977).*

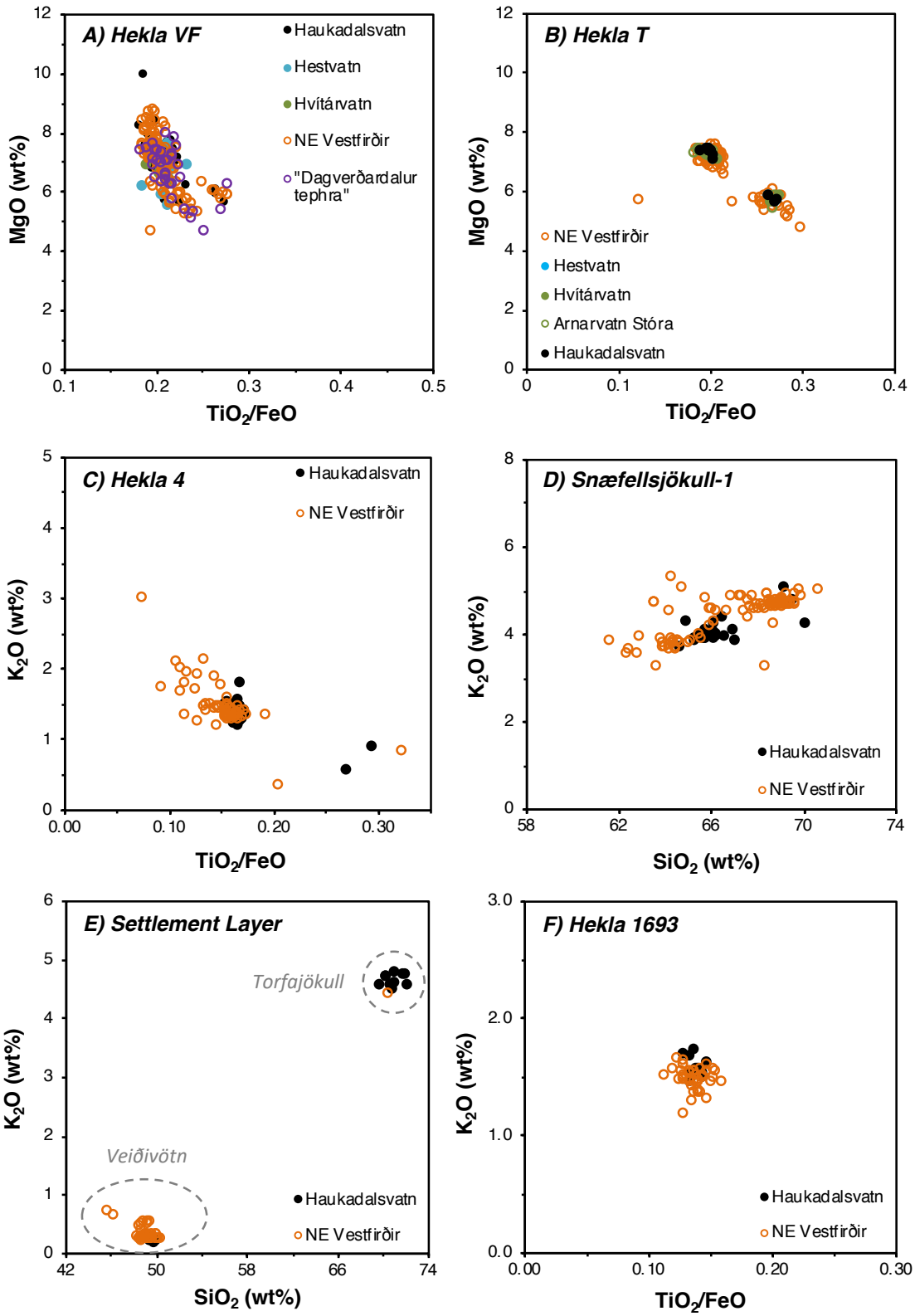

Figure 6.10. *Bi-elemental plot comparisons demonstrating the correlation of key marker tephra in Haukadalsvatn to those found in NE Vestfirðir lakes. Open purple circles in panel A represent NE Vestfirðir data from Gudmundsdóttir et al. (2018). In panels C-F, NE Vestfirðir data is a compilation of Harning et al. (2018b) and Gudmundsdóttir et al. (2018).*

6.6 Discussion

Haukadalsvatn's tephrochronological record (n=38) provides a temporally well-constrained and critical dataset for extending Iceland's Holocene tephra record to West and Northwest Iceland. The development of new marker tephra for this region of Iceland is necessary due to the dearth of more traditional marker tephra generated from some of the Holocene's largest rhyolitic eruptions, such as Hekla 5, Hekla 3 and Hekla 1104 (Larsen and Thorarinsson, 1977; Larsen et al., 1999). Furthermore, given its location between Iceland's active volcanic zones and regions of major paleoclimate research and interest, such as Greenland, establishing a framework for future (crypto)tephra investigations in more distal locations is paramount. Below, we outline some key implications gleaned from Haukadalsvatn's tephra record and how it contributes to refining our existing knowledge of Icelandic tephrochronology.

6.6.1 Grímsvötn 10 ka Series tephra

The Saksunarvatn Ash has been one of the most widespread tephra markers sourced from Iceland (Grímsvötn volcanic system) used in Northern Hemisphere tephra stratigraphies (Mangerud et al., 1986; Merkt et al., 1993; Björck et al., 1992; Grönvold et al., 1995; Birks et al., 1996). However, the volume of this basaltic tephra has been calculated to be over 450 km^3, which would categorize it as sourced from a "super volcano" 40 times larger than either the Hekla 4 or Hekla 3 eruptions, two of the largest known post-glacial explosive eruptions in Iceland (Thordarson, 2014). Despite a presumably secure age estimate from Greenland ice core records (10,300 ± 90 cal yr BP, Rasmussen et al., 2006), emerging evidence in Iceland and abroad shows that as many as 7 indistinguishable Saksunarvatn-like tephra layers were deposited between 10.4 and 9.9 cal yr BP (Jóhannsdóttir, 2007; Jennings et al., 2014; Thordarson, 2014; Harning et al., 2018b; Wastegård et al., 2018; Timms et al., 2019). Consequently, the applicability of the Saksunarvatn Ash as a key tephra marker outside of its type locality in the Faroe Islands (Mangerud et al., 1986) has been compromised, and more work is needed to better trace and correlate the Grímsvötn 10 ka Series marker tephra layers.

In Haukadalsvatn, five layers attributed to the Grímsvötn 10 ka Series tephra have been PSV-dated to 10400, 10395, 10320, 10315 and 10300 cal yr BP. Which one of these is correlated, if at all, to the „Saksunarvatn Ash" found on Greenland and the Faroe Islands remains to be determined as four of the five tephra fall within the Greenland ice cores age uncertainty (± 90 cal yr). Similarly, the lack of PSV synchronization between Vestfirðir lakes and Haukadalsvatn currently hampers correlation between these neighboring regions. As suggested by Timms et al. (2019) one possibility in linking some of these horizons across large geographical regions is by using other tephras, such as the tephra originating from Veiðivötn-Bárðarbunga found in the lake Bæjarvötn (NW Iceland) (Harning et al., 2018b), that is straddled by two Grímsvötn 10 ka Series tephra layers. Additionally, detailed analysis of major and trace element compositions may provide important opportunities to correlate layers throughout Iceland and across the North Atlantic (e.g., Davies et al., 2012; Bramham-Law et al., 2013).

6.6.2 Hekla VF tephra

A recent study used four lake sediment records from northeastern Vestfirðir to construct the first tephra stratigraphic framework for the Northwest region of Iceland (Harning et al., 2018b). By systematically tracing tephra from lake sites proximal to volcanic sources (i.e., Hestvatn and Hvítárvatn, Fig. 6.1a) to Vestfirðir, several new marker tephra layers were proposed, among them the basaltic Hekla VF tephra (9100 cal yr BP, Harning et al., 2018b). A similar study shortly followed, also using lake sediment records (n=8) collected from northeastern Vestfirðir with the goal of constructing a tephra stratigraphic framework for the region (Gudmundsdóttir et al., 2018). Despite the fact that lake sediment cores between the two studies span only a 70 km long SE-NW transect, and some lake sites are the same (e.g., Skorarvatn, Fig. 6.1b), Gudmundsdóttir et al. (2018) proposed a separate early Holocene basaltic Hekla tephra marker, termed the "Dagverðardalur tephra", and gave it the age 9500-9300 cal yr BP.

Given that the Hekla VF (or Dagverðardalur tephra) is one of the thickest tephra archived in West and Northwest Iceland (Table 6.1, Harning et al., 2018b; this study), the probability of its identification outside of Iceland is likely. Hence, deriving the best age estimate, as well as defining its name, is important for future studies in Iceland and abroad. Comparison between the major element composition of the Hekla VF and Dagverðardalur tephra demonstrates that they are identical (Fig. 6.10a, Supplemental Information). Following an assessment of the ^{14}C age constraints for the Dagverðardalur tephra, we suggest that there is reasonable likelihood that the age estimate of 9500-9300 cal yr BP is too old. The ^{14}C ages used to constrain the Dagverðardalur tephra are from terrestrial macrofossils in the lake sediment of Brattihjalli and Skorarvatn (Fig. 1B, Gudmundsdóttir et al., 2018), which when dated, are materials known to give relatively older ages due to the transportation of older organic material into lakes (Sveinbjörnsdóttir et al., 1998; Geirsdóttir et al., 2009a; Florian, 2016). Hence, the Dagverðardalur tephra ages that are several 100 years older than the age estimates of Harning et al. (2018b), which are derived from aquatic mosses with shorter residence times (Þóra Hrafnsdóttir, pers. comm.) in addition to the PSV-infered age in Haukadalsvatn (9100 cal yr BP), are expected. Ultimately, based on identical compositions (Fig. 6.10a) and a re-assessment of age constraints, we suggest that there is no distinct "Dagverðardalur tephra", but that it is in fact the Hekla VF marker tephra.

Although the depositional age and major elemental composition of the Hekla VF tephra are fairly well established, its dispersal range is still partially open to discussion. The eastern boundary of the tephra marker can be loosely delineated based on the lack of its presence in the lake Barðarlækjartjörn (Fig. 11, Eddudóttir et al., 2016), and its identification throughout Hestvatn, Hvítárvatn, Haukadalsvatn, and a number of lakes on northeastern Vestfirðir (Fig. 6.10a and 6.11, Harning et al., 2018b). Despite the fact that its western boundary is currently unknown, the distribution of lakes containing the Hekla VF suggests a moderately narrow ash plume trajectory toward the northwest (Fig. 6.11). Future studies should aim to look for the Hekla VF tephra in areas such as western Vestfirðir, Snæfellsnes peninsula and the Reykjanes peninsula in an effort to confirm whether the western boundary lies on land or perhaps even more westward at sea. This has implications for understanding Iceland's Holocene eruptive history as well as studies employing Holocene tephra-based chronologies.

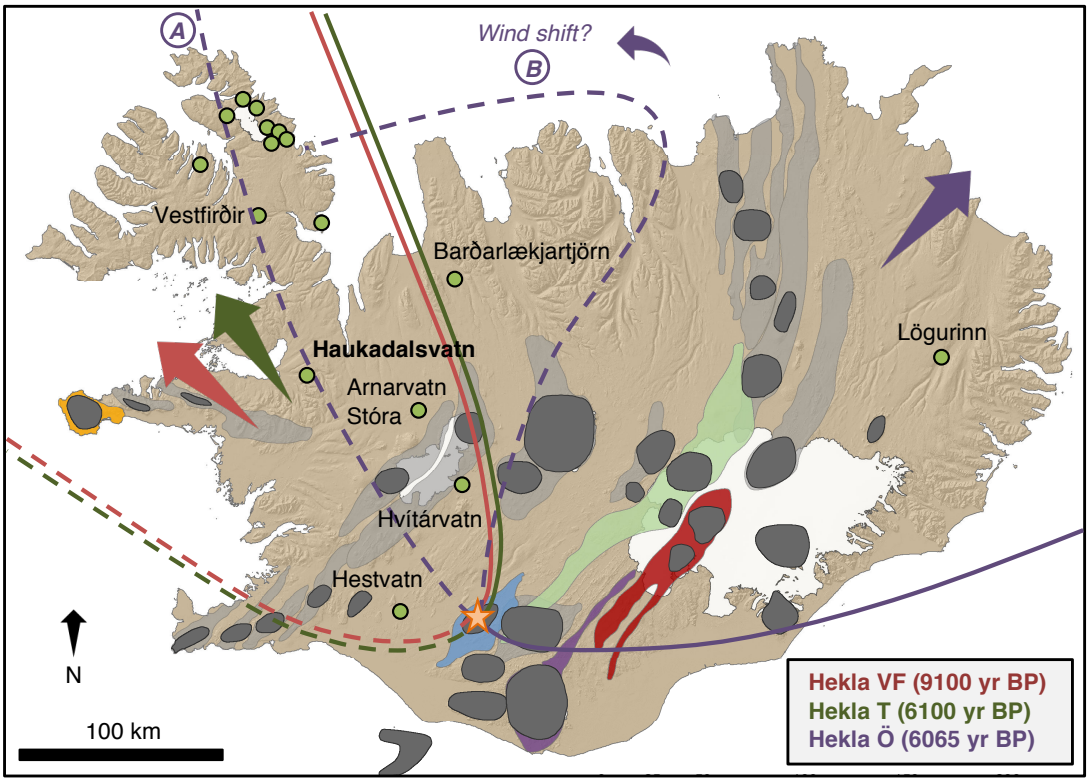

Figure 6.11. *Estimated dispersal boundaries of select early to middle Holocene Hekla tephra. Limits based on the presence/absence of tephra in lake sediment records (green circles) and soils sites (Harðardóttir et al., 2001; Jóhannsdóttir, 2007; Larsen et al., 2012; Eddudóttir et al., 2016; Harning et al., 2016a, 2016b; 2018b; Gunnarson, 2017; Gudmundsdóttir et al., 2011, 2016, 2018). For Hekla Ö, option A is after Gudmundsdóttir et al. (2018), whereas option B is suggested in this study (modified after Gudmundsdóttir et al., 2011). The orange star marks the location of the Hekla central volcano. Large arrows indicate the interpreted direction of the major tephra dispersal axis.*

6.6.3 Hekla T tephra: part of Hekla Ö or not?

Similar to the Hekla VF, another basaltic Hekla tephra layer of middle Holocene age (6100 cal yr BP) has recently been traced throughout West and Northwest Iceland, underpinning its importance as a marker tephra in this region (Fig. 6.11, Jóhannsdóttir, 2007; Larsen et al., 2012; Gunnarson, 2017; Harning et al., 2018b). However, the recent Vestfirðir study by Gudmundsdóttir et al. (2018) found a tephra of similar age that featured Hekla grains with basaltic andesite to rhyolitic compositions, in addition to the basaltic composition identified by Harning et al. (2018b). Given the strong similarity between the basaltic andesite to rhyolitic composition of the tephra on Vestfirðir and of another middle Holocene Hekla tephra found in Northeast and East Iceland, Gudmundsdóttir et al. (2018) proposed that this is the Hekla Ö tephra (Fig. 6.10b, 6065 cal yr BP, Gudmundsdóttir et al., 2011). In doing so, the previously known distribution of the Hekla Ö tephra was expanded significantly westward (Fig. 6.11, option A, Gudmundsdottir et al., 2018), despite the fact that it is not found in Arnarvatn Stóra or Hvítárvatn, where only the basaltic Hekla T is archived (Fig. 6.10b, Jóhannsdóttir, 2007; Larsen et al., 2012; Gunnarson, 2017), and that only 1 tephra shard of 115 chemically analyzed (0.9 %) in Vestfirðir lakes investigated by Harning et al. (2018b) had an andesitic composition. Given the newly proposed distribution of the Hekla Ö tephra in West Iceland, speculation has arisen regarding whether the Hekla T is part of the

same eruption that generated the Hekla Ö tephra (Gudmundsdóttir et al., 2018; Jónsson, 2018). Based on known Hekla magma products and age models employed by Gudmundsdóttir et al. (2018), we suggest that the co-eruption of the two is improbable.

First, regardless of the exact dispersal limits of the Hekla Ö tephra, it is high unlikely that the Hekla T tephra was generated during the same eruption. As we know it today, the Hekla volcanic complex features both a central volcano (1490 m asl) and a 60 km long fissure swarm, both of which have distinct magma products (Thorarinson, 1967; Jakobsson, 1979). Hekla basalt (particularly primitive, i.e., high MgO wt%) is erupted from the rift flank fissures, whereas Hekla basaltic andesite-rhyolite originates from the central volcano, undergoing multi-leveled magmatic differentiation from its basaltic magma parent sourced from deeper within the mantle (Sigmarsson et al., 1992; Sigmarsson and Steinþórsson, 2007; Moune et al., 2009; Schuessler et al., 2009). The latter central volcano eruptions often produce tephra of mixed compositions as well, starting with a short plinian to subplinian phase of rhyolitic composition, and then easing in intensity to an effusive phase characterized by andesitic to basaltic andesite magma, such as seen for the Hekla 4 eruption (Larsen and Thorarinsson, 1977). Although we cannot deny the possibility with complete certainty, there are currently no known Hekla eruptions that produced the full spectrum of magmatic compositions (Thorarinson, 1967; Larsen and Thorarinsson, 1977; Höskuldsson et al., 2007), making the speculation that the Hekla T and Hekla Ö tephra are sourced from the same event doubtful.

Second, the ^{14}C-based age models from four of the eight lakes used by Gudmundsdóttir et al. (2018) feature several unacknowledged age reversals throughout the Holocene record (Skorarvatn, Reykjarfjörður, Neðra Eyvindarfjarðarvatn, and Neðra Hvalárvatn). By accounting for some of these age reversals, it appears as though the Hekla Ö tephra was deposited during the early Holocene in the lakes Reykjarfjörður and Neðra Eyvindarfjarðarvatn (e.g., Harning et al., 2018b). Based on the comparison of the basaltic component only, Harning et al. (2018b) suggested that these tephra may in fact be the Hekla VF tephra although no basaltic andesite-rhyolitic grains have yet to be detected in the Hekla VF tephra marker. On the other hand, Neðra Hvalárvatn‘s “Hekla Ö tephra” is constrained with ^{14}C-dated humic acids, which are materials known to provide unreliable age estimates (Geirsdóttir et al., 2009a). These ^{14}C-dated humic acids constrain the tephra to the 7760-6600 cal yr BP window (Gudmundsdóttir et al., 2018), which does not fit with either Hekla VF (9070 cal yr BP) or Hekla T/Ö (6100-6065 cal yr BP) age estimates. Importantly, this reassessment demonstrates that the age models used by Gudmundsdóttir et al. (2018) to derive age estimates for tephra correlations are not reliable. Coupled with the fact that the chemical compositions of the Hekla Ö have not been replicated in other Vestfirðir lake sediments (Harning et al., 2018b) or other West and Central Icelandic lake sediment studies (Jóhannsdóttir, 2007; Larsen et al., 2012; Gunnarson, 2017; this study), suggest that the interpretation of Hekla Ö‘s presence on Vestfirðir and in West Iceland is tentative until more data and/or better age estimates can be obtained.

If the presence of the Hekla Ö tephra on Northwest Iceland is indeed bona fide, one potential would be to re-evaluate its dispersal limits as originally suggested by Gudmundsdottir et al. (2018). With the exception of the major rhyolitic Hekla eruptions (Hekla 5, 4 and 3), Hekla‘s ash plumes are typically formed over a short-lived explosive phase that feature narrow dispersal trajectories, such as for the Hekla VF and Hekla 1693 eruptions (Janebo et al., 2016; Harning et al., 2018b). Consequently, we suggest that the original Hekla Ö tephra distribution NE of of Hekla as presented by Gudmundsdottir et al. (2011) is more likely and remains the most accurate at this time. The original NE axis of dispersal is also consistent with its absence in Haukadalsvatn, Hvítárvatn, Arnarvatn Stóra

and many lakes on Vestfirðir (Fig. 6.10b). However, Hekla Ö's fragmentary and tentative deposition over portions of Northwest Iceland could have resulted when the fine grained ash component carried by the high-flying NE-trending plume dropped to lower levels in the atmosphere, where it was carried westward by shifting easterly winds (Fig. 6.11, option B).

Given our current understanding of the Hekla magma products during volcanic events, we suggest that the basaltic Hekla T (6100 cal yr BP) and the basaltic-andesite to rhyolite Hekla Ö tephra (6065 cal yr BP) were generated in separate eruptions spaced closely in time. The presence of both compositions in some Icelandic lake sediment cores as well as soil sites proximal to Hekla (Gudmundsdóttir et al., 2018; Jónsson, 2018) attests to this proposition, particularly in these low sedimentation rate environments. Because the ages derived for the two tephra are indistinguishable within calibration uncertainty, they can for all intents and purposes, be treated as a singular marker tephra if the aim is to synchronize geologic archives. However, distinguishing between the two is important for understanding distribution patterns of their respective ash plumes (Fig. 6.11), and if future studies aim to quantify volumes of erupted material. In this regard, future work should aim to firmly establish a western boundary for the Hekla T tephra marker, similar to the Hekla VF. At the same time, targeted analysis for basaltic andesite-rhyolite grains of Hekla affinity in West and Central Iceland would benefit the ongoing work aiming to define the limits of the Hekla Ö tephra (e.g., Gudmundsdóttir et al., 2018).

6.6.4 Implication of Haukadalsvatn tephra stratigraphy for identification and correlation to tephra layers in Vestfirðir and Greenland

Although 13 marker tephra can be traced between Haukadalsvatn and Northwest Iceland lake sediment records, the majority cannot. This mismatch is surprising given the close geographical location of the neighboring regions, which implies that there should be more commonalities. If the tephra from each respective site are binned for every 500 years (Fig. 6.12a and b), tephra layer frequency can provide some insight into the nature of the regional discrepancies. The dominant observation is that when Haukadalsvatn's tephra layer frequency increases (Fig. 6.12a), the Vestfirðir lakes' decreases (Fig. 6.12b), and vice versa. One possible scenario to explain this asynchronicity is the predominance for small eruptions with limited axes of dispersal, which has previously been invoked to account for the disparity just between the Vestfirðir lake records (Harning et al., 2018b). If the two tephra layer frequency records are summed (Fig. 6.12c), the frequency of eruptions during the Holocene is highest during the early and late Holocene, with relatively fewer eruptions during the middle Holocene.

Collectively, we suggest that the Haukadalsvatn (Geirsdóttir et al., 2009a, 2013, this study) and Vestfirðir tephra records (Harning et al., 2018b; Gudmundsdóttir et al., 2018) serve as templates for studies investigating tephra archived in Northwest North Atlantic geological records, such as those on Greenland. More specifically, if the trajectory of the more widespread marker tephra from Iceland (e.g., Hekla VF and Hekla T) were extrapolated to the northwest, East Greenland holds the most promise for tephra identification and correlation (e.g., Jennings et al., 2014). Perhaps with the exception of large, explosive events such as those related to the Grímsvötn 10 ka tephra series, the more distal tephra deposits in Greenland ice, lake and marine archives are likely to be preserved as cryptotephra (e.g., Zielinski et al., 1997; Grönvold et al., 1995; Mortensen et al., 2005; Abbott and Davies, 2012; Coulter et al., 2012; Jennings et al., 2014). Given the recent acquisition of lake sediment records from east Greenland (e.g., Balascio et al., 2013; 2015;

Lowell et al., 2013; Levy et al., 2014; van der Bilt et al., 2018), there is a growing opportunity to explore tephrochronology at these or neighboring locations, and perhaps, lead to improved synchronization to Icelandic paleoclimate datasets.

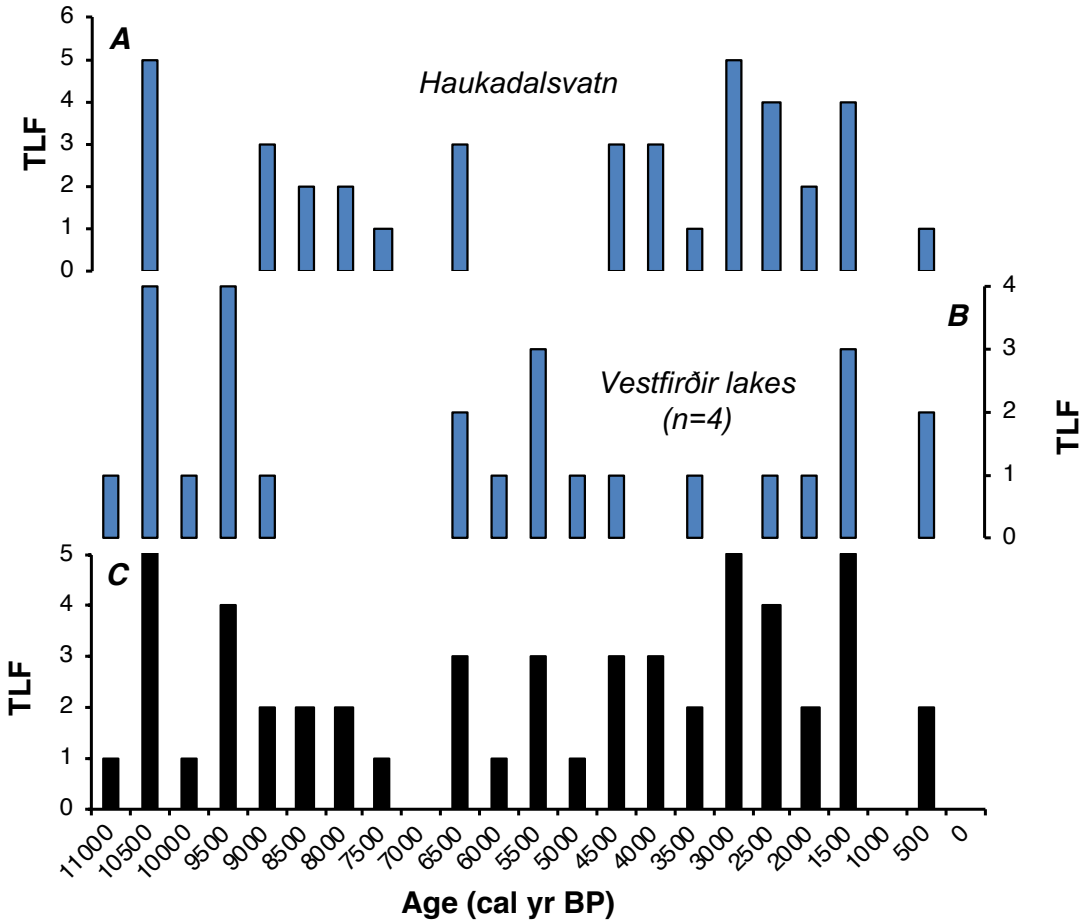

Figure 6.12. *Tephra layer frequency (TLF) in 500-yr bins for A) Haukadalsvatn, West Iceland (this study), B) Vestfirðir lakes, Northwest Iceland (n=4, Harning et al., 2018b), and C) sum of Haukadalsvatn and Vestfirðir lakes.*

6.7 Conclusions

We present a securely-dated Holocene tephra record from the lake Haukadalsvatn in West Iceland. Age control is derived from PSV synchronization to the well-dated PSV master chronology from marine core MD99-2269 on the North Iceland Shelf. Electron microprobe analyses reveal 38 different tephra layers throughout the Holocene. Identical major element composition as well as relevant stratigraphical and chronological information allow 13 of these tephra to be linked to those found on northeastern Vestfirðir, and hence, define a series of well-dated marker tephra for West and Northwest Iceland. Despite their close geographical location, comparison of Haukadalsvatn‘s tephra layer frequency record to that of Northwest Iceland‘s reveals a striking amount of asychronicity. This regional disparity is likely the result of predominately small eruptions that featured narrow ash plumes. We argue that Haukadalsvatn serves as an important template for the tephrochronology of West Iceland and for the synchronization of more distal records in the Northwest North Atlantic.

6.8 Supplemental Information

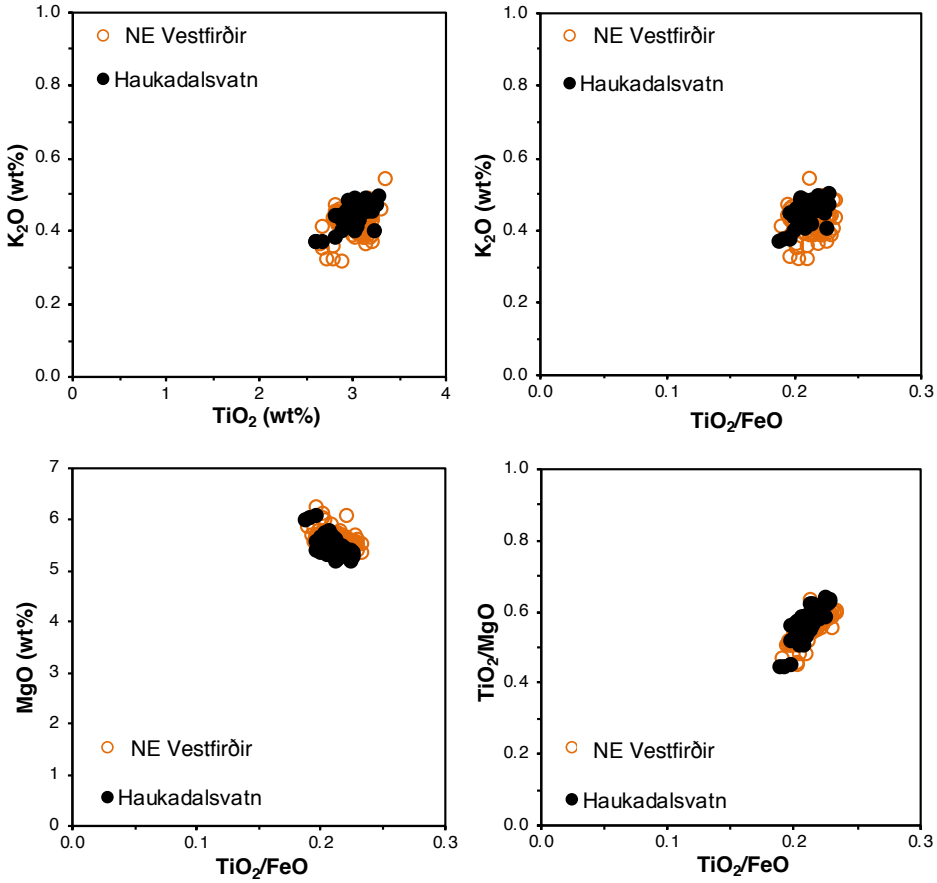

Figure S6.1. *Bi-elemental plot comparisons demonstrating the correlation of the Grímsvötn 10 ka Series marker tephra in Haukadalsvatn (n=81) to the tephra layers found in Northwest Iceland lakes (n=122, Harning et al., 2018b).*

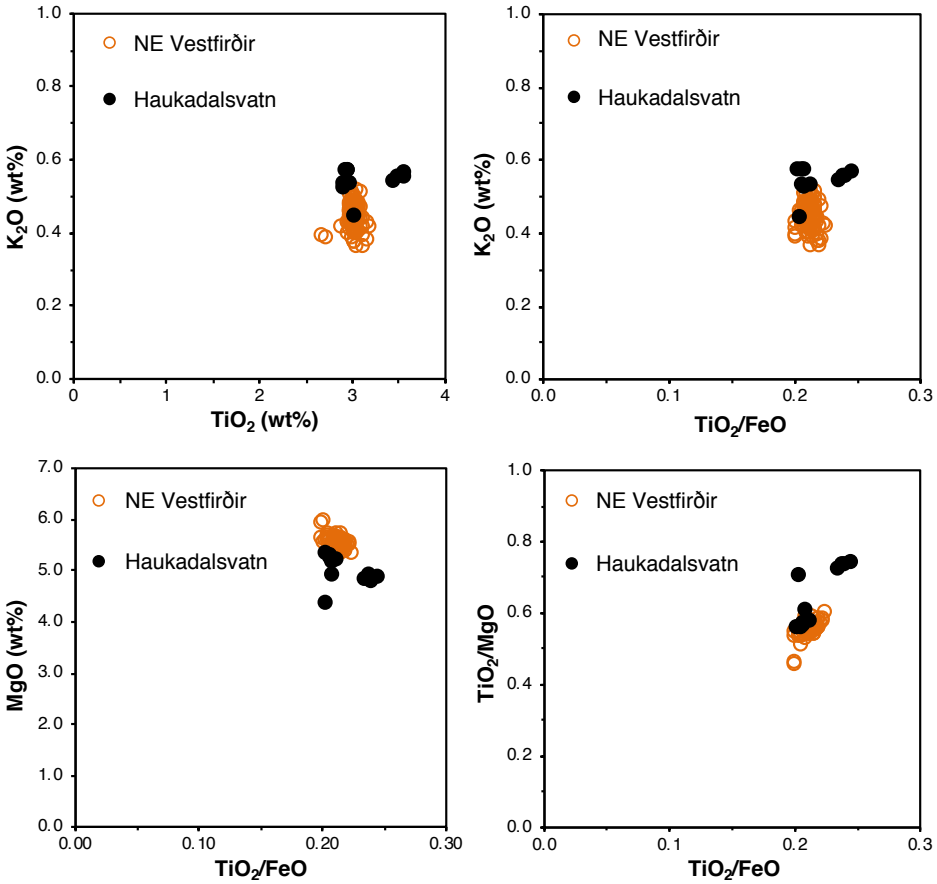

Figure S6.2. *Bi-elemental plot comparisons demonstrating the correlation of the Grímsvötn B marker tephra in Haukadalsvatn (n=11) to the tephra layers found in Northwest Iceland lakes (n=94, Harning et al., 2018b).*

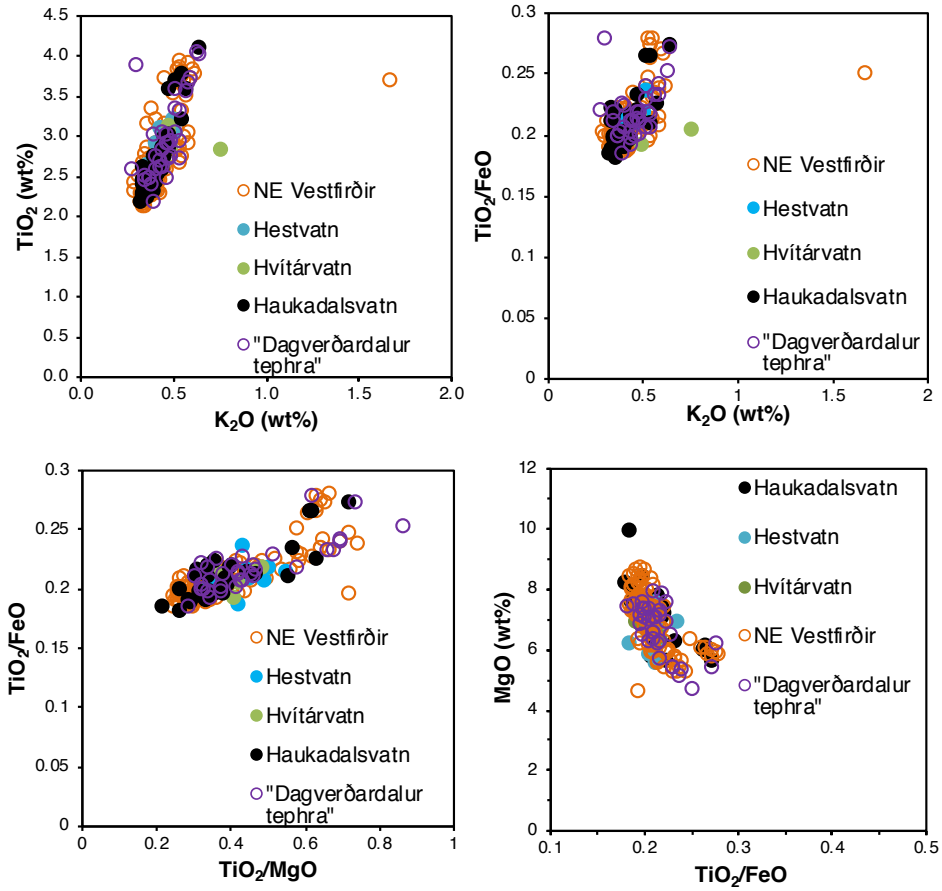

Figure S6.3. *Bi-elemental plot comparisons demonstrating the correlation of the Hekla VF marker tephra in Haukadalsvatn (n=34) to the tephra layers found in Northwest Iceland lakes (n=113, Harning et al., 2018b), Hestvatn (n=12, Jóhannsdóttir, 2007), Hvitarvatn (n=6, Jóhannsdóttir, 2007) and the "Dagverðardalur tephra" (n= 34, Gudmundsdottir et al., 2018).*

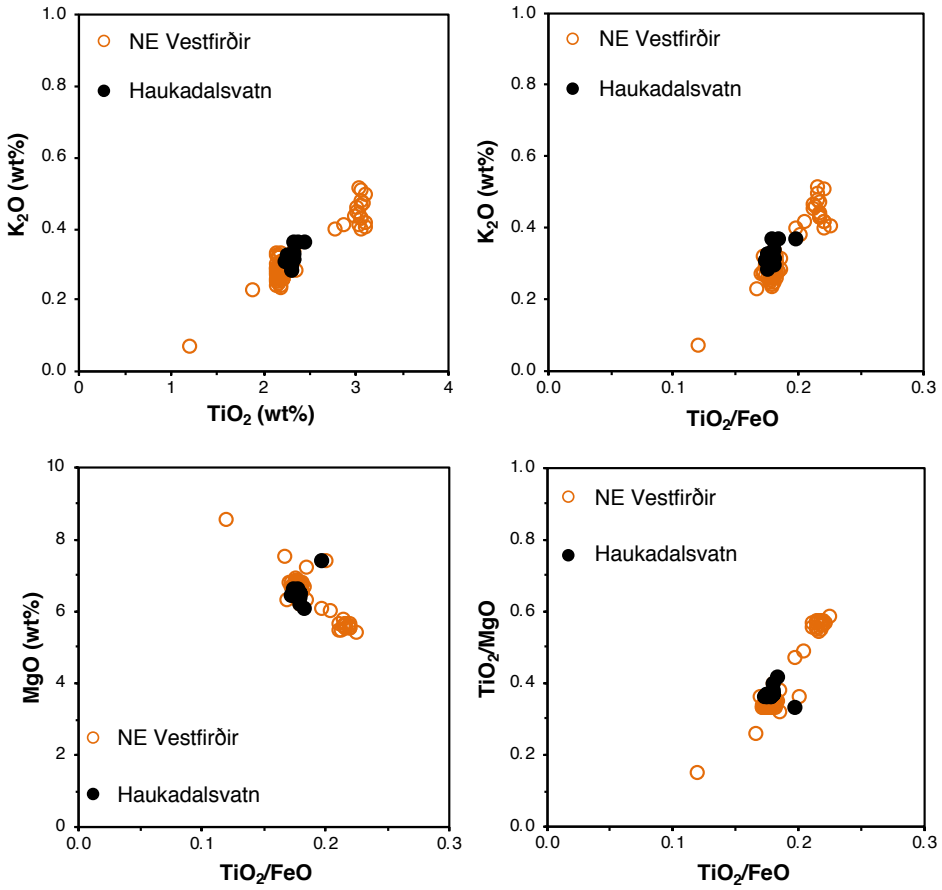

Figure S6.4. *Bi-elemental plot comparisons demonstrating the correlation of the Grímsvötn BP-2 marker tephra in Haukadalsvatn (n=12) to the tephra layers found in Northwest Iceland lakes (n=68, Harning et al., 2018b).*

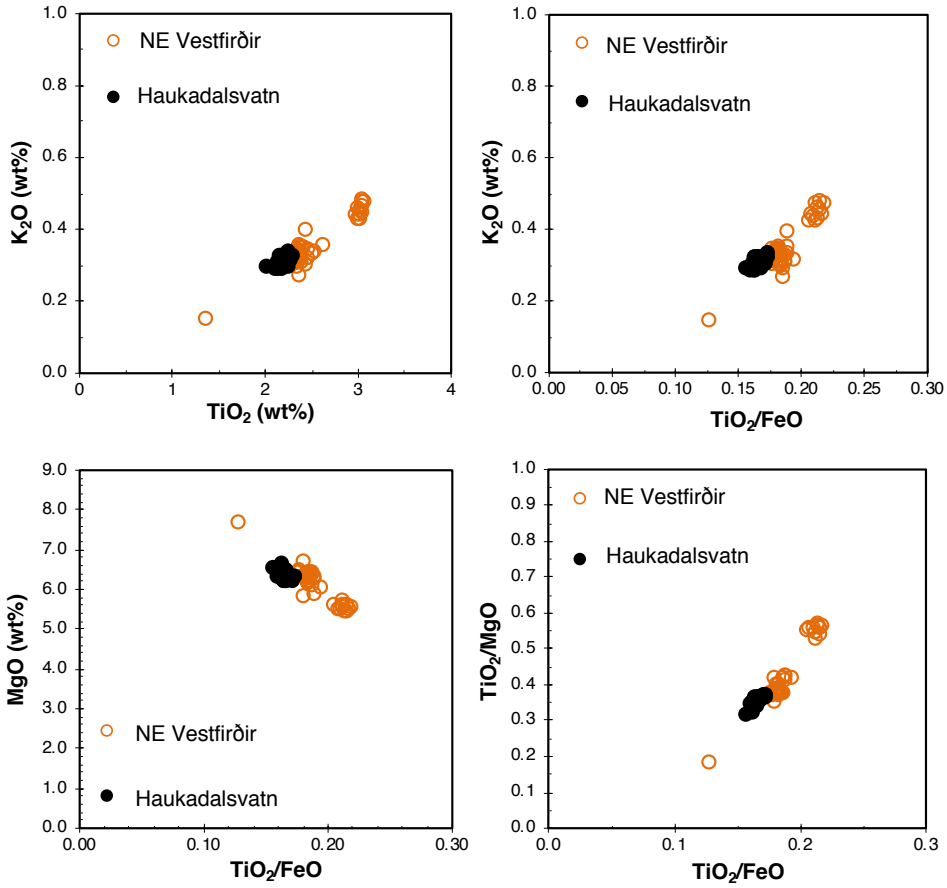

Figure S6.5. *Bi-elemental plot comparisons demonstrating the correlation of the Grímsvötn BP-1 marker tephra in Haukadalsvatn (n=12) to the tephra layers found in Northwest Iceland lakes (n=40, Harning et al., 2018b).*

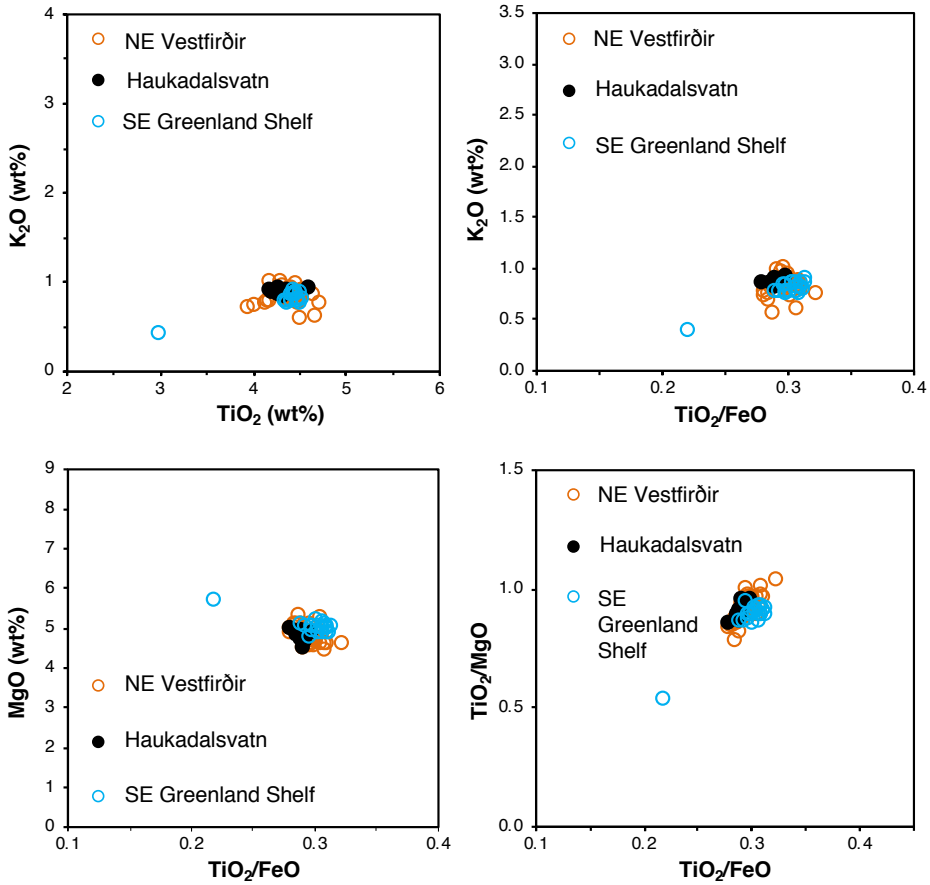

Figure S6.6. *Bi-elemental plot comparisons demonstrating the correlation of the Katla EG marker tephra in Haukadalsvatn (n=12) to the tephra layers found in Northwest Iceland lakes (n=40, Harning et al., 2018b) and on the SE Greenland Shelf (n=20, Jennings et al., 2014)*

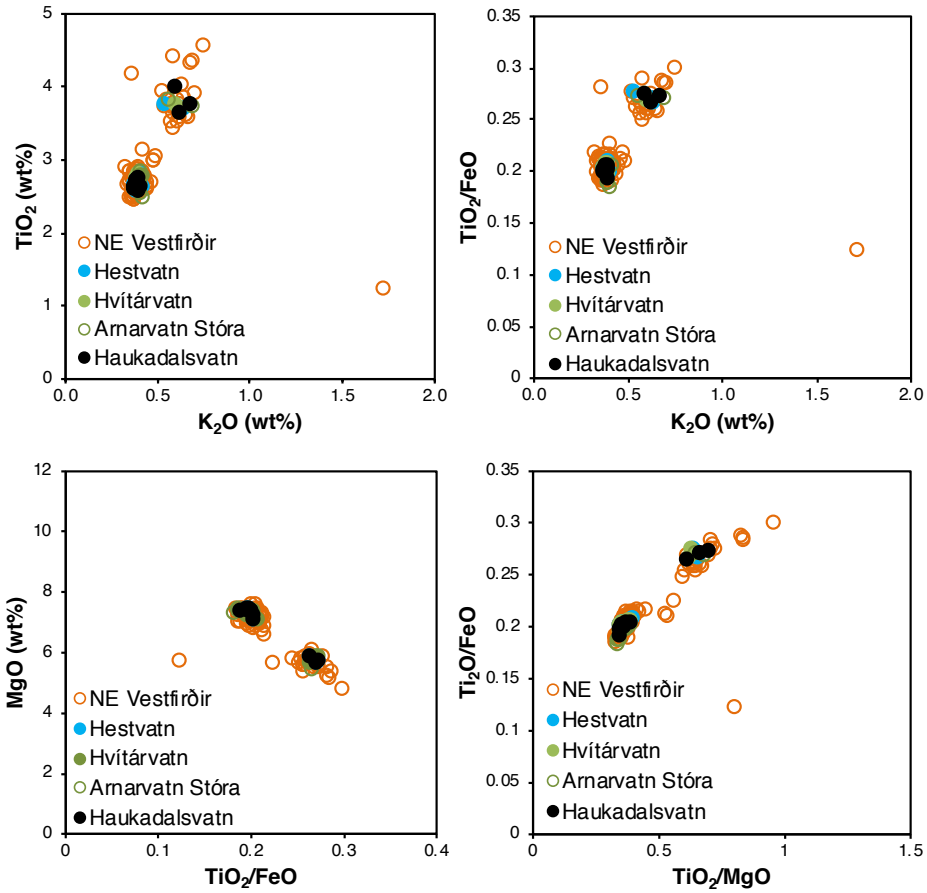

Figure S6.7. *Bi-elemental plot comparisons demonstrating the correlation of the Hekla T marker tephra in Haukadalsvatn (n=12) to the tephra layers found in Northwest Iceland lakes (Harning et al., 2018b), Hestvatn (n=11, Jóhannsdóttir, 2007), Hvitarvatn (n=11, Jóhannsdóttir, 2007) and Arnarvatn Stóra (n=15, Gunnarson, 2017).*

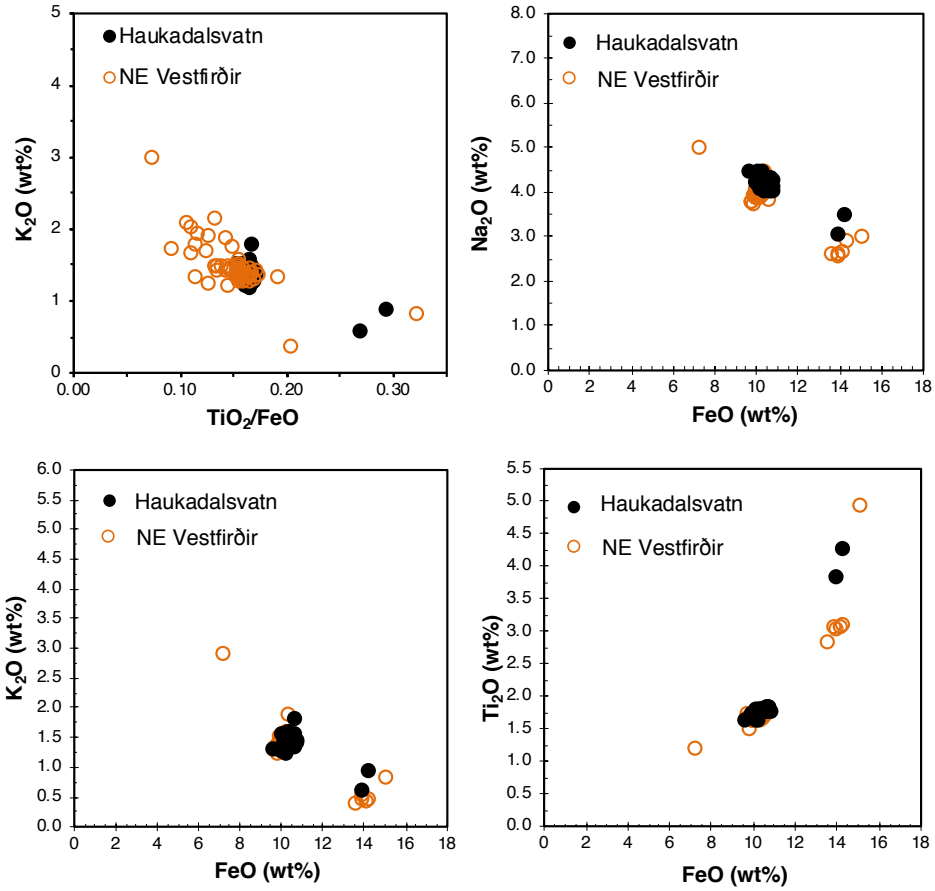

Figure S6.8. *Bi-elemental plot comparisons demonstrating the correlation of the Hekla 4 marker tephra in Haukadalsvatn (n=36) to the tephra layers found in Northwest Iceland lakes (n=37, Harning et al., 2018b).*

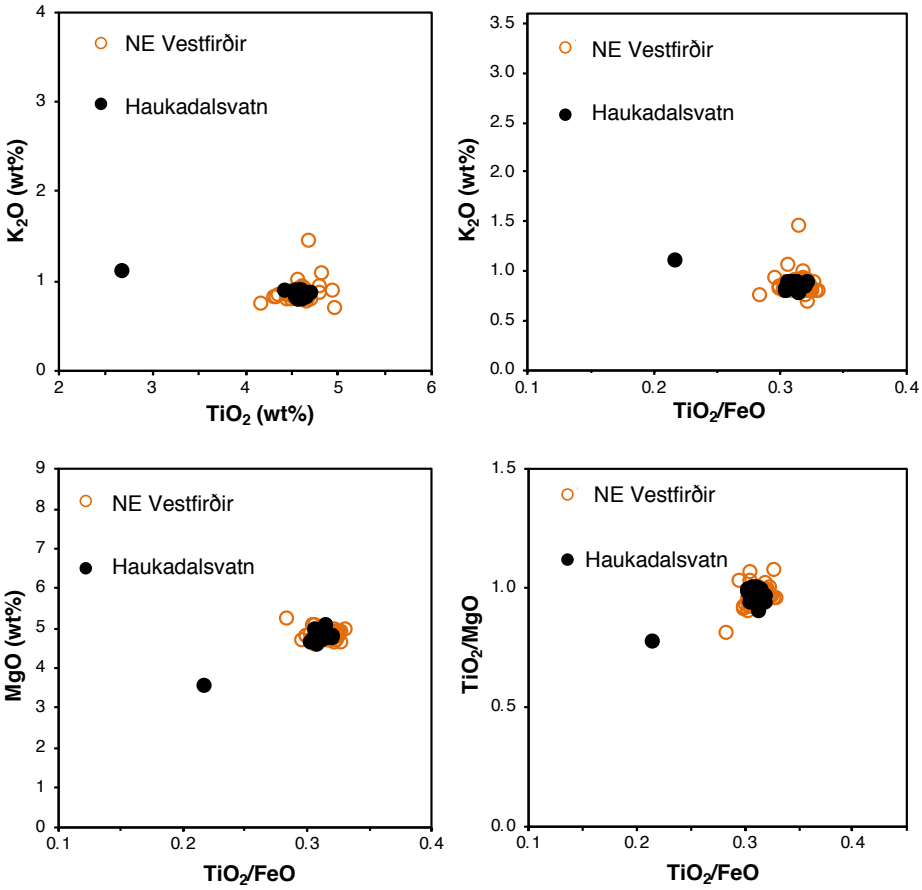

Figure S6.9. *Bi-elemental plot comparisons demonstrating the correlation of the Katla 2190 marker tephra in Haukadalsvatn (n=28) to the tephra layers found in Northwest Iceland lakes (n=69, Harning et al., 2018b).*

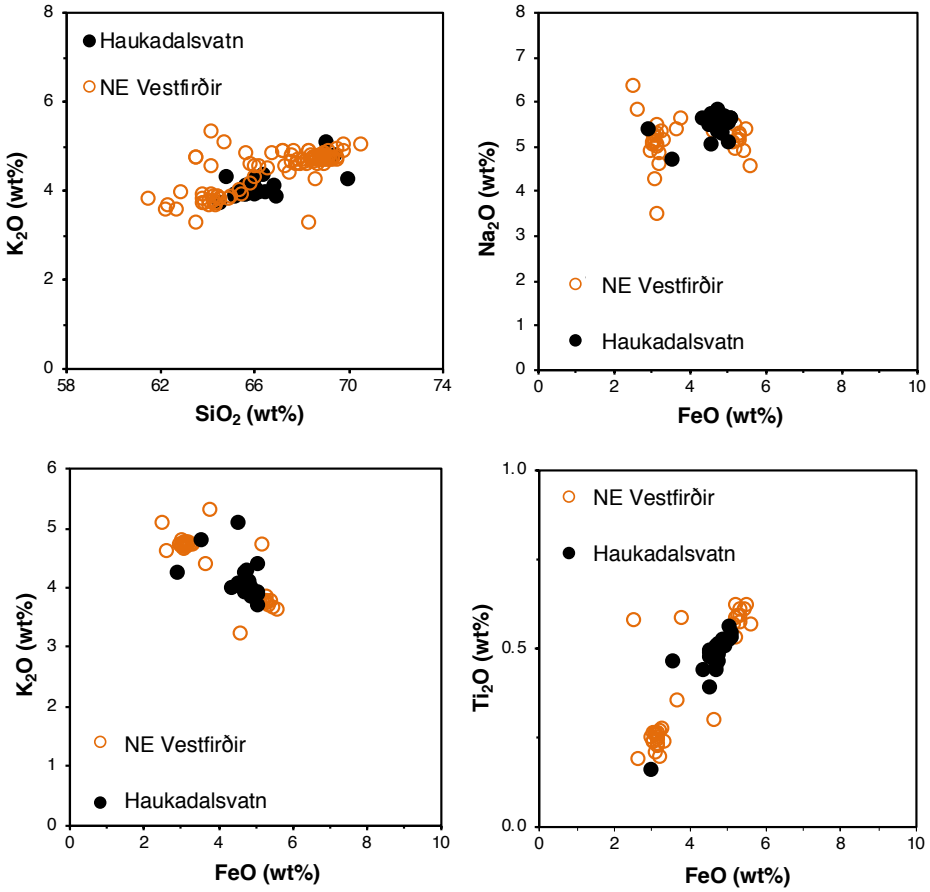

Figure S6.10. *Bi-elemental plot comparisons demonstrating the correlation of the Snæfellsjökull-1 marker tephra in Haukadalsvatn (n=25) to the tephra layers found in Northwest Iceland lakes (n=33, Harning et al., 2018b).*

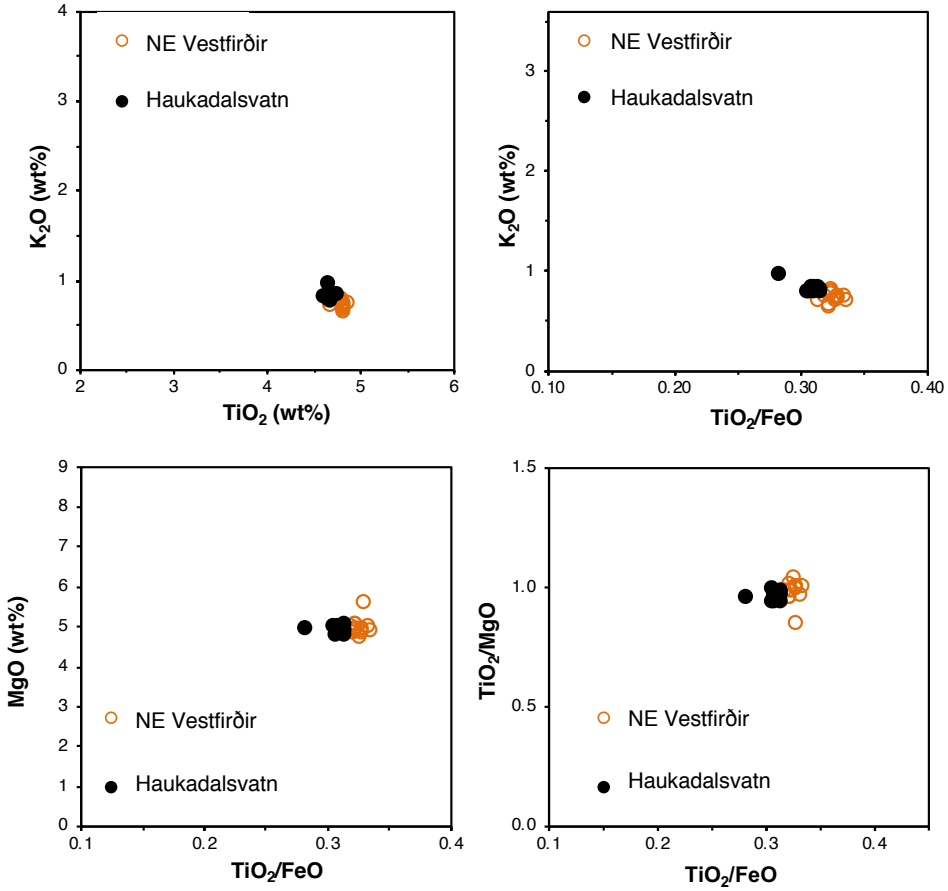

Figure S6.11. *Bi-elemental plot comparisons demonstrating the correlation of the Katla 1260 marker tephra in Haukadalsvatn (n=10) to the tephra layers found in Northwest Iceland lakes (n=14, Harning et al., 2018b).*

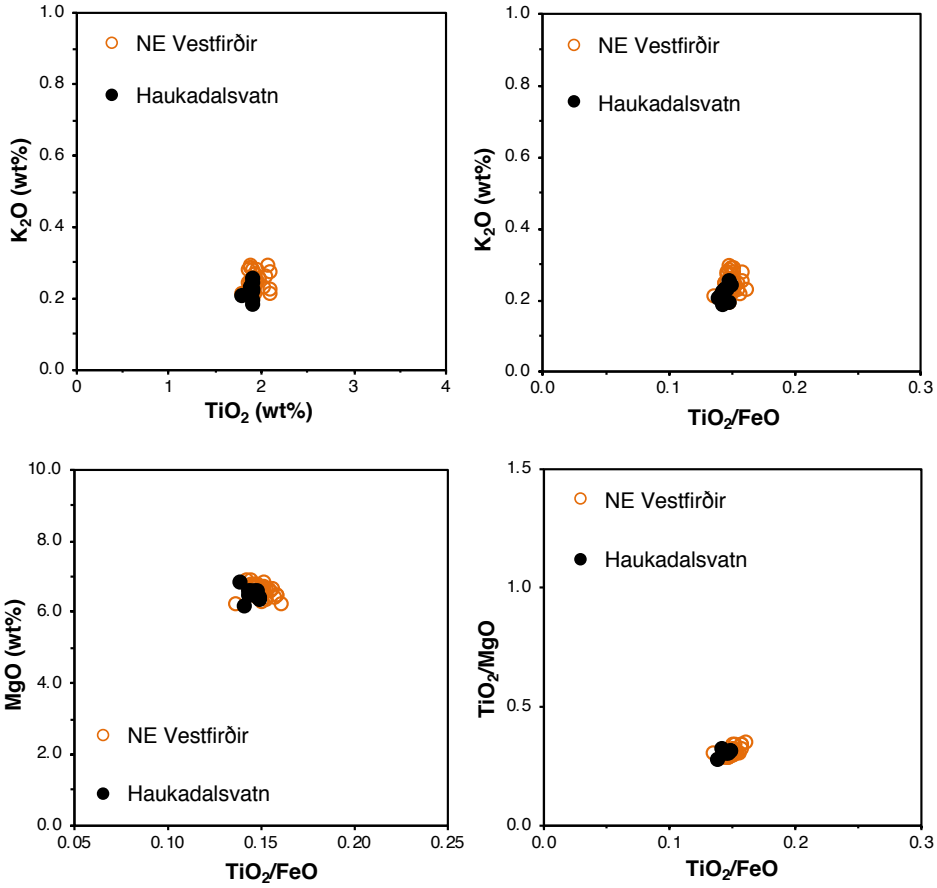

Figure S6.12. *Bi-elemental plot comparisons demonstrating the correlation of the basaltic component Settlement Layer marker tephra in Haukadalsvatn (n=10) to the tephra layers found in Northwest Iceland lakes (n=44, Harning et al., 2018b).*

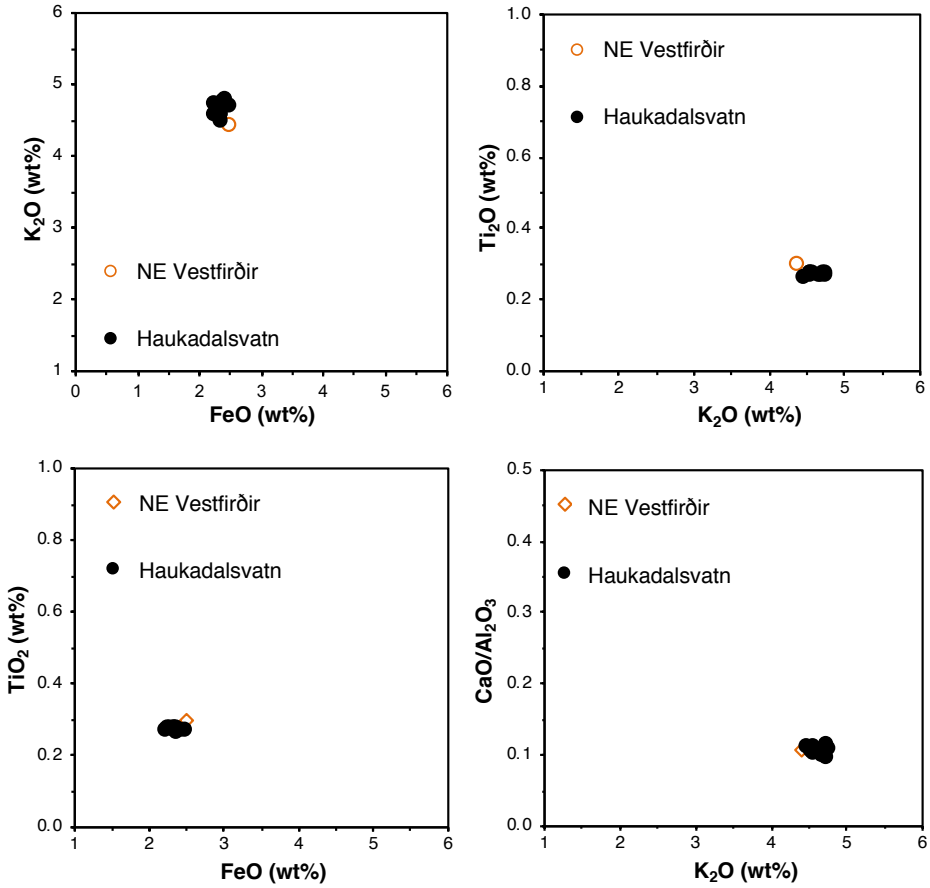

Figure S6.13. *Bi-elemental plot comparisons demonstrating the correlation of the rhyolitic component Settlement Layer marker tephra in Haukadalsvatn (n=10) to the tephra layers found in Northwest Iceland lakes (n=1, Harning et al., 2018b).*

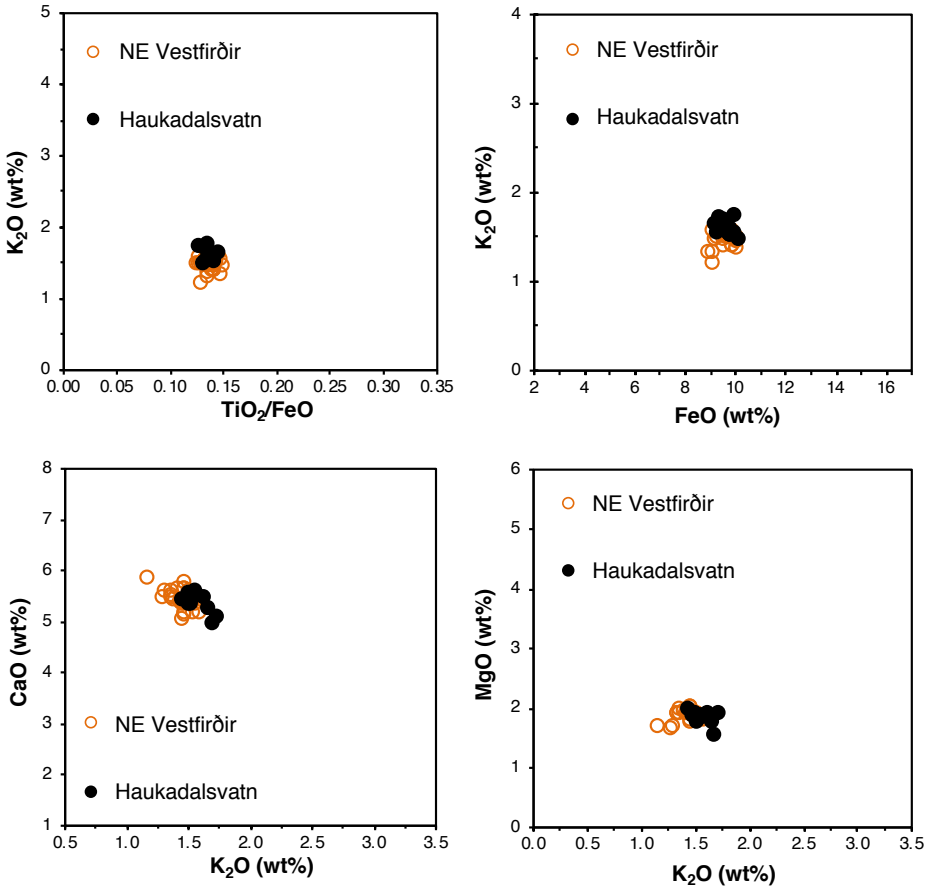

Figure S6.14. *Bi-elemental plot comparisons demonstrating the correlation of the Hekla 1693 marker tephra in Haukadalsvatn (n=12) to the tephra layers found in Northwest Iceland lakes (n=29, Harning et al., 2018b).*

7 Lipid Biomarkers Quantify Holocene Summer Temperatures in Icelandic Lakes and Soils[6]

7.1 Abstract

Iceland currently lacks reliable and continuous quantitative records of Holocene temperature. We first report downcore alkenone and branched glycerol dialkyl glycerol tetraethers (brGDGT) records that quantify Holocene temperature change in Skorarvatn, a 25-m-deep lake in northwest Iceland. Analysis of alkenones indicate that the biological producers in Skorarvatn are Group I haptophytes and, thus, allow the application of published Group I calibrations. Alkenone-based temperatures closely track smoothly decreasing Northern Hemisphere June insolation, and thus, provide a firm summer temperature baseline to assess brGDGTs. Compared to previous records from Skorarvatn, relative changes in brGDGT-inferred MSAT closely tracks biogenic silica (BSi), a proxy for qualitative summer temperature in Iceland. Furthermore, brGDGTs and BSi both show synchronous cooling at ~2.4 ka, consistent with the first late Holocene appearance and subsequent growth of the temperature-sensitive Drangajökull ice cap. However, the late Holocene soil erosion likely confounds late Holocene brGDGT lake temperatures via contamination of relic and "warmer" soil brGDGTs. In addition to the lake-based proxies, we also examine brGDGT-based temperature reconstructions from stacked soil sequences that span the last 10,000 years in the central highlands. Due to the region's proximity to the active volcanic zone, the soil sequences are separated by thick ash layers, which have diagnostic geochemical fingerprints that permit robust correlation to tephra of known age. Additionally, soil-derived records may circumvent complications associated with multiple brGDGT producers contributing to lake sediment. Using the global soil calibration, brGDGT-inferred temperatures from the soil sequence conform to local qualitative climate records and capture periods of documented abrupt climate change in Iceland. However, similar the lake, late Holocene erosion may contaminate the record and artificially imply warmer conditions at this time. Glacier modeling experiments for Drangajökull and Langjökull both pin peak Holocene Thermal Maximum (+3^{o}C modern) and lowest late Holocene (-0.8^{o}C modern) temperature estimates near those inferred from lake sediment and soil brGDGTs, as well as alkenones. Hence, these new quantitative records provide a first step towards constraining the glacier and climate sensitivity of Iceland during the Holocene, and important insight into the warming expected over the current century.

7.2 Introduction

Icelandic paleoclimate research has hemispheric relevance due to its geographic position at the confluence of major North Atlantic oceanic and atmospheric circulation patterns, both of which are integral to global heat distribution (e.g., Wunsch, 1980). A combination of proxy and model datasets have demonstrated that following deglaciation from the Icelandic Ice Sheet (Norðdahl and Ingólfsson, 2015; Patton et al, 2017), independent ice caps rapidly wasted between 10.3 and 9.2 ka, resulting in an "ice free" Iceland during the presumed Holocene Thermal Maximum (HTM, 8.9-5.5 ka) (Flowers et al., 2008; Larsen et al., 2012;

[6] Harning, D.J., Curtin, L., Geirsdóttir, Á., Miller, G.H., D'Andrea, W.J., Thordarson, T., Gunnarsdóttir, S., Sepúlveda, J. Lipid biomarkers quantify Holocene summer temperature in Iceland lakes and soils, *in prep.*

Anderson et al., 2018; Harning et al., 2016a, 2018a). Subsequent to peak warmth, continuous and high-resolution climate reconstructions reflect long-term cooling and ice cap expansion driven by the steady decline in northern hemisphere summer insolation (Larsen et al., 2011; 2012; Striberger et al., 2012; Geirsdóttir et al., 2013, 2019; Moossen et al., 2015; Harning et al., 2018b). The lowest temperatures and largest ice cap dimensions likely culminated during the Little Ice Age (LIA, 1250-1850 CE) (Flowers et al., 2007, 2008; Larsen et al., 2015; Harning et al., 2016b; Anderson et al., 2018). However, these datasets are qualitative in nature, and thus, limit our ability to assess the rate and magnitude of Holocene climate variability in Iceland.

Most quantitative reconstructions of terrestrial Holocene temperature in Iceland are based upon chironomid assemblages (Caseldine et al., 2003, 2006; Axford et al., 2007; Langdon et al., 2010). However, Icelandic chironomid communities are also confounded by substrate (Langdon et al., 2008), post-settlement soil erosion (Lawson et al., 2007), limited taxonomic resolution, and are ill-suited for large, deep lakes (Axford et al., 2009). Consequently, chironomid-based temperature reconstructions in Iceland have proven to be challenging (e.g., Holmes et al., 2016) and do not conform to the Iceland's consensus Holocene climate history. A quantitative branched glycerol dialkyl glycerol tetraether (brGDGT) record reconstructed terrestrial temperatures from a fjord sediment core in northwest Iceland (Moossen et al., 2015). However, given that brGDGTs are sourced from a range of environments (e.g., Schouten et al., 2013), the fjord record is complicated by unconstrained producer(s), variable transport times between terrestrial and marine brGDGTs, as well as sea-floor mixing. Furthermore, the fjord record preceded recent analytical improvements that remove the influence of pH-sensitive brGDGT isomers (De Jonge et al., 2013, 2014a; Hopmans et al., 2016). Considering the Icelandic glaciers respond primarily to summer temperature (Björnsson and Pálsson, 2008), glacier modeling experiments have estimated the magnitude of temperature between the HTM and the LIA required to meet reconstructed glacier dimensions (Flowers et al., 2008; Anderson et al., 2018). However, these are not continuous and do not capture the centennial-scale perturbations evident in the Holocene lake records. Hence, Iceland currently lacks reliable and continuous records of Holocene temperature.

Here, we capitalize on recent advances in the field of lipid biogeochemistry (e.g., Castañeda and Schouten, 2011; Schouten et al., 2013) to quantify Holocene temperature from a continuous lake sediment record and stacked soil sequence in Iceland. Additionally, we analyze catchment soil and lake water filtrate samples for brGDGT distributions in an effort to better constrain brGDGT sources to the lake sediment record. In the lake sediment record, we show that brGDGT and alkenone-based paleothermometers both reflect quantitative summer temperature in Iceland by comparison to a suite of high-resolution qualitative lake sediment climate proxies (Harning et al., 2018b), as well as quantitative glacier model estimates (Anderson et al., 2018). The stacked soil brGDGT-inferred temperatures also conform to local qualitative records of Holocene summer temperature (Larsen et al., 2012; Gunnarson, 2017) and glacier activity (Flowers et al., 2007, 2008; Larsen et al., 2011), providing an additional site that likely has fewer microbial sources than lake sediment. Our new continuous paleotemperature quantifications provide a critical baseline for understanding Iceland´s climate history and for assessing the performance of climate models projecting future change.

7.3 Regional Setting

7.3.1 Iceland

Iceland is a small, isolated landmass located within the northern North Atlantic at the intersection of warm, saline Atlantic currents and cool, sea-ice bearing Arctic currents (Fig. 7.1a). The high correlation between instrumental sea surface temperature (Ólafsson, 1999; Hanna et al., 2006) and coastal temperature records demonstrates the strong influence that the marine realm exerts on Iceland's terrestrial climate. Due to its position astride the mid-Atlantic ridge, the island is volcanic in origin with the oldest subaerial sectors dating back to 15 Ma (northwest) and 12.5 Ma (east) and younging to Holocene age along the axial rift (central Iceland) (Moorbath et al., 1968; Harðarson et al., 1997; Sinton et al., 2005). Consequently, the bedrock is primarily comprised of easily erodible subaerial lava successions and subglacial hyaloclastites that, over repetitive Quaternary glaciations (Geirsdóttir et al., 2007), has led to a high density of bedrock-controlled lake basins (e.g., Principato and Johnson, 2009). Furthermore, the erodible nature of the bedrock contributes to the relatively high sedimentation in lakes (Larsen et al., 2012; Geirsdóttir et al., 2013), and presence of sandy deserts in central and southern Iceland (Gísladóttir et al., 2005; Jackson et al., 2005; Arnalds, 2010).

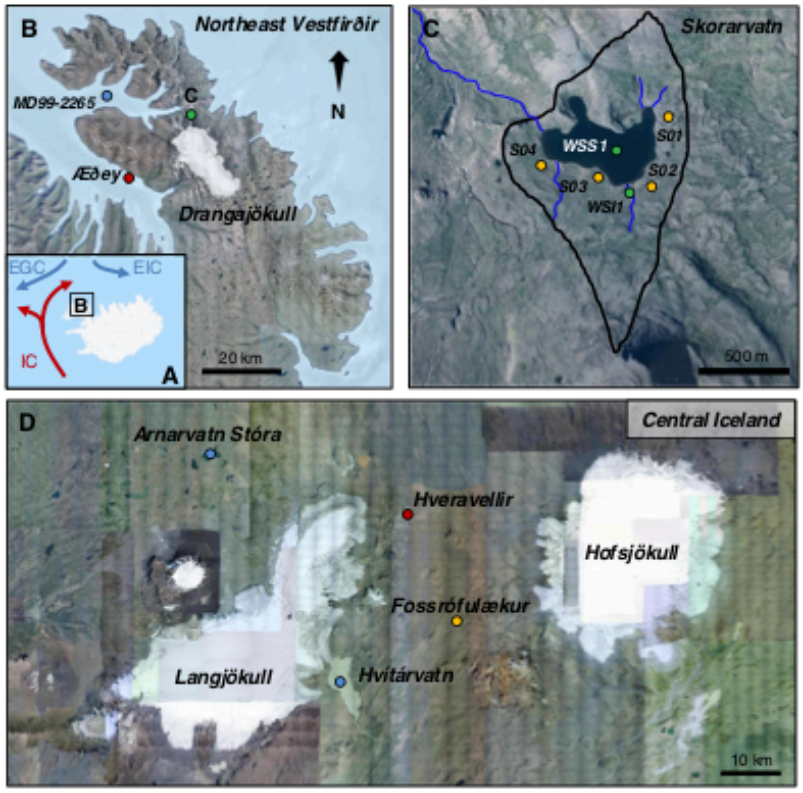

Figure 7.1. *Overview map of study locations. A) Iceland with simplified ocean currents. Red = warm, Atlantic and Blue = cool, Arctic. B) Northeastern Vestfirðir peninsula in northwest Iceland showing the local ice cap, Drangajökull and local weather station, Æðey. C) Skorarvatn and its catchment (black) and river inlets/outlets (blue). Soil sampling sites (S01- S04) marked in yellow and water sampling sites in green. D) Central highlands showing the soil site Fossrófulækur in reference to local ice caps Langjökull and Hofsjökull, and the Hveravellir weather station. 2005 base imagery courtesy of Loftmyndir ehf.*

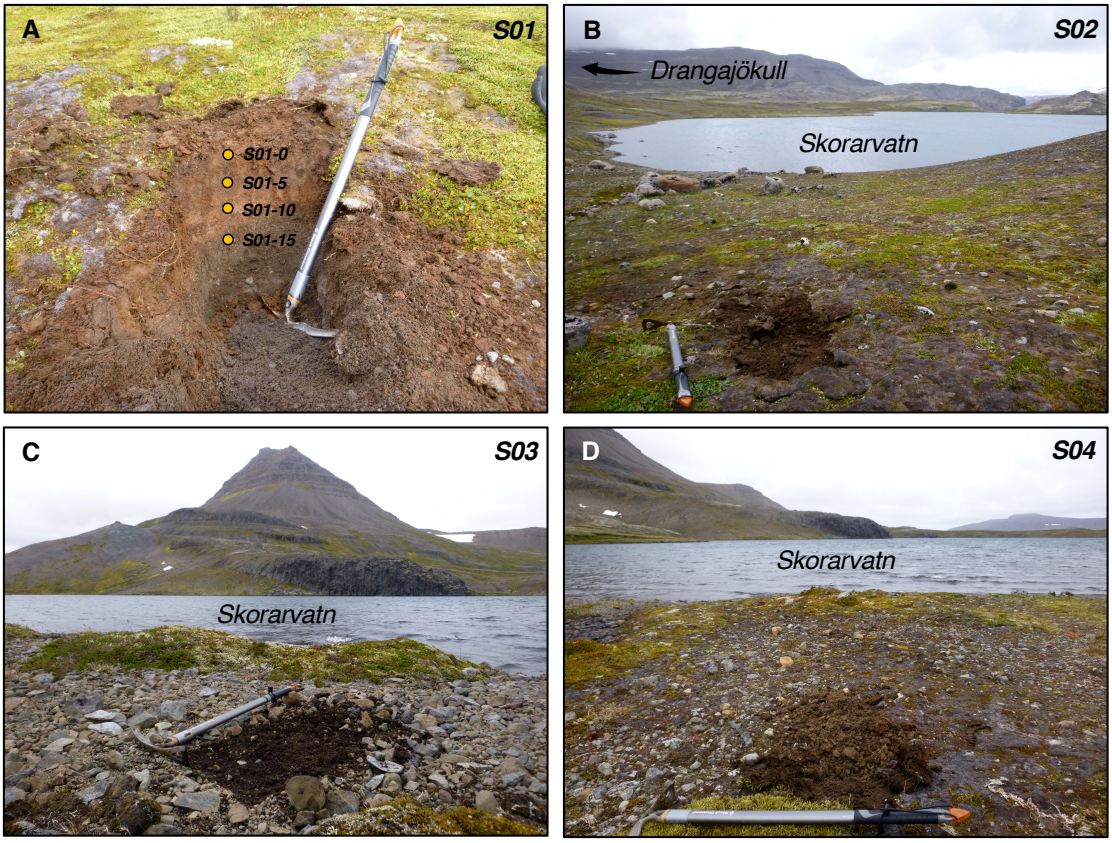

Figure 7.2. *Skorarvatn catchment soil sampling sites. Ice axe for scale (60 cm long). Photos taken August 2016.*

7.3.2 Skorarvatn

Skorarvatn (183 m asl, 66.25627°N, 22.32213°W) is a small, non-glacial lake (192 m^2) ~3 km north of the northern margin of the Drangajökull ice cap in northwest Iceland (Fig. 7.1b and 7.1c). The catchment is small (1.24 km^2) with sparse and discontinuous soil (brown andosol, Arnalds, 2004) accumulation reaching 20 cm maximum depth (Fig. 7.2). Vegetation is dominated by a variety of moss species, which tend to clump on isolated soil patches. The nearest weather station to Skorarvatn is Æðey (Fig. 7.1b, 21 m asl), which records monthly mean temperatures (1954-2011 CE) ranging from -2.0 °C in the winter months to 9.7 °C in July (Fig. 7.3a, gray line, vedur.is). Monthly mean precipitation over the same period also exhibits seasonality, reaching lowest accumulation during summer, and peaking in winter (Fig. 7.3a), likely in the form of snow (e.g., Belart et al., 2017). After applying the standard environmental lapse rate of 6.0 °C per 1000 m in elevation (Fig. 7.3a, black line), we estimate temperatures to be ~1.0 °C lower than Æðey at Skorarvatn. Following winter cooling at Skorarvatn, monthly mean temperatures rise above freezing between April and May, and reach 4 °C between May and June, which likely correspond to the timing of seasonal ice out and overturning of the water column, respectively.

Skorarvatn has a wealth of existing qualitative proxy records from lake sediment cores. These records rely on a combination of radiocarbon-dated plant macrofossils (n=7) and tephrochronology (n=5) for age control (Harning et al., 2016a, 2018a), which result in a relatively high density of chronological points throughout the record. In the early Holocene,

the deposition of the 10 ka Grímsvötn Series tephra indicates that remnants of the Icelandic Ice Sheet retreated to uncover Skorarvatn by ~10.3 ka (Harning et al., 2018a) and fully exited its catchment ~9.3 ka when sediment transitioned from glaciolacustrine to organic gyttja (Harning et al., 2016a). This local deglaciation is supported by similar ages interpreted from cosmogenic radionuclide measurements from boulders located in an adjacent fjord (Brynjólfsson et al., 2015) and numerical modeling studies of Drangajökull (Anderson et al., 2018). Subsequently, high-resolution, centennial-scale climate variability has been inferred from qualitative proxy records such as biogenic silica (BSi) and C/N ratios (Harning et al., 2016a, 2018b). These bulk proxies provide insight into local qualitative spring/summer temperatures and the severity of terrestrial catchment erosion into the lake, respectively (Harning et al., 2016a, 2016b, 2018b). In general, the combination of BSi and C/N suggest progressively cooler spring/summer temperatures through the remainder of the Holocene with punctuated episodes of cooling most clearly reflected in increased soil erosion to the lake (Harning et al., 2018b). These proxies suggest the coolest conditions likely occurred at some point during the last 2 ka, an inference supported by geological (Harning et al., 2016b) and modeling datasets (Anderson et al., 2018) that document the largest dimensions of Drangajökull at this time.

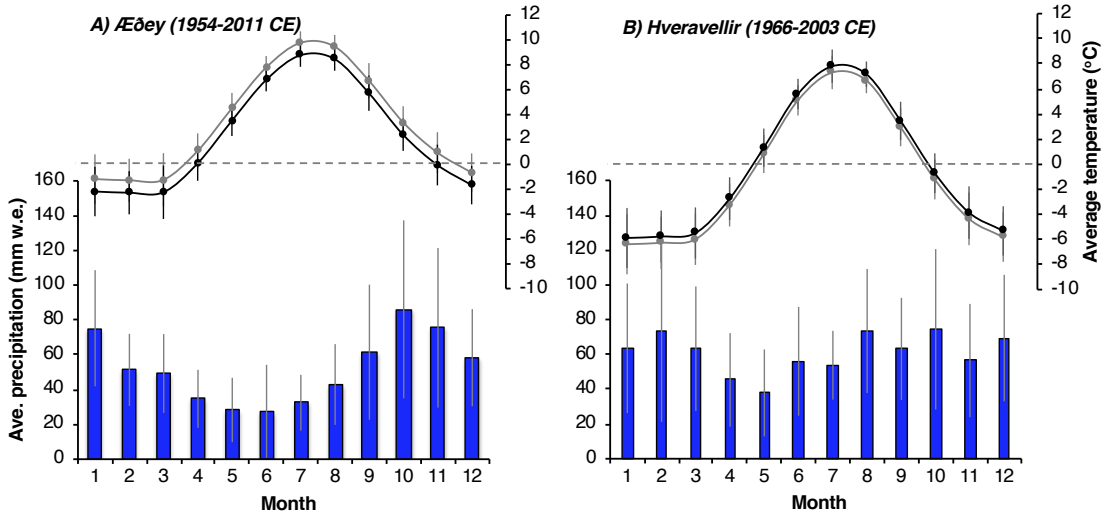

Figure 7.3. *Average monthly temperature and precipitation from two instrumental records proximal to A) Skorarvatn (Æðey) and B) Fossrófulækur (Hveravellir) (vedur.is). Gray temperature reflect those from weather station whereas black temperature reflects lapse-rate adjusted temperature (0.6 °C /100 m) for Skorarvatn (+162 m, -1 °C) and Fossrófulækur (-79 m, +0.5 °C).*

7.3.3 Fossrófulækur

Fossrófulækur is a terrestrial soil archive located in the central highlands of Iceland (562 m asl, 64.713867°N, 19.432083° W) between the Langjökull and Hofsjökull ice caps (Fig. 7.1d). The nearest weather station to Fossrófulækur is Hveravellir (Fig. 7.1d, 641 m asl), where monthly mean temperatures (1966-2003 CE) range from -6.0 °C in the winter months up to 7.3 °C in July (Fig. 7.3b, gray line, vedur.is). Monthly mean precipitation over the same period also exhibits seasonality, reaching lowest accumulation during spring, and reaching highest yet variable values in fall and winter months (Fig. 7.3b). By accounting for the

elevation lapse rate between Fossrófulækur and Hveravellir, we estimate temperatures to be ~0.5 °C higher at Fossrófulækur (Fig. 7.3b, black line).

Stacked andosol (aeolian sand and tephra) sequences have been accumulating in the central and southern Iceland deserts (22,000 km^2) since regional deglaciation in the early Holocene (Arnalds et al., 2001; Arnalds, 2004; Jackson et al., 2005; Gunnarsdóttir, 2018), and have become exposed along the flanks of rofabarð features and incised stream beds (Arnalds, 2000; Dugmore et al., 2009). The dominating dry wind direction for this area is from the north and northeast, resulting in the transport of aeolian material toward the south and southwest (Gísladóttir et al., 2005; Arnalds, 2010). Due to the region's proximity to the active volcanic zone, the soil sequences are separated by thick ash layers, which have diagnostic geochemical fingerprints that permit robust correlation to tephra of known age (e.g., Larsen et al., 1999; Óladóttir et al., 2011). However, considering that andosols lack cohesion, the soils are constantly being modified and reworked by aeolian processes (Arnalds, 2008). Hence, the massive soil packages between tephra horizons likely represent a time-average between the lower and upper tephra constraints.

Similar to Skorarvatn and northwest Iceland, a wealth of local paleoclimate and glacier history records exist from nearby lake sediment records in the central highlands. Deposition of the 10 ka Grímsvötn Series tephra in glacial lake Hvítárvatn and non-glacial lake Arnarvatn Stóra (Fig. 7.1d) indicate that both lakes emerged from underneath the retreating Icelandic Ice Sheet prior to ~10.3 ka (Larsen et al., 2012; Gunnarson, 2017). High-resolution biological and sedimentological proxy records document generally warm conditions and glacier-free catchments from 7.9 to 5.5 ka. Subsequently, mid-late Holocene cooling is reflected by similar, non-linear decrease in aquatic productivity and landscape instability in both lakes, and the nucleation and subsequent expansion of Langjökull in Hvítárvatn's catchment (Larsen et al., 2011, 2012; Gunnarson, 2017). The most severe soil erosion into the lakes culminated during the last millennium, likely as a complex combination of cooling climate, repetitive volcanic tephra deposition and extensive grazing from livestock introduced by Norse settlers (Larsen et al., 2012; Gunnarson, 2017; Geirsdóttir et al., 2013, 2019).

7.4 Methods

7.4.1 Fossrófulækur tephrochronology

Due to the inherent mobilization of soils and terrestrial organic matter in Iceland (Arnalds, 2008), age control for the Fossrófulækur soil sequences is restricted to tephra layers that exhibit minimal evidence of reworking (i.e., preservation of angularity and limited foreign material). Sixteen tephra samples were sieved to isolate glass shards between 125 and 500 μm and examined under a binocular microscope to confirm that tephra were primary layers. Tephra samples were purified by extracting crystalline rock contaminants with a magnetic separator. All samples were analyzed on a JEOL JXA-8230 SuperProbe Electron Probe Microanalyzer at the University of Iceland using a beam voltage of 15 kV, current of 10 nA (basaltic and intermediate glass) or 5 nA (silicic glass), and diameter of 5-10 μm. International glass standards (A99 for basalt, ATHO for silicic) were run before and after tephra analysis to monitor instrument drift and maintain consistency between measurements. Tephra eruption source(s) were identified following methods after Jennings et al. (2014) and Harning et al. (2018b). Major element compositional datasets and discrimination procedure

can be found in the Gunnarsdóttir (2018). Age models for each section were constructed from the tephra-based age control points in the CLAM 2.2 software package using a linear regression with 1000 iterations (Fig. 7.4) (Blaauw, 2010).

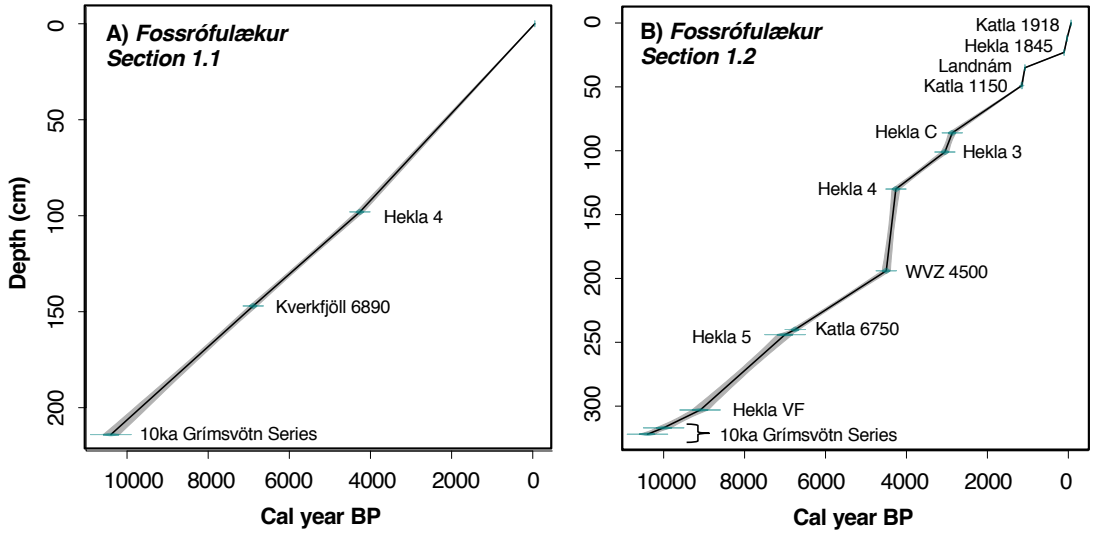

Figure 7.4. *CLAM age model for the Fossrófulækur soil sequences. Gray shaded area reflects 95% confidence interval (Blaauw, 2010). See Gunnarsdóttir (2018) for tephra compositions and discrimination plots.*

7.4.2 Skorarvatn brGDGT source sampling

In an effort to help constrain lake sediment brGDGT sources, soil and water samples were collected in August 2016 from in and around Skorarvatn. Modern catchment surface soils were collected from four locations around Skorarvatn (Fig. 7.1c and 7.2). Sites S01 and S02 had thin moss cover, whereas sites S03 and S04 were closer to the lake shore and were dominantly overlain by gravel and cobble. Considering that Site S01 on Skorarvatn's eastern shoreline was the only site that had soil accumulation over 5 cm, samples were also collected every 5 cm in depth at this site (Fig. 7.2a). The soil characteristics here transition from brown silt and sands at the top to gray coarse sand and pebbles at the bottom. Modern surface water was collected from the major river inlet along Skorarvatn's southeastern shoreline (WSI1) and from the central portion of the lake (WSS1) (Fig. 7.1c), where the sediment core was recovered from in winter 2014 (Harning et al., 2016b). Three liters of water from each location were immediately filtered through two 0.7 μm pore size GF/F filters using a small hand pump. Modern water quality measurements were taken using a Hydrolab sonde at both sites (Table 7.1).

Table 7.1. *Hydrolab water quality measurements.*

Site	Temperature (ºC)	Specific Conductivity (μS/cm)	pH	Dissolved Oxygen (mL)
WSS1	9.96	69	7.48	10.15
WSI1	8.6	63	6.97	N/A

7.4.3 Lipid biomarker analysis

Sediment subsamples (n=31) were taken from a 2.5 m lake sediment core (SKR14-6A-1N) collected in winter 2014 (Harning et al., 2016a, 2016b) and sent to Columbia University's Lamont-Doherty Earth Observatory. Freeze-dried lake sediment subsamples (~1-2 g) were solvent-extracted three times with a Dionex accelerated solvent extractor (ASE 350) using dichloromethane (DCM):methanol (9:1, v/v). Total lipid extracts (TLEs) were separated into three fractions (F1-F3) using silica gel flash chromatography after elution with hexane (4 mL), DCM (4 mL), and methanol (4 mL), respectively. At the University of Colorado Boulder, freeze dried soil samples from Skorarvatn and Fossrófulækur (~1-4 g) were extracted two times on a Dionex ASE 200 using DCM:methanol (9:1, v/v), and kept as TLEs for the brGDGT analysis. Water filtrates were extracted following a modified version of Bligh and Dyer (1959) after Wörmer et al. (2015).

After separation of the lake sediment TLEs, F2 ketone hydrocarbon fractions (containing alkenones) were quantified on a Thermo TRACE Ultra Gas Chromatograph equipped with a Flame Ionization detector (GC-FID) using a VF200MS column (60, 0.25 μm ID, 0.1 μm film thickness). U^{k}_{37} values were calculated according to the following equation (Brassell et al., 1986):

$$U^{K}_{37} = \frac{C_{37:2} - C_{37:4}}{C_{37:2} + C_{37:3} + C_{37:4}}$$

An alkenone standard was injected every 6 samples and 2 samples were measured in duplicate to monitor analytical precision of the U^{k}_{37} values, which was ±0.011 (1σ) over the course of the analysis.

For brGDGTs, aliquots of the F3 (lake sediment) and TLE (soils and water filtrate) were analyzed in the Organic Geochemistry Laboratory at the University of Colorado Boulder. Dry samples were dissolved in hexane:isopropanol (99:1, v/v), sonicated, vortexed, and then filtered using a 0.45 μm PTFE syringe filter. Prior to analysis samples were spiked with 10 ng of the C_{46} GDGT internal standard (Huguet et al., 2006). BrGDGTs were identified and quantified via high performance liquid chromatography – mass spectrometry (HPLC-MS) following modified methods of Hopmans et al. (2016) on a Thermo Scientific Ultimate 3000 HPLC interphased to a Q Exactive Focus Orbitrap-Quadrupole MS (e.g., Harning et al., under review). The HPLC was conditioned for 20 minutes between runs. Samples were analyzed on full scan mode with a mass range of 500-1500 m/z at 70,000 mass resolution. brGDGTs were identified based on their characteristic masses and elution patterns.

7.5 Results and Interpretations

7.5.1 Fossrófulækur age models and sediment accumulation rates

The age models generated for Fossfórulækur indicate relatively linear soil accumulation over the course of the records, and by extension, likely continuous records (Fig. 7.4). However, variability in the sediment accumulation rates (SAR) do exist. In soil section 1.2, shifts towards higher SAR occur between the Hekla VF and Hekla 5 tephra layers (9.1-7.0 ka),

between WVZ4500 and Hekla 4 (4.5-4.3 ka), between Hekla 3 and Hekla C (3-2.9 ka), and again between Katla 1150 and Landnám (~1.1 ka), and finally between Hekla 1845, Katla 1918, and the surface (Fig. 7.4b). We interpret each period of increased SAR to reflect lower temperatures that favor the predominance of colder, northerly winds that redistribute soils in central Iceland (e.g., Gísladóttir et al., 2005; Arnalds, 2010).

7.5.2 brGDGTs

BrGDGTs are cellular membrane lipid components biosynthesized by bacteria, which are globally ubiquitous in geologic archives such as soil and lake sediment (Sinninghe-Damsté et al., 2000; Blaga et al. 2009; Weijers et al., 2006a, 2006b, 2007; Pearson et al., 2011; De Jonge et al., 2014a; Foster et al., 2016; Naafs et al., 2017). Based on strong correlations between 16S rRNA gene copy numbers and brGDGT abundances, Acidobacteria have been suggested to represent an important biological source (Weijers et al., 2009). However, a full understanding of brGDGT producers needed for bacterial culture experiment and rigorous assessment of temperature sensitivities is still lacking. Hence, the brGDGT proxy currently rests on the assumption that the source organism(s) adjust their cell membrane structure in response to changing environmental conditions, such as temperature and pH (Weijers et al., 2007; De Jonge et al., 2014a).

The original global soil dataset showed that the degree of methylation and cyclization in nine brGDGTs, expressed as the methylation index of branched tetraethers (MBT) and the cyclisation ratio of branched tetraethers (CBT), is primarily related to mean annual air temperature (MAAT) and soil pH. Because the MBT is affected by soil pH to a lesser extent than the CBT, the CBT can correct the influence of pH on the MBT, resulting in a paleotemperature proxy for soils (Weijers et al. 2007). Using a larger soil dataset, subsequent work refined this proxy by removing two of the least abundant brGDGTs (IIIb and IIIc), resulting in a new transfer function for MAAT and pH (MBT'/CBT, Peterse et al., 2012). Further improvements in the chromatographic separation of 5-methyl and 6-methyl isomers (De Jonge et al., 2013; Hopmans et al., 2016) allow modified MBT (MBT'_{5Me}) and CBT (CBT_{5Me} and CBT') indices and calibrations, as well as new multiple regression (mr)-based MAAT calibrations for soils that rely on brGDGT subsets (De Jonge et al., 2014a; Naafs et al., 2017).

For lake sediment, the application of brGDGTs originally assumed derivation from soil in-wash, and hence, relied on the application of existing soil calibrations. However, in situ production of brGDGTs is now observed within the water column and surface sediment of lakes, particularly under reducing conditions (Bechtel et al., 2010; Naeher et al., 2014, Colcord et al., 2015, 2017; Weber et al., 2015, 2018), resulting in a variety of global (Pearson et al., 2011) and regional lake brGDGT calibrations (Zink et al., 2010; Sun et al., 2011; Loomis et al., 2012; Foster et al., 2016; Russell et al., 2018). Additionally, research in Arctic (Shanahan et al., 2013) and Antarctic/sub-Antarctic (Foster et al., 2016) lakes indicate that the distribution of brGDGTs is better correlated with mean summer air temperature (MSAT) than MAAT, consistent with peak biological activity in the brief summer months (Pearson et al., 2011; Peterse et al., 2014; Foster et al., 2016) and seasonal mixing and increased sediment flux (Loomis et al., 2014).

7.5.2.1. Skorarvatn catchment soil and water filtrate brGDGTs (modern samples)

BrGDGTs were present above the detection limit in all soil and water filtrate samples (Fig. 7.5). Different brGDGT distributions between soil and water filtrate samples suggest that soils are not the primary source for the lipids in the river inlet or lake surface water (Fig. 7.5), consistent with in situ production of brGDGTs found in suspended particulate matter of Siberian rivers (De Jonge et al., 2014b, 2015). We apply the recently revised global soil calibration to estimate temperature in the surface soils (Naafs et al., 2017) (Fig. 7.6a), given that all samples exhibit a IR_{6Me} ratio below the 0.5 threshold (c.f., Naafs et al., 2017) (Fig. 6B). Although Naafs et al. (2017) calibrate against MAAT, the soils like record a season summer (MSAT) bias due to their development at high latitudes. All calibrated surface soils underestimate MSAT by ~5-9 °C (Fig. 7.6a). Similar to the surface soils, the soil profile at site S01 also underestimates MSAT, although to a lesser degree (Fig. 7.6d). The high variability of soil temperature estimates (6.8 °C) in such a small catchment area suggests that other factors besides temperature modulate the brGDGT distributions. Interestingly, gravel surface soils (S02-S03) feature low GDGT-0/crenarchaeol values (Fig. 7.5c), whereas more organic-rich soils (S01-0 and S01-5) have higher values (Fig. 7.5c and 7.5f). The different distributions of isoprenoid GDGTs suggests that soil type may influence redox conditions, whereby the organic soils are more anoxic (e.g., Naeher et al., 2014), and dictate microbial community diversity across small areas in Iceland. Consequently, we suggest that local Icelandic calibrations are needed to accurately reflect the nuances of local microbial communitie(s) and their relationship with MSAT.

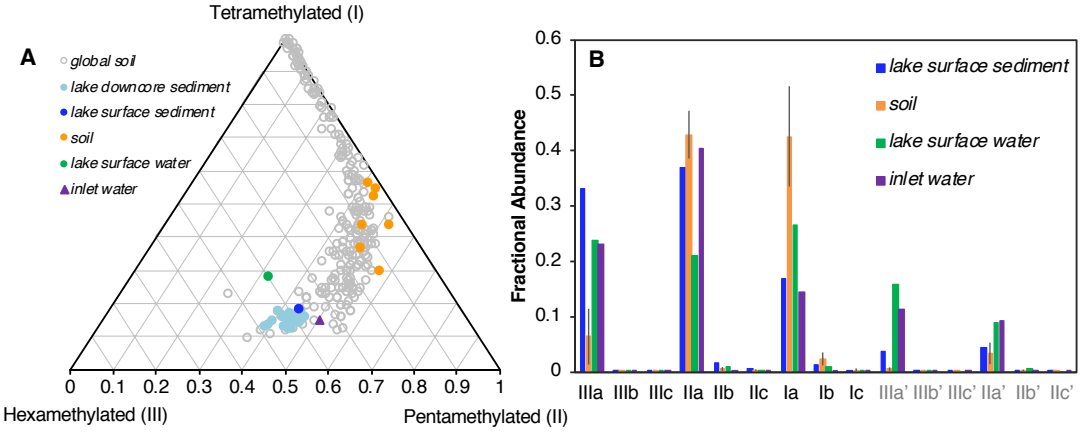

Figure 7.5. *brGDGT fractional abundances for Skorarvatn lake sediment (n=31), soil (n=7), lake surface water (n=1) and inlet water (n=1). A) Total tetra-, penta-, and hexamethylated brGDGTs in comparison to the global soil dataset (n=239, De Jonge et al., 2014a), and B) All individual brGDGTs quantified. 6-methyl isomers denoted with prime symbol in gray.*

7.5.2.2. Skorarvatn lake sediment and Fossrófulækur soil brGDGTs (paleo samples)

BrGDGTs were present above the detection limit in all lake sediment and soil samples (Fig. 7.5). Comparison of brGDGTs between Skorarvatn lake sediment, soil, lake surface water and inlet water samples show statistical differences, whereby the lake sediment samples are dominated by hexa- and pentamethylated brGDGTs, the soils by penta- and tetramethylated

brGDGTs, and both water samples by hexa- and pentamethylated brGDGTs (Fig. 7.5a). However, in contrast to the lake sediment and soils, both the lake and inlet water samples feature higher relative abundances of 6-methyl brGDGT isomers (Fig. 7.5b). The distinct distributions of brGDGTs between the four potential sources suggests that in Skorarvatn, brGDGTs are at least partially produced in situ within the water column and/or sediment, and that a lake calibration that accounts for mixed biological sources is optimal over a soil calibration. For the Fossrófulækur soil sequence, we assume a singular biological producer and explore only soil-specific calibrations for paleotemperature reconstructions. Instead of adopting calibrations that regress temperature against the MBT'$_{5Me}$ index, we rely on mr calibrations as they feature overall lower uncertainties than their MBT'$_{5Me}$ counterparts.

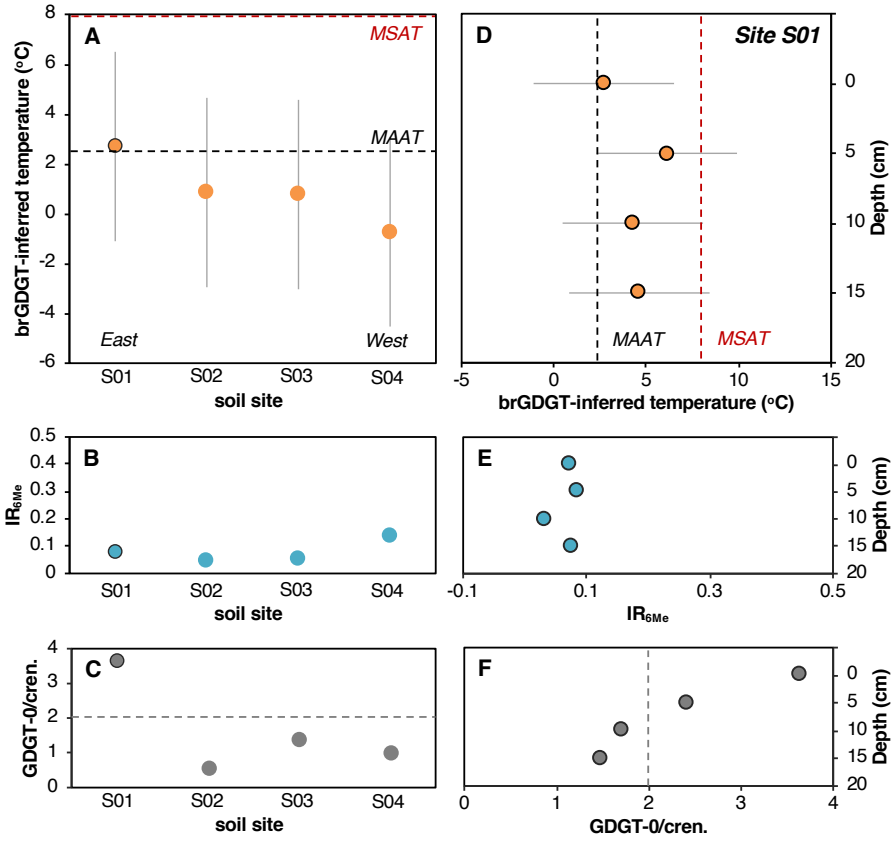

Figure 7.6. *Skorarvatn catchment soil GDGT data. A) Surface soils brGDGT temperature estimates at each of the four sites, after Naafs et al. (2017). B) Surface soil IR$_{6Me}$ ratios, after Naafs et al. (2017). C) Surface soil GDGT-0/crenarchaeol GDGT ratios, after Blaga et al. (2009) and Naeher et al. (2014). D) brGDGT temperature estimates for soil site S01 profile samples at 5-cm increments, after Naafs et al. (2017). E) Soil site S01 profile IR$_{6Me}$ ratios, after Naafs et al. (2017). C) Soil site S01 profile GDGT- 0/crenarchaeol GDGT ratios, after Blaga et al. (2009) and Naeher et al. (2014). MAAT (dashed black line) and MSAT (red dashed line) from the lapse-rate adjusted Æðey weather station (1954-2011 CE) instrumental dataset (Fig. 3) shown for reference.*

The application of various lake-specific calibrations for Skorarvatn produces a wide range of absolute temperature estimates (~16 ºC, Fig. 7.7a) (Pearson et al., 2011; Foster et al., 2016; Russell et al., 2018). Both regional calibrations (Foster et al., 2016; Russell et al., 2018) of the core top sample underestimate the 1954-2011 CE instrumental MSAT, while the global calibration does not (Pearson et al., 2011) (Fig. 7.7a). The IR$_{6Me}$ values indicate a higher proportion of 6-methyl relative to 5-methyl isomers during the early Holocene (Fig. 7.7b), which may impart a cold bias when using calibrations that do not separate the

influence of pH-sensitive 6-methyl isomers, as reflected in the Pearson et al. (2011) and Foster et al. (2016) calibrations (Fig. 7.7a). Furthermore, GDGT-0/crenarchaeol values above 2 throughout most of the record, and particularly during the early Holocene (Fig. 7.5c), suggest periodic times of lake anoxia and methanogenisis (e.g., Blaga et al., 2009; Naeher et al., 2014) that alter microbial communities and production depth in the water column also imparting a cold bias (Weber et al., 2018). Considering there is tentative evidence for in situ production in Skorarvatn (Fig. 7.5), and that Russell et al. (2018) is the only existing lake calibration that removes the influence of 6-methyl isomers, we henceforth adopt their East African lakes calibration for discussion. However, we interpret the record as relative summer temperatures due to potential cold biases and Skorarvatn's location at a high-latitude that likely results in a brGDGT bias towards summer temperatures (e.g., Shanahan et al., 2013; Peterse et al., 2014), rather than the annual brGDGT production that occurs at the equator where the Russell et al. (2018) calibration was developed.

Similar to the lake sediment record, the application of various soil calibrations (Peterse et al., 2012; De Jonge et al., 2014a; Naafs et al., 2017) for the composite Fossrófulækur soil sequence (soil sections 7.1.1 and 7.1.2) also produces a wide range of absolute temperature estimates (~27 ^{o}C, Fig. 7.7d). However, instead of during the early Holocene as seen in Skorarvatn, IR_{6Me} values are variable and peak during the latest Holocene at Fossrófulækur (Fig. 7.7e). The cold-bias introduced by including the 6-methyl isomers is reflected in the various soil calibrations as well, whereby the calibration that does not separate the two isomers (Peterse et al., 2012) produces consistently lower temperatures than the two calibrations (De Jonge et al., 2014a; Naafs et al., 2017) that do separate the isomers. The high GDGT-0/crenarchaeol values between 8.2 and 6.8 ka (Fig. 7.5f) indicate anoxic conditions (e.g., Naeher et al., 2014), which may confound quantitative temperature estimates during this period via shifting microbial communities. Considering that the latter two calibrations produce statistically identical Holocene temperature reconstructions (Fig. 7.7d), we opt for the Naafs et al. (2017) calibration for discussion as it features the lowest uncertainty (3.8 ^{o}C) compared to De Jonge et al. (2014a) (4.6 ^{o}C). Unlike the lake calibrations, however, both revised global soil calibrations produce uppermost soil temperature estimates in close agreement with local 1966-2003 CE instrumental MSAT (6.9 ^{o}C, Fig. 7.7d), strongly implying that the soil brGDGTs in the central highlands also have a summer seasonal bias.

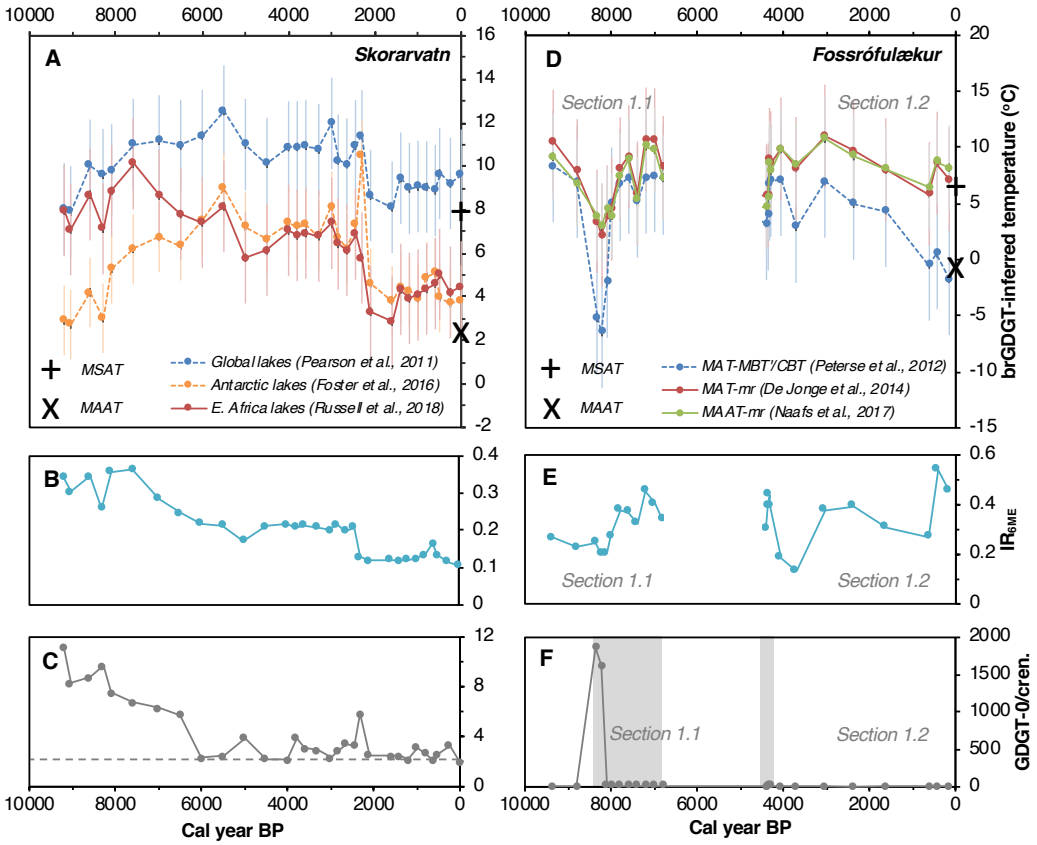

Figure 7.7. *Downcore brGDGT data for Skorarvatn lake sediment and Fossrófulækur soils. A) Lake and soil-specific multiple regression (mr) temperature calibrations for Skorarvatn. Dashed records indicate calibrations that do not separate 5- and 6-methyl isomers. B) IR_{6Me} for Skorarvatn lake sediment after Naafs et al. (2017). C) GDGT- 0/crenarchaeol for Skorarvatn lake sediment. D) Soil-specific temperature calibrations for Fossrófulækur. Dashed record indicate calibration that does not separate 5- and 6- methyl isomers. E) IR_{6Me} for Fossrófulækur soils after Naafs et al. (2017). F) GDGT- 0/crenarchaeol for Fossrófulækur soils, where gray bars denotes samples with ratios above 2. Early Holocene Fossrófulækur soils samples from section 1.1 and middle to late Holocene samples from section 1.2.*

7.5.3 Alkenones

In lacustrine environments, long-chain ketones (i.e., alkenones) are biosynthesized by photosynthetic haptophyte algae that bloom in the spring/summer following lake ice out and water overturning (Toney et al., 2010; D'Andrea et al., 2011). Haptophyte algae primarily adapt their cell membrane structure to increasing temperature by reducing the degree of unsaturation, which can be expressed as the relative abundances of C_{37} di-, tri- and tetra-unsaturated alkenones (U^{K}_{37}, Brassell et al., 1986). However, other limiting factors, such as stress induced from limited nutrients and darkness under ice cover, may result in artificially lower temperature estimates (Prahl et al., 2006). A number of lacustrine U^{K}_{37}-temperature calibrations now exist based on core-top (Zink et al., 2001; Chu et al., 2005), in situ (Toney et al., 2010; D'Andrea et al., 2011; Wang and Liu, 2013), downcore (D'Andrea et al., 2012) and culturing (Sun et al., 2007; Toney et al., 2012; Theroux et al., 2013; Nakamura et al., 2013) studies. 18S rRNA gene sequencing from lakes indicates that alkenone-producing haptophytes occupy at least three distinct phylogenetic groups (D'Andrea et al., 2006; Theroux et al., 2010) that each exhibit distinct U^{K}_{37}-temperature sensitivities (D'Andrea et

al., 2016). Recently, the Group I haptophyte has been identified as the dominant alkenone biosynthesizer in freshwater Arctic lakes, for which new in situ, phylotype-specific temperature calibrations have been developed (D'Andrea et al., 2016; Longo et al., 2016).

Alkenones were present above the detection limit in all lake sediment samples, with a notable abundance of tetra-unsaturated and isomeric tri-unsaturated alkenones (e.g., Longo et al., 2013, 2016). The abundance of tri-unsaturated isomers, expressed through the RIK_{37} index as values at 0.48-0.63, suggests that the alkenones in Skorarvatn were primarily, if not exclusively, produced by Group I haptophytes during the record (Fig. 7.8). Several samples plot just above the threshold for Group I, which may indicate a slight amount of Group II intermixing. Ongoing haptophyte DNA analyses of downcore samples will provide unamibuguous source confirmation (e.g., D'Andrea et al., 2006, 2016; Therous et al., 2010). Following tentative source identification, we adopt an in situ freshwater lake temperature calibration for Group I haptophytes from Arctic Norway that features a small standard error of ±0.7 °C (D'Andrea et al., 2016). Given that we did not measure the y-intercept between U^k_{37} and temperature in Skorarvatn, we only interpret temperature anomalies relative to the sediment core top. Reconstructed temperature estimates are highest during the early Holocene and then decrease nearly linearly through the latest Holocene. The core top temperature estimates reverse this Holocene trend with temperatures estimates ~1 °C higher than the lowest late Holocene estimates (Fig. 7.9c). We interpret the alkenone record cautiously until the complete Skorarvatn dataset becomes available.

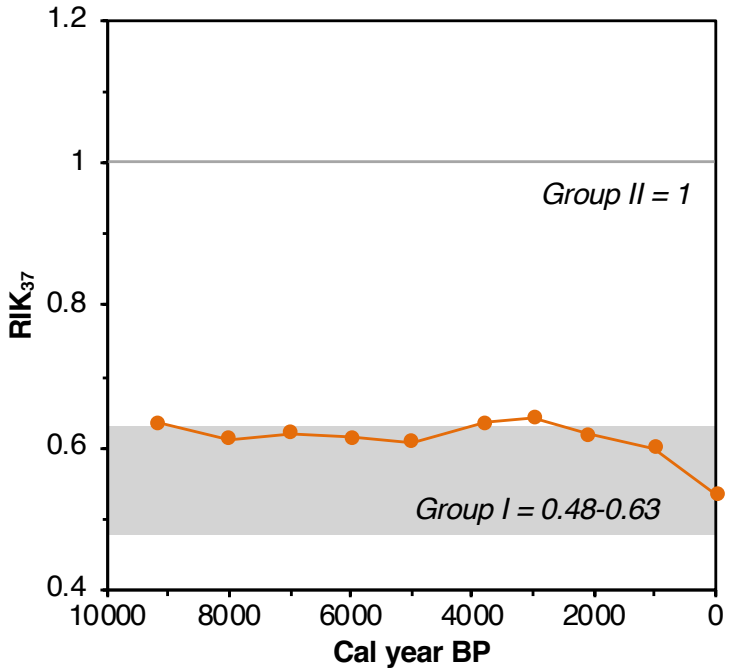

Figure 7.8. *Alkenone haptophyte source based on RIK_{37} index (after Longo et al., 2018). RIK_{37} = ($C_{37:3a}$/$C_{37:3a}$+$C_{37:3b}$), where values of 1 indicate Group II and values of 0.48- 0.63 indicate Group I haptophytes.*

7.6 Discussion

Modern studies from various Arctic locations have demonstrated that brGDGT-based temperatures more closely reflect summer temperature due to several environmental factors including temperature, sunlight, seasonal ice cover and nutrient availability, all of which vary as a function of latitude and hinder productivity during the polar winter (Pearson et al., 2011; Shanahan et al., 2013; Peterse et al., 2014; Foster et al., 2016). In the following discussion, we present the argument that this seasonal bias holds true for paleotemperature histories reconstructed from various archives in Iceland. We base this argument on comparisons to a variety of high-resolution lake sediment proxy records and glacier model simulations from nearby ice caps that have been shown to provide qualitative and quantitative summer temperature estimates, respectively. Ultimately, our new quantitative temperature estimates from both brGDGTs and alkenones have key implications for Iceland's Holocene climate and glacier history.

7.6.1 Lake sediment

Skorarvatn's wealth of qualitative paleoclimate records (Harning et al., 2016a, 2016b, 2018a, 2018b) and quantitative modeling studies from Drangajökull (Anderson et al., 2018) provide a robust framework to evaluate the veracity of our new biomarker records. The high-resolution qualitative temperature records permit the assessment of trends, whereas the quantitative modeling studies provide assessment of magnitude. Considering that there is proxy evidence for increased soil erosion into Skorarvatn beginning shortly after 3 ka (Harning et al., 2018b), as seen elsewhere in Iceland (Larsen et al., 2012; Geirsdóttir et al., 2013), we test the potential influence of older soil contributions to lake sediment brGDGT temperature estimates through the analysis of a separate and exclusive lake temperature record based on alkenones. Importantly, this test builds on the assumption that alkenone unsaturation is not influenced by increased soil erosion (and nutrient flux) into the lake, which based our literature search, has not yet been observed.

First, although alkenones have classically been interpreted as reflecting a spring temperature (e.g., Toney et al., 2010), the strong similarities between the 65°N summer insolation curve (Fig. 7.9a) and alkenones (Fig. 7.9c) suggest that in Skorarvatn the haptophytes are capturing a summer signal. This seasonal nuance is further supported by the presumed timing of ice out and lake overturning during May/June at the onset of summer (Fig. 7.3a), consistent with other high latitude lakes (D'Andrea et al., 2016; Longo et al., 2013, 2018). Second, the isolation of Skorarvatn from Drangajökull since the early Holocene (Harning et al., 2016a) should avoid any potential for differentially influenced alkenone-based water temperatures from glacier meltwater, as seen in glacier-occupied lake catchments elsewhere in the Arctic (van der Bilt et al., 2016). Collectively, we argue that the alkenone-based paleothermometer provides a firm and quantitative summer temperature baseline to assess the more complicated brGDGT record (Fig. 7.9b).

Despite slight differences in timing, both alkenones and brGDGTs record peak temperatures during the early Holocene (Fig. 7.9b-c). The relatively lower brGDGT-based temperature estimates between 9.2 and 7.6 ka may be attributed to altered redox conditions and microbial communities that impart a cold bias (see Section 7.4.2.2). BSi and C/N ratios from Skorarvatn suggest peak diatom productivity (Fig. 7.9d) and the most stable catchment of the Holocene (Fig. 7.9e) during the early Holocene as well (Harning et al., 2018b), consistent with the highest biomarker temperature estimates and peak summer insolation at 65°N (Fig. 7.9a). Modeling experiments for Drangajökull, using adjusted Renland-Agassiz

ice core $\delta^{18}O$ and diatom-based SST records, pin HTM (7.9-5.5 ka, Geirsdóttir et al., 2013) temperatures at 2.5-3 °C above the late 20th century average (Anderson et al., 2018) (Fig. 7.9). Although peak alkenone-inferred warmth precedes the classical timing of the HTM, the magnitude of peak modeling and biomarker temperature estimates are consistent. Furthermore, with the exception of one sample at 7.6 ka that overestimates model-based HTM temperature estimates, our brGDGT record is also consistent with both the model and alkenone temperature estimates.

The middle and late Holocene is characterized by a steady reduction in 65°N summer insolation (Fig. 7.9a) that resulted in local cooling, manifested by lower diatom productivity (Fig. 7.9d) and increasing contributions of terrestrial soil and woody vegetation (Fig. 7.9e) (Harning et al., 2018b). Consistent with an insolation forcing, both alkenones and brGDGTs document first-order trends toward lower relative temperatures (Fig. 7.9b-c). Major step changes in brGDGTs (i.e., cooling) occur at 8.2, 5.5 and 3-2.4 ka, which are two notable periods of local (Harning et al., 2016b; 2018b) and regional cooling (Larsen et al., 2012; Geirsdóttir et al., 2013, 2019) expressed in Icelandic paleoclimate and glacier records. The tight correlation between BSi, a qualitative summer temperature proxy in Iceland (Geirsdóttir et al., 2009a), and brGDGTs (Fig. 7.10a), further supports our conclusion that brGDGTs are primarily tracking summer temperature over the course of this record. The weaker correlation between BSi and alkenones likely reflects the currently coarse resolution of the latter (Fig. 7.10b).

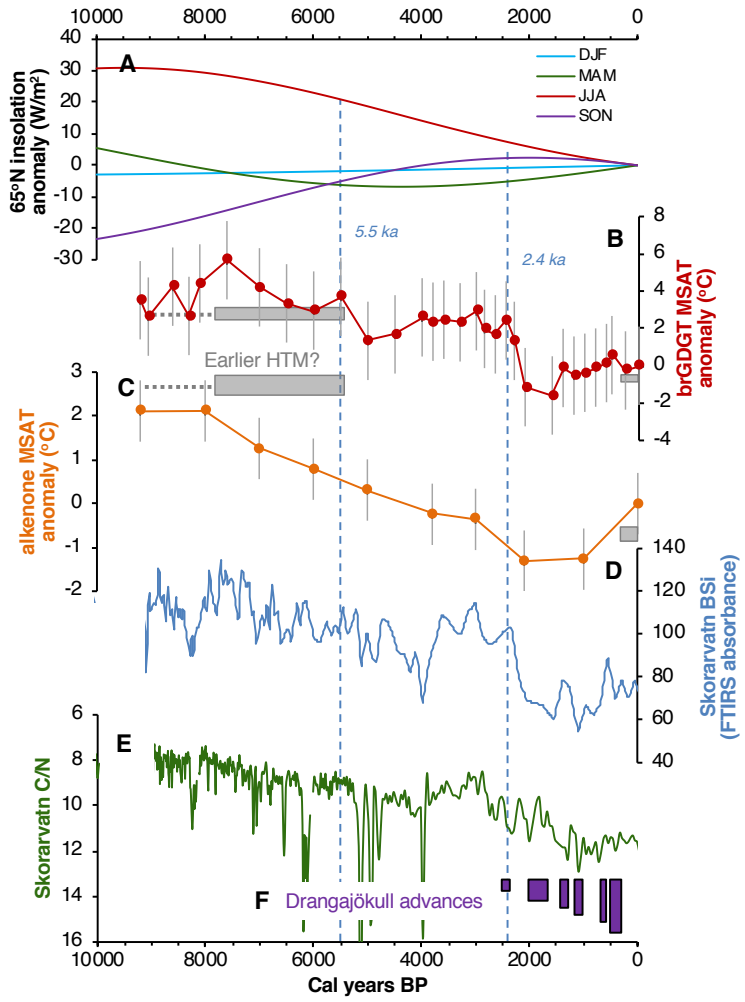

Figure 7.9. *Comparisons of regional climate records to Skorarvatn's paleotemperature records. A) Seasonal insolation curves over the last 10000 years (Laskar et al., 2004), B) brGDGT MSAT anomaly from Skorarvatn (this study), C) alkenone MSAT anomaly from Skorarvatn (this study), D) biogenic silica (BSi) record from Skorarvatn (Harning et al., 2016a), E) inverted C/N record from Skorarvatn (Harning et al., 2018b), F) Drangajökull glacier advances, where taller boxes correspond to relatively larger glacier areas (Harning et al., 2016b, 2018b). Gray boxes denote the timing and range of HTM and LIA temperatures estimated from modeling of Drangajökull (Anderson et al., 2018).*

The LIA in Iceland has classically been interpreted to have occurred between 0.7-0.1 ka, based on a combination of lake sediment proxy records (Larsen et al., 2012; Geirsdóttir et al., 2013, 2019; Harning et al., 2016b; 2018b) and ice cap reconstructions (Flowers et al., 2007, 2008; Larsen et al., 2015; Harning et al., 2016b; Anderson et al., 2018). Modeling simulations of Drangajökull estimate the lowest LIA temperatures at 0.6-0.8 °C below the late 20th century average (Anderson et al., 2018), consistent with both alkenone and brGDGT estimated temperature anomalies (Fig. 7.9b-c). However, both brGDGTs and BSi document even lower temperatures prior to the LIA, between 2.4 and 1.6 ka, with a slight warming trend setting in thereafter (Fig. 7.9b). In contrast to the implied warmth over the last millennium, C/N ratios suggest the most severe erosion of soils into Skorarvatn (Fig. 7.9e) as Drangajökull approached its maximum areal dimensions (Fig. 7.9f) - two independent arguments for colder conditions. The disparity in timing of peak cooling between brGDGTs and BSi (2.4-1.5 ka) compared to those inferred from C/N and glacier records (last 1 ka) may be related to erosion of older soils. Under such a scenario, continued catchment erosion over the last 3 ka (C/N, Fig. 7.9e) transports older soils that were produced in a prior warm period during the Holocene. Consequently, brGDGTs that are transported alongside the soils would then contaminate the latest Holocene lake sediment, producing artificially warm conditions in the downcore record. The additional nutrients delivered from terrigenous soils may then account for increased diatom productivity reflected by BSi. However, more work is needed to test this hypothesis, such as compound-specific radiocarbon-dating of Skorarvatn's late Holocene lake sediment brGDGTs (e.g., Birkholz et al., 2013).

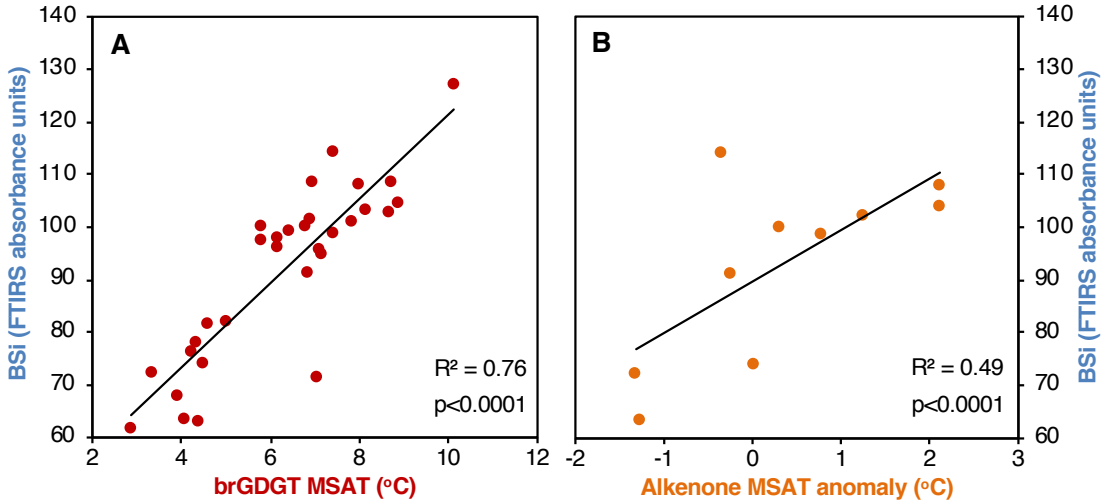

Figure 7.10. *Linear regressions between biogenic silica (BSi) from Skorarvatn (Harning et al., 2016a) and A) brGDGT MSAT and B) alkenone MSAT anomaly.*

7.6.2 Stacked soil sequence

Despite a promising brGDGT temperature record, both the analysis of brGDGTs in various sources (lake sediment, soil, water) from in and around Skorarvatn and the acknowledged late Holocene soil erosion suggest that interpreting brGDGTs from lakes in Iceland is complicated. Hence, generating a paleotemperature record from soil archives in Iceland may circumvent at least the potential issues introduced by additional unconstrained biological sources in lake systems. However, because soils lack the high-resolution of Icelandic lake sediment, we primarily limit our discussion to major trends and aberrations of the composite soil brGDGT record. In this section, we compare the soil record to the high-resolution qualitative records of climate change obtained from Hvítárvatn (Larsen et al., 2011, 2012) and from modeling studies of its local ice cap, Langjökull (Flowers et al., 2007, 2008).

Similar to the Skorarvatn lake record, high relative brGDGT-based temperatures are achieved during the early Holocene alongside peak 65ºN summer insolation (Fig. 7.11a-b). In Hvítárvatn, peak BSi after 7.9 ka indicates high diatom productivity (Fig. 7.11c), likely as the result of the highest Holocene lake temperatures (Larsen et al., 2012). The suppressed temperatures inferred from Hvítárvatn's BSi before 7.9 ka may be confounded by meltwater delivered from the waning Icelandic Ice Sheet, a yet to be stabilized catchment and/or sulfate emissions from local effusive eruptions (Larsen et al., 2012; Geirsdóttir et al., 2013; Harning et al. 2018b). Despite the assumed mixing of Iceland soils via aeolian processes that would prevent centennial-scale structure, the soil sequence captures similar trends to the lake record. Furthermore, the lowest early Holocene brGDGT temperatures are estimated to occur at 8.2 ka (Fig. 7.11b), contemporaneous with the well-known, centennial-scale "8.2 ka Event" induced by a meltwater pulse from the Laurentide Ice Sheet (Alley and Ágústsdóttir, 2005; Rohling and Pälike, 2005) that likely controlled the transient cooling reflected by low BSi and increased soil erosion into Hvítárvatn (Fig. 7.11c-d, Larsen et al., 2012). Although Langjökull is suggested to have disappeared around 10.3 ka (Larsen et al., 2012), modeling studies suggest the transient regrowth of the ice cap in response to the "8.2 ka Event" (Flowers et al., 2008). The same modeling experiments simulated peak HTM (7.9-5.5 ka) temperatures at 3-4 °C above the late 20th century average, consistent with the brGDGT dataset (Fig. 7.11b).

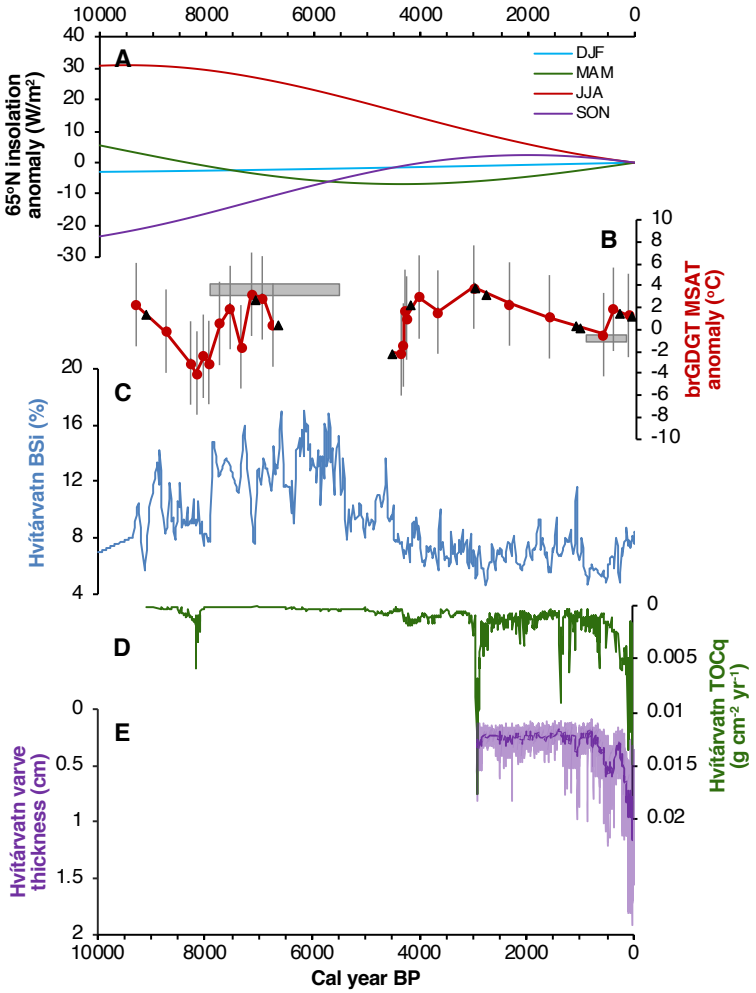

Figure 7.11. *Comparisons of regional climate records to Fossrófulækur's paleotemperature record. A) Seasonal insolation curves over the last 10000 years (Laskar et al., 2004), B) brGDGT MSAT anomaly from Fossrófulækur (this study), where black triangles marked locations of key tephra of known age, C) Hvítárvatn biogenic silica (BSi) (Larsen et al., 2012), D) inverted Hvítárvatn TOC flux (TOCq) (Larsen et al., 2012), and D) inverted Hvítárvatn varve thickness, where bold line reflects 100-year running mean (Larsen et al., 2011). Gray boxes denote the timing and range of HTM and LIA temperatures estimated from modeling of Langjökull (Flowers et al., 2008). Early Holocene Fossrófulækur soils samples from section 1.1 and middle to late Holocene samples from section 1.2.*

Following deposition of the Hekla 4 tephra (4.2 ka) in the soil sequence, we interpret a general cooling trend through to the LIA (Fig. 7.11b), in line with the continued reduction in 65ºN summer insolation (Fig. 7.11a). Local first-order cooling is supported by the observed inception of Langjökull by ~5.5 ka (Larsen et al., 2012), diminishing percent BSi (Fig. 7.11c) and increased flux of terrestrial material to Hvítárvatn (Fig. 7.11d) (Larsen et al., 2012). During the late Holocene Neoglacial period (Geirsdóttir et al., 2019), notable increases in Langjökull's size and the surrounding landscape instability occurred at 4.2 and 3.0 ka (Larsen et al., 2012). In the brGDGT soil record, periods of cooling occur at the same time (Fig. 7.11b), suggesting a shared response to cooling climate. The LIA (0.7-0.1 ka) in central Iceland is most clearly reflected in Hvítarvatn glacier and lake sediment proxy records. More specifically, peak carbon fluxes indicate the Holocene's most severe soil

erosion into Hvítarvatn (Fig. 7.11d), and varve thickness records reflect a rapidly expanding Langjökull (Fig. 7.11e), which achieved its maximum areal dimensions in the 19th Century (Larsen et al., 2011, 2012). Although brGDGT temperatures from the soil sequence match those inferred from model simulations of Langjökull (1.5 °C below the late 20th century average, Flowers et al., 2008), the brGDGTs indicate warming thereafter, inconsistent with the existing proxy datasets of Larsen et al. (2011, 2012). We suggest that similar to Skorarvatn, the warming observed in the soil reflects the erosion of older soil accumulations and contamination with relic and "warmer" brGDGTs, which was most severe during the last two millennia (Larsen et al., 2012). Interestingly, increases in percent BSi in Hvítárvatn are also observed at this time (Fig. 7.11c), suggesting the input of soil-derived nutrients may have also spurred increased diatom productivity, similar to Skorarvatn. However, given that the onset of soil erosion around Hvítárvatn is suggested to have begun as early as 5.5 ka (Larsen et al., 2012), the late Holocene soil record may have contamination of relic brGDGTs throughout this portion of the record.

7.6.3 Implications for paleoclimate

The development of continuous and quantitative terrestrial temperature records for Iceland is a vital step towards fully understanding the island's Holocene climate evolution. This is particularly necessary as existing quantitative records have shown inconsistencies with qualitative datasets. Furthermore, by adding a number of both quantitative and qualitative paleothermometers from different biological sources that each have their own confounding variables (e.g., nutrients), similarities between proxy records can begin to home in on more common variables, such as temperature. Consequently, we can gain a better appreciation for the timing o*f* temperature deviations during the Holocene and the magnitude of those changes.

First, the tight correspondence between alkenone temperatures and summer insolation receipts suggests that temperatures on Iceland were achieved during the early Holocene. Although Icelandic marine records provide evidence for a delayed HTM (Moossen et al., 2015; Kristjánsdóttir et al., 2016), possibly as a result of meltwater from the rapidly retreating Icelandic (Geirsdóttir et al., 2009b) and North American ice sheets (Barber et al., 1999; Alley and Ágústsdóttir, 2005; Jennings et al., 2015), our datasets suggest that, in contrast, terrestrial climate on Iceland was warmest during the earlier Holocene. The freshwater release from North America would have indeed impacted the local oceanography, by stratifying the water column and limiting the mixing of nutrients. Hence, the marine records may simply be recording the freshwater variable and masking the overall warmth at this time. The earlier Holocene warmth that is being observed from Skorarvatn is in line with *other* recent studies. On Baffin Island, a combination of geological glacier proxies and modeling demonstrate smaller than present glacier dimensions during the early Holocene (Pendleton et al, in review) and the presence of early Holocene thermophilic mollusc around Svalbard that currently live 1000 km further south (Mangerud and Svendsen, 2017), all suggest that summer insolation was the primary forcing for early Holocene North Atlantic climate.

Secondly, the cooling observed at 2.4 ka in Skorarvatn was the largest variation in brGDGT-inferred temperature of the record. Although we hesitate to interpret the absolute magnitude until a local calibration is developed, the abrupt nature of the cooling suggests a highly significant event (e.g., Harning et al., 2018b). Also occurring at ~2.4 ka was a tropical eruption that featured the largest negative radiative forcing of the last 2.5 ka (Sigl et al., 2015) as well as a centennial-scale shift to the negative mode of the North Atlantic

Oscillation (NAO, Olsen et al., 2012). In the North Atlantic, a negative NAO mode pushes the prevailing westerlies southward, which then allows colder, northerly winds to dominate (Hurrell et al., 2003). Collectively, the cooling observed in our biomarker records to two triggers (volcanism and NAO-) highlights the sensitivity of the paleothermometers to temperature variability. Furthermore, given that brGDGTs, alkenones, and BSi all independently document cooling, the number of confounding variables can be greatly reduced, leaving temperature as the primary control.

7.7 Conclusions

We present three quantitative lipid biomarker temperature records from Iceland, paired brGDGTs and alkenones in a lake from northwest Iceland (Skorarvatn) and a brGDGT record from a soil sequence in central Iceland. The analysis of soils and water filtrates from Skorarvatn suggests in situ production of brGDGTs within the lake, which in addition to a lack of local calibration, currently hampers brGDGT interpretations. However, the strong similarities between brGDGTs, alkenones and other local records of climate and glacier variability, suggests that brGDGTs will add valuable information to Iceland's emerging Holocene climate history once local calibrations are developed and we can better constrain the biological sources. The brGDGT record from the Holocene soil sequence conforms to local lake paleoclimate and glacier records as well. Despite the assumed mixing of soils via aeolian processes, the soils appear to capture centennial-scale climate variability. Both the lake and soil brGDGTs records suggest that increased soil erosion of the last two millennia may confound these record through the contamination of relic and "warmer" brGDGTs.

7.8 Acknowledgements

This study has been supported by the Icelandic Center for Research (RANNIS #163431051, 130775051, 141573052), the University of Iceland Research Fund, Columbia University's Chevron Student Initiative Fund and the University of Colorado Boulder's Geology Department.

8 Sea Ice Control on Winter Subsurface Temperatures of the North Iceland Shelf over the Last Millennium[7]

8.1 Abstract

To date, Holocene oceanographic reconstructions along the North Iceland Shelf (NIS) have employed a variety of sea-surface temperature (SST) and sea ice proxies. However, the SST proxies tend to have a seasonal bias toward spring/summer SST, and thus, only provide a discrete snapshot of surface conditions during one season. Furthermore, SST proxies can be influenced by additional confounding variables resulting in markedly different Holocene temperature reconstructions between proxy datasets. Here, we expand Iceland's marine paleoclimate toolkit with TEX_{86}^{L}; a paleotemperature proxy based on the distribution of archaeal glycerol dibiphytanyl glycerol tetraether (GDGT) lipids. First, we develop a local Icelandic calibration from 21 surface sediment samples covering a wide environmental gradient across Iceland's insular shelves. Locally calibrated GDGT results demonstrate that: 1) TEX_{86}^{L} reflects winter subsurface (0-200 m) temperatures on the NIS, and 2) our calibration produces more realistic temperature estimates with substantially lower uncertainty (S.E. ±4 °C) over global calibrations. Second, we apply this new calibration to a high-resolution marine sediment core collected from the central NIS (B997-316 GGC, 658 m depth). Age control, constrained by ^{14}C dates, shows a linear sedimentation rate over the last millennium. To test the veracity of the GDGT subsurface temperatures, we analyze quartz and calcite wt% and a series of highly branched isoprenoid alkenes, including the sea ice biomarker IP_{25}, from the same core. The sediment records demonstrate that: 1) subsurface conditions lag the surface by ~100 years and 2) periods of thick sea ice during the Little Ice Age may have warmed the subsurface due to winter insulation.

8.2 Introduction

The steep oceanographic (temperature, salinity, and nutrient) gradients caused by the presence of Arctic and Atlantic Ocean currents surrounding Iceland have made the insular shelves targets for northern North Atlantic climate change studies since the last deglaciation (Knudsen et al., 2004; Ólafsdóttir et al., 2010). Throughout the Holocene, the strength and latitudinal position of these currents has varied on centennial timescales, impacting terrestrial climate (Larsen et al., 2012; Geirsdóttir et al., 2013, 2018; Harning et al., 2018), as well as the status of Icelandic ice caps (Larsen et al., 2011; Brynjólfsson et al., 2015; Harning et al., 2016a, 2016b). As the North Atlantic is the region that exhibits the largest meridional heat flux of the Northern Hemisphere (Wunsch, 1980), and the area of deep-

[7] Harning, D.J., Andrews, J.T., Belt, S.T., Cabedo-Sanz, P., Geirsdóttir, Á., Miller, G.H., Dildar, N., Sepúlveda, J., 2019. Sea ice control on winter subsurface temperatures of the North Iceland Shelf over the last millennium. Paleoceanography and Paleoclimatology, *under review*.

water formation that drives the Atlantic Meridional Overturning Circulation (AMOC), changes in local climate also have widespread global consequence (Denton & Broecker, 2008; Buckley & Marshall, 2016). Thus, gaining a more comprehensive understanding of the past oceanographic conditions in this region of the North Atlantic is not only key to understanding past episodes of climate change, but also critical to contextualize circulation changes under a currently warming climate (Spielhagen et al., 2011; Caesar et al., 2018; Thornalley et al., 2018).

Over recent decades, numerous marine sediment core studies have generated surface and bottom water temperature proxy records based on Mg/Ca and $\delta^{18}O$ of benthic and planktonic foraminifera, calcite wt%, the alkenone unsaturation index ($U_{37}^{K\prime}$) and biotic species assemblages, such as dinoflagellates and diatoms (Andersen et al., 2004; Castañeda et al., 2004; Giraudeau et al., 2004; Smith et al., 2005; Solignac et al., 2006; Bendle and Rosell-Melé, 2007; Justwan et al., 2008; Ran et al., 2008; Ólafsdóttir et al., 2010; Jiang et al., 2015; Moossen et al., 2015; Kristjánsdóttir et al., 2016). Sea surface temperature (SST) proxies derived from phytoplankton result in a bias toward spring/summer SST and are influenced by additional confounding variables (i.e., salinity, nutrients, and depth habitat of biota, e.g., Prahl et al., 2006; Chival et al., 2014), resulting in markedly different Holocene temperature reconstructions around Iceland (Kristjánsdóttir et al., 2016). As an example, the Little Ice Age (LIA, 1250-1850 CE) is believed to be the coldest multi-centennial climate anomaly of the Holocene in Iceland, yet the coldest Holocene conditions inferred from alkenones (Kristjánsdóttir et al., 2016), dinocysts (Solignac et al., 2006) and diatoms (Andersen et al., 2004; Justwan et al., 2008) occur earlier, between 4 and 2 ka. Although the cooling observed in some proxies between 4 and 2 ka may be linked to long-term changes in the AMOC (Hall et al., 2004) and/or North Atlantic Oscillation (Orme et al., 2018), expanding Iceland's quantitative proxy toolkit may help reconcile proxy discrepancies.

In this study, we focus on quantifying the distribution of archaeal glycerol dibiphytanyl glycerol tetraethers (GDGTs) archived in marine sediment from the North Iceland Shelf (NIS). Although never used to reconstruct marine paleoclimate around Iceland, GDGT distributions have been shown to reflect modern winter subsurface (0-200 m) temperatures around Iceland (Rodrigo-Gámiz et al., 2015), the North Sea (Herfort et al., 2006), Skagerrak (Rueda et al., 2009), and Antarctica (Kim et al., 2010, 2012). Assuming temperature is the dominant control on the distribution of GDGTs on the NIS (Schouten et al., 2013 and references therein), but acknowledging that at least part of the variability could also be explained by confounded effects such as ammonia oxidation rates (Hurley et al., 2016), we improve absolute subsurface temperature estimates by developing a local Icelandic calibration based on the analysis of surface sediments. We then apply this local calibration to our late Holocene marine sediment core record. A suite of additional oceanographic surface climate proxies from the same core allow us to explore lead-lag relationships between NIS surface and subsurface over time, and to test the veracity of GDGTs as paleotemperature proxies around Iceland.

8.3 Regional Setting

Today, the NIS represents the boundary where Arctic and Atlantic Ocean currents intercept (Fig. 8.1a-b, Stefánsson, 1962; Hopkins, 1991; Belkin et al., 2009). This front separates the cool, low salinity and sea-ice-bearing East Icelandic Current (EIC, 1 to 4 ^{o}C) to the north from the warmer and more saline Atlantic waters carried by the North Iceland Irminger Current (NIIC, 5 to 8 ^{o}C) on the inner and mid-shelf (Orvik et al., 2001). The density

differences between the two water masses result in modern vertical stratification along the NIS, such that the NIIC overlies the denser and cooler Upper Arctic Intermediate Waters (<0 °C, UAIW) (Fig. 8.1c). Within 70-100 km from Iceland's northern coastline, freshwater run-off and summer heating modify the NIIC surface waters and form "coastal surface waters" (Fig. 8.1c), which then disintegrate during the following winter (Stefánsson, 1962; Ólafsson et al., 2008). The onset of this stratification in early spring triggers the spring bloom of phytoplankton (Zhai et al., 2012).

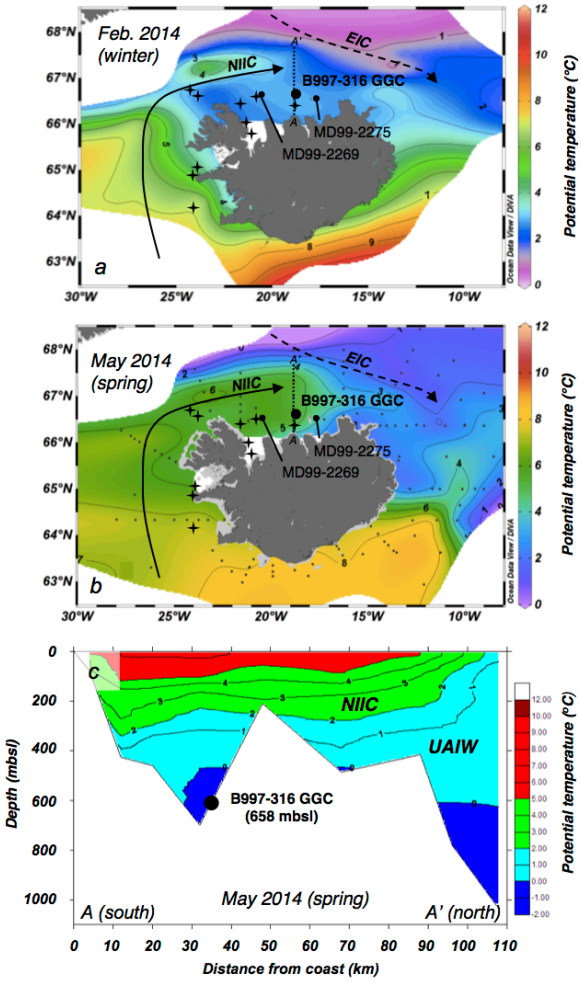

Figure 8.1. *A) Overview maps of modern Icelandic oceanography. A) February 2014 and B) May 2014 50 m depth potential temperature integrated from local CTD stations. Marine sediment cores (black dots) and used B997 surface sediment sample locations (black + and B997-316 GGC core site) are marked. C) May 2014 S-N trending cross section of NIS bathymetry and vertical potential temperature structure along the Siglunes transect (A-A' in panels A and B) and through the B997-316 GGC marine sediment core site. Data from Hafrannsóknastofnun (Marine and Freshwater Research Institute, http://www.hafro.is/Sjora/).*

Atlantic waters provide the primary source of nutrients (i.e., phosphate, nitrate, silica) to the Icelandic shelves. Due to the greater influence of nutrient-deficient polar waters, NIS nutrient concentrations are considerably lower compared to those along the south of Iceland, where Atlantic waters dominate (Stefánsson, 1968; Stefánsson & Ólafsson, 1991). Although the freshwater run-off from Iceland is key for the seasonal stratification and phytoplankton blooms along the NIS, it has negligible direct effects on nitrate and phosphate concentrations throughout the water column (Stefánsson & Ólafsson, 1991). In terms of modern oxygen saturation, the eastern NIS has similar values to those of waters south of

Iceland, which may suggest relatively high rates of productivity for both locations (Stefánsson & Ólafsson, 1991). However, given that the NIS is rather limited in available nutrients, the relatively high oxygen saturation on the NIS may also relate to higher solubility of the colder Arctic waters.

Sea ice is also an integral component of the NIS. Iron oxide data on detrital grains suggest that drift ice is predominately sourced from east and southeast Greenland but also from as far as Canada and Russia, with the latter distal sources dramatically increasing in abundance over the last 1 ka (Andrews et al., 2009a; Darby et al., 2017). The presence of the IP_{25} biomarker - a proxy for seasonal sea ice extension - in core-top sediment along the NIS, and its absence from Iceland's southern and western shelves further supports the dominance of drift ice origins over local sea ice production (Axford et al., 2011; Cabedo-Sanz et al., 2016). When present, sea ice limits the exchange of heat, gases and moisture between the ocean and atmosphere, in addition to insulating the colder polar atmosphere from the relatively warmer ocean during winter (Thorndike et al., 1975; Maykut, 1978, 1982). Due to Iceland's close proximity to the instrumental (post-1870 CE) sea ice edge (Divine & Dick, 2007), past changes in sea ice advection along the EIC have resulted in profound changes in local marine and terrestrial climate (Moros et al., 2006; Massé et al., 2008; Miller et al., 2012; Cabedo-Sanz et al., 2016).

8.4 Methods

8.4.1 Surface and Marine Core Sediments

During July 1997, the cooperative USA/Icelandic *Bjarni Sæmundsson* B997 research cruise visited 30 locations across Iceland's western and northern shelves (Helgadóttir, 1997). At each location, marine surface sediments were collected using a grab sampler. Previous studies have used these surface samples to describe the regional distributions of foraminifera $\delta^{18}O$ (Smith et al., 2005), quartz wt % (Andrews & Eberl, 2007), and the sea ice biomarker IP_{25} (Cabedo-Sanz et al., 2016). We selected a subset (n=11) of these marine surface sediment samples for biomarker analyses to help construct a local Icelandic GDGT calibration (Fig. 8.1). As many of the 30 surface sediment locations were spatially clustered, our selection provides a representative sample from each geographical location the cruise covered, and, thus optimizes our local calibration by spanning the full range of oceanographic conditions present around Iceland today. The B997 cruise also recovered a suite of piston and gravity sediment cores. In this study, we focus on giant gravity core B997-316 GGC (2.47 m long) from the central North Iceland Shelf (66.75°N, 18.79°W, 658 mbsl, Fig. 8.1) (Helgadóttir, 1997). Sediment (~1 cm^3) was subsampled every six cm for minerological and biomarker analyses.

8.4.2 Age Control

Four radiocarbon-based age control points are derived from a combination of mollusks (*T. equalis*) and benthic foraminifera (*N. labradorica* and *G. auriculata arctica*) sampled from the B997-316 GGC core (Table 8.1). Two mollusks (*T. equalis*) were sampled from the near surface sediment of an adjacent short gravity core, B997-316 SGC (Table 1), to confirm that the tops of the sediment cores are modern and that no surface sediments were lost during coring. Samples were prepared for AMS radiocarbon dating at the Institute of Arctic and

Alpine Research (INSTAAR) ^{14}C Preparation Lab and analyzed at the University of California Irvine.

Table 8.1. *Radiocarbon information. ^{14}C ages calibrated in Calib 7.1 (Stuiver et al., 2018) using the MARINE13 calibration curve (Reimer et al., 2013) and a ΔR of 0.*

Sediment core	Sediment depth (cm)	Lab ID	Material	$\delta^{13}C$ (‰)	Conventional ^{14}C date ± σ	ΔR	Calibrated age ± σ
B997-316 SGC	7.5	GRL-1691-S	mollusk (*T. equalis*)	0.62	294 ± 91	0	<400
B997-316 SGC	18	GRL-1690-S	mollusk (*T. equalis*)	-7.2	402 ± 38	0	<400
B997-316 GGC	49.5	CURL-18624	foraminifera (*N. labradorica* and *G. auriculata arctica)*	-14	1030 ± 15	0	600 ± 35
B997-316 GGC	135	CURL-19693	mollusk (*T. equalis*)	-9	1040 ± 15	0	620 ± 25
B997-316 GGC	160	CURL-19511	mollusk (*T. equalis*)	-8.5	1075 ± 15	0	645 ± 15
B997-316 GGC	212.5	CURL-20191	mollusk (*T. equalis*)	-5	1245 ± 15	0	780 ± 35

8.4.3 Minerological Analyses

Quantitative X-ray diffraction (qXRD) analysis was conducted on the <2 mm sediment fraction using the method developed by Eberl (2003) and used extensively on sediment samples on other B997- cores (Andrews & Eberl, 2007; Andrews et al., 2009a; Andrews, 2009). Comparison between qXRD weight percent estimates on known mineral mixtures and replicate analyses indicate that the errors on the weight percent estimates of both are in the range of ±1 %. For B997-316 GGC, we focus on the identification of quartz as a proxy to reconstruct the incursion of drift ice into Icelandic waters (i.e., sea ice and/or icebergs), and calcite as a proxy of ocean productivity (Andrews et al., 2001).

8.4.4 Biomarker Analyses

At the University of Plymouth, freeze-dried subsamples (~1-2 g) from core B997-316 GGC were extracted for biomarkers by ultrasonication using dichloromethane:methanol (2:1, v/v). Samples were initially spiked with an internal standard (9-octylheptadec-8-ene, 9-OHD, 10 μL; 10 μg mL^{-1}) to permit quantification of highly branched isoprenoid (HBI) alkenes. Total lipid extracts (TLEs) were separated into three fractions (F1-F3) using silica column chromatography, after elution with hexane (6 mL), hexane:methylacetate (80:20, v/v, 6 mL), and methanol (4 mL), respectively. The F1 fraction contained aliphatic hydrocarbons including highly branched isoprenoids (HBIs; i.e., IP_{25}, $C_{25:2}$ and $C_{25:3}$), whereas F2 contained lipids with hydroxyl functional groups, including GDGTs. At the University of Colorado Boulder, freeze dried marine surface sediment samples (~3-7 g) were extracted three times on a Dionex accelerated solvent extractor (ASE 200) using dichloromethane:methanol (9:1, v/v) at 100 °C and 2000 psi, and kept as TLEs for the GDGT analysis.

The IP_{25} ($C_{25:1}$), diene II ($C_{25:2}$) and triene Z ($C_{25:3}$) biomarkers were analyzed at the University of Plymouth as described by Belt et al. (2012, 2015). Analysis of the F1 was performed via gas chromatography-mass spectrometry (GC-MS) following the methods and operating conditions of Belt et al. (2012) on an Agilent 7890A GC coupled to a 5975 series mass selective detector fitted with an Agilent HP-5ms column (30 m x 0.25 mm x 0.25 mm). Mass spectrometric analyses were carried out in selected ion monitoring mode. The identification of IP_{25} (Belt et al., 2007), diene II (Belt et al., 2007) and triene Z (Belt et al., 2000) was based on their characteristic GC retention indices (RI_{HP5MS} = 2081, 2082, and 2044 for IP_{25}, diene II, and triene Z, respectively) and mass spectra (Belt, 2018). Quantification of lipids was achieved by comparison of mass spectral responses of selected ions (IP_{25}, *m/z* 350; diene II, *m/z* 348; triene Z, *m/z* 346) with those of the internal standard (9-OHD, *m/z* 350) and normalized according to their respective response factors and sediment masses (Belt et al., 2012). Analytical reproducibility was monitored using a standard sediment with known abundances of biomarkers for every 14-16 sediment samples extracted (analytical error 4%, n = 31).

For GDGTs, we analyzed aliquots of the F2 from B997-316 GGC and aliquots of the TLE from marine surface sediment samples in the Organic Geochemistry Laboratory at the University of Colorado Boulder. Dry samples were dissolved in hexane:isopropanol (99:1, v/v), sonicated, vortexed, and then filtered using a 0.45 μm PTFE syringe filter. Prior to analysis samples were spiked with 10 ng of the C_{46} GDGT internal standard (Huguet et al., 2006). Isoprenoid GDGTs were identified and quantified via high performance liquid chromatography – mass spectrometry (HPLC-MS) following modified methods of Hopmans et al. (2016) on a Thermo Scientific Ultimate 3000 HPLC interphased to a Q Exactive Focus Orbitrap-Quadrupole MS. Rather than starting at 18% hexane:isopropanol (9:1, v/v) (Hopmans et al., 2016), we began our eluent gradient with 30% hexane:isopropanol (9:1, v/v) to shorten retention and overall run times without compromising the chromotographic separation of GDGTs. The HPLC was conditioned for 20 minutes between runs. Samples were analyzed on full scan mode with a mass range of 500-1500 *m/z* at 70,000 mass resolution. GDGTs were identified based on their characteristic masses and elution patterns. We adopt the TEX_{86}^{L} index to reflect relative changes in temperature, which is a modification of the original TEX_{86} index (Schouten et al., 2002) constructed for temperatures <15 °C (Kim et al., 2010, 2012):

$$TEX_{86}^{L} = \log\left(\frac{[GDGT-2]}{[GDGT-1]+[GDGT-2]+[GDGT-3]}\right)$$

8.4.5 Local Icelandic TEX_{86}^{L} Calibration

Since the largest uncertainty in the temperature relationship of GDGTs in global calibrations is at the low end of the temperature spectrum (<5 °C, Kim et al., 2010, 2012), we targeted a network of local marine surface sediments (Fig. 8.1) to develop a local calibration and reduce proxy uncertainties for paleotemperature reconstruction on the NIS. We supplemented our 11 surface sediment samples with 10 previously published surface sediment samples from around Iceland (Table 8.2, Rodrigo-Gámiz et al., 2015) to generate a more comprehensive GDGT calibration that spans a larger geographical area than obtainable using B997 cruise samples alone. Therefore, we were also able to cover a greater variability of ocean masses as well as a larger temperature gradient. To calibrate the TEX_{86}^{L} index, climatological mean temperatures from 1995-2004 were obtained from the World Ocean Atlas (WOA09, Locarnini et al., 2010) at the quarter-degree pixel where each surface sediment site is located. Seasonal (spring, summer, fall, winter) and annual SST estimates, in addition to 0-10 m, 0-

20 m, 0-30 m, 0-40 m, 0-50 m, 0-60 m, 0-70 m, 0-80 m, 0-90 m, 0-100 m, 0-125 m, 0-150 m, 0-175 m, 0-200 m depth temperature integrations, were each regressed against the 21 core top TEX_{86}^{L} index values (Rodgrio-Gámiz et al., 2015; this study) to assess which portion of the water column and which season the GDGT distributions most closely correspond to around Iceland.

Table 8.2. *Surface sediment calibration information. * indicates data from Rodrigo-Gámiz et al. (2015).*

Site ID	Latitude	Longitude	Water depth (mbsl)	TEX_{86}^{L}
B997-313	66.617000°	-23.933000°	213	-0.67
B997-315	66.736000°	-24.332000°	217	-0.69
B997-316	66.746000°	-18.792000°	658	-0.68
B997-319	66.447000°	-18.843000°	422	-0.72
B997-324	66.527000°	-21.152000°	281	-0.65
B997-334	66.410000°	-21.880000°	112	-0.70
B997-329	65.965000°	-21.294000°	112	-0.68
B997-331	66.136000°	-21.591000°	165	-0.71
B997-344	64.836000°	-24.369000°	284	-0.61
B997-346	64.927000°	-24.129000°	320	-0.63
B997-347	63.928000°	-24.482000°	327	-0.64
Station 1*	62.000317°	-15.999183°	2255	-0.49
Station 7*	61.498550°	-24.172250°	1628	-0.51
Station 3*	63.366200°	-16.628267°	240	-0.59
Station 5*	63.583267°	-22.143733°	188	-0.62
Station 6*	63.238233°	-22.561417°	315	-0.61
Station 8*	64.293183°	-24.147083°	260	-0.62
Station 10*	66.677450°	-24.179500°	241	-0.64
Station 11*	66.633317°	-20.833433°	367	-0.63
Station 13*	67.501633°	-15.069217°	884	-0.71
Station 14*	66.303100°	-13.972817°	262	-0.68

8.5 Results and Interpretations

8.5.1 Age Model

An age model for the B997-316 GGC sediment core was generated in the CLAM software using the Marine13 calibration curve (ΔR=0, Reimer et al., 2013) and a smooth spline regression over 1000 iterations (Blaauw, 2010). The calibrated benthic foraminifera date from 49.5 cm depth produced an age reversal in the initial model, and thus, was identified as an outlier and removed from the final age model (Fig. 8.2). The ~400-year difference between the calibrated age of the foraminifera and that estimated from the model may relate to changes in ΔR resulting from variable water masses (Eiríksson et al., 2004; Wanamaker et al., 2012). The two mollusks from the adjacent short gravity core (B997-316 SGC) both returned conventional ^{14}C ages ≤ 400 years, confirming modern sediment at the core tops, and validating the extrapolation of the B997-316 GGC age model to the surface (Fig. 8.2). Even though our age model only uses the three lowermost mollusks, when it is applied to the proxy datasets (Fig. 8.3), the interpreted period of the Little Ice Age (LIA) is consistent with previous age ranges in Iceland (Geirsdóttir et al., 2009; Larsen et al., 2011, 2012). Therefore, we contend that our age estimates are robust and that the sedimentation rate at the B997-316GGC site is relatively linear over the last millennium.

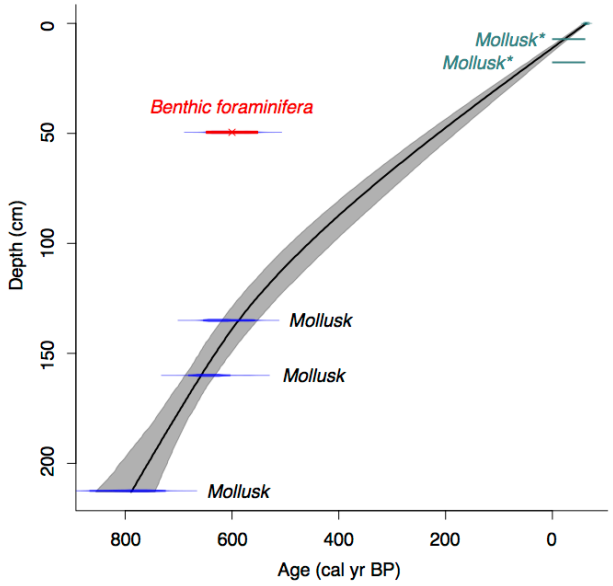

Figure 8.2. *CLAM age model. Gray shaded area denotes the 95% confidence envelope (Blaauw, 2010). Teal and asterisked mollusk ages are from the adjacent short gravity core, B997-316 SGC, and not used as age control points in the model. Radiocarbon information provided in Table 1.*

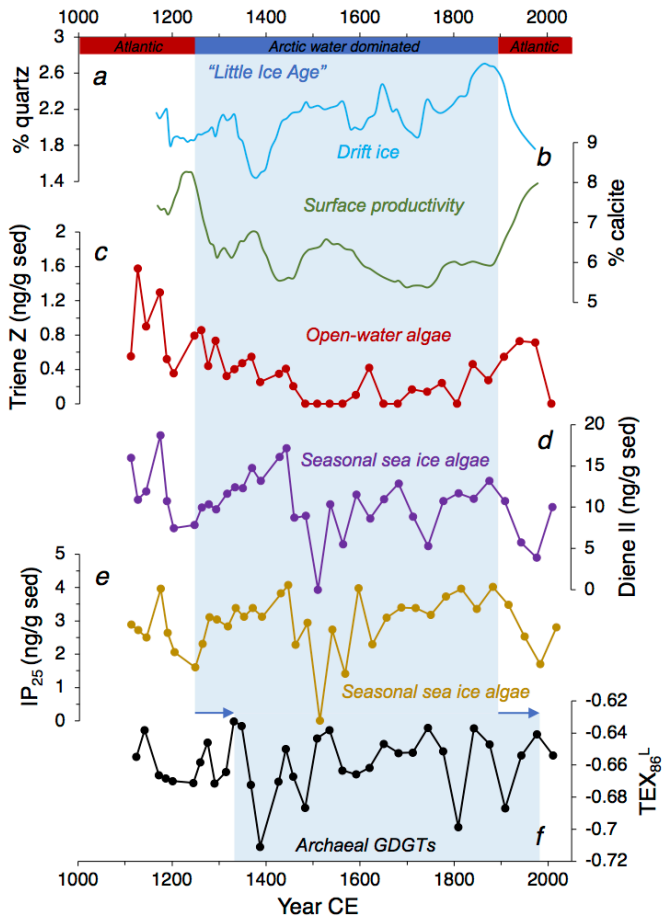

Figure 8.3. *B997-316 GGC marine sediment core climate proxies over the last millennium. A) % quartz, B) % calcite, C) triene Z concentrations, D) diene II concentrations, E) IP_{25} concentrations, and F) TEX_{86}^{L}. Blue boxes highlight colder, LIA-like conditions reflected in the surface climate proxies (A-E) and the subsurface proxy (F).*

8.5.2 Minerological Analyses

In Icelandic waters, the two minerals quartz and calcite are qualitative indicators that reflect the incursion of drift ice (i.e., sea ice and/or icebergs) and marine surface productivity, respectively (Andrews et al., 2001, 2009a). In years when cold low-salinity Arctic water dominates, sea ice (% quartz) increases and surface productivity (% calcite) decreases due to the development of a well stratified water column. The opposite is seen in the proxies during years characterized by warm and saline Atlantic waters, which reduces sea ice presence and mixes the water column resulting in higher productivity. Unsurprisingly, % quartz and calcite generally show an inverse relationship over the last millennium in B997-316 GGC, which can be interpreted as the relative dominance of Arctic versus Atlantic waters at this location (Fig. 8.3a-b).

Percent quartz ranges from 1.4 to 2.7 %, whereas calcite ranges from 5.4 to 8.3 % (Fig. 8.3a-b). Recent analyses using mineral mixtures with known quartz wt % of 3.5 and 1.5 (Andrews et al., 2018) confirm that these small amounts of quartz can be correctly measured. Prior to ~1250 CE, quartz is relatively low, and calcite is the highest of the record, suggesting a dominance of warmer Atlantic waters at this time. Subsequently, quartz begins a gradual yet quasi-episodic rise towards its peak abundance at ~1900 CE. On the other hand, calcite

appears to decline more sharply to lower values after ~1250 CE and remain relatively low through ~1900 CE, when it rises to levels near its pre-1250 CE state. Based on these two minerals, the period between 1250 and 1900 CE was likely characterized by cooler Arctic waters that favored the advection of drift ice, vertical stratification and lower surface productivity on the NIS. Following 1900 CE, the conditions reverted back to a dominance of warmer Atlantic waters that favored restricted sea drift transport and higher surface productivity (Fig. 8.3).

8.5.3 Highly-branched isoprenoid (HBI) alkenes

The analysis of the biomarker IP_{25} (Belt et al., 2007), a monounsaturated C_{25} HBI biosynthesized by Arctic sea ice diatoms (Belt et al., 2008; Brown et al., 2014), has gained recent traction as a novel proxy for spring/summer sea ice conditions around Iceland (Massé et al., 2008; Andrews et al., 2009b; Sicre et al., 2013; Cabedo-Sanz et al., 2016; Xiao et al., 2017). Although the IP_{25} biomarker is well-preserved in Arctic and sub-Arctic marine sediment and routinely applied in paleo sea ice reconstructions as old as 5.3 Ma (Stein et al., 2016), questions remain regarding its vertical transport, degradation processes, and environmental controls (see reviews by Belt & Müller, 2013; Belt, 2018). Notably, the interpretation of its presence (or lack thereof) can be ambiguous. IP_{25} below the limit of detection has often been interpreted as reflecting either a lack of seasonal sea ice cover, or permanent and thick sea ice that inhibits light penetration needed for sea ice diatoms to photosynthesize and grow. However, this is likely an over-simplification of a broader range of scenarios that result in absent IP_{25} (Belt, 2018). In any case, further information may be obtained by the complimentary analysis of certain open-water phytoplankton biomarkers (i.e., brassicasterol or dinosterol, Müller et al., 2011).

Based on a distinctively heavy stable carbon isotopic composition, in addition to similar concentration profiles to IP_{25} across Arctic marine surface sediment, the di-unsaturated HBI diene II also has an Arctic sea ice diatom source (Belt et al., 2008; Cabedo-Sanz et al., 2013; Brown et al., 2014), and is made by some Antarctic sea ice algae as well (Belt et al., 2016). In contrast, a tri-unsaturated HBI (hereafter, triene Z) is biosynthesized by certain open-water diatoms (Belt et al., 2000, 2008, 2015; Rowland et al., 2001), and sources for the Arctic and Antarctic have recently been identified (Belt et al., 2017). Importantly, the presence (or lack thereof) of triene Z, like certain phytoplankton sterols, may potentially help differentiate between open-water or thick sea ice conditions inferred from IP_{25} and diene II in the Arctic (Cabedo-Sanz et al., 2013; Smik et al., 2016; Köseoğlu et al., 2018). However, since sterols may also be derived from other (e.g., terrestrial) sources in addition to sea ice algae (Huang & Meinschein, 1976; Volkman, 1986; Volkman et al., 1998; Belt et al., 2013, 2018), we limit our analysis here to triene Z only.

HBIs were detected in all downcore samples, with the exception of 96.5 cm depth (1509 CE), where no triene Z, diene II or IP_{25} were detected (Fig. 8.3c-e). Concentrations ranged from near detection up to 1.6 ng/g sediment for triene Z, up to 19 ng/g sediment for diene II, and up to 4 ng/g sediment for IP_{25}. Triene Z exhibited the highest concentrations prior to 1200 CE, while its abundance diminished to very low or undetectable between ~1200 and 1800 CE (Fig. 8.3c). Triene Z then rises to higher concentrations up through 2000 CE. The similar relative trends of diene II and IP_{25} concentrations suggest that both HBIs are likely sourced from sea ice algae around Iceland, similar to other Arctic (Brown et al., 2014) and Antarctic locations (Collins et al., 2013). Periods of synchronous reductions of diene II and IP_{25} concentrations occur at ~1170-1290 CE, 1450-1650 CE, and 1880 CE-present.

The similar overall trends between % calcite and triene Z abundance suggest that both proxies indicate temperate water surface productivity (Fig. 8.3b-c). Hence, in years where warmer Atlantic waters dominate, both % calcite and triene Z abundance increase, while the opposite trend should dominate during years characterized by cooler Arctic waters. The detection of both IP_{25} and % quartz throughout the record suggests that sea ice has been a persistent feature at this location of the NIS over the last 1 ka, even during intervals when elevated % calcite and triene Z suggest an increased influence of warmer Atlantic waters. Regarding periods of reduced diene II and IP_{25} concentrations, those between ~1170-1290 CE and 1880 CE-present likely reflect periods of diminished seasonal sea ice as the co-occurrence of increased triene Z concentrations reflect conditions indicative of warmer Atlantic waters. However, the reduction of diene II and IP_{25} from 1450-1650 CE may reflect a period of thick, perennial sea ice as triene Z was mostly undetectable (Fig. 8.3c-e).

8.5.4 Glycerol dibiphytanyl glycerol tetraethers (GDGTs)

Changes in the degree of cyclization (number of cyclopentane moieties) in GDGTs have classically been interpreted to represent a physiological response of marine ammonia oxidizing Thaumarchaeota to changes in *in situ* temperature (e.g., Schouten et al., 2002). Thus, the TEX_{86} paleothermometer index has been empirically linked to annual or winter subsurface (0-200 m depth) water temperature in global data sets (Schouten et al., 2002; Kim et al., 2010, 2012). However, recent studies have shown that several other environmental and geochemical factors can have confounding effects with temperature and thus influence the degree of cyclization, such as growth phase (Elling et al., 2014), ammonia oxidation rates (Hurley et al., 2016), and oxygen concentrations (Qin et al., 2015). Also, unlike the $\delta^{18}O$ of planktic foraminifera, GDGTs do not seem to be influenced by variations in salinity (Wuchter et al., 2004, 2005; Elling et al., 2015). Even though Thaumarchaeota occur throughout the entire water column, a recent study along a latitudinal transect in the western Atlantic Ocean demonstrated that the most likely water depths where GDGTs are produced from and exported to marine sediment is around 80-250 m (Hurley et al., 2018), similar to evidence for archaea abundance maxima at 200 m depths in the Pacific Ocean (Karner et al., 2001). Considering that Thaumarchaeota are chemolithoautotrophs that perform ammonia oxidation (conversion of NH_4^+ to NO_2^-), they are typically more abundant around the primary NO_2^- maximum near the base of the photic zone (Francis et al., 2005; Church et al., 2010; Hurley et al., 2018), and are thus most productive when there is minimized phytoplanktic competition over NH_4^+ (Schouten et al., 2013). In the case of the Arctic region, the latter occurs during the less productive winter months when photosynthesis for sea surface species is inhibited, which may explain the seasonal winter temperature bias of GDGTs in this region (Rodrigo-Gámiz et al., 2015). Finally, GDGTs appear to be relatively resistant to oxic degradation (Schouten et al., 2004), and thus, likely reflect original living conditions once deposited in the sedimentary record.

GDGTs were present above the detection limits in all marine sediment core samples (Supplement Fig S8.1). The calculated TEX_{86}^L index ranged from -0.71 to -0.63 (Fig. 8.3f). The record displays high variability and a rather constant first order trend towards the present, in addition to the occurrence of two intervals of substantial decreases in TEX_{86}^L values during 1350-1530 CE and 1745-1975 CE. Both periods are preceded by periods of relatively higher TEX_{86}^L values during 1110-1350 CE and 1530-1745 CE, respectively.

8.5.5 Local Icelandic TEX_{86}^{L} Calibration

GDGTs were also detected and above detection limits in all B997 marine surface sediments samples (n=11, Supplemental Fig S2). TEX_{86}^{L} values of these samples ranged from -0.72 to -0.61 (Table 8.2). The 10 marine surface sediment samples from Rodrigo-Gámiz et al. (2015) span a greater geographical and environmental range around Iceland, and hence exhibit a greater range of TEX_{86}^{L} values (-0.71 to -0.49, Table 8.2). When we use the combined set of Icelandic marine surface sediment samples (n=21), the regression analysis demonstrates that the integration of winter temperatures from the top 200 m of the water column provides the best regression coefficients (R^2=0.73, p<0.001) compared to the integration of other seasonal temperatures and the mean annual value (Figs. 8.4a-b). Thus, sedimentary values around Iceland most likely represent winter subsurface temperatures that integrate a signal of the uppermost 200 m of the water column.

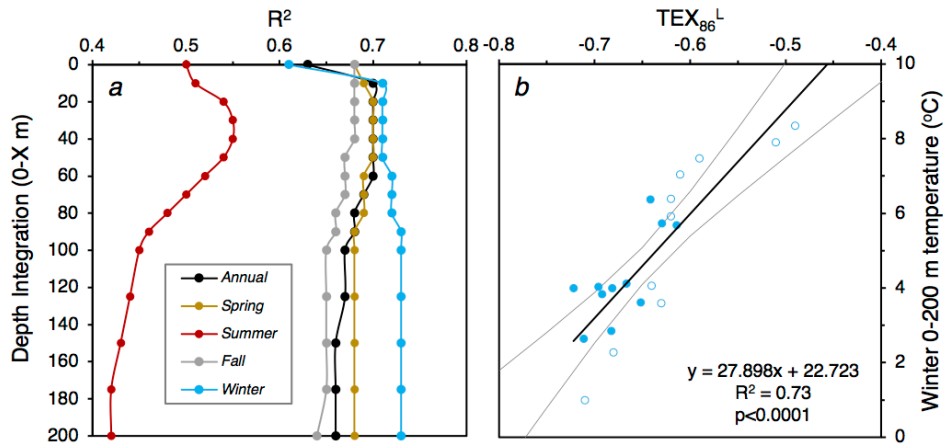

Figure 8.4. *Regression analysis summary of surface sediment GDGT calibration. A) Correlation coefficient (R^2) of the 21 surface sediment TEX_{86}^{L} values against seasonal and annual temperature depth integrations. B) Calibration of Icelandic marine surface sediment TEX_{86}^{L} values against winter 0-200 m temperature, where gray lines denote the 95% confidence envelope. Surface sediment data shown as closed circles (this study) and open circles (Rodrigo-Gámiz et al., 2015).*

8.6 Discussion

8.6.1 Local Icelandic TEX_{86}^{L} vs. Regional Arctic Calibration

When our combined Icelandic data set is supplemented with more marine surface sediment samples from the greater northern North Atlantic region (Kim et al., 2010), the correlation coefficients of our winter subsurface (0-200 m) temperature regression is substantially reduced (R^2 = 0.43 vs. 0.73, Supplemental Fig S8.3). This suggests that a local Icelandic calibration is optimal over hemispheric-scale calibrations, and perhaps, more accurately captures the nuances of local Icelandic oceanography. We hypothesize that the poorer performance of a more regional GDGT calibration for the North Atlantic region may relate to the inclusion of: 1) surface samples from locations that experience different oceanographic environments than Iceland (e.g., Hudson Bay), and/or 2) samples from higher latitude (e.g., Svalbard and the Barents Sea) that are less "responsive" in terms of GDGT

cyclization as they fall under the colder end of the spectrum in the global TEX_{86}^{L} calibration, which is characterized by a higher uncertainty and deviation from linearity (Kim et al., 2010). The standard error in our Icelandic winter temperature calibration for 0-200 m (±0.4 ^{o}C), is also an order of magnitude lower than the error derived from global low temperature calibrations (e.g., 4.0 ^{o}C, Kim et al., 2010; 2.8 ^{o}C, Kim et al., 2012). The reduced uncertainty achieved in our Icelandic calibration highlights the growing need for the continued development and application of regional calibrations in future biomarker-based paleoclimate reconstructions (e.g., Kaiser et al., 2015; Foster et al., 2016; Russell et al., 2018). This is particularly important in areas where the temperature relationship of GDGTs deviates from the overall linear correlation observed in global calibrations (i.e., cold and warm regions).

Despite the reduced uncertainty compared to global calibrations, the regression coefficient for the Icelandic winter subsurface temperature calibration (R^2=0.73) is comparatively lower than the global calibration (R^2=0.86-0.87; Kim et al., 2010, 2012). The unconstrained confounding influence of ammonia-oxidation on the degree of GDGT cyclization (e.g., Hurley et al., 2016), with values both above and below the 1:1 relationship (Fig. 8.4b), may contribute to the scatter of our dataset. Although specific ammonia (NH_4^+) and nitrite (NO_2^-) information for this region is currently unavailable, reduced (enhanced) ammonia oxidation rates in the water column throughout the year would result in increased (decreased) degree of cyclization, thus yielding higher and lower temperatures, respectively (Hurley et al., 2016). If ammonia oxidation rates are driven by changes in ammonia supply and utilization (e.g., reduced nutrient availability in Arctic waters, or competition with phytoplankton), we cannot separate the influence of nutrient variability on the Icelandic TEX_{86}^{L} values with our current dataset. While oxygen availability has also been shown to influence the degree of cyclization in GDGTs (Qin et al., 2015), this factor is unlikely to affect the distribution of GDGTs around Iceland as these waters are relatively well-mixed and ventilated today (Stefánsson & Ólafsson, 1991), and presumably have been since the early Holocene (Kristjánsdóttir et al., 2016). With all controlling factors considered, we suggest that our local TEX_{86}^{L} calibration improves the temperature estimates for Icelandic winter subsurface waters. Given that ammonia availability and oxidation rates may also affect the index, interpretation of TEX_{86}^{L} paleo records can also be more conservatively interpreted as a record of Arctic water variability, whereby lower TEX_{86}^{L} reflects the presence of colder and more nutrient-limited waters.

When different TEX_{86}^{L} calibrations are applied to our down core B997-316 GGC record, our data reveal rapid and abrupt temperature variability on the NIS during the last millennium (Fig. 8.5). However, the existing annual SST (Kim et al., 2010) and annual subsurface TEX_{86}^{L} calibrations developed for polar regions (Kim et al., 2012) produce temperature fluctuations of up to 5 ^{o}C over the course of decades, which is inconsistent with the magnitude of SST changes observed in other NIS proxy records over the entire Holocene (e.g., Andersen et al., 2004; Bendle & Rosell-Melé, 2007; Jiang et al., 2015; Kristjánsdóttir et al., 2016). Thus, global calibrations do not seem to be appropriate for this area. However, by applying our local winter subsurface temperature calibration, the magnitude of estimated subsurface temperatures is not only reduced to ranges more comparable to other records and proxies but, importantly, also captures the modern instrumental winter subsurface temperature (within calibration uncertainty) at the B997-316 GGC site (4 ^{o}C, Fig. 8.5), further reinforcing the application of our local Icelandic TEX_{86}^{L} calibration.

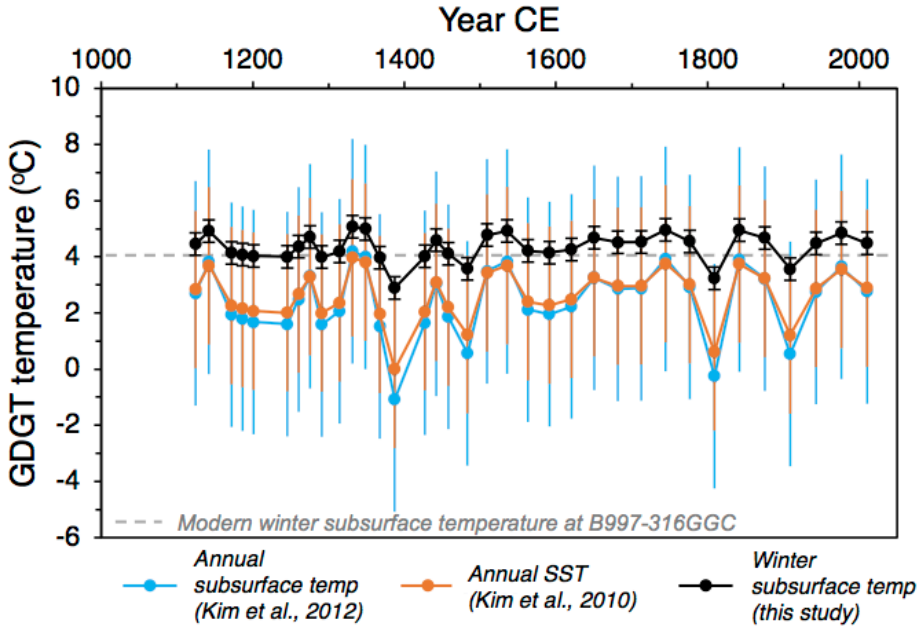

Figure 8.5. *Comparison of the available TEX_{86}^{L} temperature calibrations on the B997-316 GGC sediment record. Icelandic winter subsurface temperature (this study), annual SST (Kim et al., 2010) and annual subsurface temperature (Kim et al., 2012). Modern winter subsurface temperature at the B997-316 GGC site marked with gray dashed line. Note: the standard error of the winter subsurface temperature (±0.4ºC) is shown, but hardly visible given the diameter of the data points.*

8.6.2 NIS Surface and Subsurface Climate Variability Over the Last Millennium

The variability of IP_{25} has been applied routinely to marine sediment around Iceland as a means to track changes in seasonal sea ice (Massé et al., 2008; Andrews et al., 2009b; Sicre et al., 2013; Cabedo-Sanz et al., 2016). Similar to these previous studies, IP_{25} concentrations in B997-316 GGC increase abruptly during the 13th century, and with the exception of the period 1450-1650 CE, remain elevated until the 19th century when concentrations begin to diminish (Fig. 8.6a). By employing statistical analyses on IP_{25} abundances and 11 other marine climate proxy datasets from marine sediment core MD99-2263, Andrews et al. (2009b) showed that a major regime shift in the marine climate off NW Iceland commenced after 1200 CE, possibly linked to a strengthening high-pressure ridge over Greenland in winter/spring that favored stronger north/northwesterly winds and increased drift ice export to Iceland. Our mineral and HBI records consistently reflect major shifts in surface conditions at a similar time and in the same direction (Fig. 8.3a-e), reinforcing the observed regime shift in marine climate, and increase of sea ice in particular, during the 13th century (Ogilvie & Jónsson, 2001; Massé et al., 2008; Andrews et al., 2009b; Sicre et al., 2013; Cabedo-Sanz et al., 2016). The consistency of our surface productivity and sea ice proxy records in reflecting the established understanding of marine climate over the last millennium on the NIS supports the fidelity of the B997-316 GGC marine sediment record, and therefore, the interpretation of the GDGT record.

Regardless of which calibration is employed to obtain quantitative GDGT-based temperature estimates, the relative changes of the temperature record remain the same (Fig. 8.5). From this, two pronounced (albeit oscillatory) centennial-scale cold anomalies at the

B997-316 GGC study site are observed over the last millennium; at 1350-1530 CE and then at 1745-1975 CE. These two cold anomalies, inferred from subsurface winter temperatures statistically below the record mean, broadly align with when surface productivity (% calcite and triene Z) and seasonal sea ice proxies (% quartz, diene II, IP_{25}) suggest greater dominance of colder Arctic waters at this site (~1250-1900 CE, Fig. 8.6). Furthermore, a quantitative, high-resolution alkenone SST record from marine core MD99-2275, located 50 km to the east of B997-316 GGC (Fig. 1a), documents steady cooling throughout this interval (Fig. 8.6b, Sicre et al., 2011). If the total time span of the GDGT-based cold anomalies is considered to reflect the LIA-like conditions of the subsurface during winter (1350-1975 CE), the timing for the onset and termination appear to lag the LIA-like conditions at the surface (1250-1900 CE) by ~100 years (Fig. 8.6). The surface proxies likely reflect the onset and termination of the LIA cold anomaly, manifested on the NIS in abrupt and persistent increases in seasonal sea ice, reduced northward heat transport and cooler SSTs in response to large and sustained stratospheric volcanic sulfate injection (Zhong et al., 2010; Miller et al., 2012; Sicre et al., 2013; Slawinska & Robock, 2018). The phase relationship between surface proxies and GDGTs suggests that it may have taken ~100 years for the oceanographic response to radiative forcing to propagate to the subsurface.

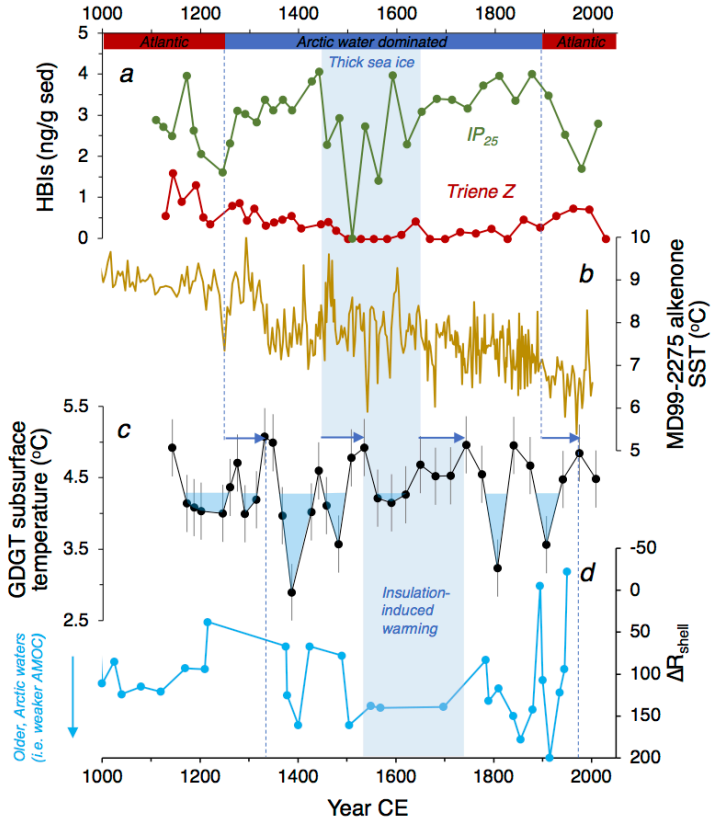

Figure 8.6. *Comparison of select B997-316 GGC marine climate proxies to other well-dated, high-resolution Icelandic NIS marine climate records. A) B997-316 GGC IP_{25} and triene Z concentrations (this study), B) MD99-2275 alkenone-inferred SST (Sicre et al., 2011), C) B997-316 GGC GDGT-inferred subsurface temperatures, with values below the record mean highlighted in blue (this study), and D) schlerochronological ΔR record, where increases in ΔR_{shell} values reflect the incursion of older, Arctic waters and a weaker AMOC (Wanamaker et al., 2012). Vertical blue bars highlight the period of interpreted thick sea ice, and then the delayed associated insulation/warming of the subsurface. Dashed blue lines bound the inferred periods of LIA-like conditions for the surface (A-B) and subsurface (C).*

Given our interpretation of TEX_{86}^{L} as a proxy for the presence of Arctic waters, the period between the two GDGT-inferred cold anomalies (~1530-1745 CE) may suggest a reduction in the dominance of this colder Arctic water mass at this time. However, in contrast, the surface proxies reflect a continued dominance of the Arctic sea-ice-laden waters through this period, as does the alkenone SST record from MD99-2275 (Fig. 8.6). It should also be noted that between 1450-1650 CE, the combination of IP_{25} and triene Z suggest thicker and more permanent sea ice at the B997-316 site (Fig. 8.6a), and that additional IP_{25} records from the NIS also reflect increases in seasonal sea ice at this time (Massé et al., 2008; Andrews et al., 2009b; Cabedo-Sanz et al., 2016). Although Icelandic documentary evidence is too sparse between 1430 and 1530 CE to confirm these proxy records, the greater number of historical records for the early 17th century do describe years of extensive sea ice (Ogilvie & Jónsson, 2001), consistent with the IP_{25} proxy datasets. If our interpretation of sea ice conditions is valid and thick sea ice conditions are indeed maintained through the following winter at the B997-316 site, the insulating effects of sea ice may result in a warming of winter subsurface waters, as reflected by our GDGT record (Fig. 8.6c). Similar to the phasing of the onset and termination of the LIA in surface versus subsurface marine climate proxies, the GDGTs lag the surface proxies by ~100 years during this interval (Fig. 8.6c). Furthermore, the thickening of sea ice at 1450 CE at our site coincides with the local intensification of LIA cooling reflected in the synchronous advance of Icelandic ice caps (Larsen et al., 2011; Harning et al., 2016a), and reduced Icelandic lake productivity (Geirsdóttir et al., 2013, 2018; Harning et al., 2018). Previous data-modeling comparisons have shown that this climate shift was likely forced by another episode of high stratospheric sulfate loading from explosive tropical volcanism (Miller et al., 2012; Slawinska & Robock, 2018).

Following the termination of thick sea ice conditions at 1650 CE, rising IP_{25} and triene Z concentrations suggest the return to seasonal sea ice conditions that favored the productivity of sea ice and open water algae at the B997-316 site (Fig. 8.6a). The change in sea ice conditions is the likely mechanism for the return of cooler subsurface temperatures at 1745 CE, inferred from low GDGT temperature anomalies (Fig. 8.6c). We hypothesize that as the sea ice became less thick during spring, possibly spurred by the trapped subsurface winter heat, the winter ice pack would have also thinned accordingly. Consequently, a thinner winter sea ice pack would have facilitated increased heat flux from the ocean to the colder overlying atmosphere, as reflected by lower GDGT-based subsurface temperatures.

8.6.3 Comparison to AMOC-Sensitive Climate Records

Given that we propose the TEX_{86}^{L} paleothermometer may also serve as an indicator of water mass variability, we also compare our data with an absolutely-dated schlerochronological ΔR record from the vicinity of B997-316 GGC (Fig. 8.6d, Wanamaker et al., 2012). Since age control is independently constrained by shell growth increments, the ^{14}C values derived from the known-age mollusk shells serve as a water mass tracer, whereby increased ΔR_{shell} reflects older Arctic waters and, by extension, a weaker AMOC (Wanamaker et al., 2012). Both TEX_{86}^{L}-based cold anomalies broadly coincide with increases in ΔR_{shell} values (Fig. 8.6c-d), supporting our proxy interpretation of GDGT distributions on the NIS as an indicator of Arctic- versus Atlantic-sourced waters. Importantly, when the TEX_{86}^{L} values increase between 1530 and 1745 CE, ΔR_{shell} values remain consistently higher (Fig. 8.6d), suggesting the continued dominance of sea ice bearing Arctic waters on the NIS, consistent with our interpretations for thick sea ice that may have insulated and warmed the subsurface waters during winter. Thus, we suggest that at times when there is not thick sea ice (i.e.,

seasonal or no sea ice) present on the NIS, TEX_{86}^{L} may tentatively serve as a water mass tracer. However, further caution must be exercised if thick sea ice conditions prevail, such that TEX_{86}^{L} may counterintuitively reflect warmer, yet still Arctic, waters. Given that the schlerochronological **Δ**R record is limited to the last 1350 years, the extension of TEX_{86}^{L} through Holocene and deglacial marine sediment records may provide further insight into centennial to millennial changes of AMOC variability along the NIS.

8.7 Conclusion

Consistent with the community's growing comprehension of GDGT-based temperature records at high latitudes, we show that archaeal isoprenoid GDGT distributions (TEX_{86}^{L}) around Iceland predominately reflect winter subsurface (0-200 m) temperatures. Furthermore, by developing a local calibration based on a network of surface sediment samples, reconstructed NIS subsurface temperature estimates and uncertainty are improved upon those obtained from regional and global calibrations. The TEX_{86}^{L} subsurface temperature record from the NIS captures the cooling likely associated with the LIA (1250-1900 CE), as seen in additional surface proxies (sea ice and marine productivity) from the same sediment core. However, the LIA onset, intensification, and termination of the subsurface lags those changes of the surface, suggesting that it may have taken ~100 years for changes at the surface to propagate to the subsurface during the late Holocene. We propose that the development of thick sea ice conditions during the intensification of the LIA around 1450 CE insulated the subsurface in winter, resulting in apparently warmer seasonal subsurface waters. Comparison of the TEX_{86}^{L} record against a securely-dated schlerochronological record of NIS water mass variability support its use as both a tracer of Arctic/Atlantic water masses as well as winter subsurface temperature. Considering that the NIS shell record only extends back 1350 years, the development of a Holocene length TEX_{86}^{L} record from the NIS may provide new insight into changes of AMOC variability in this region of the northern North Atlantic.

8.8 Acknowledgements

We kindly thank the caption, crew, and scientific staffs of the 1997 *Bjarni Sæmundsson* (B997) cruise for their considerable assistance in obtaining marine sediment cores and surface samples. The B997 cruise was principally supported by the Marine Research Institute of Iceland, with the University of Colorado's participation supported by NSF grant #ATM-9531397. Biomarker analyses were supported by internal CU funding awarded to JS and a grant from the CU Retired Faculty Association to JTA. DJH has been supported by an Icelandic Center for Research (RANNÍS) Doctoral Student Grant #163431051. PCS and STB acknowledge support from the RANNÍS Grant of Excellence #141573052 awarded to ÁG and GHM.

8.9 Supplemental Information

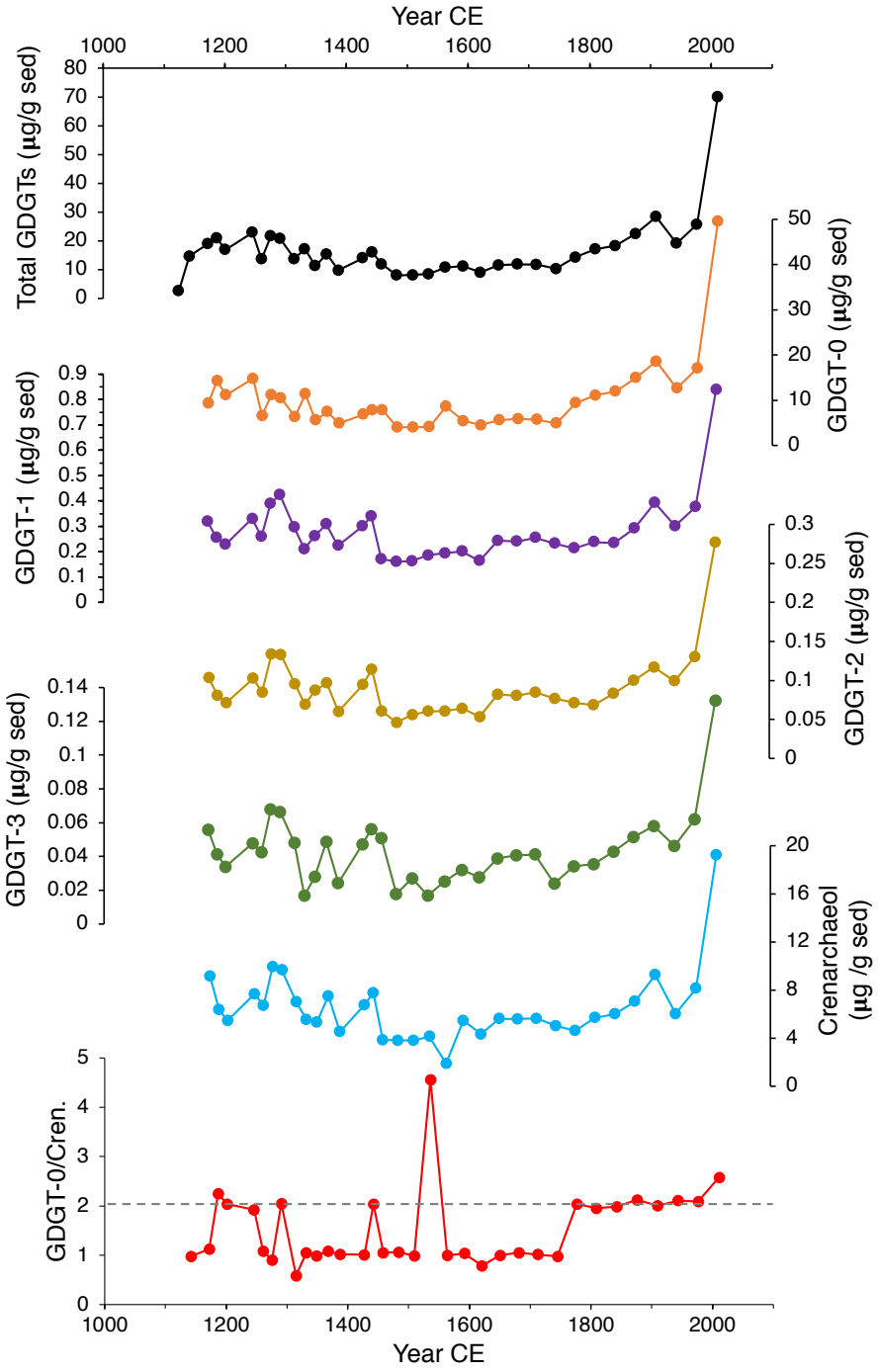

Figure S8.1: *GDGT concentrations in B997-316 GGC marine sediment samples. GDGT-0/crenarchaeol ratios >2 suggest the presence of methanogenic Eukaryotes, which produce the same GDTGs as marine Thaumarchaeota, but with different distributions (Blaga et al., 2009). Thus, when methanogenic Eukaryotes are present, take caution with the* TEX_{86}^{L} *ratios.*

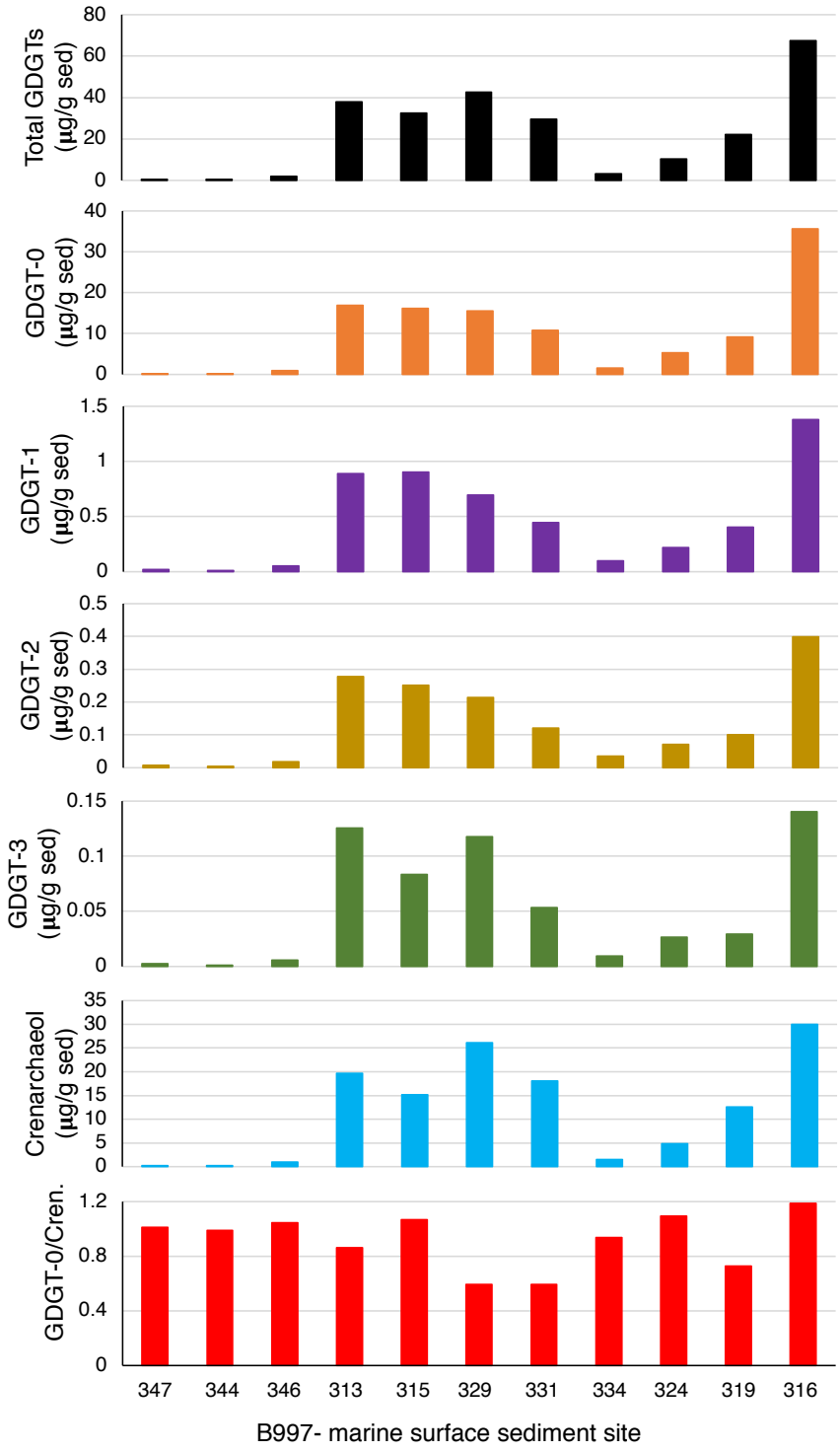

Figure S8.2: GDGT concentrations in B997 marine surface sediment samples. Sample labels are abbreviated (i.e., 347 = B997-347) and ordered geographically from the southwestern-most (347) to the northeastern-most (316).

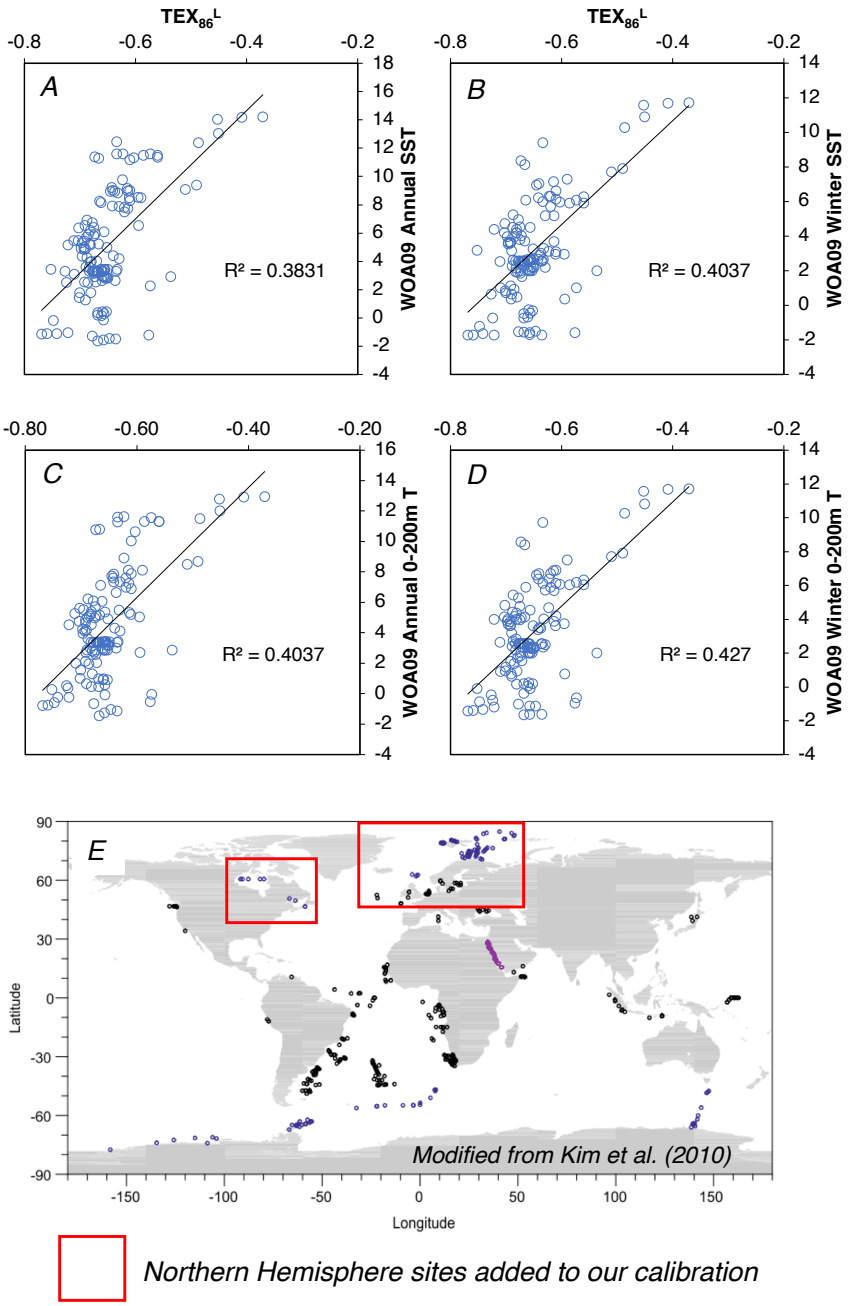

Figure S8.3: *Using samples selected from the global calibration of Kim et al. (2010), we tested whether we could improve the local calibration by extending the range of samples, and thus, the environmental gradient. We applied the same calibration techniques as described for our local Icelandic calibration in the main text (Section 3.5). A) Annual SST, B) Winter SST, C) Annual 0-200 m T, and D) Winter 0-200 m T. The deviation from linearity and higher uncertainty of temperature estimates is clearly shown by the samples from the colder regions (<5 °C) and concomitant lower TEX_{86}^{L} ratios. Panel E highlights the northern hemisphere samples included from the global calibration of Kim et al. (2010).*

9 Conclusions and Future Work

9.1 Conclusions

This dissertation capitalized on and merged a range of analytical techniques in an effort to refine our understanding of Icelandic climate variability, glacier extent, and tephrochronology during the Holocene epoch. By extension, it has helped confirm emerging theories of Icelandic Holocene climate, elucidate a more glacier nuanced history and opened the door to a number of new questions. All of these achievements are critical for evaluating modeling simulations aiming to forecast the poorly constrained climate of the coming century. Here, I briefly review the major research questions and the how they have, at least partially, been answered under this dissertation.

1) What was the Holocene history of Drangajökull, in northwest Iceland? Did it survive early Holocene warmth, or did it behave similarly to other Icelandic ice caps that melted to smaller than present dimensions before 9 ka? If the latter, when did it nucleate during the middle to late Holocene Neoglaciation, and how does this compare to other Icelandic ice cap reconstructions? Chapters 1 and 2 used two glaciers proxies (threshold lake sediment records and emerging dead vegetation from receding ice margins) to provide firm constraints on the Holocene activity of Drangajökull. Ultimately, our novel datasets suggest that similar to other Icelandic ice caps (e.g., Langjökull and Vatnajökull), Drangajökull likely disappeared shortly after 9.2 ka during early Holocene warmth and renucleated during the late Holocene, by ~2.3 ka. This is an important conclusion as a contemporary study using similar threshold lake methods suggested the Holocene persistence of Drangajökull (Schomacker et al., 2016), which had vital implications for numerical modeling studies (Anderson et al., 2018). The conclusions drawn from our Drangajökull records, particularly its late appearance, also paved the way refining our understanding of late Holocene Neoglaciation of Icelandic ice caps (Geirsdóttir et al., 2019), which illustrated their time-transgressive inception as a result of subglacial topographic thresholds.

2) What was the Holocene climate history of the Vestfirðir peninsula, northwest Iceland? Was it non-linear as seen elsewhere in Iceland? And if so, can those punctuations be linked to known climate drivers and feedback mechanisms? Chapter 3 helped confirm the non-linear response of Iceland's climate to the monotonic reduction in NH summer insolation, via the high-resolution analyses of lake sediment records and the generation of qualitative climate proxy records. Furthermore, the climate punctuations replicated in both of the well-dated lake records were linked to a number of internal and external climate drivers (e.g., early Holocene freshwater pulses, low total solar irradiance, explosive and effusive volcanism, and the NAO) and amplifiers (e.g., ocean/sea-ice feedbacks). The two climate proxy records from Skorarvatn and Tröllkonuvatn also contributed to a 7-lake record synthesis from a wide variety of catchment styles that all showed similar climate punctuations throughout the Holocene in Iceland (Geirsdóttir et al., 2019).

3) How has local and hemispheric volcanism impacted Icelandic paleoclimate? Chapter 2 and 3 explored the climate development of Northwest Iceland during the Holocene and potential triggers for abrupt cooling events against the backdrop of smoothly decreasing NH summer insolation. Of the potential triggers, local and global volcanism stood out as frequent mechanisms. During the early and middle Holocene, extended periods of Icelandic effusive volcanism emitted substantial amounts of sulfate that likely contributed to cooling

between 8.7 and 7.9 ka, and then at ~6.6 ka. During the late Holocene, sulfate emissions from explosive tropical volcanos, particularly at ~2.4 and during the LIA likely contributed to the two most pronounced episodes of cooling on Northwest Iceland identified in this dissertation. Considering that NH summer insolation exhibited minimal percent changes during the latest Holocene, amplifier(s), such as ocean/sea-ice feedbacks are required in order result in such a large climatic response.

4) Can we quantify the Holocene temperature history of Iceland with emerging organic geochemical toolsets to gain an appreciation for the glacier and climate sensitivity in Iceland during the Holocene? Chapters 6 and 7 applied lipid biomarker thermometers to sedimentary archives in an effort to quantify Holocene temperature. On Iceland, alkenones appear to be the most straightforward and promising method to capture quantitative temperature in lake sediments records as a result of a single biological source with known temperature sensitivity. brGDGTs were tested in lake sediment, soils and water filtrates but are complicated by a variety of unconstrained biological sources, late Holocene soil erosion, and a lack of local calibrations. In the marine realm, isoprenoid GDGTs have added new insight into the late Holocene marine paleoclimate of Iceland by capturing winter subsurface temperature variability and the influence from variable seasonal sea ice conditions. Additionally, the reduced uncertainty achieved in our local Icelandic calibration for marine GDGTS demonstrates the improvement temperature estimates that will likely be obtained from lakes and soil brGDGTs once they have their own respective Icelandic calibrations. Ultimately, the local calibrations for brGDGTs, as well as alkenones, are needed to address the climate and glacier sensitivity of Iceland during the Holocene.

9.2 Future Work

Over the course of the last 6 years, my immersion in this dissertation has brought about a multitude of questions and potential directions for further research. Some of these were inspired directly from the questions and methods I relied on, as well as from the numerous conversations that I had with our lab group and the network of researchers at large. Similarly, more tangential questions that would rely on the application of new techniques to new questions emerged through equally important discussions. Consequently, I do not take these to be entirely my own but acknowledge inspiration taken from the vast amount of existing knowledge developed over decades of research and all the individuals I have been fortunate enough to continually explore these questions with. I lay these shared suggestions for future work out below, separated by their immediate relevance, i.e., directly related to the targeted dissertation research questions, or tangentially related suggestions that would contribute to the greater knowledge of Icelandic paleoclimate.

9.2.1 Directly Relevant

One of the initial revelations from this dissertation was that although the early Holocene deglaciation of Icelandic ice caps appears to be coeval, the mid-late Holocene nucleation was spatio-temporally asynchronous (Larsen et al., 2011, 2012; Striberger et al., 2012; Geirsdóttir et al., 2013, 2019; Harning et al., 2016a, b; Anderson et al., 2018). However, these current deductions are only based on three ice caps; Drangajökull (northwest), Langjökull (central) and Vatnajökull (southeast), which does not provide a comprehensive picture. Furthermore, evidence from tephra-based datasets indicate that Katla has produced phreatomagmatic eruptions continuously throughout the Holocene, which may suggest that

Mýrdalsjökull persisted through peak early Holocene warmth (Óladóttir et al., 2007). Despite the fact that phreatomagmatic eruptions from Katla could also be generated from a lake occupying its crater instead of an ice cap, open questions clearly remain regarding the proposed „ice free“ early Holcoene landscape in Iceland (e.g., Geirsdóttir et al., 2019). Hence, reconstructing the pattern of early Holocene demise and subsequent Neoglaciation of Iceland from additional icecaps and glaciers (e.g., Hofsjökull, Mýrdalsjökull, Tröllaskagi) through threshold lake sediment, and potentially emerging dead vegetation at high-elevation ice divides, would be illuminating (Fig. 9.1). Such datasets would also complement and cross-validate ongoing glacier modeling work targeting the same question.

Figure 9.1: *Location of major ice caps and glaciers (Tröllaskagi) in Iceland.*

Second, the final chapter of this dissertation demonstrated the considerable reduction in temperature estimate uncertainty achieved from local GDGT calibrations in the marine realm around Iceland. The terrestrial brGDGT records generated in this dissertation, however, relied on global temperature calibrations based on old analytical techniques that feature high uncertainty or regional calibrations from far-flung locations (i.e., equatorial East Africa) where brGDGTs are likely sensitive to different variables and seasons than Iceland. Hence, developing local temperature calibrations for brGDGTs (both lake sediment and soil) based on improved chromatographic separation (e.g., Hopmans et al., 2016) would greatly improve our existing temperature records by providing absolute temperature estimates, and importantly, reduced temperature uncertainties. These temperature calibrations could be generated from either core-top, in situ, and/or instrumental methods. Such improved calibrations would also enable the quantification of the climate and glacier sensitivity of Iceland during the Holocene.

Third, a major uncertainty in the utility of brGDGTs in lake sediment is whether their dominant source originates from terrestrial soils or is produced within the lake, in addition to from which season. One option to tackle this uncertainty would be to perform a comprehensive study at lakes, where we collect soils and suspended particles in tributary waters from the catchment, suspended particles in lake water (epilimnion, metalimnion and hypolimnion), and lake surface sediment seasonally, in addition to sinking lake particles (via moored sediment traps with monthly collection cups) throughout a full year cycle.

Exploration of the distribution of both core (fossil) and intact (in situ living signal) brGDGTs in each sample in and around these lakes may shed light on their in situ production, sources, and mixing in the environment. Furthermore, brGDGTs sources in lake sediment can be assessed by comparing the compound-specific $\delta^{13}C$ of brGDGTs (Pancost and Sinninghe Damsté, 2003; Weijers et al., 2010; Weber et al., 2015; Colcord et al., 2017) where those produced in situ feature significantly more depleted isotopes than those from catchment soils. Additionally, we may be able to assess changes in in situ lake brGDGT production over time by analyzing a novel, presumably aquatic, hexamethylated brGDGT found in lake sediment from a Swiss mountain lake that seems to be absent in catchment soils (Weber et al., 2015). Furthermore, the residence time of brGDGTs in soils and lake sediment can be assessed by means of compound-specific ^{14}C (e.g., Birkholz et al., 2013), which may shed light on the mobilization and potential contamination of sedimentary records from older brGDGTs.

Fourth, the final chapter demonstrated the utility of GDGTs for reconstructing winter subsurface temperatures on the North Iceland Shelf, which sheds new light on paleotemperature reconstructions from different seasons and water depths than previously existed. However, a major shortcoming in that study is that the record only reached through the last millennium. Hence, there is significant opportunity to extend the TEX_{86}^{L}-based records spatio-temporally through the network of Holocene-length marine sediment cores available from the North Iceland Shelf. Such records could provide insight into several different questions, such as whether periods of thick sea in past also induced subsurface warming during winter. Additionally, the subsurface may be less prone to short-term climate variability, which may explain some of the inconsistencies between SST reconstructions. If the latter is indeed the case, then TEX_{86}^{L} may be important to reconstructing major Holocene temperature trends along the highly dynamic North Iceland Shelf, without the superimposition of SST "noise".

Finally, continued work on refining and establishing a master Icelandic tephrochronology through more detailed and securely-dated lake sediment records is paramount. The high-resolution tephra age estimates derived from Haukadalsvatn's secure PSV age model highlights the potential for better tephrochronological records than the ones that currently rely on radiocarbon dating methods. Additionally, although Icelandic tephra research can be likely be sustained entirely on its own tephra products, emerging work from other locations in the Arctic highlight the opportunity to identify foreign (crypto)tephra. Such studies have recently isolated and confirmed the presence of ultra-distal cryptotephra originating from volcanic sources in Kamchatka that have reached Greenland (Cook et al., 2018) and locations as far as Svalbard, over 14,000 km away (van der Bilt et al., 2017). Greenland ice cores and paleoenvironmental records have also identified tephra from other locations, such as the North American Cascades (Fiacco et al., 1993; Zdanowicz et al. 1999; Jensen et al., 2014; Blockley et al., 2015) and China (Sun et al., 2014). Developing paleoclimate record synchronizations through these means will permit better assessment of leads and lags in the climate system across the northern hemisphere (e.g., Lane et al., 2013).

9.2.2 Tangentially Relevant

The following thoughts are questions and goals that have been spurred from my general dissertation research, post-doc proposals, or exposure to visiting researchers that target questions outside the dissertation's focus.

First, late Holocene soil erosion has classically been linked to the arrival of Norse settlers at the end of the first millennium CE. However, emerging datasets from lakes

demonstrate that the onset of erosion preceded settlement, and that other factors, such as deteriorating climate and repetitive tephra deposition from local volcanism, also likely played a role (Geirsdóttir et al., 2009, 2019). Constraining human activities through the Holocene would help determine and separate human environmental impacts from those caused by a deteriorating climate or volcanic eruptions. Diagnostic biomarkers (fecal sterols from humans and their livestock and polycyclic aromatic hydrocarbons (PAHs) from biomass burning) archived in lake sediment would be beneficial in this regard as they can record the appearance of human agency in a lake's catchment (e.g., D'Anjou et al., 2012). Since the microbially-mediated degradation pathways of plant and animal sterols in the intestinal tracts of higher mammals (e.g., omnivores vs. herbivores, including humans) are distinctive (e.g., Bull et al., 2002), different organisms produce characteristic breakdown products of sterols, namely fecal sterol or 5β-stanols. Most animals, particularly carnivorous animals, transform cholesterol into 5β-coprostanol, while herbivorous ruminant grazing animals such as sheep and cattle degrade sitosterol (a plant-derived phytosterol) into 5β-stigmastanol in their guts. Fecal sterols and the 5β-coprostanol/5β-stigmastanol ratio have been used in archeological and paleoclimate studies to detect human waste (human/carnivore), livestock grazing (livestock/herbivore), and fertilization by manure (Evershed et al., 1997; Bull et al., 2001, 2002; Tyagi et al., 2007; D'Anjou et al., 2012). The absence of large herbivorous mammals and humans in Iceland prior to settlement means that increases in the occurrence of fecal sterols over natural background values should mark the arrival of humans and associated livestock in the catchment, which could be traced regionally. Preliminary work has already showed the high potential for success of fecal sterols in Icelandic lakes for answering questions about human settlement (C. Florian, 2017, pers. comm.).

Polycyclic aromatic hydrocarbons (PAHs) can be formed during the incomplete combustion of landscape burning by humans or natural wildfires, as well as by the microbial modification of biogenic precursors during low-temperature diagenesis (Lima et al., 2005; Simoneit, 2002). Here the focus would be on pyrogenic PAHs as indicators of human activity (biomass burning). Since the molecular distribution of PAHs can be related to the temperature at which these compounds are formed, their presence in sedimentary archives reveal the source and temperature of their formation (Laflamme and Hites, 1978; Meyers, 2003; Simoneit, 1998; Yunker et al., 2011; Wakeham et al., 1980); with low temperature fires generating alkyl-substituted PAHs, whereas high temperature fires (coal or hydrocarbon burning) favor the production of parent compounds (e.g., Simoneit, 1998). Pyrogenic PAHs have been successfully applied as tracers of human activity and wildfires in lake sediments (D'Anjou et al., 2012; Musa Bandowe et al., 2014). Thus, along with fecal sterols, and bile acids, PAHs offer great potential as indicators of human occupation, particularly those related to Norse Settlement (D'Anjou et al., 2012), and landscape alteration in Icelandic records.

Second, paleoecological studies traditionally rely on pollen and plant macrofossils in sediment cores to reconstruct past vegetation. However, pollen production of many Arctic species is low and pollen records are obscured by long-distant transport from southern species (Birks and Birks, 2000; Birks et al., 2003; Caseldine et al., 2006). The latter is highlighted by the fact that following early Holocene deglaciation in Iceland, lake sediment records include pollen from exotic trees, such as Pinus, Quercus, Corylus, Alnus, and Ulmus (Caseldine et al., 2006; Eddudóttir et al., 2015), that have never been reported as macrofossils in Iceland. Pollen is also restricted to seed-bearing taxa, and taxonomic resolution is limited (Williams et al. 2004; Birks and Birks, 2015). Macrofossils offer higher taxonomic resolution and a more local signal, but sample size is low and rarely captures the

full range of vegetation (Anderson-Carpenter et al., 2011; Alsos et al., 2016). Sedimentary ancient DNA (sedaDNA) preserved in lake sediment adds valuable paleoecological information not obtainable from pollen and macrofossils studies (Pedersen et al., 2013; Alsos et al., 2016; Parducci et al., 2017; Alsos et al., 2018). Improved plant reference libraries (Willerslev et al., 2014) enable sedaDNA to provide more taxa overall than macrofossils (Alsos et al., 2016) or pollen (Alsos et al., 2018; Niemeyer et al., 2017; Edwards et al., 2018) and the strong match between lake sediment DNA and catchment vegetation surveys suggests sedaDNA has a local origin (Alsos et al., 2018; Niemeyer et al., 2017; Sjögren et al., 2017; Edwards et al., 2018). Hence, reconstructing vegetation communities in Iceland with sedaDNA would provide more reliable datasets to understand open questions regarding the early Holocene plant establishment, the maximum elevation of birch trees prior to human deforestation, and the role of dispersal vector(s) and/or climate constraints the biotic evolution. By extension, these questions would help us understand the potential future of vegetation in a warmer future, which is currently a poorly constrained feedback in climate models.

One final thought is extending quantitative Icelandic climate records beyond the Holocene epoch. An underlying theme in this dissertation's research was quantifying how much warmer was the early Holocene than present, and how ice caps and the regional environment adapted, in order to better anticipate future change over the coming century. Unfortunately, given the extensive and repetitive ice sheets that recurred throughout Iceland's history, records are typically limited to the Holocene. In eastern Iceland, pre-Holocene climate change has been deduced from pollen assemblages preserved in lignite beds (Mudie and Helgason, 1983; Duncan and Helgason, 1998), from periods deeper in Earth's history characterized by considerably higher temperatures with larger temperature oscillations than today (Zachos et al., 2001). At 10.72 Ma the pollen indicates climate deterioration that is contemporaneous with ~70 m global sea level drop of the brief global glaciation event Mi6 (Duncan and Helgason, 1998). Subsequently, between 10 and 9.5 Ma, the pollen assemblages suggest a temperature decrease of ~10 ^{o}C (Mudie and Helgason, 1983). However, these records are temporally limited and can be improved upon with new analytical methods. In addition to lignite beds, Miocene and Pliocene-age lava flow sequences in eastern Iceland (Moorbath et al., 1968; McDougall et al., 1976; Kristjansson et al., 1995) also straddle units of welded tuff (Walker, 1962; Geirsdóttir and Eiríksson, 1994; Geirsdóttir et al., 2007). Basaltic and rhyolitic tuffs such as these are comprised of hydrated volcanic glass (Cerling et al., 1985), whose δD signature is directly correlated to the environmental water that it was originally deposited in (Friedman, Gleason, Sheppard, and Rude, 1993; Friedman, Gleason, and Warden, 1993; Seligman et al., 2016). Consequently, using Ar-Ar and paleomagnetic reversal age constraints on the lavas (B. Óskarsson, 2018, pers. comm.), the δD of hydrated glass in Icelandic tuff deposits can be used to reconstruct past climate, as previously demonstrated for a range of tephra spanning the late Pleistocene to early Cenozoic in other global locations (Mulch et al., 2008; Canavan et al., 2014; Porter et al., 2016). Considering that the δD of plant wax alkanoic acids has been shown to reflect summer temperature in Iceland during the Holocene (L. Curtin, 2018, unpublished data), the prospect of applying a similar concept to different and much older archives to quantitatively reconstruct Miocene and Pliocene cooling in Iceland is tantalizing. Although the inception of intermittent and full glaciation in Iceland is considered to occur during the late Pliocene (5-3 Ma) and start of the Quaternary (~2.6 Ma), respectively (Geirsdóttir and Eiríksson, 1994; Geirsdóttir et al., 2007), insight from cooling trends preceding these events may shed new light on Iceland's regional response to global cooling (Zachos et al., 2001), characterized by the emergence of glaciers on Greenland by 7 Ma (Larsen et al., 1994).

References

Abbott, P.M., Davies, S.M., 2012. Volcanism and the Greenland ice-cores: the tephra record. Earth-Science Reviews, 173-191.

Adrian, R., O'Reilly, C.M., Zagarese, H., Baines, S.B., Hessen, D.O., Keller, W., Livingstone, D.M., Sommaruga, R., Straile, D., Van Donk, E., Weyhenmeyer, G.A., Winder, M., 2009. Lakes as sentinels of climate change. Limnology and Oceanography 54, 2283-2297.

Alley, R.B., Ágústdóttir, A.M., 2005. The 8k event: cause and consequences of a major Holocene abrupt climate change. Quaternary Science Reviews 24, 1123-1149.

Alsos, I.G., Lammers, Y., Yoccoz, N.G., Jørgensen, T., Sjögren, P., Gielly, L., Edwards, M.E., 2018. Plant DNA metabarcoding of lake sediment: How does it represent the contemporary vegetation. PLoS ONE 13, 1-23.

Alsos, I.G., Sjögren, P., Edwards, M.E., Landvik, J.Y., Gielly, L., Forwick, M., Coissac, E., Brown, A.G., Jakobsen, L.V., Føreid, M.K., Pedersen, M.W., 2016. Sedimentary ancient DNA from Lake Skartjørna, Svalbard: Assessing the resilience of arctic flora to Holocene climate change. The Holocene 26, 627-642.

Andersen, C., Koç, N., Jennings, A.E., Andrews, J.T., 2004. Nonuniform response of the major surface currents in the Nordic Seas to insolation forcings: Implications for the Holocene climate variability. Paleoceanography 19, 1-16.

Andresen, C.S., Bond, G., Kuijpers, A., Knutz, P.C., Björck, S., 2005. Holocene variability at multidecadal time scales detected by sedimentological indicators in a shelf core NW off Iceland. Marine Geology 214, 323-338.

Anderson-Carpenter, L.L., McLachlan, J.S., Jackson, S.T., Kuch, M., Lumibao, C.Y., Poinar, H.N., 2011. Ancient DNA from lake sediments: Bridging the gap between paleoecology and genetics. BMC Evolutionary Biology 11, 1-15.

Anderson, L.S., Flowers, G.E., Jarosch, A.H., Aðalgeirsdóttir, G.Th., Geirsdóttir, Á., Miller, G.H., Harning, D.J., Þorsteinsson, Þ., Magnússon, E., Pálsson, F., 2018. Holocene glacier and climate variations in Vestfirðir, Iceland, from the modeling of Drangajökull ice cap. Quaternary Science Reviews 190, 39-56.

Anderson, R.K., Miller, G.H., Briner, J.P., Lifton, N.A., DeVogel, S.B., 2008. A millennial perspective on Arctic warming from ^{14}C in quartz and plants emerging from beneath ice caps. Geophysical Research Letters 35, 1-5.

Andrews, J.T., 2009. Seeking a Holocene drift ice proxy: non-clay mineral variations from the SW to N-central Iceland shelf: trends, regime shifts, and periodicities. Journal of Quaternary Science 24, 664-676.

Andrews, J.T., Belt, S.T., Ólafsdóttir, S., Massé, G., Vare, L.L., 2009. Sea ice and marine climate variability for NW Iceland/Denmark Strait over the last 2000 cal. yr BP. The Holocene 5, 775-784.

Andrews, J.T., Caseldine, C., Weiner, N.J., Hatton, J., 2001. Late Holocene (ca. 4 ka) marine and terrestrial environmental change in Reykjarfjördur, north Iceland: climate and/or settlement?. Journal of Quaternary Science 16, 133-143.

Andrews, J.T., Darby, D.A., Eberl, D.D., Jennings, A.E., Moros, M., Ogilvie, A., 2009. A robust multi-site Holocene history of drift ice off northern Iceland: Implications for North Atlantic climate. The Holocene 19, 71-78.

Andrews, J.T., Eberl, D.D., 2007. Quantitative mineralogy of surface sediments on the Iceland shelf, and application to down-core studies of Holocene ice-rafted sediments. Journal of Sedimentary Research 77, 469-479.

Andrews, J.T., Geirsdóttir, Á., Hardardóttir, J., Principato, S., Grönvold, K., Kristjansdóttir, G.B., Helgadóttir, G., Drexler, J., Sveinbjörnsdóttir, A., 2002. Distribution, sediment magnetism and geochemistry of the Saksunarvatn (10180 ± 60 cal. yr BP) tephra in marine, lake, and terrestrial sediments, northwest Iceland. Journal of Quaternary Science 17, 731-745.

Andrews, J.T., Helgadottir, G., Geirsdottir, Á., Jennings, A.E., 2001. Multicentury-scale records of carbonate (hydrographic?) variability on the N. Iceland margin over the last 5000 yrs. Quaternary Research 56, 199-206.

Andrews, J.T., Jónsdóttir, I., Geirsdóttir, Á., 2018. Tracking Holocene drift-ice limits on the NW/SW Iceland shelf: comparing proxy data with observation and historical evidence. Arctic, Antarctic, and Alpine Research, **in press**.

Arnalds, Ó., 2000. The Icelandic "rofabard" soil erosion features. Earth Surface Processes and Landforms 25, 17-28.

Arnalds, Ó., 2004. Volcanic soils of Iceland. Catena 56, 3-20.

Arnalds, Ó., 2008. Soils of Iceland. Jökull 58, 409-421.

Arnalds, Ó., 2010. Dust sources and deposition of aeolian materials in Iceland. Icelandic Agricultural Sciences 23, 3-21.

Arnalds, Ó., Gísladóttir, F.O., Sigurjónsson, H., 2001. Sandy deserts of Iceland: an overview. Journal of Arid Environments 47, 359-371.

Arnalds, O., Gretarsson, E., 2001. Soil map of Iceland. Agricultural Research Institute, Reykjavík.

Axford, Y., Geirsdóttir, Á., Miller, G.H., Langdon, P.G., 2009. Climate of the Little Ice Age and the past 2000 years in northeast Iceland inferred from chironomids and other lake sediment proxies. Journal of Paleolimnology 41, 7-24.

Axford, Y., Miller, G.H., Geirsdóttir, Á., Langdon, P.G., 2007. Holocene temperature history of northern Iceland inferred from subfossil midges. Quaternary Science Reviews 26, 3344-3358.

Balascio, N.L., D'Andrea, W.J., Bradley, R.S., 2015. Glacier response to North Atlantic climate variability during the Holocene. Climate of the Past 11, 1587-1598.

Balascio, N.L., D'Andrea, W.J., Bradley, R.S., Perren, B.B., 2013. Biogeochemical evidence for hydrologic changes during the Holocene in a lake sediment record from southeast Greenland. The Holocene 23, 1428-1439.

Barber, D.C., Dyke, A., Hillaire-Marcel, C., Jennings, A.E., Andrews, J.T., Kerwin, M.W., Bilodeau, G., McNeely, R., Southon, J., Morehead, M.D., Gagnon, J.-M., 1999. Forcing of the cold event of 8,200 years ago by catastrophic drainage of Laurentian lakes. Nature 400, 344-348.

Bechtel, A., Smittenberg, R.H., Bernasconi, S.M., Schubert, C.J., 2010. Distribution of branched and isoprenoid tetraether lipids in an oligotrophic and a eutrophic Swiss lake: Insights into sources and GDGT-based proxies. Organic Geochemistry 41, 822-832.

Belart, J.M.C., Berthier, E., Magnússon, E., Anderson, L.S., Pálsson, F., Thorsteinsson, T., Howat, I.M., Aðalgeirsdóttir, G., Jóhannesson, T., Jarosch, A.H., 2017. Winter mass balance of Drangajökull ice cap (NW Iceland) derived from satellite sub-meter stereo images. The Cryosphere 11, 1501-1517.

Belkin, I.M., Cornillon, P.C., Sherman, K., 2009. Fronts in large marine ecosystems. Progress in Oceanography 81, 223-236.

Belt, S.T., 2018. Source-specific biomarkers as proxies for Arctic and Antarctic sea ice. Organic Geochemistry 125, 277–298.

Belt, S.T., Allard, W.G., Massé, G., Robert, J.-M., Rowland, S.J., 2000. Highly branched isoprenoids (HBIs): Identification of the most common and abundant sedimentary isomers. Geochimica and Cosmochimica Acta 64, 3839-3851.

Belt, S.T., Brown, T.A., Navarro Rodriguez, A., Cabedo Sanz, P., Tonkin, A., Ingle, R., 2012. A reproducible method for the extraction, identification and quanitification of the Arctic sea ice proxy IP_{25} from marine sediments. Analytical Methods 4, 704-713.

Belt, S.T., Brown, T.A., Smik, L., Assmy, P., Mundy, C.J., 2018. Sterol identification in floating Arctic sea ice algal aggregates and the Antarctic sea ice diatom Berkeleya adeliensis. Organic Geochemistry 118, 1-3.

Belt, S.T., Brown, T.A., Smik, L., Tatarek, A., Wiktor, J., Stowasser, G., Assmy, P., Allen, C.S., Husum, K., 2017. Identification of C_{25} highly branched isoprenoid (HBI) alkenes in diatoms of the genus Rhizosolenia in polar and sub-polar marine phytoplankton. Organic Geochemistry 110, 65–72.

Belt, S.T., Brown, T.A., Ringrose, A.E., Cabedo-Sanz, P., Mundy, C.J., Gosselin, M., Poulin, M., 2013. Quantitative measurement of the sea ice diatom biomarker IP_{25} and sterols

in Arctic sea ice and underlying sediments: Further considerations for palaeo sea ice reconstructions. Organic Geochemistry 62, 33-45.

Belt, S.T., Cabedo-Sanz, P., Smik, L., Navarro-Rodriguez, A., Berben, S.M.P., Knies, J., Husum, K., 2015. Identification of paleo Arctic winter sea ice limits and the marginal ice zone: Optimised biomarker-based reconstructions of late Quaternary Arctic sea ice. Earth and Planetary Science Letters 431, 127-139.

Belt, S.T., Massé, G., Rowland, S.J., Poulin, M., Michel, C., LeBlanc, B., 2007. A novel chemical fossil of palaeo sea ice: IP_{25}. Organic Geochemistry 38, 16-27.

Belt, S.T., Massé, G., Vare, L.L., Rowland, S.J., Poulin, M., Sicre, M.-A., Sampei, M., Fortier, L., 2008. Distinctive ^{13}C isotopic signature distinguishes a novel sea ice biomarker in Arctic sediments and sediment traps. Marine Chemistry 112, 158-167.

Belt, S.T., Müller, J., 2013. The Arctic sea ice biomarker IP_{25}: a review of current understanding, recommendations for future research and applications in palaeo sea ice reconstructions. Quaternary Science Reviews 79, 9-25.

Belt, S.T., Smik, L., Brown, T.A., Kim, J.-H., Rowland, S.J., Allen, C.S., Gal, J.-K., Shin, K.-H., Lee, J.I., Taylor, K.W.R., 2016. Source identification and distribution reveals the potential of the geochemical Antarctic sea ice proxy $IPSO_{25}$. Nature Communications 7, 1-10.

Bendle, J.A.P., Rosell-Melé, A., 2007. High-resolution alkenone sea surface temperature variability on the north Icelandic shelf: implications for Nordic Seas palaeoclimatic development during the Holocene. The Holocene 17, 9-24.

Berger, A., Loutre, M.F., 1991. Insolation values for the climate of the last 10 million years. Quaternary Science Reviews 10, 297-317.

Bergthórsson, P., 1969. An estimate of drift ice and temperature in Iceland in 1000 years. Jökull 19, 94-101.

Birkholz, A., Smittenberg, R.H., Hajdas, I., Wacker, L., Bernasconi, S.M., 2013. Isolation and compound specific radiocarbon dating of terrigenous branched glycerol dialkyl glycerol tetraethers (brGDGTs). Organic Geochemistry 60, 9-19.

Birks, H. H., 2003. The importance of plant macrofossils in the reconstruction of Lateglacial vegetation and climate: examples from Scotland, western Norway, and Minnesota, USA. Quaternary Science Reviews 22, 453-473.

Birks, H.H., Gulliksen, S., Haflidason, H., Mangerud, J., Possnert, G., 1996. New radiocarbon dates from the Vedde ash and Saksunarvatn ash western Norway. Quaternary Research 127, 119-127.

Birks, H.H., Birks, H.J.B., 2000. Future uses of pollen analysis must include plant macrofossils. Journal of Biogeography 27, 31-35.

Birks, H.J.B., and Birks, H.H., 2015. How have studies of ancient DNA from sediments contributed to the reconstruction of Quaternary floras? New Phytologist, doi: 10.1111/nph.13657.

Björck, S., Ingólfsson, Ó., Haflidason, H., Hallsdóttir, M., Anderson, N.J., 1992. Lake Torfadalsvatn: a high resolution record of the North Atlantic ash zone I and the last glacial-interglacial environmental changes in Iceland. Boreas 21, 15-22.

Björnsson, H., Pálsson, F., 2008. Iceland glaciers. Jökull 58, 365-386.

Björnsson, H., Pálsson, F., Gudmundsson, S., Magnússon, E., Adalgeirsdóttir, G., Jóhannesson, T., Berthier, E., Sigurdsson, O., Thorsteinsson, T., 2013. Contribution of Icelandic ice caps to sea level rise: Trends and variability since the Little Ice Age. Geophysical Research Letters 40, 1546-1550.

Blaauw, M., 2010. Methods and code for 'classical' age-modeling of radiocarbon sequences. Quaternary Geochronology 5, 512-518.

Blair, C.L., Geirsdóttir, Á., Miller, G.H., 2015. A high-resolution multi-proxy lake record of Holocene environmental change in southern Iceland. Journal of Quaternary Science 30, 281-292.

Bligh, E.G., Dyer, W.J., 1959. A rapid method of total lipid extraction and purification. Canadian Journal of Biochemistry and Physiology 37, 911-917.

Blindheim, J., Malmberg, S.A., 2005. The mean sea level pressure gradient across the Denmark Strait as an indicator of conditions in the North Iceland Irminger Current. In: Drange, H., Dokken, T., Furevik, T., Gerdes, R., Berger, W. (Eds.), The Nordic Seas: An Integrated Perspective. In: Geophys. Monogr., vol. 158, pp. 65-71.

Blockley, S.P.E., Edwards, K.J., Schofield, J.E., Pyne-O'Donnell, S.D.F., Jensen, B.J.L., Matthews, I.P., Cook, G.T., Wallace, K.L., Froese, D., 2015. First evidence of cryptotephra in palaeoenvironmental records associated with Norse occupation sites in Greenland. Quaternary Geochronology 27, 145-157.

Bond, G., Kromer, B., Beer, J., Muscheler, R., Evans, M.N., Showers, W., Hoffmann, S., Lotti-Bond, R., Hajdas, I., Bonani, G., 2001. Persistent solar influence on North Atlantic climate during the Holocene. Science 294, 2130-2136.

Boygle, J., 1999. Variability of tephra in lake and catchment sediments, Svínavatn, Iceland. Global and Planetary Change 21, 129-149.

Braconnot, P., Harrison, S.P., Kageyama, M., Bartlein, P.J., Masson-Delmotte, V., Abe-Ouchi, A., Otto-Bliesner, B., Zhao, Y., 2012. Evaluation of climate models using palaeoclimatic data. Nature Climate Change 2, 417-424.

Brader, M.D., Lloyd, J.M., Barlow, N.L.M., Norðdahl, H., Bentley, M.J., Newton, A.J., 2017. Postglacial relative sea-level changes in northwest Iceland: Evidence from isolation basins, coastal lowlands and raised shorelines. Quaternary Science Reviews 169, 114-130.

Bradwell, T., Dugmore, A.J., Sugden, D.E., 2006. The Little Ice Age glacier maximum in Iceland and the North Atlantic Oscillation: Evidence from Lambatungnajökull, southeast Iceland. Boreas 35, 61-80.

Bramham-Law, C.W.F., Theuerkauf, M., Lane, C.S., Mangerud, J., 2013. New findings regarding the Saksunarvatn Ash in Germany. Journal of Quaternary Science 28, 248-257.

Brassell, S.C., Eglington, G., Marlowe, I.T., Pflaumann, U., Sarnthein, M., 1986. Molecular stratigraphy: a new tool for climatic assessment. Nature 320, 129-133.

Briner, J.P., Stewart, H.A.M., Young, N.E., Philipps, W., Losee, S., 2010. Using proglacial-threshold lakes to constrain fluctuations of the Jakobshavn Isbræ ice margin, western Greenland, during the Holocene. Quaternary Science Reviews 29, 3861-3874.

Bronk Ramsey, C., 2009. Bayesian analysis of radiocarbon dates. Radiocarbon, 51, 337-360.

Brown, T.A., Belt, S.T., Tatarek, A., Mundy, C.J., 2014. Source identification of the Arctic sea ice proxy IP_{25}. Nature Communications 5, 4197.

Brynjólfsson, S., Schomacker, A., Guðmundsdóttir, E.R., Ingólfsson, Ó., 2015. A 300-year surge history of the Drangajökull ice cap, northwest Iceland, and its maximum during the 'Little Ice Age'. The Holocene 7, 1-17.

Brynjólfsson, S., Schomacker, A., Ingólfsson, Ó., 2014. Geomorphology and the Little Ice Age extent of the Drangajökull ice cap, NW Iceland, with focus on its three surge-type outlets. Geomorphology 213, 292-304.

Brynjólfsson, S., Schomacker, A., Ingólfsson, Ó., Keiding, J.K., 2015. Cosmogenic ^{36}Cl exposure ages reveal a 9.3 ka BP glacier advance and the Late Weichselian-Early Holocene glacial history of the Drangajökull region, northwest Iceland. Quaternary Science Reviews 126, 140-157.

Buckley, M.W., Marshall, J., 2016. Observations, inferences, and mechanisms of the Atlantic Meridional Overturning Circulation: A review. Journal of Geophysics 54, 5-63.

Büntgen, U., Myglan, V.S., Ljungqvist, F.C., McCormick, M., Di Cosmo, N., Sigl, M., Jungclaus, J., Wagner, S., Krusic, P.J., Esper, J., Kaplan, J.O., de Vaan, M.A.C., Luterbacher, J., Wacker, L., Tegel, W., Kirdyanov, A.V., 2016. Cooling and societal change during the Late Antique Little Ice Age from 536 to around 660 AD. Nature Geoscience 9, 231-236.

Bull, I.D., Evershed, R.P., Betancourt, P.P., 2001. An organic geochemical investigation of the practice of manuring at a Minoan site on Pseira Island, Crete. Geoarchaeology 16, 223-242.

Bull, I.D., Lockheart, M.J., Elhmmali, M.M., Roberts, D.J., Evershed, R.P., 2002. The origin of faeces by means of biomarker detection. Environment International 27, 647-654.

Cabedo-Sanz, P., Belt, S.T., Jennings, A.E., Andrews, J.T., Geirsdóttir, Á., 2016. Variability in drift ice export from the Arctic Ocean to the North Iceland Shelf over the last 8000 years: A multi-proxy evaluation. Quaternary Science Reviews 146, 99-115.

Cabedo-Sanz, P., Belt, S.T., Knies, J., Husum, K., 2013. Identification of contrasting seasonal sea ice conditions during the Younger Dryas. Quaternary Science Reviews 79, 74-86.

Caesar, L., Rahmstorf, S., Robinson, A., Feulner, G., Saba, V., 2018. Observed fingerprint of a weakening Atlantic Ocean overturning circulation. Nature 556, 191-198.

Canavan, R.R., Carrapa, B., Clementz, M.T., Quade, J., DeCelles, P.G., Schoenbohm, L.M., 2014. Early Cenozoic uplift of the Puna Plateau, Central Andes, based on stable isotope paleoaltimetry of hydrated volcanic glass. Geology 42, 447-450.

Caseldine, C., Geirsdóttir, Á., Langdon, P., 2003. Efstadalsvatn – a multi-proxy study of a Holocene lacustrine sequence from NW Iceland. Journal of Paleolimnology 30, 55-73.

Caseldine, C., Langdon, P.G., Holmes, N., 2006. Early Holocene climate variability and the timing and extent of the Holocene Thermal Maximum (HTM) in northern Iceland. Quaternary Science Reviews 25, 2314-2331.

Castañeda, I.S., Schouten, S., 2011. A review of molecular organic proxies for examining modern and ancient lacustrine environments. Quaternary Science Reviews 30, 2851-2891.

Castañeda, I., Smith, L.M., Kristjánsdóttir, G.B., Andrews, J.T., 2004. Temporal changes in Holocene $\delta^{18}O$ records from the northwest and central North Iceland Shelf. Journal of Quaternary Science 19, 321-334.

Cerling, T.E., Brown, F.H., Bowman, J.R., 1985. Low-temperature alteration of volcanic glass: hydration, Na, K, ^{18}O and Ar mobility. Chemical Geology 52, 281-293.

Chivall, D., M'Boule, D., Sinke-Schoen, D., Sinninghe Damsté, J.S., Schouten, S., van der Meer, M.T.J., 2014. Impact of salinity and growth phase on alkenone distributions in coastal haptophytes. Organic Geochemistry 67, 31-34.

Christensen, C.L., 2013. Multi-proxy responses of Icelandic lakes to Holocene tephra perturbations. MSc thesis. University of Colorado, Boulder, CO. p. 203.

Chu, G.Q., Sun, Q., Li, S.Q., Zheng, M.P., Jia, X.X., Lu, C.F., Liu, J.Q., Liu, T.S., 2005. Long-chain alkenone distributions and temperature dependence in lacustrine surface sediments from China. Geochimica et Cosmochimica Acta 69, 4985–5003.

Church, M.J., Wai, B., Karl, D.M., DeLong, E.F., 2010. Abundances of crenarchaeal amoA genes and transcripts in the Pacific Ocean. Environmental Microbiology 12, 679-688.

Colcord, D.E., Cadieux, S.B., Brassell, S.C., Castañeda, I.S., Pratt, L.M., White, J.R., 2015. Assessment of branched GDGTs as temperature proxies in sedimentary records from several small lakes in southwestern Greenland. Organic Geochemistry 82, 33-41.

Colcord, D.E., Pearson, A., Brassell, S.C., 2017. Carbon isotope composition of intact branched GDGT core lipids in Greenland lake sediments and soils. Organic Geochemistry 110, 25-32.

Collins, L.G., Allen, C.S., Pike, J., Hodgson, D.A., Weckström, K., Massé, G., 2013. Evaluating highly branched isoprenoid (HBI) biomarkers as a novel Antarctic sea-ice proxy in deep ocean glacial age sediments. Quaternary Science Reviews 79, 87-98.

Compton, K., Bennett, R.A., Hreinsdóttir, S., 2015. Climate-driven vertical acceleration of Icelandic crust measured by continuous GPS geodesy. Geophysical Research Letters 42, 643-750.

Conley, D.J., Schelske, C.L., 2001. Biogenic silica. In: J.P. Smol, Birks, H.J.B. and Last, W.M. (eds), 2001. Tracking Environmental Change Using Lake Sediments. Volume 3:Terrestrial, Algal, and Siliceous Indicators. Kluwer Academic Publishers, Dordecht, The Netherlands.

Cook, E., Portnyagin, M., Ponomareva, V., Bazanova, L., Svensson, A., Garbe-Schönberg, D., 2018. First identification of cryptotephra from the Kamchatkan Peninsula in a Greenland ice core: Implications of a widespread marker deposit that links Greenland to the Pacific northwest. Quaternary Science Reviews 181, 200-206.

Coulter, S.E., Pilcher, J.R., Plunkett, G., Baillie, M., Hall, V.A., Steffensen, J.P., Vinther, B.M., Clausen, H.B., Johnsen, S.J., 2012. Holocene tephras highlight complexity of volcanic signals in Greenland ice cores. Journal of Geophysical Research Atmospheres 117, 1-11.

Crochet, P., Jóhannesson, T., Jónsson, T., Sigurðsson, O., Björnsson, H., Pálsson, F., Barstad, I., 2007. Estimating the spatial distribution of precipitation in Iceland using a linear model of orographic precipitation. Journal of Hydrometeorology 8, 1285-1306.

Damby, D.E., Horwell, C.J., Larsen, G., Thordarson, T., Tomatis, M., Fubini, B., Donaldson, K., 2017. Assessment of the potential respiratory hazard of volcanic ash from future Icelandic eruptions: a study of archived basaltic to rhyolitic ash samples. Environmental Health 16, 1-15.

D'Andrea, W.J., Huang, Y., Fritz, S.C., Anderson, N.J., 2011. Abrupt Holocene climate change as an important factor for human migration in West Greenland. Proceedings of the National Academy of Sciences 108, 9765-9769.

D'Andrea, W.J., Lage, M., Hughes, J.B., Laatsch, A.D., Amaral-Zettler, L.A., Sogin, M.L., Huang Y., 2006. Alkenone producers inferred from well-preserved 18S rDNA in Greenland lake sediments. Journal of Geophysical Research – Biogeosciences 111, G03013.

D'Andrea, W.J., Theroux, S., Bradley, R.S., Huang, X., 2016. Does phylogeny control U^{k}_{37}-temperature sensitivity? Implications for lacustrine alkenone paleothermometry. Geochimica et Cosmochimica Acta 175, 168-180.

D'Andrea, W. J., Vaillencourt, D.A., Balascio, N.L., Werner, A., Roof, S.R., Retelle, M., Bradley, R.S., 2012. Mild Little Ice Age and unprecedented recent warmth in an 1800 year lake sediment record from Svalbard. Geology 40, 1007-1010.

D'Anjou, R.M., Bradley, R.S., Balascio, N.L., Finkelstein, D.B., 2012. Climate impacts on human settlement and agricultural activities in northern Norway revealed through sediment biogeochemistry. Proceedings of the National Academy of Sciences 109, 20332-20337.

Darby, D.A., Andrews, J.T., Belt, S.T., Jennings, A.E., Cabedo-Sanz, P., 2017. Holocene cyclic records of ice-rafted debris and sea ice variations on the East Greenland and Northwest Iceland margins. Arctic, Antarctic, and Alpine Research 49, 649-672.

Davies, S.M., 2015. Cryptotephras: the revolution in correlation and precision dating. Journal of Quaternary Science 30, 114-130.

Davies, S.M., Abbott, P.M., Pearce, N.J.G., Wastegård, S., Blockley, S.P.E., 2012. Integrating the INTIMATE records using tephrochronology: rising to the challenge. Quaternary Science Reviews 36, 11-27.

Davies, S.M., Abbott, P.M., Meara, R.H., Pearce, N.J.G., Austin, W.E.N., Chapman, M.R., Svensson, A., Bigler, M., Rasmussen, T.L., Rasmussen, S.O., Farmer, E.J., 2014. A North Atlantic tephrostratigraphical framework for 130-60 ka b2k: new tephra discoveries, marine-based correlations, and future challenges.

Davies, S.M., Elmquist, M., Bergman, J., Wohlfarth, B., Hammarlund, D., 2007. Cryptotephra sedimentation processes within two lacustrine sequences from west central Sweden. The Holocene 3, 319-330.

Davies, S.M., Larsen, G., Wastegård, S., Turney, C.S.M., Hall, V.A., Coyle, L., Thordarson, T., 2010. Widespread dispersal of Icelandic tephra: how does the Eyjafjöll eruption of 2010 compare to past Icelandic events? Journal of Quaternary Science 25, 605-611.

De Jonge, C., Hopmans, E.C., Stadnitskaia, A., Rijpstra, W.I.C., Hofland, R., Tegelaar, E., Sinninghe Damsté, J.S., 2013. Identification of novel penta- and hexamethylated branched glycerol dialkyl glycerol tetraethers in peat using HPLC-MS^2, GC-MS and GC-SMB-MS. Organic Geochemistry 54, 78-82.

De Jonge, C., Hopmans, E.C., Zell, C.I., Kim, J.-H., Schouten, S., Sinninghe Damsté, J.S., 2014a. Occurrence and abundance of 6-methyl branched glycerol dialkyl glycerol tetraethers in soils: Implications for palaeoclimate reconstruction. Geochimica et Cosmochimica Acta 141, 97-112.

De Jonge, C., Stadnitskaia, A., Fedotov, A., Sinninghe Damsté, J.S., 2015. Impact of riverine suspended particulate matter on the branched glycerol dialkyl glycerol tetraether composition of lakes: The outflow of the Selenga River in Lake Baikal (Russia). Organic Geochemistry 83-84, 241-252.

De Jonge, C., Stadnitskaia, A., Hopmans, E.C., Cherkashov, G., Fedotov, A., Sinninghe Damsté, J.S., 2014b. In situ produced branched glycerol dialkyl glycerol tetraethers in suspended particulate matter from the Yenisei River, Eastern Siberia. Geochimica et Cosmochimica Acta 125, 476-491.

Denton, G.H., Broecker, W.S., 2008. Wobbly ocean conveyor circulation during the Holocene? Quaternary Science Reviews 27, 1939-1950.

de Vernal, A., Gersonde, R., Goosse, H., Seidenkrantz, M.-S., Wolff, E.W., 2013. Sea ice in the paleoclimate system: the challenge of reconstructing sea ice from proxies – an introduction. Quaternary Science Reviews 79, 1-8.

Dickson, R.R., Meincke, J., Malmberg, S.-A., Lee, A.J., 1988. The "Great Salinity Anomaly" in the Northern North Atlantic 1968-1982. Progress in Oceanography 20, 103-151.

Divine, D.V., Dick, C. 2007. March through August Ice Edge Positions in the Nordic Seas, 1750-2002, Version 1. Boulder, Colorado USA. NSIDC: National Snow and Ice Data Center.

Dugmore, A.J., Church, M.J., Mairs, K.-A., McGovern, T.H., Perdikaris, S., Vésteinsson, O, 2007. Abandoned farms, volcanic impacts, and woodland management: revisiting Þjórsárdalur, the "Pompeii of Iceland". Arctic Anthropology 44, 1-11.

Dugmore, A.J., Cook, G.T., Shore, J.S., Newton, A.J., Edwards, K.J., Larsen, G., 1995. Radiocarbon dating tephra layers from Britain and Iceland. Radiocarbon 37, 379-388.

Dugmore, A.J., Gísladóttir, G., Simpson, I.A., Newton, A., 2009. Conceptual models of 1200 years of Icelandic soil erosion reconstructed using tephrochronology. Journal of the North Atlantic 2, 1-18.

Duncan, R., Helgason, J., 1998. Precise dating of the Holmatindur cooling event in eastern Iceland: Evidence for mid-Miocene bipolar glaciation. Journal of Geophysical Research 103, 397-404.

Eberl, D.D., 2003. User guide to RockJock: A program for determining quantitative mineralogy from X-ray diffraction data. United States Geological Survey, Open File Report 03-78, 40 pp, Washington, DC.

Eddudóttir, S.D., Erlendsson, E., Gísladóttir, G., 2015. Life on the periphery is tough: Vegetation in Northwest Iceland and its responses to early-Holocene warmth and later climate fluctuations. The Holocene 25, 1437-1453.

Eddudóttir, S. D., Erlendsson, E., Gísladóttir, G., 2017. Effects of the Hekla 4 tephra on vegetation in Northwest Iceland, Vegetation History and Archaeobotany 25, 1–14.

Eddudóttir, S.D., Erlendsson, E., Tinganelli, L., Gísladóttir, G., 2016. Climate change and human impact in a sensitive ecosystem: the Holocene environment of the Northwest Icelandic highland margin. Boreas September, 1-14.

Edwards, M.E., Alsos, I.G., Yoccoz, N., Coissac, E., Goslar, T., Gielly, L., Haile, J., Langdon, C.T., Tribsch, A., Binney, H.A., von Stedingk, H., Taberlet, P., 2018. Metabarcoding of modern soil DNA gives a highly local vegetation signal in Svalbard tundra. The Holocene 28, 1-11.

Egilsson, K., 2015. Umhverfi Skorarvatns vestan Drangajökuls á nútíma: Rannsókn á veðurvísum úr setkjarna SKR14-5A-1N-01. B.S. thesis, University of Iceland, Reykjavík.

Eiríksson, J., Knudsen, K.L., Haflidason, H., Heinemeier, J., Símonarson, L.A., 2000a. Chronology of late Holocene climatic events in the northern north Atlantic based on AMS ^{14}C dates and tephra markers from the volcano Hekla, Iceland. Journal of Quaternary Science 15, 573-580.

Eiríksson, J., Knudsen, K.L., Haflidason, H., Henriksen, P., 2000b. Late-glacial and Holocene palaeoceanography of the North Icelandic shelf. Journal of Quaternary Science 15, 23-42.

Eiríksson, J., Larsen, G., Knudsen, K.L., Heinemeier, J., Símonarson, L.A., 2004. Marine reservoir age variability and water mass distribution in the Iceland Sea. Quaternary Science Reviews 23, 2247-2268.

Elling, F.J., Könneke, M., Lipp, J.S., Becker, K.W., Gagen, E.J., Hinrichs, K.-U., 2014. Effects of growth phase on the membrane lipid composition of the thaumarchaeon Nitrosopumilus maritimus and their implications for archaeal lipid distributions in the marine environment. Geochimica et Cosmochimica Acta 141, 579-597.

Elling, F.J., Könneke, M., Mußmann, M., Greve, A., Hinrichs, K.-U., 2015. Influence of temperature, pH, and salinity on membrane lipid composition and TEX_{86} of marine planktonic thaumarchaeal isolates. Geochimica et Cosmochimica Acta 171, 238-255.

Evershed, R.P., Bethell, P.H., Reynolds, P.J., Walsh, N.J., 1997. 5β-stigmastanol and related 5β-stanols as biomarkers of manuring: analysis of modern experimental material and assessment of the archaeological potential. Journal of Archaeological Science 24, 485-495.

Fiacco, R.J., Palais, J.M., Germani, M.S., Zielinski, G.A., Mayewski, P.A., 1993. Characteristics and possible source of a 1479 A.D. Volcanic ash layer in a Greenland ice core. Quaternary Research 39, 267-273.

Finnsson, H., 1796. Um Mannfækkun af Hallærum á Íslandi. Rit Lærdómslistafélags 14, 30-226.

Florian, C.R., 2016. Multi-proxy reconstructions of Holocene environmental change and catchment biogeochemistry using algal pigments and stable isotopes preserved in lake sediment from Baffin Island and Iceland. Ph.D. thesis, University of Colorado, Boulder and University of Iceland, Reykjavík.

Florian, C.R., Miller, G.H., Fogel, M.L., Wolfe, A.P., Vinebrooke, R.D., Geirsdóttir, Á., 2015. Algal pigments in Arctic lake sediments record biogeochemical changes due to Holocene climate variability and anthropogenic change. Journal of Paleolimnology 54, 53-69.

Flowers, G.E., Björnsson, H., Geirsdóttir, A., Miller, G.H., Clarke, G.K.C., 2007. Glacier fluctuation and inferred chronology of Langjökull ice cap through the Little Ice Age. Quaternary Science Reviews 26, 2337-2353.

Flowers, G.E., Björnsson, H., Geirsdóttir, Á., Miller, G.H., Black, J.L., Clarke, G.K.C., 2008. Holocene climate conditions and glacier variation in central Iceland from physical modelling and empirical evidence. Quaternary Science Reviews 27, 797-813.

Foster, L.C., Pearson, E.J., Juggins, S., Hodgson, D.A., Saunders, K.M., Verleyen, E., Roberts, S.J., 2016. Development of a regional glycerol dialkyl glycerol tetraether (GDGT)-temperature calibration for Antarctic and sub-Antarctic lakes. Earth and Planetary Science Letters 433, 370-379.

Francis, C.A., Roberts, K.J., Beman, J.M., Santoro, A.E., Oakley, B.B., 2005. Ubiquity and diversity of ammonia-oxidizing archaea in water columns and sediments of the ocean. Proceedings of the National Academy of Sciences 102, 14683-14688.

Friedman, I., Gleason, J., Sheppard, R.A., Gude, A.J., 1993. Deuterium fractionation as water diffuses into silicic volcanic ash. Geophysical Monograph 78, 321-323.

Friedman, I., Gleason, J., Warden, A., 1993. Ancient climate from deuterium content of water in volcanic glass. Geophysical Monograph 78, 309-319.

Gardner, A.S., Moholdt, G., Cogley, J.G., Wouters, B., Arendt, A.A., Wahr, J., Berthier, E., Hock, R., Pfeffer, W.T., Kaser, G., Ligtenberg, S.R.M., Bolch, T., Sharp, M.J., Hagen, J.O., van den Broeke, M.R., Paul, F., 2013. A reconciled estimate of glacier contributions to sea level rise: 2003 to 2009. Science 340, 852–7.

Gathorne-Hardy, F.J., Erlendsson, E., Langdon, P.G., Edwards, K.J., 2009. Lake sediment evidence for late Holocene climate change and landscape erosion in western Iceland. Journal of Paleolimnology 42, 413-426.

Geirsdóttir, Á., 2004. Extent and chronology of Glaciation in Iceland. In: Ehlers, J., Gibbard, P. (Eds.), Quaternary Glaciations - Extent and Chronology of Glaciation. Part I. INQUA Commission on Glaciation 2004, Work Group 5, Elsevier B.V., p. 175-182.

Geirsdóttir, Á., Andrews, J.T., Ólafsdóttir, S., Helgadóttir, G., Hardardóttir, J., 2002. A 36 ky record of iceberg rafting and sedimentation from north-west Iceland. Polar Research 21, 291-298.

Geirsdóttir, Á., Eiríksson, J., 1994. Growth of an intermittent ice sheet in Iceland during the late Pliocene and early Pleistocene. Quaternary Research 42, 115-130.

Geirsdóttir, Á., Miller, G.H., Andrews, J.T., 2007. Glaciation, erosion, and landscape evolution of Iceland. Journal of Geodynamics 43, 170-186.

Geirsdóttir, Á., Miller, G.H., Andrews, J.T., Harning, D.J., Anderson, L.S., Larsen, D.J., Florian, C., Thordarson, T., 2019. The onset of Neoglaciation in Iceland and the 4.2 ka event. Climate of the Past Discussions 15, 25-40.

Geirsdóttir, Á., Miller, G.H., Axford, Y., Ólafsdóttir, S., 2009. Holocene and latest Pleistocene climate and glacier fluctuations in Iceland. Quaternary Science Reviews 28, 2107-2118.

Geirsdóttir, Á., Miller, G.H., Larsen, D.J., Ólafsdóttir, S., 2013. Abrupt Holocene climate transitions in the northern North Atlantic region recorded by synchronized lacustrine records in Iceland. Quaternary Science Reviews 70, 48-62.

Geirsdóttir, A., Miller, G.H., Thordarson, T., Ólafsdóttir, S., 2009. A 2000 year record of climate variations reconstructed from Haukadalsvatn, West Iceland. Journal of Paleolimnology 41, 95-115.

Giraudeau, J., Jennings, A.E., Andrews, J.T., 2004. Timing and mechanisms of surface and intermediate water circulation changes in the Nordic Seas over the last 10,000 cal years: a view from the North Iceland shelf. Quaternary Science Reviews 23, 2127-2139.

Gísladóttir, F.Ó., Arnalds, Ó., Gísladóttir, G., 2005. The effect of landscape and retreating glaciers on wind erosion in south Iceland. Land Degradation and Developments 16, 177-187.

Grönvold, K., Óksarsson, N., Johnsen, S.J., Clausen, H.B., Hammer, C.U., Bond, G., Bard, E., 1995. Ash layers from Iceland in the Greenland GRIP ice core correlated with oceanic and land sediments. Earth and Planetary Science Letters 135, 149-155.

Grove, J.M., 1988. The Little Ice Age. Methuen, London, UK, 498 pp.

Guðlaugsdóttir, H., Steen-Larsen, H.C., Sjolte, J., Masson-Delmotte, V., Werner, M., Sveinbjörnsdóttir, Á.E., 2018. The influence of volcanic eruptions on weather regimes over the North Atlantic simulated by ECHAM5/MPI-OM ensemble runs from 800 to 2000 CE. Atmospheric Research 213, 211-223.

Gudmundsdóttir, E.R., Larsen, G., Björck, S., Ingólfsson, Ó., Striberger, J., 2016. A new high-resolution Holocene tephra stratigraphy in eastern Iceland: improving the Icelandic and North Atlantic tephrochronology. Quaternary Science Reviews 150, 234-249.

Gudmundsdóttir, E.R., Larsen, G., Eiríksson, J, 2011. Two new Icelandic tephra markers: the Hekla Ö tephra layer, ~6060 cal yr BP and Hekla DH tephra layer, ~6650 cal yr BP – land-sea correlation of Mid Holocene tephra layers. Holocene 21, 629-639.

Gudmundsdóttir, E.R., Larsen, G., Eiríksson, J, 2012. Tephra stratigraphy on the North Icelandic shelf: extending tephrochronology into marine sediments off North Iceland. Boreas 41, 719-734.

Gudmundsdóttir, E.R., Schomacker, A., Brynjólfsson, S., Ingólfsson, Ó., Larsen, N.K., 2018. Holocene tephrostratigraphy in Vestfirðir, NW, Iceland. Journal of Quaternary Science 33, 827-839.

Gunnarsdóttir, S., 2018. Holocene environmental changes in the central highlands of Iceland as recorded in soils. M.S. thesis, University of Iceland, Reykjavík.

Gunnarson, S.R., 2017. Climate and landscape evolution in the west Central Highlands, Iceland. M.S. thesis, University of Iceland, Reykjavík.

Haflidison, H., Eiríksson, J, Kreveld, S., 2000. The tephrochronology of Iceland and the North Atlantic region during the Middle and Late Quaternary: a review. Journal of Quaternary Science 15, 3-22.

Haflidison, H., Larsen, G., Ólafsson, G., 1992. The recent sedimentation history of Thingvallavatn, Iceland. Oikos 64, 80-95.

Haflidason, H., Regnéll, C., Pyne-O'Donnell, S., Svendsen, J.I., 2018. Extending the known distribution of the Vedde Ash into Siberia: occurrence in lake sediments from the Timan Ridge and the Ural Mountains, northern Russia. Boreas XXX.

Hall, I.R., Bianchi, G.G., Evans, J.R., 2004. Centennial to millenial scale Holocene climate-deep water linkage in the North Atlantic. Quaternary Science Reviews 23, 1529-1536.

Hanna, E., Jónsson, T., Ólafsson, J., Valdimarsson, H., 2006. Icelandic coastal sea surface temperature records constructed: putting the pulse on air-sea-climate interactions in the northern North Atlantic. Part I: Comparison with HadISST1 open-ocean surface temperatures and preliminary analysis of long-term patterns and anomalies of SSTs around Iceland. Journal of Climate 19, 5652-5667.

Hansen, B., Østerhus, S., 2000. North Atlantic Nordic Seas exchanges. Progress in Oceanography 45, 109-208.

Harðardóttir, J., Geirsdóttir, Á., Thordarson, T., 2001. Tephra layers in a sediment core from Lake Hestvatn, southern Iceland; implications for evaluating sedimentation processes and environmental impacts on a lacustrine system caused by tephra fall deposits in the surrounding watershed. Spec. Publs int. Ass. Sediment 30, 225-246.

Harðarson, B.S., Fitton, J.G., Ellam, R.M., Pringle, M.S., 1997. Rift relocation – A geochemical and geochronological investigation of a palaeo-rift in northwest Iceland. Earth and Planetary Science Letters 153, 181-196.

Harðarson, B.S., Fitton, J.G., Hjartarson, Á., 2008. Tertiary volcanism in Iceland. Jökull 58, 161-178.

Harning, D.J., Andrews, J.T., Belt, S.T., Cabedo-Sanz, P., Dildar, N., Geirsdóttir, Á., Miller, G.H., Sepúlveda, J., 2019. Sea ice control on winter subsurface temperatures of the North Iceland Shelf over the last millennium. Paleoceanography and Paleoclimatology, under review.

Harning, D.J., Geirsdóttir, Á., Miller, G.H., 2018. Punctuated Holocene climate of Vestfirðir, Iceland, linked to internal/external variables and oceanographic conditions. Quaternary Science Reviews 189, 31-42.

Harning, D.J., Geirsdóttir, Á., Miller, G.H., Anderson, L., 2016. Episodic expansion of Drangajökull, Vestfirðir, Iceland, over the last 3 ka culminating in its maximum dimension during the Little Ice Age. Quaternary Science Reviews 152, 118-131.

Harning, D.J., Geirsdóttir, Á., Miller, G.H., Zalzal, K., 2016. Early Holocene deglaciation of Drangajökull, Vestfirðir, Iceland. Quaternary Science Reviews 153, 192-198.

Harning, D.J., Geirsdóttir, Á., Thordarson, T., Miller, G.H., 2018. Climatic control on Icelandic volcanic activity during the mid-Holocene: COMMENT. Geology 46, e443.

Harning, D.J., Thordarson, T., Geirsdóttir, Á., Zalzal, K., Miller, G.H., 2018. Provenance, stratigraphy and chronology of Holocene tephra from Vestfirðir, Iceland. Quaternary Geochronology 46, 59-76.

Hayward, C., 2012. High spatial resolution electron probe microanalysis of tephra and melt inclusions without beam-induced chemical modification. The Holocene 22, 119-125.

Helgadóttir, G., 1997. Paleoclimate (0 to >14 ka) of W and NW Iceland: an Iceland/USA contribution to P.A.L.E. Cruise Report B9-97 R/V Bjarni Sæmundsson RE 30 17th-30th July 1997. No. 62, Marine Research Institute of Iceland, Reykjavík, Iceland.

Herfort, L., Schouten, S., Boon, J.P., Sinninghe Damsté, J.S., 2006. Application of TEX_{86} temperature proxy to the southern North Sea. Organic Geochemistry 37, 1715-1726.

Hjort, C., Ingólfsson, Ó., Norðdahl, H., 1985. Late Quaternary geology and glacier history of Hornstrandir, Northwest Iceland: A reconnaissance study. Jökull 35, 9-29.

Holmes, N., Langdon, P.G., Caseldine, C.J., Wastegård, S., Leng, M.J., Croudace, I.W., Davies, S.M., 2016. Climatic variability during the last millennium in Western Iceland from lake sediment records. The Holocene, 1-16.

Hopkins, T.S., 1991. The GIN Sea – A synthesis of its physical oceanography and literature review 1972-1985. Earth Science Reviews 30, 175-318.

Hopmans, E.C., Schouten, S., Sinninghe Damsté, J.S., 2016. The effect of improved chromatography on GDGT-based palaeoproxies. Organic Geochemistry 93, 1-6.

Horwell, C.J., Baxter, P.J., Hillman, S.E., Calkins, J.A., Damby, D.E., Delmelle, P., Donaldson, K., Dunster, C., Fubini, B., Kelly, F.J., Le Blond, J.S., Livi, K.J.T., Murphy, F., Nattrass, C., Sweeney, S., Tetley, T.D., Thordarson, T., Tomatis, M., 2013. Physiochemical and toxicological profiling of ash from the 2010 and 2011 eruptions of Eyjafjallajökull and Grímsvötn volcanoes, Iceland using a rapid respiratory hazard assessment protocol. Environmental Research 127, 63-73.

Höskuldsson, Á., Óskarsson, N., Pedersen, R., Grönvold, K., Vogjörð, K., Ólafsdóttir, R., 2007. The millennium eruption of Hekla in February 2000. Bulletin of Volcanology 70, 169-182.

Huang, W.-Y., Meinschein, W., 1976. Sterols as ecological indicators. Geochimica et Cosmochimica Acta 43, 739-745.

Huguet, C., Hopmans, E.C., Febo-Ayala, W., Thompson, D.H., Sinninghe Damsté, J.S., Schouten, S., 2006. An improved method to determine the absolute abundance of glycerol dibiphytanyl glycerol tetraether lipids. Organic Geochemistry 37, 1036-1041.

Hurley, S.J., Elling, F.J., Könneke, M., Buchwald, C., Wankel, S.D., Santoro, A.E., Lipp, J.S., Hinrichs, K.-U., Pearson, A., 2016. Influence of ammonia oxidation rate on thaumarchaeal lipid composition and the TEX_{86} temperature proxy. Proceedings of the National Academy of Sciences 113, 7762-7767.

Hurley, S.J., Lipp, J.S., Close, H.G., Hinrichs, K.-U., Pearson, A., 2018. Distribution and export of isoprenoid tetraether lipids in suspended particulate matter from the water column of the Western Atlantic Ocean. Organic Geochemistry 116, 90-102.

Hurrell, J.W., Kushnir, Y., Ottersen, G., Visbeck, M., 2003. An Overview of the North Atlantic Oscillation. Geophysical Monograph, 134, 1-35.

Ingólfsson, Ó., Benediktsson, Í.Ö, Schomacker, A., Kjær, K.H., Brynjólfsson, S., Jónsson, S.A., Korsgaard, N.J., Johnson, M.D. 2016. Glacial geological studies of surge-type glaciers in Iceland - Research status and future challenges. Earth-Science Reviews 152, 37-69.

IPCC, 2013. In: Stocker, T.F., Qin, D., Plattner, G.-K., Tignor, M., Allen, S.K., Boschung, J., Nauels, A., Xia, Y., Bex, V., Midgley, P.M. (Eds.), Climate Change 2013: The Physical Science Basis. Contribution of Working Group I to the Fifth Assessment Report of the Intergovernmental Panel on Climate Change. Cambridge University Press, Cambridge, United Kingdom and New York, NY, USA.

Jackson, M.G., Oskarsson, N., Trønnes, R.G., McManus, J.F., Oppo, D.W., Grönvold, K., Hart, S.R., Sachs, J.P., 2005. Holocene loess deposition in Iceland: Evidence for millennial-scale atmosphere-ocean coupling in the North Atlantic. Geology 33, 509-512.

Jagan, A., 2010. Tephra stratigraphy and geochemistry from three Icelandic lake cores: a new method for determining source volcano of tephra. M.S. thesis, The University of Edinburgh, Edinburgh.

Jakobsson, S.P., 1979. Petrology of recent basalts of the Eastern Volcanic Zone, Iceland. Acta Naturalia Islandica 26, 1-103.

Jakobsson, S.J., Jónasson, K., Sigurdsson, L.A., 2008. The three igneous rock series of Iceland. Jökull 58, 117-138.

Janebo, M.H., Thordarson, T., Houghton, B.F., Bonadonna, C., Larsen, G., Carey, R.J., 2016. Dispersal of key subplinan-Plinian tephras from Hekla volcano, Iceland: implications for eruption source parameters. Bulletin of Volcanology 78, 1-16.

Japan Meteorological Agency, 2006. Characteristics of Global Sea Surface Temperature Analysis Data (COBE-SST) for Climate Use. Monthly Report on Climate System Separated 12, 116.

Jennings, A.E., Andrews, J.T., Pearce, C., Wilson, L., Ólafsdóttir, S., 2015. Detrital carbonate peaks on the Labrador shelf, a 13-7 ka template for freshwater forcing from the Hudson Strait outlet of the Laurentide Ice Sheet into the subpolar gyre. Quaternary Science Reviews 107, 62-80.

Jennings, A.E., Thordarson, T., Zalzal, K., Stoner, J., Hayward, C., Geirsdóttir, Á., Miller, G., 2014. Holocene tephra from Iceland and Alaska in SE Greenland Shelf Sediments. In: Austin, W.E.N., Abbott, P.M., Davies, S.M., Pearce, N.J.G., and Wastegård, S. (eds) Marine Tephrochronology. Geological Society, London, Specical Publications, 398.

Jensen, B.J.L., Pyne-O'Donnell, S.D., Plunkett, G., Froese, D.G., Hughes, P.D.M., Sigl, M., McConnell, J.R., Amesbury, M.J., Blackwell, P.G., van den Bogaard, C., Buck, C.E., Charman, D.J., Clague, J.J., Hall, V.A., Koch, J., Mackay, H., Mallon, G., McColl, L., Pilcher, J.R., 2014. Transatlantic distribution of the Alaskan White river ash. Geology 42, 875-878.

Jiang, H., Muscheler, R., Björck, S., Seidenkrantz, M-S., Olsen, J., Sha, L., Sjolte, J., Eiríksson, J., Ran, L., Knudsen, K-L., Knudsen, M.F., 2015. Solar forcing of Holocene summer sea-surface temperatures in the northern North Atlantic. Geology 43, 2-5.

Jóhannesson, H., 2014. Geological Map of Iceland. Bedrock Geology. 1:600,000. 2nd Edition. Icelandic Institute of Natural History.

Jóhannesson, T., Björnsson, H., Magnússon, E., Guðmundsson, S., Pálsson, F., Sigurðsson, O., Thorsteinsson, T., Berthier, E., 2013. Ice-volume changes, bias estimation of mass-balance measurements and changes in subglacial lakes derived from lidar mapping of the surface of Icelandic glaciers. Annals of Geology 54, 63-74.

Jóhannsdóttir, G.E., 2007. Mid-Holocene to late glacial tephrochronology in west Iceland as revealed in three lacustrine environments. M.S. thesis, University of Iceland, Reykjavík.

Jónsson, D.F., 2018. Mid-Holocene eruptive activity in the Hekla volcanic system. M.S. thesis, University of Iceland, Reykjavík.

Jónsson, O., 1945. Ódáðahraun I–III. Bókaútgáfan Norðri, Akureyri.

Justwan, A., Koc, N., Jennings, A.E., 2008. Evolution of the Irminger and East Icelandic Current systems through the Holocene, revealed by diatom-based sea surface temperature reconstructions. Quaternary Science Reviews 27, 1571-1582.

Kaiser, J., Schouten, S., Kilian, R., Arz, H.W., Lamy, F., Sinninghe Damsté, J.S., 2015. Isoprenoid and branched GDGT-based proxies for surface sediments from marine, fjord and lake environments in Chile. Organic Geochemistry 89-90, 117-127.

Kalliokoski, M., Wastegård, S., Saarinen, T., 2019. Rhyolitic and dacitic component of the Askja 1875 tephra in southern and central Finland: first step towards a Finnish tephrochronology. Journal of Quaternary Science 34, 29-39.

Karner, M.B., DeLong, E.F., Karl, D.M., 2001. Archaeal dominance in the mesopelagic zone of the Pacific Ocean. Nature 409, 507-510.

Kim, J.-H., van der Meer, J., Schouten, S., Helmke, P., Willmott, V., Sangiorgi, F., Koç, N., Hopmans, E. C., Sinninghe Damsté, J. S., 2010. New indices and calibrations derived from the distribution of crenarchaeal isoprenoid tetraether lipids: Implications for past sea surface temperature reconstructions. Geochimica et Cosmochimica Acta 74, 4639–4654.

Kim, J.-H., Crosta, X., Willmott, V., Renssen, H., Bonnin, J., Helmke, P., Schouten, S., Sinninghe Damsté, J.S., 2012. Holocene subsurface temperature variability in the eastern Antarctic continental margin. Geophysical Research Letters 39, 3-8.

Kirkbride, M.P., Dugmore, A.J., 2006. Responses of mountain ice caps in central Iceland to Holocene climate change. Quaternary Science Reviews 25, 1692-1707.

Kirkbride, M.P., Dugmore, A.J., 2008. Two millennia of glacier advances from southern Iceland dated by tephrochronology. Quaternary Research 70, 398-411.

Knudsen, K.L., Eirikson, J., Jansen, E., Jiang, H., Rytter, F., Gudmundsdottir, E.R., 2004. Paleoceanographic changes off North Iceland through the last 1200 yrs: foraminifera, stable isotopes, diatomes and ice rafted debris. Quaternary Science Reviews 23, 2231-2246.

Knudsen, M.F., Seidenkrantz, M.-S., Jacobsen, B.H., Kuijpers, A., 2011. Tracking the Atlantic Multidecadal Oscillation through the last 8,000 years. Nature Communications 2, 178.

Korte, M., Brown, M.C., Gunnarson, S.R., Nilsson, A., Panovska, S., Wardinski, I., Constable, C.G., 2019. Refining Holocene geochronologies using palaeomagnetic records. Quaternary Geochronology 50, 47-74.

Koch, L., 1945. 'The East Greenland Ice', Meddelelser om Grønland 130, Kommisionen for Videnskabelige Undersøgelser i Grønland, Copenhagen.

Köseoğlu, D., Belt, S.T., Smik, L., Yao, H., Panieri, G., Knies, J., 2018. Complementary biomarker-based methods for characterizing Arctic sea ice conditions: A case study comparison between multivariate analysis and the PIP_{25} index. Geochimica et Cosmochimica Acta 222, 406-420.

Kristjánsdóttir, G.B., Moros, M., Andrews, J.T., Jennings, A.E., 2016. Holocene Mg/Ca, alkenones, and light stable isotope measurements on the outer North Iceland shelf (MD99-2269): A comparison with other multi-proxy data and sub-division of the Holocene. The Holocene 27, 1-11.

Kristjánsdóttir, G.B., Stoner, J.S., Jennings, A.E., Andrews, J.T., Grönvold, K., 2007. Geochemistry of Holocene cryptotephras from the North Iceland Shelf (MD99-2269): intercalibration with radiocarbon and palaeomagnetic chronostratigraphies. The Holocene 17, 155-176.

Kristjansson, L., Gudmundsson, A., Haraldsson, H., 1995. Stratigraphy and paleomagnetism of a 3-km-thick Miocene lava pile in the Mjoifjörður area, eastern Iceland. Geol Rundsch 84, 813-830.

Kuno, H., 1968. Differentiation of basaltic magmas. In: Hess, H.H., Poldervaart, A. (eds) Basalts: The Poldervaart Treatise on Rocks of Basaltic Composition. Interscience, New York, 2, 623-688.

Kvamme, T., Mangerud, J., Furnes, H., Ruddiman, W.F., 1989. Geochemistry of Pleistocene ash zones in cores from the North Atlantic. Norsk Geologisk Tidsskrift 69, 251-272.

Lacasse, C., 2001. Influence of climate variability on the atmospheric transport of Icelandic tephra in the subpolar North Atlantic. Global and Planetary Change 29, 31-55.

Lacasse, C., Sigurdsson, H., Jóhannesson, H., Paterne, M., Carey, S., 1995. Source of Ash Zone 1 in the North Atlantic. Bulletin of Volcanology 57, 18-32.

Laflamme, R.E., Hites, R.A., 1978. The global distribution of polycyclic aromatic hydrocarbons in recent sediments. Geochimica et Cosmochimica Acta 42, 289-303.

Lane, C.S., Blockley, S.P.E., Mangerud, J., Smith, V.C., Lohne, Ø.S., Tomlinson, E.L., Matthews, I.P., Lotter, A.F., 2012. Was the 12.1 ka Icelandic Vedde Ash one of a kind? Quaternary Science Reviews 33, 87-99.

Lane, C.S., Brauer, A., Blockley, S.P.E., Dulski, P., 2013. Volcanic ash reveals time-transgressive abrupt climate change during the Younger Dryas. Geology 41, 1251-1254.

Langdon, P.G., Caseldine, C.J., Croudace, I.W., Jarvis, S., Wastegård, S., Crowford, T.C., 2011. A chironomid-based reconstruction of summer temperatures in NW Iceland since AD 1650. Quaternary Research 75, 451-460.

Langdon, P.G., Leng, M.J., Holmes, N., Caseldine, C.J., 2008. Environmental controls on modern chironomid faunas from NW Iceland and implications for reconstructing climate change. Journal of Paleolimnology 40, 273-293.

Langdon, P.G., Leng, M.J., Holmes, N., Caseldine, C.J., 2010. Lacustrine evidence of early-Holocene environmental change in northern Iceland: a multiproxy palaeoecology and stable isotope study. The Holocene 20, 205-214.

Larsen, D.J., Miller, G.H., Geirsdóttir, Á., Thordarson, T., 2011. A 3000-year varved record of glacier activity and climate change from the proglacial lake Hvítárvatn, Iceland. Quaternary Science Reviews 30, 2715-2731.

Larsen, D.J., Miller, G.H., Geirsdóttir, Á., Ólafsdóttir, S., 2012. Non-linear Holocene climate evolution in the North Atlantic: a high-resolution, multi-proxy record of glacier activity and environmental change from Hvítárvatn, central Iceland. Quaternary Science Reviews 39, 14-25.

Larsen, D.J., Geirsdóttir, Á., Miller, G.H., 2015. Precise chronology of Little Ice Age expansion and repetitive surges of Langjökull, central Iceland. Geology 43, 1-4.

Larsen, G., 1982. Gjóskutímatal jökuldals or nágrennis. In: Thórarinsdóttir, H., Óskarsson, Ó., Steinthórsson, S. and Einarsson, T. (eds) Eldur er í Norðri. Sögufélag, Reykjavík, 51-65.

Larsen, G., 1984. Recent volcanic history of the Veiðivötn fissure swarm, southern Iceland – an approach to volcanic risk assessment. Journal of Volcanology and Geothermal Research 22, 33-58.

Larsen, G., Dugmore, A.J., Newton A.J., 1999. Geochemistry of historical-age silicic tephras in Iceland. Holocene 9, 463-471.

Larsen, G., Eiríksson, J., 2008. Holocene tephra archives and tephrochronology in Iceland – a brief overview. Jökull 58, 229-250.

Larsen, G., Eiríksson, J., Knudsen, K.L., Heinemeier, J., 2002. Correlation of late Holocene terrestrial and marine tephra markers, north Iceland: implications for reservoir age changes. Polar Research 21, 283-290.

Larsen, G, Thorarinsson, S., 1977. H-4 and other acid Hekla tephra layers. Jökull 27, 27-46.

Larsen, H.C., Saunders, A.D., Clift, P.D., Begét, J., Wei, W., Spezzaferri, S., Ali, J., Cambray, H., Demant, A., Fitton, G., Fram, M.S., Fukuma, K., Gieskes, J., Holmes, M.A., Hunt, J., Lacasse, C., Larsen, L.M., Lykke-Andersen, H., Meltser, A., Morrison, M.L., Nemoto, N., Okay, N., Saito, S., Sinton, C., Stax, R., Vallier, T.L., Vandamme, D., Werner, R., 1994. Seven million years of glaciation in Greenland. Science 264, 952-955.

Laskar, J., Robutel, P., Gastineau, M., Correia, A.C.M., Levrard, B., 2004. A long-term numerical solution for the insolation quantities of the Earth. Astronomy and Astrophysics 428, 261-285.

Lawson, I.T., Gathorne-Hardy, F.J., Church, M.J., Newton, A.J., Edwards, K.J., Dugmore, A.J., Einarsson, Á., 2007. Environmental impacts of the Norse settlement palaeoenvironmental data from Mývatnssveit, northern Iceland. Boreas 36, 1-19.

Lawson, I.T., Swindles, G.T., Plunkett, G., Greenberg, D., 2012. The spatial distribution of Holocene cryptotephras in north-west Europe since 7 ka: implications for understanding ash fall events from Icelandic eruptions. Quaternary Science Reviews 41, 57-66.

Legates, D.R., Willmott, C.J., 1990. Mean seasonal and spatial variability in global surface air temperature. Theoretical and Applied Climatology 41, 11-21.

Levy, L.B., Kelly, M.A., Lowell, T.V., Hall, B.L., Hempel, L.A., Honsaker, W.M., Lusas, A.R., Howley, J.A., Axford, Y.L., 2014. Holocene fluctuations of Bregne ice cap, Scoresby Sund, east Greenland: a proxy for climate along the Greenland Ice Sheet margin. Quaternary Science Reviews 92, 357-368.

Libby, W.F., Anderson, E.C., Arnold, J.R., 1946. Age determination by radiocarbon content: world-wide assay of natural radiocarbon. Science 109, 227-228.

Lima, A.L.C., Farrington, J.W., Reddy, C.M., 2005. Combustion-derived polycyclic aromatic hydrocarbons in the environment – a review. Environmental Forensics 6, 109-131.

Locarnini, R.A., Mishonov, A.V., Antonov, J.I., Boyer, T.P., Garcia, H.E., Baranova, O.K., Zweng, M.M., Johnson, D.R., 2010. World Ocean Atlas 2009, Volume 1: Temperature. S. Levitus, Ed. NOAA Atlas NESDIS 68, U.S. Government Printing Office, Washington, D.C., 184 pp.

Longo, W.M., Dillon, J.T., Tarozo, R., Salacup, J.M., Huang, Y., 2013. Unprecedented separation of long chain alkenones from gas chromatography with a poly (trifluoropropylmethylsiloxane) stationary phase. Organic Geochemistry 65, 12803-12808.

Longo, W.M., Huang, Y., Yao, Y., Zhao, J., Giblin, A.E., Wang, X., Zech, R., Haberzettl, T., Jardillier, L., Toney, J., Liu, Z., Krivonogov, S., Kolpakova, M., Chu, G., D'Andrea, W.J., Harada, N., Nagashima, K., Sato, M., Yonenobu, H., Yamada, K., Gotanda, K., Shinozuka, Y., 2018. Widespread occurrence of distinct alkenones from Group I haptophytes in freshwater lakes: Implications for paleotemperature and paleoenvironmental reconstructions. Earth and Planetary Science Letters 492, 239-250.

Longo, W.M., Theroux, S., Giblin, A.E., Zheng, Y., Dillon, J.T., Huang, Y., 2016. Temperature calibration and phylogenetically distinct distributions for freshwater alkenones: Evidence from northern Alaskan lakes. Geochimica et Cosmochimica Acta 180, 177-196.

Loomis, S.E., Russell, J.M., Heureux, A.M., D'Andrea, W.J., Sinninghe Damsté, J.S., 2014. Seasonal variability of branched glycerol dialkyl glycerol tetraethers (brGDGTs) in a temperate lake system. Geochimica et Cosmochimica Acta 144, 173-187.

Loomis, S.E., Russell, J.M., Ladd, B., Street-Perrott, F.A., Sinninghe Damsté, J.S., 2012. Calibration and application of the branched GDGT temperature proxy in East African lake sediments. Earth and Planetary Science Letters 357-358, 277-288.

Lowe, D.J., 2011. Tephrochronology and its application: A review. Quaternary Geochronology 6, 107-153.

Lowell, T.V., Hall, B.L., Kelly, M.A., Bennike, O., Lusas, A.R., Honsaker, W., Smith, C.A., Levy, L.B., Travis, S., Denton, G.H., 2013. Late Holocene expansion of Istorvet ice cap, Liverpool Land, east Greenland. Quaternary Science Reviews 63, 128-140.

MacDonald, G.A., Katsura, T., 1964. Chemical composition of Hawaiian lavas. Journal of Petrology 5, 82-133.

MacDonald, R., McGarvie, D.W., Pinkerton, H., Smith, R.L., Palacz, Z.A., 1990. Petrogenic evolution of the Torfajökull volcanic complex, Iceland I. Relationship between the magma types. Journal of Petrology 31, 429-459.

Magnússon, E., Belart, J.M.C., Pálsson, F., Ágústsson, H., Crochet, P., 2016. Geodetic mass balance record with rigorous uncertainty estimates deduced from aerial photographs and LiDAR data – a case study from Drangajökull ice cap, NW Iceland. The Cryosphere Discussions 9, 4733-4785.

Magnússon, E., Belart, J.M.C., Pálsson, F., Anderson, L.S., Gunnlaugsson, Á.Þ., Berthier, E., Ágústson, H., Geirsdóttir, Á., 2016. The subglacial topography of Drangajökull ice cap, NW-Iceland, deduced from dense RES-profiling. Jökull 66, 1-26.

Mangerud, J., Furnes, H., Jóhansen, J., 1986. A 9000-year-old ash bed on the Faroe Islands. Quaternary Research 26, 262-265.

Mangerud, J., Svendsen, J.I., 2018. The Holocene Thermal Maximum around Svalbard, Arctic North Atlantic; molluscs show early and exceptional warmth. The Holocene 28, 65-83.

Margreth, A., Dyke, A.S., Gosse, J.C., Telka, A.M., 2014. Neoglacial ice expansion and late Holocene cold-based ice cap dynamics on Cumberland Peninsula, Baffin Island, Arctic Canada. Quaternary Science Reviews 91, 242-256.

Massé, G., Rowland, S.J., Sicre, M-A., Jacob, J., Jansen, E., Belt, S., 2008. Abrupt climate changes for Iceland during the last millennium: Evidence from high resolution sea ice reconstructions. Earth and Planetary Science Letters 269, 565-569.

Masson-Delmotte, V., M. Schulz, A. Abe-Ouchi, J. Beer, A. Ganopolski, J.F. González Rouco, E. Jansen, K. Lambeck, J. Luterbacher, T. Naish, T. Osborn, B. Otto-Bliesner, T. Quinn, R. Ramesh, M. Rojas, X. Shao and A. Timmermann, 2013: Information from Paleoclimate Archives. In: Climate Change 2013: The Physical Science Basis. Contribution of Working Group I to the Fifth Assessment Report of the Intergovernmental Panel on Climate Change [Stocker, T.F., D. Qin, G.-K. Plattner, M. Tignor, S.K. Allen, J. Boschung, A. Nauels, Y. Xia, V. Bex and P.M. Midgley (eds.)]. Cambridge University Press, Cambridge, United Kingdom and New York, NY, USA.

Mayewski, P.A., Rohling, E.E., Stager, J.C., Karlén, W., Maasch, K.A., Meeker, L.D., Meyerson, E.A., Gasse, F., van Kreveld, S., Holmgren, K., Lee-Thorp, J., Rosqvist, G., Rack, F., Staubwasser, M., Schneider, R.R., Steig, E.J., 2004. Holocene climate variability. Quaternary Research 62, 243-255.

Maykut, G.A., 1978. Energy exchange over young sea ice in the central Arctic. Journal of Geophysical Research 83, 3646-3658.

Maykut, G.A., 1982. Large-scale heat exchange and ice production in the central Arctic. Journal of Geophysical Research 87, 7971-7984.

McDougall, I., Kristjansson, L., Sæmundsson, K., 1984. Magnetostratigraphy and geochronology of northwest Iceland. Journal of Geophysical Research 89, 7029-7060.

McDougall, I., Watkins, N.D., Kristjansson, L., 1976. Geochronology and paleomagnetism of a Miocene-Pliocene lava sequence at Bessastadaa, Eastern Iceland. American Journal of Science 276, 1078-1095.

McKay, N.P., Kaufman, D.S., Michelutti, N., 2008. Biogenic silica concentration as a high-resolution, quantitative temperature proxy at Hallet Lake, south-central Alaska. Geophysical Research Letters 35, 4-9.

Merkt, J., Müller, H., Knabe, W., Müller, P., Wieser, T., 1993. The early Holocene Saksunarvatn tephra found in lake sediments in NW Germany. Boreas 22, 93-100.

Meyers, P., 2003. Applications of organic geochemistry to paleolimnological reconstructions: a summary of examples from the Laurentian Great Lakes. Organic Geochemistry 34, 261-289.

Miller, G.H., Alley, R.B., Brigham-Grette, J., Fitzpatrick, J.J., Polyak, L., Serreze, M.C., White, J.W.C., 2010. Arctic amplification: can the past constrain the future? Quaternary Science Reviews 29, 1779-1790.

Miller, G.H., Geirsdóttir, Á., Zhong, Y., Larsen, D.J., Otto-Bliesner, B.L., Holland, M.M., Bailey, D.A., Refsnider, K.A., Lehman, S.J., Southon, J.R., Anderson, C., Björnsson, H., Thordarson, T., 2012. Abrupt onset of the Little Ice Age triggered by volcanism and sustained sea-ice/ocean feedbacks. Geophysical Research Letters 39, 1-5.

Miller, G.H., Landvik, J.Y., Lehman, S.J., Southon, J.R., 2017. Episodic Neoglacial snowline descent and glacier expansion on Svalbard reconstructed from the ^{14}C ages of ice-entombed plants. Quaternary Science Reviews 155, 67-78.

Miller, G.H., Lehman, S.J., Refsnider, K.A., Southon, J.R., Zhong, Y., 2013. Unprecendented recent summer warmth in Arctic Canada. Geophysical Research Letters 40, 5745-5751.

Moorbath, S., Sigurdsson, H., Goodwin, R., 1968. K-Ar ages of the oldest exposed rocks in Iceland. Earth and Planetary Science Letters 4, 197-205.

Moossen, H., Bendle, J., Seki, O., Quillman, U., Kawamura, K., 2015. North Atlantic Holocene climate evolution recorded by high-resolution terrestrial and marine biomarker records. Quaternary Science Reviews 129, 111-117.

Moros, M., Andrews, J.T., Eberl, D.D., Jansen, E., 2006. Holocene history of drift ice in the northern North Atlantic: evidence for different spatial and temporal modes. Paleoceanography 21, 1-10.

Mortensen, A.K., Bigler, M., Grönvold, K., Steffensen, J.P., Johnsen, S.J., 2005. Volcanic ash layers from the Last Glacial Termination in the NGRIP ice core. Journal of Quaternary Science 20, 209-219.

Moune, S., Holtz, F., Botcharnikov, R.E., 2009. Sulphur solubility in andesitic to basaltic melts: implications for Hekla volcano. Contributions to Minerology and Petrology 157, 691-707.

Mudie, P.J., Helgason, J., 1983. Palynological evidence for Miocene climatic cooling in eastern Iceland about 9.8 Myr age. Nature 303, 689-692.

Mulch, A., Sarna-Wojcicki, A.M., Perkins, M.E., Chamberlain, C.P., 2008. A Miocene to Pleistocene climate and elevation record of the Sierra Nevada (California). Proceedings of the National Academy of Sciences 105, 6819-6824.

Müller, J., Wagner, A., Fahl, K., Stein, R., Prange, M., Lohmann, G., 2011. Towards quantitative sea ice reconstructions in the northern North Atlantic: a combined biomarker and numerical modelling approach. Earth and Planetary Science Letters 306, 137-148.

Müller, J., Werner, K., Stein, R., Fahl, K., Moros, M., Jansen, E., 2012. Holocene cooling culminates in sea ice oscillations in Fram Strait. Quaternary Science Reviews 47, 1-14.

Musa Bandowe, B.A., Srinivasan, P., Seelge, M., Sirocko, F., Wilcke, W., 2014. A 2600-year record of past polycyclic aromatic hydrocarbons (PAHs) deposition at Holzmaar (Eifel, Germany). Palaeogeography, Palaeoclimatology, Palaeoecology 401, 111-121.

Naeher, S., Peterse, F., Smittenberg, R.H., Niemann, H., Zigah, P.K., Schubert, C.J., 2014. Sources of glycerol dialkyl glycerol tetraethers (GDGTs) in catchment soils, water column and sediments of Lake Rotsee (Switzerland) – Implications for the application of GDGT-based proxies for lakes. Organic Geochemistry 66, 164-173.

Nakamura, H., Sawada, K., Araie, H., Suzuki, I., Shiraiwa, Y., 2013. Long chain alkenones, alkenones and alkenoates produced in the haptophyte alga Chrysotila lamellose CCMP1307 isolated from a salt marsh. Organic Geochemistry 66, 90-97.

Nesje, A., Dahl, S.O., Thun, T., Nordli, Ø, 2008. The 'Little Ice Age' glacial expansion in western Scandinavia: summer temperature or winter precipitation?. Climate Dynamics 30, 789-801.

Niemann, H., Stadnitskaia, A., Wirth, S.B., Gilli, A., Anselmetti, F.S., Sinninghe Damsté, J.S., Schouten, S., Hopmans, E.C., Lehmann, M.F., 2012. Bacterial GDGTs in Holocene sediments and catchment soils of a high Alpine lake: application of the MBT/CBT-paleothermometer. Climate of the Past 8, 889-906.

Niemeyer, B., Epp, L.S., Stoof-Leichsenring, K., Pestryakova, L.A., Herzschuh, U., 2017. A comparison of sedimentary DNA and pollen from lake sediments in recording vegetation composition at the Siberian treeline. Molecular Ecology Resources 17, e46-e62.

Norðdahl, H., Ingólfsson, Ó., 2015. Collapse of the Icelandic ice sheet controlled by sea-level rise? Arktos 1, 1-18.

Oerlemans, J., 2005. Extracting a climate signal from 169 glacier records. Science 308, 675-7.

Ogilvie, A.E.J., Jónsson, T., 2001. "Little Ice Age" research: A perspective from Iceland. Climatic Change 48, 9-52.

Óladóttir, B.A., Larsen, G., Sigmarsson, O., 2011. Holocene volcanic activity at Grímsvötn, Bárdarbunga and Kverkfjöll subglacial centres beneath Vatnajökull, Iceland. Bulletin of Volcanology 73, 1187-1208.

Óladóttir, B.A., Larsen, G., Þórðarson, Þ., Sigmarsson, O., 2006. The Katla volcano S-Iceland: Holocene tephra stratigraphy and eruption frequency. Jökull 55, 53-74.

Óladóttir, B.A., Sigmarsson, O., Larsen, G., 2011. Provenance of basaltic tephra from Vatnajökull subglacial volcanoes, Iceland, as determined by major- and trace-element analyses. Holocene 21, 1037-1048.

Óladóttir, B.A., Sigmarsson, O., Larsen, G., Thordarson, T., 2007. Katla volcano, Iceland: magma composition, dynamics and eruption frequency as recorded by Holocene tephra layers. Bulletin of Volcanology 70, 475-493.

Óladóttir, B.A., Thordarson, T., Larsen, G., Sigmarsson, O., 2007. Survival of the Mýrdalsjökull ice cap through the Holocene thermal maximum: evidence from sulphur contents in Katla tephra layers (Iceland) from the last ~8400 years. Annals of Glaciology 45, 183-188.

Óladóttir, B.A., Sigmarsson, O., Larsen, G., 2018. Tephra productivity and eruption flux of the subglacial Katla volcano, Iceland. Bulletin of Volcanology 80, 1-16.

Ólafsdóttir, S., Geirsdóttir, Á., Miller, G.H., Stoner, J.S., Channell, J.E.T., 2013. Synchronizing Holocene lacustrine and marine sediment records using paleomagnetic secular variation. Geology 41, 535-538.

Ólafsdóttir, S., Jennings A., Geirsdóttir, Á., 2010. Holocene variability of the North Atlantic Irminger current on the south- and northwest shelf of Iceland. Marine Micropaleontology 77, 101-118.

Ólafsson, J., 1999. Connections between oceanic conditions off N-Iceland, Lake Mývatn temperature, regional wind direction variability and the North Atlantic Oscillation. Rit Fiskideildar 16, 41-57.

Ólafsson, J., Ólafsdóttir, S.R., Briem, J., 2008. Vatnsföll og vistkerfi strandsjávar. Náttúrufræðingurinn 76, 95-108.

Olsen, J., Anderson, N.J., Knudsen, M.F., 2012. Variability of the North Atlantic Oscillation over the past 5,200 years. Nature Geoscience 5, 1-14.

Orme, L.C., Miettinen, A., Divine, D., Husum, K., Pearce, C., Van Nieuwenhove, N., Born, A., Mohan, R., Seidenkrantz, M.-S., 2018. Subpolar North Atlantic sea surface temperature since 6 ka BP: Indications of anomalous ocean-atmosphere interactions at 4-2 ka BP. Quaternary Science Reviews 194, 128-142.

Orvik, K.A., Skagseth, Ø., Mork, M., 2001. Atlantic inflow to the Nordic Seas: current structure and volume fluxes from moored current meters, VM-ADCP and SeaSoar-CTD observations, 1995-1999. Deep-Sea Research 48, 937-957.

Paillard, D., Labeyrie, L., Yiou, P., 1996. Macintosh program performs time-series analysis. Eos Transactions American Geophysical Union 77, 379.

Pancost, R.D., Sinninghe Damsté, J.S., 2003. Carbon isotopic compositions of prokaryotic lipids as tracers of carbon cycling in diverse settings. Chemical Geology 195, 29–58.

Parducci, L., Bennett, K.D., Ficetola, G.F., Alsos, I.G., Suyama, Y., Wood, J.R., Pedersen, M.W., 2017. Ancient plant DNA in lake sediments. New Phytologist 214, 924-942.

Patton, H., Hubbard, A., Bradwell, T., Schomacker, A., 2017. The configuration, sensitivity and rapid retreat of the Late Weichselian Icelandic ice sheet. Earth-Science Reviews 166, 223-245.

Pearson, E.J., Juggins, S., Talbot, H.M., Weckström, J., Rosén, P., Ryves, D.B., Roberts, S.J., Schmidt, R., 2011. A lacustrine GDGT-temperature calibration from the Scandinavian Arctic to Antarctic: Renewed potential for the application of GDGT-paleothermometry in lakes. Geochimica et Cosmochimica Acta 75, 6225-6238.

Pedersen, M.W., Ginolhac, A., Orlando, L., Olsen, J., Andersen, K., Holm, J., Funder, S., Willerslev, E., Kjær, K.H., 2013. A comparative study of ancient environmental DNA to pollen and macrofossils from lake sediments reveals taxonomic overlap and additional plant taxa. Quaternary Science Reviews 75, 161–168.

Pendleton, S.L., Miller, G.H., Anderson, R.A., Crump, S.E., Zhong, Y., Jahn, A., Geirsdóttir, Á., 2017. Episodic Neoglacial expansion and rapid 20th century retreat of a small ice cap on Baffin Island, Arctic Canada, and modeled temperature change. Climate of the Past 13, 1527-1537.

Pendleton, S.L., Miller, G.H., Lifton, N., Lehman, S.J., Southon, J., Crump, S.E., Anderson, R.S., 2019. Rapidly receding Arctic Canada glaciers revealing landscapes continuously ice-covered for more than 40,000 years. Nature Communications 10, 1-8.

Pendleton, S.L., Miller, G.H., Lifton, N., Young, N., 2019. Cryosphere response resolves conflicting evidence for the timing of peak Holocene warmth on Baffin Island, Arctic Canada. Quaternary Science Reviews, in review.

Peterse, F., van der Meer, J., Schouten, S., Weijers, J.W.H., Fierer, N., Jackson, R.B., Him, J.-H., Sinninghe Damsté, J.S., 2012. Revised calibration of the MBT-CBT

paleotemperature proxy based on branched tetraether membrane lipids in surface soils. Geochimica et Cosmochimica Acta 96, 215-229.

Peterse, F., Vonk, J.E., Holmes, R.M., Giosan, L., Zimov, N., Eglington, T.I., 2014. Branched glycerol dialkyl glycerol tetraethers in Arctic lake sediments: Sources and implications for paleothermometry at high latitudes. Journal of Geophysical Research: Biogeosciences 119, 1738-1754.

Plunkett, G., Pilcher, J.R., 2018. Defining the potential source region of volcanic ash in northwest Europe during the Mid- to Late Holocene. Earth-Science Reviews 179, 20-37.

Porter, J., Froese, D.G., Feakins, S.J., Bindeman, I.N., Mahony, M.E., Pautler, B.G., Reichart, G.-J., Sanborn, P.T., Simpson, M.J., Weijers, J.W.H., 2016. Multiple water isotope proxy reconstruction of extremely low last glacial temperatures in Eastern Beringia (Western Arctic). Quaternary Science Reviews 137, 113-125.

Prahl, F.G., Mix, A.C., Sparrow, M.A., 2006. Alkenone paleothermometry: Biological lessons from marine sediment records off western South America. Geochimica et Cosmochimica Acta 70, 101-117.

Prahl, F.G., Wakeham, S.G., 1987. Calibration of unsaturation patterns in long-chain ketone compositions for palaeotemperature assessment. Nature 330, 533-537.

Principato, S.M., 2008. Geomorphic evidence for Holocene glacial advances and sea level fluctuations on eastern Vestfirðir, northwest Iceland. Boreas 37, 132-145.

Principato, S., Geirsdóttir, Á., Jóhannsdóttir, G.E., Andrews, J.T., 2006. Late Quaternary glacial and deglacial history of eastern Vestfirðir, Iceland using cosmogenic isotope (^{36}Cl) exposure ages and marine cores. Journal of Quaternary Science 21, 271-285.

Principato, S.M., Johnson, J.S., 2009. Using GIS to quantify patterns of glacial erosion on northwest Iceland: Implications for independent ice sheets. Arctic, Antarctic and Alpine Research 41, 128-137.

Qin, W., Carlson, L.T., Armbrust, E.V., Devol, A.H., Moffett, J.W., Stahl, D.A., Ingalls, A.E., 2015. Confounding effects of oxygen and temperature on the TEX_{86} signature of marine Thaumarchaeota. Proceedings of the National Academy of Sciences 112, 10979-10984.

Quillmann, U., Jennings, A.E., Andrews, J.T., 2010. Reconstructing Holocene palaeoclimate and palaeoceanography in Ísafjarðardjúp, northwest Iceland, from two fjord records overprinted by relative sea-level and local hydrographic changes. Journal of Quaternary Science 25, 1144-1159.

Quillmann, U., Marchitto, T.M., Jennings, A.E., Andrews, J.T., Friestad, B.F., 2012. Cooling and freshening at 8.2 ka on the NW Iceland Shelf recorded in paired δ^{18}O and Mg/Ca measurements of the benthic foraminifer Cibicides lobatulus. Quaternary Research 78, 528-539.

Rahmstorf, S., Box, J.E., Feulner, G., Mann, M.E., Robinson, A., Rutherford, S., Schaffernicht, E.J., 2015. Exceptional twentieth-century slowdown in Atlantic Ocean overturning circulation. Nature Climate Change 5, 1–6.

Ran, L., Knudsen, K.L., Eiríksson, J., 2008. A high-resolution Holocene diatom record on the North Icelandic Shelf. Boreas 37, 399-413.

Rasmussen, S.O., Andersen, K.K., Svensson, A.M., Steffensen, J.P., Vinther, B.M., Clausen, H.,B., Siggaard-Andersen, M.-L., Johnsen, S.J., Larsen, L.B., Dahl-Jensen, D., Bigler, M., Röthlisberger, R., Fischer, H., Azuma-Goto, K., Hansson, M.E., Ruth, U., 2006. Anew Greenland ice core chronology for the last glacial termination. Journal of Geophysical Research 111, 1-16.

Rawlins, M.A., Steele, M., Holland, M.M., Adam, J.C., Cherry, J.E., Francis, J.A., Groisman, P.Y., Hinzman, L.D., Huntington, T.G., Kane, D.L., Kimball, J.S., Kwok, R., Lammers, R.B., Lee, C.M., Lettenmaier, D.P., Mcdonald, K.C., Podest, E., Pundsack, J.W., Rudels, B., Serreze, M.C., Shiklomanov, A., Skagseth, Ø., Troy, T.J., Vörösmarty, C.J., Wensnahan, M., Wood, E.F., Woodgate, R., Yang, D., Zhang, K., Zhang T., 2010. Analysis of the Arctic system for freshwater cycle intensification: Observations and expectations. Journal of Climate 23, 5715–5737.

RCoreTeam, 2014. R: a Language and Environment for Statistical Computing: R Foundation for Statistical Computing, Vienna, Austria, 2012. Open access available at: http://cran.r-project.org.

Reimer, P.J., Bard, E., Bayliss, A., Beck, W.J., Blackwell, P.G., Brock Ramsey, C., Buck, C.E., Cheng, H., Edwards, R.L., Friedrich, M., Grootes, P.M., Guilderson, T.P., Haflidason, H., Hajdas, I., Hatté, C., Heaton, T.J., Hoffmann, D.L., Hogg, A.G., Hughen, K.A., Kaiser, K.F., Kromer, B., Manning, S.W., Niu, M., Reimer, R.W., Richards, D.A., Scott, E.M., Southon, J.R., Staff, R.A., Turney, C.S.M., van der Plicht, J., 2013. Intcal13 and Marine13 radiocarbon age calibration curves 0-50,000 years cal BP. Radiocarbon 55, 1869-1887.

Riehle, P.J., Meyer, C.E., Miyaok, R.T., 1999. Data on Holocene tephra (volcanic ash) deposits in the Alaska Peninsula and Lower Cook Inlet region of the Aleutian Volcanic Arc, Alaska. United States Geological Survey Open-file Report 99-135, www.avo.alaska.edu.

Rodrigo-Gámiz, M., Rampen, S.W., de Haas, H., Baas, M., Schouten, S., Sinninghe-Damsté, J.S., 2015. Constraints on the applicability of the organic temperature proxies Uk37′, TEX_{86} and LDI in the subpolar region around Iceland. Biogeosciences 12, 6573-6590.

Rohling, E.J., Pälike, H., 2005. Centennial-scale climate cooling with a sudden cold event around 8,200 years ago. Nature 434, 975-979.

Rowland, S.J., Allard, W.G., Belt, S.T., Massé, G., Robert, J.-M., Blackburn, S., Frampton, D., Revill, A.T., Volkman, J.K., 2001. Factors influencing the distributions of polyunsaturated terpenoids in the diatom, Rhizosolenia setigera. Phytochemistry 58, 717-728.

Rueda, G., Rosell-Melé, A., Escala, M., Gyllencreutz, R., Backman, J., 2009. Comparison of instrumental and GDGT-based estimates of sea surface and air temperatures from the Skaggerak. Organic Geochemistry 40, 287-291.

Russell, J.M., Hopmans, E.C., Loomis, S.E., Liang, J., Sinninghe Damsté, J.S., 2018. Distributions of 5- and 6-methyl branched glycerol dialkyl glycerol tetraethers (brGDGTs) in East African lake sediment: Effects of temperature, pH, and new lacustrine paleotemperature calibrations. Organic Geochemistry 117, 56-69.

Schmid, M.M.E., Dugmore, A.J., Vésteinsson, O., Newton, A.J., 2017. Tephra isochrons and chronologies of colonisation. Quaternary Geochronology 40, 56-66.

Schomacker, A., Brynjólfsson, S., Andreassen, J.M., Gudmundsdóttir, E.R., Olsen, J., Odgaard, B.V., Håkansson, L., Ingólfsson, Ó., Larsen, N.K., 2016. The Drangajökull icecap, northwest Iceland, persisted into the early-mid Holocene. Quaternary Science Reviews 148, 66-84.

Schouten, S., Hopmans, E.C., Schefuss, E., Sinninghe Damsté, J.S., 2002. Distributional variations in marine crenarchaeotal membrane lipids: a new tool for reconstructing ancient sea water temperatures? Earth and Planetary Science Letters 204, 265-274.

Schouten, S., Hopmans, E.C., Sinninghe Damsté, J.S., 2004. The effect of maturity and depositional redox conditions on archael tetraether lipid palaeothermomtry. Organic Geochemistry 35, 567-571.

Schouten, S., Hopmans, E.C., Sinninghe Damsté, J.S., 2013. The organic geochemistry of glycerol dialkyl glycerol tetraether lipids: A review. Organic Geochemistry 54, 19-61.

Schuessler, J.A., Schoenberg, R., Sigmarsson, O., 2009. Iron and lithium isotope systematics of the Hekla volcano, Iceland – Evidence for Fe isotope fractionation during magma differentiation. Chemical Geology 258, 78-81.

Schweinsberg, A.D., Briner, J.P., Miller, G.H., Bennike, O., Thomas, E.K., 2017. Local glaciation in West Greenland linked to North Atlantic Ocean circulation during the Holocene. Geology 45, 1-4.

Schweinsberg, A.D., Briner, J.P., Miller, G.H., Lifton, N.A., Bennike, O., Graham,B.L., 2018. Holocene mountain glacier history in the Sukkertoppen Iskappe area, southwest Greenland. Quaternary Science Reviews 197, 142-161.

Seligman, A.N., Bindeman, I.N., Watkins, J.M., Ross, A.M., 2016. Water in volcanic glass: From volcanic degassing to secondary hydration. Geochimica et Cosmochimica Acta 191, 216-238.

Serreze, M.C., Barry, R.G., 2011. Processes and impacts of Arctic amplification: A research synthesis. Global and Planetary Change 77, 85-96.

Shanahan, T.M., Hughen, K.A., Van Mooy, B.A.S., 2013. Temperature sensitivity of branched and isoprenoid GDGTs in Arctic lakes. Organic Geochemistry 64, 119-128.

Shindell, D.T., Schmidt, G.A., Mann, M.E., Rind, D., Waple, A., 2001. Solar forcing of regional climate during the Maunder Minimum. Science 294, 2149-2152.

Sicre, M.-A., Hall, I.R., Mignot, J., Khodri, M., Ezat, U., Truong, M-X., Eiríksson, J., Knudsen, K-L., 2011. Sea surface temperature variability in the subpolar Atlantic over the last two millennia. Paleoceanography 26, 1-10.

Sicre, M.-A., Khodri, M., Mignot, J., Eiríksson, J., Knudsen, K.-L., Ezat, U., Closset, I., Nogues, P., Massé, G., 2013. Sea surface temperature and sea ice variability in the subpolar North Atlantic from explosive volcanism of the late thirteenth century. Geophysical Research Letters 40, 5526-5539.

Sigl, M., Winstrup, M., McConnell, J.R., Welten, K.C., Plunkett, G., Ludlow, F., Büntgen, U., Caffee, M., Chellman, N., Dahl-Jensen, D., Fischer, H., Kipfstuhl, S., Kostick, C., Maselli, O.J., Mekhaldi, F., Mulvaney, R., Muscheler, R., Pasteris, D.R., Pilcher, J.R., Salzer, M., Schüpbach, S., Steffensen, J.P., Vinther, B.M., Woodruff, T.E., 2015. Timing and climate forcing of volcanic eruptions for the past 2,500 years. Nature 253, 543-549.

Sigmarsson, O., Condomines, M., Fourcade, S., 1992. A detailed Th, Sr and O isotope study of Hekla: differentiation processes in an Icelandic Volcano. Contributions to Minerology and Petrology 112, 20-34.

Sigmarsson, O., Steinþórsson, S., 2007. Origin of Icelandic basalts: A review of their petrology and geochemistry. Journal of Geodynamics 32, 87-100.

Sigurdsson, H., Sparks, R.S.J., 1981. Petrology of rhyolitic and mixed magma ejecta from the 1875 eruption of Askja, Iceland. Journal of Petrology 22, 41-84.

Sigurgeirsson, M.Á., Hauptfleisch, U., Newton, A., Einarsson, Á., 2013. Dating of the Viking age Landnám tephra sequence in Lake Mývatn sediment, north Iceland. Journal of the North Atlantic 21, 1-11.

Sigvaldason, G., Annertz, K., Nilsson, M., 1992. Effect of glacier unloading/deloading on volcanism: postglacial volcanic eruption rate of the Dyngjufjöll area, central Iceland. Bulletin of Volcanology 54, 385-392.

Simoneit, B.R.T., 1998. Biomarker PAHs in the Environment. In: Neilson A.H. (eds) PAHs and Related Compounds. The Handbook of Environmental Chemistry (Anthropogenic Compounds), vol 3/3I. Springer, Berlin, Heidelberg.

Simoneit, B.R.T., 2002. Biomass burning – a review of organic tracers for smoke from incomplete combustion. Applied Geochemistry 17, 129-162.

Sinninghe Damsté, J.S., Hopmans, E.C., Pancost, R.D., Schouten, S., Geenevasen, J.A.J., 2000. Newly discovered non-isoprenoid dialkyl diglycerol tetraether lipids in sediments. Journal of the Chemical Society, Chemical Communications 23, 1683–1684.

Sinton, J., Grönvold, K., Sæmundsson, K., 2005. Post-glacial eruptive history of the Western Volcanic Zone, Iceland. Geochemistry, Geophysics, Geosystems 6, 1-34.

Sjögren, P., Edwards, M.E., Gielly, L., Langdon, C.T., Croudace, I.W., Merkel, M.K.F., Fonville, T., Alsos, I.G., 2017. Lake sedimentary DNA accurately records 20th Century introductions of exotic conifers in Scotland. New Phytologist 213, 929-941.

Skrzypek, G., Paul, D., Wojtuń, B., 2008. Stable isotope composition of plants and peat from Arctic mire and geothermal area in Iceland. Polish Polar Research 29, 365-376.

Slater, L., Jull, M., McKenzie, D., Grönvold, K., 1998. Deglaciation effects on mantle melting under Iceland: results from the northern volcanic zone. Earth and Planetary Science Letters 164, 151-164.

Slawinska, J., Robock, A., 2018. Impact of volcanic eruptions on decadal to centennial fluctuations of Arctic sea ice extent during the last millennium and on initiation of the Little Ice Age. Journal of Climate 31, 2145-2167.

Smik, L., Cabedo-Sanz, P., Belt, S.T., 2016. Semi-quantitative estimates of paleo Arctic sea ice concentration based on source-specific highly branched isoprenoid alkenes: A further development of the PIP_{25} index. Organic Geochemistry 92, 63-69.

Smith, L.M., Andrews, J.T., Castañeda, I.S., Kristjánsdóttir, G.B., Jennings, A.E., Sveinbjörnsdóttir, Á.E., 2005. Temperature reconstructions for SW and N Iceland waters over the last 10 cal ka based on $\delta^{18}O$ records from planktic and benthic foraminifera. Quaternary Science Reviews 24, 1723-1740.

Solanki, S.K., Usoskin, I.G., Kromer, B., Schüssler, M., Beer, J., 2004. Unusual activity of the Sun during the recent decades compared to the previous 11,000 years. Nature 431, 1084-1087.

Solignac, S., Giraudeau, J., de Vernal, A., 2006. Holocene sea surface conditions in the western North Atlantic: Spatial and temporal heterogeneities. Paleoceanography 21, 1-6.

Solomina, O.N., Bradley, R.S., Jomelli, V., Geirsdóttir, Á., Kaufman, D.S., Koch, J., McKay, N.P., Masiokas, M., Miller, G., Nesje, A., Nicolussi, K., Owen, L.A., Putnam, A.E., Wanner, H., Wiles, G., Yang, B., 2016. Glacier fluctuations during the past 2000 years. Quaternary Science Reviews 149, 61-90.

Spielhagen, R.F., Werner, K., Sørensen, S.A., Zamelczyk, K., Kandiano, E., Budeus, G., Husum, K., Marchitto, T.M., Hald, M., 2011. Enhanced modern heat transfer to the Arctic by warm Atlantic water. Science 311, 450-453.

Stefánsson, U., 1962. North Icelandic Waters. Rit Fiskideildar III. Bind, vol 3.

Stefánsson, U., 1968. Dissolved nutrients, oxygen and water masses in the Northern Irminger Sea. Deep-Sea Research 15, 541-575.

Stefánsson, U., Ólafsson, J., 1991. Nutrients and fertility of Icelandic waters. Rit fiskideildar, 1-56.

Stein, R., Fahl, K., Schreck, M., Knorr, G., Niessen, F., Forwick, M., Gebhardt, C., Jensen, L., Kaminski, M., Kopf, A., Matthiessen, J., Jokat, W., Lohmann, G., 2016. Evidence for

ice-free summers in the late Miocene central Arctic Ocean. Nature Communications 7, 11148.

Steinhilber, F., Beer, J., Fröhlich, C., 2009. Total solar irradiance during the Holocene. Geophysical Research Letters 36, 1-5.

Stoner, J.S., Jennings, A., Kristjánsdóttir, G.B., Dunhill, G., Andrews, J.T., Hardardóttir, J., 2007. A paleomagnetic approach toward refining Holocene radiocarbon-based chronologies: Paleoceanographic records from the north Iceland (MD99-2269) and east Greenland (MD99-2322) margins. Paleoceanography 22, 1-23.

Stötter, J., Wastl, M., Caseldine, C., Häberle, T., 1999. Holocene palaeoclimatic reconstruction in northern Iceland: approaches and results. Quaternary Science Reviews 18, 457-474.

Striberger, J., Björck, S., Benediktsson, Í.Ö., Snowball, I., Uvo, C.B., Ingólfsson, Ó., Kjær, K., 2011. Climatic control of the surge periodicity of an Icelandic outlet glacier. Journal of Quaternary Science 26, 561-565.

Striberger, J., Björck, S., Holmgren, S., Hamerlík, L., 2012. The sediments of Lake Lögurinn – A unique proxy record of Holocene glacial meltwater variability in eastern Iceland. Quaternary Science Reviews 38, 76-88.

Stroeve, J., Holland, M.M., Meier, W., Scambos, T., Serreze, M., 2007. Arctic sea ice decline: Faster than forecast. Geophysical Research Letters 34, 1–5.

Stuiver, M., Reimer, P.J., Reimer, R.W., 2018. CALIB 7.1 [WWW program] at http://calib.org, accessed 2018-11-16.

Sun, C., Plunkett, G., Liu, J., Zhao, H., Sigl, M., McConnell, J.R., Pilcher, J.R., Vinther, B., Steffensen, J.P., Hall, V., 2014. Ash from Changbaishan Millennium eruption recorded in Greenland ice: implications for determining the eruption's timing and impact. Geophysical Research Letters 41, 694-701.

Sun, Q., Chu, G., Liu, M., Xie, M., Li, S., Ling, Y., Wang, X., Shi, L., Jia, G., Lü, H., 2011. Distributions and temperature dependence of branched glycerol dialkyl glycerol tetraethers in recent lacustrine sediments from China and Nepal. Journal of Geophysical Research: Biogeosciences 116, 1-12.

Sun, Q., Chu, G.Q., Liu, G.X., Li, S., Wang, X.H., 2007. Calibration of alkenone unsaturation index with growth temperature for a lacustrine species, Chrysotila lamellosa (Haptophyceae). Organic Geochemistry 38, 1226-1234.

Sveinbjörnsdóttir, Á.E., Heinemeier, J., Kristensen, P., Rus, N., Geirsdóttir, Á., Harðardóttir, J., 1998. ^{14}C AMS dating of Icelandic lake sediments. Radiocarbon 40, 865-872.

Svenden, J.I., Landvik, J.Y., Mangerud, J., Miller, G.H., 1987. Postglacial marine and lacustrine sediments in Lake Linnévatnet, Svalbard. Polar Research 5, 281-283.

Sweet, S.K., Griffin, K.L., Steltzer, H., Gough, L., Boelman, N.T., 2015. Greater deciduous shrub abundance extends tundra peak season and increases modeled net CO_2 uptake. Global Change Biology 21, 2394-2409.

Theroux, S., D'Andrea, W.J., Toney, J., Amaral-Zettler, L., Huang Y., 2010. Phylogenetic diversity and evolutionary relatedness of alkenone-producing haptophyte algae in lakes: implications for continental paleotemperature reconstructions. Earth and Planetary Science Letters 300, 311-320.

Theroux, S., Toney, J., Amaral-Zettler, L., Huang, Y.S., 2013. Production and temperature sensitivity of long chain alkenones in the cultured haptophyte Pseudoisochrysis paradoxa. Organic Geochemistry 62, 68-73

Thorarinsson, S., 1944. Tefrokronologiska studier på Island. Geografiska Annaler XXVI, 1-217.

Thorarinsson, S., 1967. The eruptions of Hekla in historical times: a tephrochronological study. In: Einarsson, T., Kjartansson, G., Thorarinsson, S. (eds) The eruption of Hekla 1947-1948. Societas Scientiarum Islandica, Reykjavik, 1-177.

Thordarson, T., 2014. The widespread ~10ka Saksunarvatn tephra is not a product single eruption. AGU Fall Meeting Abstracts.

Thordarson, T., Geirsdóttir, Á., Miller, G.H., 2012. Framework for the tephra stratigraphy and chronology in western Iceland for the last 12 ka. 2012 Nordic Winter Meeting, Reykjavík.

Thordarson, T., Höskuldsson, Á., 2008, Postglacial volcanism in Iceland. Jökull 58, 197-228.

Thordarson, T., Larsen, G., 2007. Volcanism in historical time: Volcano types, eruptions styles and eruptive history. Journal of Geodynamics 43, 118-152.

Thordarson, T., Miller, D.J., Larsen, G., Self, S., Sigurdsson, H., 2001. New estimates of sulfur degassing and atmospheric mass-loading by the 934 AD Eldgjá eruption, Iceland. Journal of Volcanology and Geothermal Research 108, 33-54.

Thordarson, T., Self, S., Miller, D.J., Larsen, G., Vilmundardóttir, E.G., 2003. Sulphur release from flood lava eruptions in the Veidivötn, Grímsvötn and Katla volcanic systems, Iceland. In: Oppenheimer, C., Pyle, D.M. and Barclay, J. (eds) Volcanic Degassing. Geological Society, London, Specical Publications, 213, 103-121.

Thordarson, T., Self, S., Óskarsson, N., Hulsebosch, T., 1996. Sulphur, chlorine, and fluorine degassing and atmospheric loading by the 1783-1784 AD Laki (Skaftár Fires) eruption in Iceland. Bulletin of Volcanology 58, 205-225.

Thoroddsen, Þ., 1916-1917. Árferði á Íslandi í þúsund ár (The climate of Iceland through one thousand years), Hið íslenska fræðafélag, Copenhagen.

Thornalley, D.J.R., Oppo, D.W., Ortega, P., Robson, J.I., Brierley, C.M., Davis, R., Hall, I.R., Moffa-Sanchez, P., Rose, N.L., Spooner, P.T., Yashayaev, I., Keigwin, L.D., 2018.

Anomalously weak Labrador Sea convection and Atlantic overturning during the past 150 years. Nature 556, 227-232.

Thorndike, A.S., Rothrock, D.A., Maykut, G.A., Colony, R., 1975. The thickness distribution of sea ice. Journal of Geophysical Research 80, 4501-4513.

Timms, R.G.O., Matthews, I.P., Lowe, J.J., Palmer, A.P., Weston, D.J., MacLeod, A., Blockley, S.P.E., 2019. Establishing tephrostratigraphic frameworks to air the study of abrupt climatic and glacial transitions: a case study of the Last Glacial-Interglacial Transition in the British Isles (c. 16-8 ka BP). Earth-Science Reviews, in press.

Toney, J.L., Huang, Y., Fritz, S.C., Baker, P.A., Grimm, E., Nyren, P., 2010. Climatic and environmental controls on the occurrence and distributions of long chain alkenones in lakes of the interior United States. Geochimica et Cosmochimica Acta 74, 1563– 1578.

Toney, J., Theroux, S., Andersen, R.A., Coleman, A., Amaral-Zettler, L., Huang Y., 2012. Culturing of the first 37:4 predominant lacustrine haptophyte: geochemical, biochemical, and genetic implications. Geochimica et Cosmochimica Acta 78, 51–64.

Trouet, V., Esper, J., Graham, N.E., Baker, A., Scourse, J.D., Frank, D.C., 2009. Persistent positive North Atlantic Oscillation mode dominated the Medieval Climate Anomaly. Science 324, 78-80.

Tyagi, P., Edwards, D.R., Coyne, M.S., 2007. Use of selected chemical markers in combination with a multiple regression model to assess the contribution of domesticated animal sources of fecal pollution in the environment. Chemosphere 69, 1617-1624.

van der Bilt, W.G.M., D'Andrea, W.J., Bakke, J., Balascio, N.L., Werner, J.P., Gjerde, M., Bradley, R.S., 2018. Alkenone-based reconstructions reveal four-phase Holocene temperature evolution for High Arctic Svalbard. Quaternary Science Reviews 183, 204-213.

van der Bilt, W.G.M., Lane, C.S., Bakke, J., 2017. Ultra-distal Kamchatkan ash on Arctic Svalbard: Towards hemispheric cryptotephra correlation. Quaternary Science Reviews 164, 230-235.

van der Bilt, W.G.M., Rea, B., Spagnolo, M., Roerdink, D.L., Jørgensen, S.L., Bakke, J., 2018. Novel sedimentological fingerprints link shifting depositional processes to Holocene climate transitions in East Greenland. Global and Planetary Change 164, 52-64.

Vésteinsson, O., McGovern, T.H., 2012. The peopling of Iceland. Norwegian Archaeological Review 45, 206-218.

Volkman, J.K., 1986. A review of sterol markers for marine and terrigenous organic matter. Organic Geochemistry 9, 83-99.

Volkman, J.K., Barrett, S.M., Blackburn, S.I., Mansour, M.P., Sikes, E.L., Gelin, F., 1998. Microalgal biomarkers: a review of recent developments. Organic Geochemistry 29, 1163-1179.

Wakeham, S.G., Schaffner, C., Giger, W., 1980. Polycyclic aromatic hydrocarbons in recent lake sediments – II. Compounds derived from biogenic precursors during early diagenesis. Geochimica et Cosmochimica Acta 44, 415-429.

Walker, G.P.L., 1962. Tertiary welded tuffs in eastern Iceland. Quarterly Journal of the Geological Society 118, 275-290.

Wanamaker, A.D., Butler, P.G., Scourse, J.D., Heinemeier, J., Eiríksson, J., Knudsen, K.L., Richardson, C.A., 2012. Surface changes in the North Atlantic meridional overturning circulation during the last millennium. Nature Communications 3, 1-7.

Wang, Z., Liu, W., 2013. Calibration of the $U^{K'}_{37}$ index of long-chain alkenones with the in-situ water temperature in Lake Qinghai in the Tibetan Plateau. Climate Science Bulletin 58, 803-808.

Wang, Y., Wooller, M., 2006. The stable isotopic (C and N) composition of modern plants and lichens from northern Iceland: with ecological and paleoenvironmental implications. Jökull 56, 27-38.

Wanner, H., Solomina, O., Grosjean, M., Ritz, S.P., Jetel, M., 2011. Structure and origin of Holocene cold events. Quaternary Science Reviews 30, 3109-3123.

Wastegård, S., Gudmundsdóttir, E.R., Lind, E.M., Timms, R.G.O., Björck, S., Hannon, G.E., Olsen, J., Rundgren, M., 2018. Towards a Holocene tephrochronology for the Faroe Islands, North Atlantic. Quaternary Science Reviews 195, 195-214.

Wastegård, S., Hall, V.A., Hannon, G.E., van den Bogaard, C., Pilcher, J.R., Sigurgeirsson, M.Á., Hermanns-Auðardóttir, M., 2003. Rhyolitic tephra horizons in northwestern Europe and Iceland from the AD 700s-800s: a potential alternative for dating first human impact. The Holocene 13, 277-283.

Wastl, M., Stötter, J., Caseldine, C., 2001. Reconstruction of Holocene variations of the upper limit of tree or shrub birch growth in northern Iceland based on evidence from Vesturárdalur-Skíðadalur, Tröllaskagi. Arctic, Antarctic, and Alpine Research 33, 191-203.

Weber, Y., Sinninghe Damsté, J.S., Zopfi, J., De Jonge, C., Gilli, A., Schubert, C.J., Lepori, F., Lehmann, M.F., Niemann, H., 2018. Redox-dependent niche differentiation provides evidence for multiple bacterial sources of glycerol tetraether lipids in lakes. Proceedings of the National Academy of Sciences 115, 10926-10931.

Weber, Y., De Jonge, C., Rijpstra, I.C., Hopmans, E.C., Stadnitskaia, A., Schubert, C.J., Lehmann, M.F., Sinninghe Damsté, J.S., Niemann, H., 2015. Identification and carbon isotope composition of a novel branched GDGT isomer in lake sediments: Evidence for lacustrine branched GDGT production. Geochimica et Cosmochimica Acta 154, 118-129.

Weijers, J.W.H., Panoto, E., van Bleijswijk, J., Schouten, S., Rijpstra, W.I.C., Balk, M., Stams, A.J.M., Sinninghe Damsté, J.S., 2009. Constraints on the biological source(s) of the orphan branched tetraether membrane lipids. Geomicrobiology Journal 26, 402-414.

Weijers, J.W.H., Schouten, S., Hopmans, E.C., Geenevasen, J.A.J., David, O.R.P., Coleman, J.M., Pancost, R.D., Sinninghe Damsté, J.S., 2006a. Membrane lipids of mesophilic

anaerobic bacteria thriving in peats have typical archaeal traits. Environmental Microbiology 8, 648-657.

Weijers, J.W.H., Schouten, S., Spaargaren, O.C., Sinninghe Damsté, J.S., 2006b. Occurrence and distribution of tetraether membrane in soils: implications for the use of the BIT index and the TEX86 SST proxy. Organic Geochemistry 37, 1680–1693.

Weijers, J.W.H., Schouten, S., van den Donker, J.C., Hopmans, E.C., Sinninghe Damsté, J.S., 2007. Environmental controls on bacterial tetraether membrane lipid distribution in soils. Geochimica et Cosmochimica Acta 71, 703-713.

Weijers, J.W.H., Wiesenberg, G.L.B., Bol, R., Hopmans, E.C., Pancost, R.D., 2010. Carbon isotopic composition of branched tetraether membrane lipids in soils suggest a rapid turnover and a heterotrophic life style of their source organism(s). Biogeosciences 7, 2959–2973.

Willerslev, E., Davison, J., Moora, M., Zobel, M., Coissac, E., Edwards, M.E., Lorenzen, E.D., Vestergård, M., Gussarova, G., Haile, J., Craine, J., Gielly, L., Boessenkool, S., Epp, L.S., Pearman, P.B., Cheddadi, R., Murray, D., Bråthen K.A., Yoccoz, N., Binney, H., Cruaud, C., Wincker, P., Goslar, T., Alsos, I.G., Bellemain, E., Brysting, A.K., Elven, R., Sønstebø, J.H., Murton, J., Sher, A., Rasmussen, M., Rønn, R., Mourier, T., Cooper, A., Austin, J., Möller, P., Froese, D., Zazula, G., Pompanon, F., Rioux, D., Niderkorn, V., Tikhonov, A., Savvinov, G., Roberts, R.G., MacPhee, R.D.E., Gilbert, M.T.P., Kjær, K., Orlando, L., Brochmann, C., Taberlet, P., 2014. Fifty thousand years of Arctic vegetation and megafaunal data. Science 506, 46-57.

Williams, J.W., Shuman, B.N., Webb, T., Bartlein, P.J., Leduc, P.L., 2004, Late-Quaternary vegetation dynamics in North America: Scaling from taxa to biomes. Ecological Monographs 74, 309–334.

Wörmer, L., Lipp, J.S., Hinrichs, K.U., 2015. Comprehensive analysis of microbial lipids in environmental samples through HPLC-MS protocols. In Hydrocarbon and Lipid Microbiology, p. 289-317. Springer, Berlin, Heidelberg.

Wuchter, C., Schouten, S., Coolen, M.J.L., Sinninghe Damsté, J.S., 2004. Temperature-dependent variation in the distribution of tetraether membrane lipids of marine Crenarchaeota: implications for TEX_{86} paleothermometry. Paleoceanography 19, 1-10.

Wuchter, C., Schouten, S., Wakeham, S.G., Sinninghe Damsté, J.S., 2005. Temporal and spatial variation in tetraether membrane lipids of marine Crenarchaeota in particulate organic matter: implications for TEX_{86} paleothermometry. Paleoceanography 20, 1-11.

Wunsch, C., 1980. Meridional heat flux of the North Atlantic Ocean. Proceedings of the National Academy of Sciences 77, 5043-5047.

Xiao, X., Zhao, M., Knudsen, K.L., Sha, L., Eiríksson, J., Gudmundsdóttir, E., Jiang, H., Guo, Z., 2017. Deglacial and Holocene sea-ice variability north of Iceland and response to ocean circulation changes. Earth and Planetary Science Letters 472, 14-24.

Yunker, M.B., Macdonald, R.W., Snowdon, L.R., Fowler, B.R., 2011. Alkane and PAH biomarkers as tracers of terrigenous organic carbon in Arctic Ocean sediments. Organic Geochemistry 42, 1109-1146.

Zachos, J., Pagani, M., Sloan, L., Thomas, E., Billups, K., 2001. Trends, rhythms, and aberrations in global climate 65 Ma to present. Science 292, 686-693.

Zdanowicz, C.M., Zielinski, G.A., Germani, M.S., 1999. Mount Mazama eruption: Calendrical age verified and atmospheric impact assessed. Geology 27, 621-624.

Zhai, L., Guðmundsson, K., Miller, P., Peng, W., Guðfinnsson, H., Debes, H., Hátun, H., White III, G.N., Hernández Walls, R., Sathyendranath, S., Platt, T., 2012. Phytoplankton phenology and production around Iceland and Faroes. Continental Shelf Research 37, 15-25.

Zheng, Y., Tarozo, R., Huang, Y., 2017. Optimizing chromatographic resolution for simultaneous quantification of long chain alkenones, alkenoates and their double bond positional isomers. Organic Geochemistry 111, 136-143.

Zhong, Y., Miller, G.H., Otto-Bliesner, B.L., Holland, M.M., Bailey, D.A., Schneider, D.P., Geirsdóttir, Á., 2010. Centennial-scale climate change from decadally-paced explosive volcanism: a coupled sea ice-ocean mechanism. Climate Dynamics 37, 2373-2387.

Zielinski, G.A., Mayewski, P.A., Meeker, L.D., Grönvold, K., Germani, M.S., Whitlow, S., Twickler, M.S., Taylor, K., 1997. Volcanic aerosol records and tephrochronology of the Summit, Greenland, ice cores. Journal of Geophysical Research 102, 625-640.

Zink, K.G., Leythaeuser, D., Melkonian, M., Schwark, L., 2001. Temperature dependency of long-chain alkenone distributions in recent to fossil limnic sediments in lake waters. Geochimica et Cosmochimca Acta 65, 253–257.

Zink, K.G., Vandergoes, M.J., Mangelsdorf, K., Dieffenbacher-Krall, A.C., Schwark, L., 2010. Application of bacterial glycerol dialkyl glycerol tetraethers (GDGTs) to develop modern and past temperature estimates from New Zealand lakes. Organic Geochemistry 41, 1060-106.